Nano- and microplastics in the environment : presence, effects and their role as a Trojan horse for other pollutants

Celia Trujillo Lacasa

THÈSE

UNIVERSITE DE PAU ET DES PAYS DE L'ADOUR

École doctorale des sciences exactes et leurs applications

Présentée et soutenue le 05 de mai de 2023

par **Celia TRUJILLO LACASA**

pour obtenir le grade de docteur
de l'Université de Pau et des Pays de l'Adour
Spécialité : Chimie analytique et environnement

NANO- AND MICROPLASTICS IN THE ENVIRONMENT: PRESENCE, EFFECTS AND THEIR ROLE AS A TROJAN HORSE FOR OTHER POLLUTANTS

MEMBRES DU JURY

RAPPORTEURS

• Yolanda MADRID ALBARRÁN	Professeure / Université Complutense de Madrid- Espagne
• Antonio MOREDA PIÑEIRO	Professeur / Université de Saint-Jacques de Compostelle- Espagne

EXAMINATEURS

• Stéphanie REYNAUD	Directrice de recherche / Université de Pau et des Pays de l'Adour- France
• Mónica IGLESIAS JUNCA	Professeure / Université de Gérone - Espagne

DIRECTEURS

• Francisco LABORDA GARCÍA	Professeur/ Université de Saragosse - Espagne
• Ryszard LOBINSKI	Directeur de recherche/ CNRS-IPREM- France

UNIVERSITÉ DE PAU ET DES PAYS DE L'ADOUR

Universidad Zaragoza 1542

INSTITUTO UNIVERSITARIO DE INVESTIGACIÓN EN CIENCIAS AMBIENTALES DE ARAGÓN

UNIVERSIDAD DE ZARAGOZA

INSTITUTE OF ANALYTICAL SCIENCES AND PHYSICO-CHEMISTRY FOR ENVIRONMENT AND MATERIALS

UNIVERSITÉ DE PAU ET DES PAYS DE L'ADOUR

NANO- AND MICROPLASTICS IN THE ENVIRONMENT:

PRESENCE, EFFECTS AND THEIR ROLE AS A TROJAN HORSE FOR OTHER POLLUTANTS

CELIA TRUJILLO LACASA

DOCTORAL THESIS 2023

Departamento de
Química Analítica
Universidad Zaragoza

Francisco Laborda García, Professor at the University of Zaragoza and Ryszard Lobinski, Researcher Director at the CNRS,

CERTIFY

that this thesis manuscript:

"NANO- AND MICROPLASTICS IN THE ENVIRONMENT: PRESENCE, EFFECTS AND THEIR ROLE AS A TROJAN HORSE FOR OTHER POLLUTANTS"

has been carried out under their supervision by Celia Trujillo Lacasa in the Department of Analytical Chemistry of the Faculty of Sciences of the University of Zaragoza and at the University of Pau, to qualify for the title of Doctor in Analytical Science in Chemistry for the University of Zaragoza and the title of Doctor in Analytical Chemistry for the University of Pau.

And,

AUTHORISE

the presentation of this report to be defended to the corresponding Thesis Committe.

Zaragoza, 13 of February 2023

Francisco Laborda García

Ryszard Lobinski

Different parts of this Doctoral Thesis have been carried out in collaboration with the following companies, research groups and support services:

- Water and Environmental Health Group, Department of Chemical Engineering and Environmental Technology, University of Zaragoza.

- Chemical Analysis and Electron Microscopy of Materials Services of the General Research Support Service of the University of Zaragoza.

- Analytical, Physical and Theoretical Chemistry Department of IPREM UMR 5254 (CNRS-UPPA), Pau, France .

This work has been carried out in the frame of the projects:

- RTI2018-096111-B-100 of the Spanish Ministry of Science, Innovation and Universities, co-funded by ERDF "A way of making Europe".
- PID2021-123203OB-I00 of the Spanish Ministry of Science and Innovation (MCIN/AEI/10.13039/501100011033) co-funded by ERDF.
- E29_17R of the Government of Aragon, co-funded by ERDF "Building Europe from Aragon".
- University of Zaragoza for awarding a grant (PI-PRD/2018-001) to carry out a joint thesis between the University of Zaragoza and the University of Pau.

“It always seems impossible until it is done”

Nelson Mandela

Cuando empecé esta aventura, parecía que este momento estaba muy lejos de suceder. Sin embargo, ha llegado definitivamente y es necesario recordar a todas aquellas personas que lo han hecho posible.

Sin duda gran parte de esta tesis corresponde a mis directores Francisco Laborda y Ryszard Lobinski, sin los cuales me hubiera encontrada perdida en este caótico mundo que es la ciencia. Agradecer a Francisco Laborda todo el apoyo y el tiempo que me ha dedicado durante estos años, ya que a pesar de tener una agenda ajetreada siempre disponía de tiempo para comentar cualquier duda o resultado. Agradecer también Ryszard Lobinski, por proporcionarme consejo científico y darme la oportunidad de realizar una tesis en cotutela dentro de un centro de investigación de renombre.

También agradecer a los miembros del Grupo de Espectroscopía Analítica y Sensores (GEAS), los cuales han sido una parte importante de mis días durante estos últimos años. A Eduardo Bolea, el cual siempre se encontraba dispuesto a ayudar en cualquier tipo de tarea y que tristemente ha tenido que sufrir con el mejor humor posible nuestros desvaríos varios en los cafés. A Josefina Pérez, por la diligencia mostrada ante cualquier problema que le presentaba y que ha tenido que soportar las eternas jornadas de microscopia con la máxima entereza, aunque en ocasiones fuera tarea imposible. A Sierra Jiménez y Teresa Gómez, las cuales no pueden existir en mi mente la una sin la otra, y que gracias a su buen humor se han convertido en compañeras necesarias de congreso. También agradecer a Juan Ramón Castillo y Gemma Cepría, aunque ya no están, siempre serán unas figuras indispensables del GEAS.

Mención especial a mis compañeros de Laboratorio; Ana Cris, David, Dea, Isabel, Khaoula y Mariam, los cuales han hecho que la vida en el laboratorio fuera soportable y divertida. A Ana Cris, mi compañera de laboratorio y "fechorías", que comenzó esto conmigo. A David, a pesar de resultar en ocasiones insufrible por su tranquilidad y chistes malos, se hacía querer muy al final. A Dea, por animar el ambiente del laboratorio con su música y expandir nuestro vocabulario castellano-cubano. A Isabel, a pesar de aparecer en la recta

final del doctorado ha resultado ser un apoyo incondicional, aunque presente cierto odio oculto a mi persona. A Khaoula, por sus abrazos sorpresa, su locura y su felicidad, la cual repartía a cualquiera que la necesitara. A Mariam, mi compañera de viajes y la cual, aunque intente hacerse la dura sé que me tiene cariño. Gracias a todos por esos cafés de como mucho 30 minutos, por las historias desternillantes que los llenaban, por esos desayunos de chocolate con churros y por el apoyo moral en los momentos de bajón científico.

Agradecer también a todas aquellas personas que han pasado más o menos tiempo por el GEAS, pero que sin duda han formado parte importante de esta etapa. A Laura y Vanessa, por darnos consejos sobre la dura vida de un doctorando. A Bianca, por revolucionar durante unos meses nuestro laboratorio y la vida. A Sebastiano, por traer su buen rollo y proporcionarnos frases para la posteridad. Y a tantos otros que han aportado su granito de arena.

A su vez agradecer a todo el personal y profesores del Departamento de Química analítica. En especial al personal de Servicio Central de Análisis: Maite, Ana y Teresa, las cuales siempre han estado dispuestas a echar una mano.

Agradecer a Aubin Thibault de Chanvalon, por ser uno de los pilares científicos durante mi estancia en el IPREM y guiarme para conseguir el mejor resultado.

Agradecer enormemente a Javier Jimenez-Lamana, no solo por ser uno de mis apoyos científicos en el IPREM, si no también por ser un apoyo durante mi estancia en Pau y ayudarme con los problemas que han ido surgiendo a lo largo de esta cotutela.

Por supuesto agradecer a Rossana, Silvia, Mikel, Fran, Yaidel, Claudia y Gustavo, por los ánimos para sobrellevar los problemas derivados de la vida en el laboratorio, por los planes improvisados y por hacer que mi experiencia en Pau fuera increíble e irrepetible.

Y por último agradecer a mi máximo apoyo, mi familia. En especial a mis padres; sin los cuales este viaje no hubiera sido posible. Gracias por enseñarme a no rendirme, a ser constante y valorar las cosas de la vida. Gracias por apoyarme en todos los pasos que ha dado en mi vida. Gracias por luchar siempre para darme las mejores oportunidades. Gracias por todo.

SUMMARY

Today, plastic is a widely used material in a variety of sectors. As a result, much of the plastic ends up as waste in the environment, making it a global problem. It is estimated that around 80% of the plastics produced are discarded into the environment. Some of these plastics end up as nanoplastics and microplastics in aquatic systems. The presence of these plastics presents problems due to their size and ability to adsorb and transport emerging pollutants, and consequently facilitate their ingestion by living organisms. The understanding of the effects of micro- and nanoplastics is still limited, largely due to the lack of robust methods for their detection and quantification.

In this context, this PhD thesis has aimed at the development of an analytical method for the detection, size characterisation and quantification of plastic microparticles by ICP-MS operated in single particle mode using microsecond dwell times. This method allowed the detection of polystyrene particles up to 1.2 µm in size by ^{13}C isotopic tracing and was used to analyse for microplastics in personal care products and those released from food packagings. An analytical platform was also developed for the analysis of environmental samples, such as river water, by combination of SP-ICP-MS, field emission scanning electron microscopy and Raman spectroscopy. The use of this platform allowed us to determine the presence and chemical identity of plastic microparticles in the analysed river water samples. Also, the adsorption capacity of environmental nanoplastics for emerging pollutants, such as gadolinium-based contrast agents, and their ability to act as competitors of natural colloids were studied. The ability of nanoplastics to act as vectors of emerging pollutants under environmental conditions was demonstrated.

TABLE OF CONTENTS

AF4	Asymmetric flow field-flow fractionation
AFM	Atomic force microscopy
ATR-FTIR	Attenuated total reflectance Fourier transform spectroscopy
AuNPs	Gold nanoparticles
CFU	Colony forming unit
Cps	Counts per second
DLS	Dynamic light scattering
DOM	Dissolved organic carbon
EDX	Energy dispersive X-ray spectroscopy
EEA	Ethylene copolymer
ENPTs	Environmental nanoplastics
FESEM	Field emission scanning electron microscopy
FTIR	Fourier-transform infrared spectroscopy
GBCAs	Gadolinium-based contrast agents
GPGP	Great Pacific garbage patch
HDPE	High density polyethylene
HW	Hardwater
ICP-MS	Inductively coupled plasma mass spectrometry
ICP-OES	Atomic emission spectroscopy with inductively coupled plasma
IS	Ionic strengh
LDPE	Low-density polyethylene
LOD	Limit of detection
LODnumber	Number concentration detection limit
LODsize	Size detection limit
LOQ	Limit of quantification

MALS	Multiangle light scattering
MBE	Mass budget error
MPs	Microplastics
NPs	Nanoparticles
NPTs	Nanoplastics
NTA	Nanoparticle tracking analysis
PA	Polyamide
PAHs	Polycyclic aromatic hydrocarbons
PAN	Polyacrylonitrile
PC	Polycarbonate
PCBs	Polychlorinated biphenyls
PE	Polyethylene
PES	Polyethersulfone
PET	Polyethylene terephthalate
PIB	Polyisobutene
PMMA	Poly(methyl methacrylate)
PMP	Polymethylpentene
POPs	Persistent organic pollutants
PP	Polypropylene
PS	Polystyrene
PSD	Particle size distribution
PUR	Polyurethane
PVA	Poly(vinyl alcohol)
PVC	Polyvinyl chloride
PVF	Polyvinyl fluoride

Py-GC-MS	Pyrolysis gas chromatography mass spectrometry
RW	River water
SEM	Scanning electron microscopy
SLS	Static light scattering
SP-ICP-MS	Single particle inductively coupled plasma mass spectrometry
SW	Sea water
TED-GC-MS	Thermo-extraction and desorption gas chromatography mass spectrometry
TEM	Transmission electron microscopy
UV	Ultraviolet light
µFTIR	Fourier-transform infrared microspectroscopy
µRaman	Raman microscopy

1. Plastics today

Plastics are organic high-molecular weight long-chain polymers produced from fossil raw materials, such as oil or gas. They are divided into two groups, thermoplastics, and thermosets.[1,2] The former, which can melt when heated and harden when cooled, include polyethylene (PE), polypropylene (PP), polyvinyl chloride (PVC), polyethylene terephthalate (PET) and polystyrene (PS). The second group, which undergoes chemical transformations when heated, creating a three-dimensional network, includes polyurethane (PUR), unsaturated polyester, epoxy resins and melamine resin.[3]

The first synthetic plastic, bakelite, made in 1907 by Leo Hendrik Baekeland, initiated a new era in material science.[1,4] From the beginning of the 20th century, the use of plastics in the world has increased exponentially. Currently, the most used plastics are polyethylene, polypropylene, polyvinyl chloride, polyethylene terephthalate, polyurethane, and polystyrene.[3,5] Their world production passed in 2018 from 359 million tons to 368 million tons in 2019 and is rising.[3] Among the countries with the largest production of plastics, China had a 31% share of global production in 2019.[3]

Over 8 million tons of plastics are released every year into the marine ecosystem.[6] They accumulate in ocean gyres in certain areas of the globe. One of the most known is the Great Pacific garbage patch (GPGP) in the North Pacific, which occupies around 1.6 million km^2.[7]

Plastics are used in a variety form in consumer products, cosmetics, or food, which can lead to the presence of microplastics and nanoplastics available for human consumption. They release was reported from take-away food containers[8] and plastic bottles.[9–11] Microplastics and nanoplastics were also found in consumer food products, such as milk,[12] salt[13–17] or tea.[18] Consequently, plastics can enter the food chain of different organisms.

2. Microplastics and nanoplastics: state of art

No standardised definition is currently available for microplastics and nanoplastics. In many cases the classifications used make it difficult to compare the results obtained in different studies. [19] Figure 1 shows a representation of the classification of plastics in different studies. The main difference among these definitions is related to the particle size.

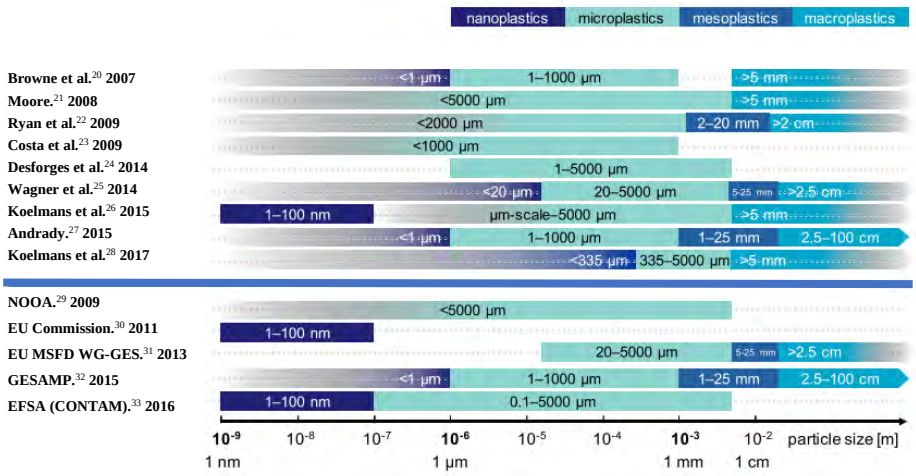

Figure 1. Examples of differences in the categorization of plastic debris according to size as applied (and/or defined) in scientific literature and in institutional reports. It should be noted that this does not represent an exhaustive overview of all size classes used.[19]

Plastics are divided, according to size, in four large groups: macroplastics, mesoplastics, microplastics and nanoplastics. In general, macroplastics are understood as plastics with sizes between 5 mm[20,21,26,28] and 2.5 mm.[22,25,27,31,32] The size of mesoplastics is 1 mm and 25 mm,[22,25,27,31,32] but they are often not considered as a separate class. In the case of plastics referred to as microplastics, the particle size range varied in different studies: 1-5000 µm,[24,25,28,31] 0.1-5000 µm[21,22,26,33] or 1-1000 µm.[20,23,27,32] Frias *et al.*,[4] defined microplastics as "any synthetic solid particle or polymeric matrix, with regular or irregular shape and with size ranging from 1 µm to 5 mm, of either primary or secondary manufacturing origin, which are insoluble in water". In the case of

nanoplastics, their size ranges tend to be marked between 1-100 nm or below 1 µm. Gigault *et al.*,[34] defined nanoplastics as "particles within a size ranging from 1 to 1000 nm resulting from the degradation of industrial plastic objects and can exhibit a colloidal behaviour".

2.1. Formation of nanoplastics and microplastics

The formation of micro- and nanoplastics from macro- and mesoplastics needs action of various processes, which will not only modify the particle size but also the surface characteristics. These processes include mechanical degradation, photodegradation, thermal degradation and biodegradation.[35,36]

2.1.1. Mechanical degradation

Mechanical degradation is based on the degradation of plastics due to their breakdown by external forces. The degradation is produced when the forces apply an excessive stress on plastic, which results in breaking molecular chains and in the formation of a pair of free radicals. In the presence of oxygen, these radicals can form peroxy radicals. The radicals produced due to the stress originate from the main backbone part of the plastic in the stressed region.[37–39] These external forces can be due to friction between the plastic with another material. An example of this mechanical degradation is the abrasion between the tire and the road, which leads the release of fragments of the tire surface as a result of friction.[38] In the environment, frictions can be caused by the action of sea waves, freezing, wind, sand, collisions with rocks or by human activities (e.g., soil cultivation and crop rotation). [39,40]

2.1.2. Photodegradation

Photodegradation is the degradation of plastics due to the action of light (visible, infrared and UV light). The UV fraction of light has the greatest effect on plastics, in particular UVB (290 - 315 nm) and UVA (315 - 400 nm)

radiation.[38,40] This degradation process takes place in the outer layer of plastics and can reach a depth of µm, depending on the type of plastic.[40]

The photodegradation process is based on three steps: initiation, propagation, and termination. In the initiation step, UV energy breaks the chemical bonds of the polymer chains and promotes the formation of free radicals. The propagation step is based on a series of reactions common to all polymers with a carbon backbone. These reactions lead to the generation of hydroperoxide species which favour the subsequent reactions leading to autoxidation. The termination step occurs when free radicals are absorbed to create inert products. This step is reached naturally by reaction with stabilisers in the plastic.[5,37–39,41] In order to be able to continue this process, another non-oxidised layer must be applied. Figure 2 depicts the photodegradation process.

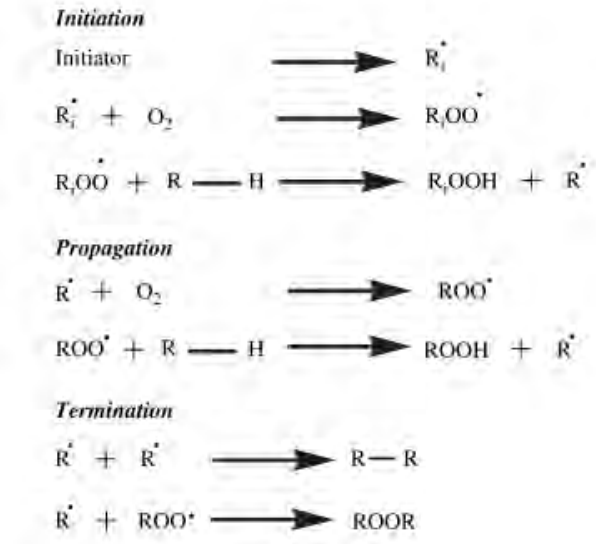

Figure 2. Diagram of the photodegradation process, showing the 3 stages of the process: Initiation, propagation and terminiantion.[37]

2.1.3. Thermal degradation

Thermal degradation is based on the degradation of plastics due to high temperatures. The degradation depends on the characteristics of antioxidant

additives in the polymers, which determine the temperature at which the process will take place.[37,38]

The degradation process begins when the polymer has sufficient heat to overcome the energy barrier, so that free radicals can be generated from the polymer chains. Free radicals can react with oxygen to produce hydroperoxides, which can then cleave to form hydroxyl free radicals and alkoxy radicals. The first part of the process is like in photodegradation. This reaction will self-propagate along the polymer until the energy supply is interrupted or when inert products are formed due to the collision of two radicals.[5,37,38] In the environment, this type of degradation occurs in environments where plastics are exposed to direct sunlight.[38]

2.1.4. Biodegradation

Biodegradation is based on the degradation of plastics due to the biochemical transformation by microorganisms. The degree of biodegradation is controlled by the physiochemical characteristics of the polymer (surface area, molecular weight, chemical structure, elasticity...). Microbes involved in biodegradation include bacteria, fungi, algae, and protozoa. This type of degradation can occur at various structural levels (molecular, macromolecular, microscopic, and macroscopic).[36,37,39,41,42] This degradation is strongly influenced by the type of plastic, which can be hydrolysable or non-hydrolysable, depending on the presence or absence of ester or amide groups. The non-hydrolysable plastics include PE, PP and PVC, as they have a lignin-like structure, making their degradation difficult.[38,40]

The degradation process involves three steps: bio-fragmentation, assimilation, and mineralization (Figure 3).

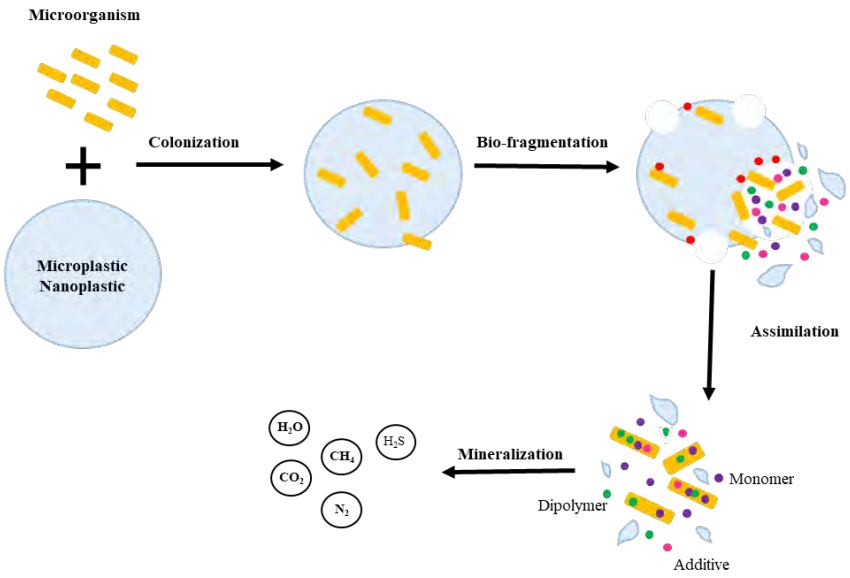

Figure 3. Diagram representing the biodegradation carried out by micro-organisms, showing the 3 stages: bio-fragmentation, assimilation, and mineralisation. [40]

Bio-fragmentation is produced following a microorganism adhesion to the polymer surface and/or its penetration into the pores of the polymer. The released extracellular substances act on the carbon skeleton of the polymer, producing oligomers, dimers, and monomers, which can pass through the microorganism semi- permeable membrane, in a process known as assimilation. These absorbed compounds are transformed into CO_2, H_2O, CH_4, H_2S and N_2 by different metabolic pathways.[5,36–41]

3. Principal analytical techniques for the detection, characterization, and quantification of nanoplastics and microplastics

The exposure of humans to nano- and microplastics requires techniques allowing their detection, characterization, and quantification in a wide variety of samples. Currently, there is no single technique that allows us to determine the composition, shape, size, and concentration of these particles. Therefore, in

general, the characterisation of these nano- and microplastics is carried out at two levels, the physical one and the chemical one. The physical characterization usually refers to the description of a material according to its particle size, particle size distribution (PSD), shape and surface area. The agglomeration/aggregation state can be included here, as it can be assessed by particle size. A chemical characterisation of a particle includes its elemental and/or molecular composition, a chemical formula with a specific stoichiometry, chemical state of the elements and molecular structure-conformation, whenever possible.[43]

3.1. Microscopy

Microscopy techniques are widely used to obtain information about size, shape, aggregation state and surface properties of the plastics. They include optical microscopy, electron microscopy and atomic force microscopy.

Optical microscopy is often used to carry out the first examination of a sample. Because it is a simple and inexpensive technique, it can be performed at the sampling site. However, it has a few disadvantages which are related to its inability to distinguish plastics from other particles. The minimum size to be visualised is around 10 μm.[44,45]

Electron microscopy is one of the most widely used techniques for the analysis of nanomaterials, but for the analysis of plastics it tends to be used as a complementary technique. Two types of electron microscopy can be used: Scanning Electron Microscopy (SEM) and Transmission Electron Microscopy (TEM). In order to identify and quantify elements, SEM and TEM tend to be combined with energy dispersive X-ray spectroscopy (EDX).[46,47] These techniques are expensive, the analysis times are long and sample preparation laborious.

SEM uses a high intensity electron beam to irradiate the sample, the interaction between the beam and the sample produces secondary electrons

which are used to obtain the image. The particle size detection limit is ca. 3 nm.[44,45,47–49] TEM detects the transmission electron beam through the sample requiring high electron acceleration voltages and ultra-thin sample cross-sections.[44,45,47,50] Although this technique has a size detection limit of 1 nm,[44] its use for plastics is hampered by low contrast due to the weak elastic interactions of plastics with electrons.[47]

In atomic force microscopy (AFM) the sample image is formed by passing over the sample a small tip of very stiff conductive material which is attached to the end of cantilever. For the formation of the image, the deflection of the tip through the sample, which is caused by electrostatic or van der Waals interactions, is recorded.[47] This technique provides images with high resolution around 0.3 nm and 3D images of the surface structure. In addition, it allows investigation of the surface of non-conductive polymers. Problems can be caused by damage to the tip due to interaction with the sample. In some cases, fragments may be released, which, in the case of adhesive polymers, can produce incorrect images.[44,45,47,50]

3.2. Light scattering techniques

Several techniques are based on the application of laser light scattering on the particles to obtain information about particle size, particle size distribution (PSD) or aggregation state. The most used techniques for the analysis of plastics are dynamic light scattering (DLS), nanoparticle tracking analysis (NTA) and multi angle light scattering (MALS).

The DLS technique is based on the measurement of the fluctuations of intensity of a laser beam on the sample due to the Brownian motion of the particles present. Specifically, DLS allows the determination of the hydrodynamic diameter (d_h), PSD and the aggregation state of the particle. On the other hand, it presents problems when used for samples with large particles, with high polydispersity and in complex matrices. Its working size range is fixed between 10 nm to 3 µm at concentrations of mg L^{-1}.[44–46]

Nanoparticle tracking analysis (NTA), like DLS, is based on the measurement of the Brownian motion of the particles. However, in this case, a microscope and a digital camera are applied to record and transform the movement using the viscosity and temperature of the medium to obtain information about the particles. Like in DLS, it is possible to obtain information about (d_h) and PSD as well as the number concentration. NTA works best on polydisperse and complex samples but is more difficult to use than DLS. This technique can be operated for particles with sizes between 10 - 1000 nm while the working concentration range is of 10^9 - 10^{12} L^{-1}. [44,46,51]

MALS, also known as static light scattering (SLS), provides measurement of physical properties that are derived from the angular dependency of the light scattered by particles. The scattering provides information about the particle size and the radius of gyration (d_g). The working range is between 10 - 1000 nm. The main problem of MALS is that requires cleaner samples than DLS.[44–46,50]

All these scattering techniques can be online coupled to separation techniques such as asymmetric flow field-flow fractionation (AF4), avoiding the problems arising from polydispersity and the presence of interferent particles.[44–46]

3.3. Spectroscopic techniques

Spectroscopic techniques are used for the chemical identification of particles present in samples. Among these techniques, the most used are Fourier-transform infrared spectroscopy (FTIR) and Raman spectroscopy.

FTIR is based on the irradiation of the sample by infrared light (wave number range 400 - 4000 cm^{-1} for mid-IR) which, depending on the molecular structure of the sample, is absorbed and subsequently measured, either in reflection or transmission mode. This technique allows a direct and non-destructive analysis and provides additional information about the physicochemical weathering of plastics. However, this technique has limitations

related to the lower size limit to be analysed, which is set at ca. 20 µm. When samples with smaller particle sizes (< 10 µm) need to be analysed, it is necessary to use micro-Fourier-transform infrared spectroscopy (µFTIR), which is based in the coupling of FTIR with microscopy. By using µFTIR we can not only get information about particle composition but also perform particle quantification. However, dry samples are required for its use, and it is less sensitive in comparison with Raman spectroscopy.[44,45,47–50,52]

Raman spectroscopy is based on the vibrational movements of the molecules caused by the laser radiation of a particle, which causes the re-emission of light at wavelengths characteristic of specific atomic groups. The obtained spectra correspond to the chemical structure of the particles analysed, acting as a fingerprint of the particle. In comparison with FTIR, Raman spectroscopy offers a better spatial resolution, a better sensitivity to non-polar functional groups and a lower interference caused by water. Micro-Raman (µRaman) allows the analysis of particles down to 0.5 µm.

The main problem of Raman spectroscopy is the risk of degrading polymers due to the high temperatures caused by the laser.[44,47–49]

3.4. Thermo-analytical techniques

Thermoanalytical techniques allow the identification of the types of plastics through the degradation of the particles and the analysis of the degradation products by chromatographic techniques. The chromatograms (pyrograms) obtained allow the simultaneous identification of different polymers and associated organic additives. However, information about size or shape of the particles is missed. Among the most used thermoanalytical techniques are pyrolysis gas chromatography mass spectrometry (Py-GC-MS) and thermo-extraction and desorption (TED-GC-MS).[44,45,48,50]

In Py-GC-MS, the sample is thermally degraded in an inert atmosphere and the pyrolysis fragments of the polymer structure can be separated by gas

chromatography and characterised by mass spectrometry. The analysis requires a small amount of dry sample (ng - µg) and can be used to simultaneously identify polymer types and associated organic plastic additives.[44,45,48,50]

TED-GC-MS combines a thermal extraction of the products of thermogravimetric analysis on a solid-phase adsorber, which are subsequently thermally desorbed in gas chromatographic mass spectrometry to allow the identification of the polymer. The method requires milligram sample quantities and does not require pre-concentration or particle selection. The measurement times are shorter than those in Py-GC-MS.[44,45,48,50]

4. Objectives

The occurrence of micro- and nanoplastics in the environment can produce several direct effects inherent to their very nature, but also a series of indirect ones related to their capacity to adsorb and transport different types of pollutants, magnifying their potential effects on living organisms. Therefore, information about their occurrence, distribution and effects in the environment is necessary. Although the number of studies of these topics has increased in recent years, they are still very limited, largely due to the lack of analytical methods to detect, characterise and quantify micro- and nanoplastics in different systems.

The objectives of this thesis were:

- The development of an analytical methodology based on single particle ICP-MS for the detection of plastic particles by carbon isotopic tracing, as well as its validation for the analysis of samples containing this type of particles.
- Investigation of the presence of microplastics in consumer products and environmental samples
- A study of the role of micro/nanoplastics as vectors of other emerging pollutants.

After a general introduction, the thesis has been structured in three different chapters, in which each chapter deals with the scientific background, the experimental conditions, the results and the discussion corresponding to the challenges mentioned above. The first chapter is focused on the development of a methodology based on SP-ICP-MS for the analysis of plastic particles. The second chapter focuses on the application of the previously developed methodology for the detection of microplastics in river water through screening analysis. The third chapter focuses on the study of the adsorptive performance of plastics in the presence of emerging pollutants such as gadolinium-based contrast agents. Finally, the thesis manuscript ends with a conclusion.

The information presented in the first chapter was published in Talanta *(Laborda, F., Trujillo, C. & Lobinski, R. Analysis of microplastics in consumer products by single particle-inductively coupled plasma mass spectrometry using the carbon-13 isotope. Talanta, 221, 121486 (2021))* and in a technical note (*Laborda, F., Trujillo, C. & Lobinski, R. Unlocking Carbon-13 with Single Particle ICP-MS: Feasibility Study for Microplastic Detection. Perkin Elmer (2022)*). The results presented in chapters two and three, are in the process of preparation for publication.

5. References

1. Chalmin, P. Field Actions Science Reports The history of plastics: from the Capitol to the Tarpeian Rock. Field Actions Science Reports, 19, 5–11 (2019).

2. Su, L., Xiong, X., Zhang, Y., Wu, C., Xu, X., Sun, C. & Shi, H. Global transportation of plastics and microplastics: A critical review of pathways and influences. Science of the Total Environment, 831, 154884 (2022).

3. PlasticsEurope. Plastics – the Facts 2020. PlasticEurope (2020).

4. Frias, J. & Nash, R. Microplastics: Finding a consensus on the definition. Marine Pollution Bulletin, 138, 145–147 (2019).

5. Ali, S. S., Elsamahy, T., Koutra, E., Kornaros, M., El-Sheekh, M., Abdelkarim, E. A., Zhu, D. & Sun, J. Degradation of conventional plastic wastes in the environment: A review on current status of knowledge and future perspectives of disposal. Science of The Total Environment, 771, 144719 (2021).

6. Naik, R. K., Naik, M. M., D'Costa, P. M. & Shaikh, F. Microplastics in ballast water as an emerging source and vector for harmful chemicals, antibiotics, metals, bacterial pathogens and HAB species: A potential risk to the marine environment and human health. Marine Pollution Bulletin, 149, 110525 (2019).

7. Lebreton, L., Slat, B., Ferrari, F., Sainte-Rose, B., Aitken, J., Marthouse, R., Hajbane, S., Cunsolo, S., Schwarz, A., Levivier, A., Noble, K., Debeljak, P., Maral, H., Schoeneich-Argent, R., Brambini, R. & Reisser, J. Evidence that the Great Pacific Garbage Patch is rapidly accumulating plastic. Scientific Reports, 8, 4666 (2018).

8. Du, F., Cai, H., Zhang, Q., Chen, Q. & Shi, H. Microplastics in take-out food containers. Journal of Hazardous Materials, 399, 122969 (2020).

9. Winkler, A., Santo, N., Ortenzi, M. A., Bolzoni, E., Bacchetta, R. & Tremolada, P. Does mechanical stress cause microplastic release from plastic water bottles?. Water Research, 166, 115082 (2019).

10. Mason, S. A., Welch, V. G. & Neratko, J. Synthetic Polymer Contamination in Bottled Water. Frontiers in Chemistry, 6 (407) (2018).

11. Robertson, I. Aplication note: FT-IR Microscopic Analysis of Microplastics in Bottled Water. PerkinElmer (2018).

12. Kutralam-Muniasamy, G., Pérez-Guevara, F., Elizalde-Martínez, I. & Shruti, V. C. Branded milks – Are they immune from microplastics contamination?. Science of The Total Environment ,714, 136823 (2020).

13. Kim, J.-S., Lee, H.-J., Kim, S.-K. & Kim, H.-J. Global Pattern of Microplastics (MPs) in Commercial Food-Grade Salts: Sea Salt as an Indicator of Seawater MP Pollution. Environmental Science & Technology, 52, 12819–12828 (2018).

14. Yang, D., Shi, H., Li, L., Li, J., Jabeen, K. & Kolandhasamy, P. Microplastic Pollution in Table Salts from China. Environmental Science & Technology, 49, 13622–13627 (2015).

15. Seth, C. K. & Shriwastav, A. Contamination of Indian sea salts with microplastics and a potential prevention strategy. Environmental Science and Pollution Research, 25, 30122–30131 (2018).

16. Iñiguez, M. E., Conesa, J. A. & Fullana, A. Microplastics in Spanish Table Salt. Scientific Reports, 7, 8620 (2017).

17. Peixoto, D., Pinheiro, C., Amorim, J., Oliva-Teles, L., Guilhermino, L. & Vieira, M. N. Microplastic pollution in commercial salt for human consumption: A review. Estuarine, Coastal and Shelf Science, 219, 161–168 (2019).

18. Hernandez, L. M., Xu, E. G., Larsson, H. C. E., Tahara, R., Maisuria, V. B. & Tufenkji, N. Plastic Teabags Release Billions of Microparticles and Nanoparticles into Tea. Environmental Science & Technology, 53, 12300–12310 (2019).

19. Hartmann, N. B., Hüffer, T., Thompson, R. C., Hassellöv, M., Verschoor, A., Daugaard, A. E., Rist, S., Karlsson, T., Brennholt, N., Cole, M., Herrling, M. P., Hess, M. C., Ivleva, N. P., Lusher, A. L. & Wagner, M. Are We Speaking the Same Language? Recommendations for a Definition and Categorization Framework for Plastic Debris. Environmental Science & Technology, 53, 1039–1047 (2019).

20. Browne, M., Galloway, T., & Thompson, R. Microplastics-an emerging contaminant of potential concern?. Integrated Environmental Assessment and Management, 3 (4), 458–458 (2008).

21. Moore, C. J. Synthetic polymers in the marine environment: A rapidly increasing, long-term threat. Environmental Research, 108, 131–139 (2008).

22. Ryan, P. G., Moore, C. J., van Franeker, J. A. & Moloney, C. L. Monitoring the abundance of plastic debris in the marine environment. Philosophical Transactions of the Royal Society B: Biological Sciences, 364, 1999–2012 (2009).

23. Costa, M. F., Ivar Do Sul, J. A., Silva-Cavalcanti, J. S., Araújo, M. C. B., Spengler, Â. & Tourinho, P. S. On the importance of size of plastic fragments and pellets on the strandline: A snapshot of a Brazilian beach. Environmental Monitoring and Assessment, 168, 299–304 (2010).

24. Desforges, J.P.W., Galbraith, M., Dangerfield, N. & Ross, P.S. Widespread distribution of microplastics in subsurface seawater in the NE Pacific Ocean. Marine Pollution Bulletin, 79, 94–99 (2014).

25. Wagner, M., Scherer, C., Alvarez-Muñoz, D., Brennholt, N., Bourrain, X., Buchinger, S., Fries, E., Grosbois, C., Klasmeier, J., Marti, T., Rodriguez-Mozaz, S., Urbatzka, R., Vethaak, A. D., Winther-Nielsen, M. & Reifferscheid, G. Microplastics in freshwater ecosystems: what we know and what we need to know. Environmental Science Europe, 26, 12 (2014).

26. In: Bergmann, M., Gutow, L. & Klages, M. (Eds.). Marine Anthropogenic Litter. Springer (2015).

27. Andrady, A. L. Plastics and Environmental Sustainability. Wiley (2015)

28. Koelmans, A. A., Kooi, M., Law, K. L. & Van Sebille, E. All is not lost: deriving a top-down mass budget of plastic at sea. Environmental Research Letters, 12 (11), 114028 (2017).

29. Arthur, C., Baker, J. & Bamford, H. Proceedings of the International Research Workshop on the Occurrence , Effects , and Fate of Microplastic Marine Debris. (2009).

30. Commission, T., European, T. & Joint, C. Commission recommendations. Nursing Standard, 24, 6–6 (2010).

31. European Commission. Guidance on Monitoring of Marine Litter in European Seas. (2013).

32. GESAMP. Sources, fate and effects of microplastics in the marine environment:A global assessment. (2015).

33. EFSA Panel. Presence of microplastics and nanoplastics in food, with particular focus on seafood. EFSA Journal, 14, (2016).

34. Gigault, J., Halle, A. ter, Baudrimont, M., Pascal, P. Y., Gauffre, F., Phi, T. L., El Hadri, H., Grassl, B. & Reynaud, S. Current opinion: What is a nanoplastic? Environmental Pollution, 235, 1030–1034 (2018).

35. Wang, T., Wang, L., Chen, Q., Kalogerakis, N., Ji, R. & Ma, Y. Interactions between microplastics and organic pollutants: Effects on toxicity, bioaccumulation, degradation, and transport. Science of the Total Environment, 748, 142427 (2020).

36. Manzoor, S., Naqash, N., Rashid, G. & Singh, R. Plastic Material Degradation and Formation of Microplastic in the Environment: A Review. Materials Today: Proceedings, 56, 3254–3260 (2022).

37. Singh, B. & Sharma, N. Mechanistic implications of plastic degradation. Polymer Degradation and Stability, 93, 561–584 (2008).

38. Zhang, K., Hamidian, A. H., Tubić, A., Zhang, Y., Fang, J. K. H., Wu, C. & Lam, P. K. S. Understanding plastic degradation and microplastic formation in the environment: A review. Environmental Pollution, 274, 116554 (2021).

39. Bacha, A.-U.-R., Nabi, I. & Zhang, L. Mechanisms and the Engineering Approaches for the Degradation of Microplastics. ACS ES&T Engineering, 1 (11), 1481–1501 (2021).

40. Duan, J., Bolan, N., Li, Y., Ding, S., Atugoda, T., Vithanage, M., Sarkar, B., Tsang, D. C. W. & Kirkham, M. B. Weathering of microplastics and interaction with other coexisting constituents in terrestrial and aquatic environments. Water Research, 196, 117011 (2021).

41. Du, H., Xie, Y. & Wang, J. Microplastic degradation methods and corresponding degradation mechanism: Research status and future perspectives. Journal of Hazardous Materials, 418, 126377 (2021).

42. Yang, H., Chen, G. & Wang, J. Microplastics in the marine environment: Sources, fates, impacts and microbial degradation. Toxics, 9, 1–19 (2021).

43. Laborda, F. & Bolea, E. Reference Module in Chemistry, Molecular Sciences and Chemical Engineering. Elsevier (2018).

44. Schwaferts, C., Niessner, R., Elsner, M. & Ivleva, N. P. Methods for the analysis of submicrometer- and nanoplastic particles in the environment. TrAC Trends in Analytical Chemistry, 112, 52–65 (2019).

45. Ali, I., Cheng, Q., Ding, T., Yiguang, Q., Yuechao, Z., Sun, H., Peng, C., Naz, I., Li, J. & Liu, J. Micro- and nanoplastics in the environment: Occurrence, detection, characterization and toxicity – A critical review. Journal of Cleaner Production, 313, 127863 (2021).

46. Laborda, F., Bolea, E., Cepriá, G., Gómez, M. T., Jiménez, M. S., Pérez-Arantegui, J. & Castillo, J. R. Detection, characterization and quantification of inorganic engineered nanomaterials: A review of techniques and methodological approaches for the analysis of complex samples. Analytica Chimica Acta, 904, 10–32 (2016).

47. Mariano, S., Tacconi, S., Fidaleo, M., Rossi, M. & Dini, L. Micro and Nanoplastics Identification: Classic Methods and Innovative Detection Techniques. Frontiers in Toxicology, 3, 1–17 (2021).

48. Silva, A. B., Bastos, A. S., Justino, C. I. L., da Costa, J. P., Duarte, A. C. & Rocha-Santos, T. A. P. Microplastics in the environment: Challenges in analytical chemistry - A review. Analytica Chimica Acta, 1017, 1–19 (2018).

49. Tirkey, A. & Upadhyay, L. S. B. Microplastics: An overview on separation, identification and characterization of microplastics. Marine Pollution Bulletin, 170, 112604 (2021).

50. Ivleva, N. P. Chemical Analysis of Microplastics and Nanoplastics: Challenges, Advanced Methods, and Perspectives. Chemical Reviews, 121, 11886–11936 (2021).

51. Lambert, S. & Wagner, M. Characterisation of nanoplastics during the degradation of polystyrene. Chemosphere, 145, 265–268 (2016).

52. Ateia, M., Ersan, G., Alalm, M. G., Boffito, D. C. & Karanfil, T. Emerging investigator series: microplastic sources, fate, toxicity, detection, and interactions with micropollutants in aquatic ecosystems – a review of reviews. Environmental Science: Processes & Impacts, 24, 172–195 (2022).

1. Analysis of microplastics by single particle inductively coupled plasma mass spectrometry using carbon-13

1.1. Introduction

1.1.1. Theoretical basis of SP-ICP-MS

An ICP-MS instrument when used at high readout frequencies can be converted into a particle counting device, providing particle-by-particle information. The fundamentals of single particle inductively coupled plasma mass spectrometry (SP-ICP-MS) measurements were established by Degueldre *et al*.,[1] By nebulising a dilute suspension of particles in an ICP-MS and measuring an isotope of the element present in the particles at a high data acquisition frequency (≥100 Hz), a series of events corresponding to individual particles over a continuous baseline is obtained, as shown in Figure 1.1(a).

The events signal intensity is obtained from the sum of the different individual readings recorded. This summed-up intensity is related to the mass of the element in the particle, and thus to its size, if additional information on the composition, density and shape of the particle is available. The frequency of the events is proportional to the number concentration of the particles. The dissolved species present in a sample are homogeneously distributed in all the aerosol droplets formed in the system, while the particles are found randomly in some of them. The dissolved species produce a constant signal corresponding to the baseline, while the particles produce individual signal events. Both signals are recorded in time resolved mode in a time scan.

The raw time scans (Figure 1.1(a)) are processed by plotting the intensity of the events against their frequency, obtaining histograms as shown in Figure 1.1(b), where the first distribution is due to the background and/or the presence of dissolved forms of the measured element and the second one to the particles themselves. At the same time, the mass of element per particle, the size distribution (if information about the shape, composition and density are known) or, alternatively, the equivalent size distribution (if a specific shape, composition and density are only assumed) can be obtained from the intensity event

distribution of Figure 1.1(b) (Figure 1.1(c)). For this purpose, the intensity histogram of the particle events is transformed into the corresponding particle size distribution considering the nebulisation efficiency, the sample flow rate and the mass concentration calibration with a dissolved standard.[2]

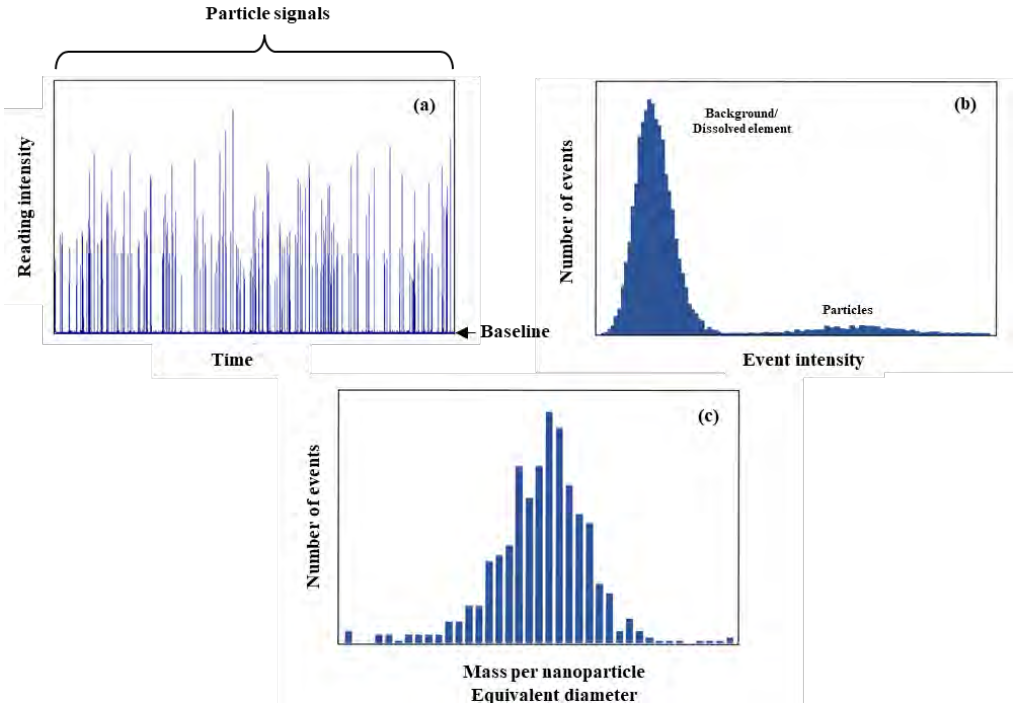

Figure 1.1. (a) Time scan of suspension containing nanoparticles and dissolved forms of the same element. (b) Event intensity histogram of data from (a). (c) Mass per nanoparticle/size distribution of spherical nanoparticles calculated from the second intensity distribution in (b).[3]

1.1.2. Particle detection in SP-ICP-MS

The criteria used for detection of particle events will affect to the characterisation and quantification of the particles. This is especially relevant when high levels of baseline intensity are present, either because of the high concentration of dissolved forms of the analyte or because of polyatomic interferences present. This criterion is based on the so-called critical value (Y_C),

which is defined as the instrument response above which an observed signal is attributed to the presence of a particle.[4]

This critical value can be established by different strategies. In general, its calculation is based on an n sigma criterion, in which Y_C is calculated from the average baseline intensity (Y_B) and a multiple of its standard deviation (σ_B), through the following expression:[4]

$$Y_C = Y_B + n\,\sigma_B \tag{1.1}$$

In general, the coefficients used comprise values for the parameter *n* ranging from 3 to 8, however the most used are 3σ[5–7] and 5σ.[4,8,9] Depending on the criterion used, the number of false positives, understood as baseline readings erroneously considered as particles, can be significant. For the normal baseline distribution, the application of a 3σ criterion leads to 0.135% of detected events being false positives, while using a 5σ criterion, their occurrence can be practically eliminated in a variety of acquisition conditions.[4] The main objective of using such a restrictive criterion is to avoid the occurrence of false positives, which would be recorded as particles, negatively affecting the number concentration detection limits.

1.1.3. Signal processing in SP-ICP-MS

In standard ICP-MS, when a solution with an element mass concentration X^M is nebulised, the relationship between the signal Y_R (ions counted per unit time) and the mass concentration can be expressed as: [4]

$$Y_R = K_R X^M = K_{intro} K_{ICPMS} K_M X^M \tag{1.2}$$

where K_R is the analytical sensitivity obtained from a conventional calibration (signal intensity in cps versus element mass concentration), $K_{intro}(=\eta Q_{sam})$ which is a factor with sample introduction, where η is the analyte transport efficiency and Q_{sam} is the sample introduction rate, K_{ICPMS} is the detection

efficiency, which represents the ratio of the number of ions detected versus the number of atoms of the analyte of the measured isotope introduced in the ICP; and $K_M(AN_{AV}/M_M)$ is a factor related to the element measured, where A refers to the atomic abundance of the isotope under consideration, N_{AV} the Avogadro number and M_M the atomic mass of the element.

As discussed above, when a sufficiently dilute particle suspension is measured in single particle mode, each particle is recorded as a single event. Under these conditions, the number of counted particle events (Y_N) during a given acquisition time (t_i) is directly related to the particle number concentration (X^N):[2]

$$Y_N = K_N X^N = K_{intro} t_i X^N = \eta Q_{sam} t_i X^N \quad (1.3)$$

where K_N is the analytical sensitivity obtained from a calibration of the number concentration (number of particle events counted versus number concentration). K_N is related only to the sample introduction process and the acquisition time and is independent of the nature of the nanoparticles if they are nebulised in the same way as dissolved species.

The net intensity of each particle event ($S_P = Y - Y_B$) where Y is the raw intensity and Y_B is the mean intensity of the base line distribution, (both measured in counts), is proportional to the number of atoms of the element monitored in each detected particle, and hence to the mass of element per particle (m_p):[4]

$$S_P = K_{ICPMS} K_M m_p \quad (1.4)$$

When the composition, shape and density of the particle are known, the mass of element per particle can be related to the size of the particle. For a solid, homogeneous and spherical particle, the equation 1.4 can be written as:[2]

$$S_P = K_d d^3 = \frac{1}{6}\pi\rho F_P K_{ICPMS} K_M d^3 \quad (1.5)$$

where K_d is the slope obtained from a size calibration (net event intensity vs. particle diameter cubed), d is the diameter, ρ the density, F_P the mass fraction of the element in the particle. The diameter of a particle, can be calculated as:[4]

$$d = \left(\frac{S_P}{K_d}\right)^{1/3} \tag{1.6}$$

if particle size standards of the same chemical composition are available to obtain K_d empirically. Alternatively, the diameter can be estimated from the following expression:[4]

$$d = \left(\frac{S_P}{\frac{1}{6}\pi\rho F_P K_{ICPMS} K_M}\right)^{1/3} \tag{1.7}$$

Both approaches are shown in Figure 1.2. Since the second approach involves the use of dissolved standards, the behaviour of the element in dissolved and particulate forms must be the same in the plasma. K_{ICPMS} can be calculated from equation (1.2), once K_R is determined from a calibration with dissolved standards, and Q_{sam} and η are known:[10]

$$K_{ICPMS} = \frac{K_R}{\eta Q_{sam} \frac{AN_{AV}}{M_M}} \tag{1.8}$$

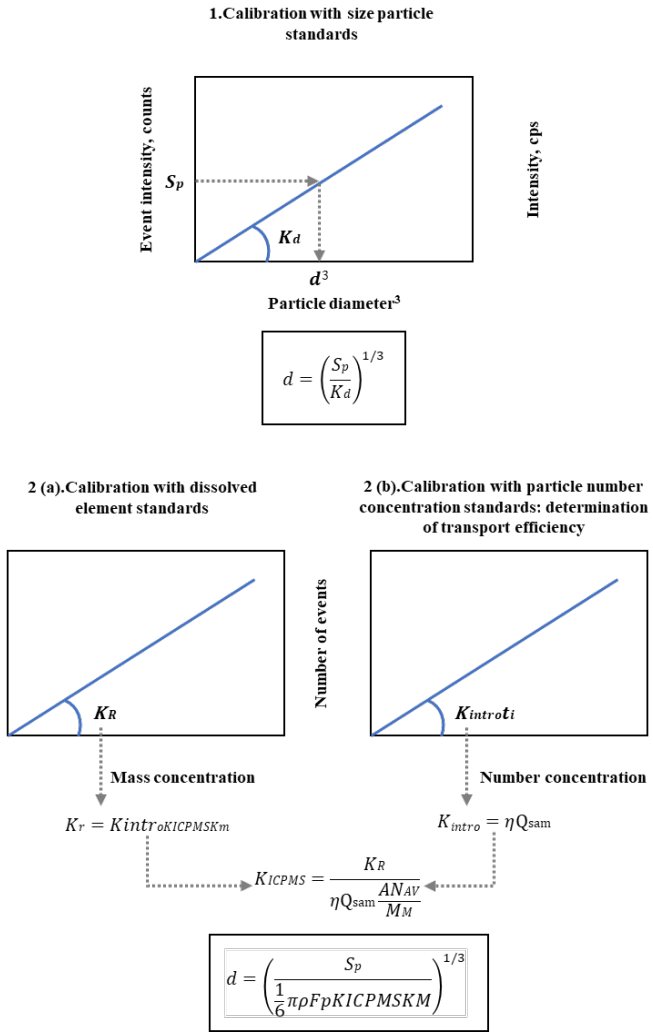

Figure 1.2. Approaches to the determination of particle size: (1) direct determination from calibration with particle size standards and (2) indirect determination from dissolved standards once the transport efficiency and sample flow rate are known.

Whereas Q_{sam} is determined by direct measurement (e.g., gravimetrically), there are several methods for calculation of η. If number concentration standards are available and each recorded event represents a single

particle, the number of particle events counted (Y_N) during an acquisition time (t_i) is directly related to the number concentration of particles (X^N):[11]

$$Y_N = K_{intro} t_i X^N \quad (1.9)$$

K_{intro} can be determined from Equation 1.9 and η can be calculated once Q_{sam} is known. This is the basis of the frequency method proposed by Pace *et al.*[7] for determination of the transport efficiency (Figure 1.2(2)) based on the number concentration. Pace *et al.*,[7] developed another method based on particle size, referred to as particle size method. In this method, a size nanoparticle standard and dissolved element standards are required to estimate the analyte nebulisation efficiency. Recently, Cuello-Nuñez *et al.*,[12] developed a gravimetric method for the calculation of η based on the dynamic measurement of mass fluxes to determine the nebulisation efficiency of the sample, avoiding the use of nanoparticle standards.

1.1.4. Limitations of carbon determination by ICP-MS

Carbon is an element which is not routinely analysed by ICP-MS. However, it has attracted some attention with respect to the measurement of its isotope ratios[13], the monitoring of organic species separated by liquid chromatography[14,15] or field flow fractionation,[16,17] and its use as an internal standard in laser ablation ICP-MS.[18,19] Some of the reasons why carbon is not routinely determined by ICP-MS are the low sensitivity for the element and its high background levels. Carbon sensitivity is limited by its low ionisation efficiency (approx. 5%) due to its high ionisation potential (11.26 eV), together with its low transmission at the ICP-MS interface due to space charge effects.[20] The background level for this element tends to be considerable because carbon is a ubiquitous element either in the form of carbon dioxide in air and water and contamination in argon as CO_2, CO and hydrocarbons. As a result of these limitations, achievable detection limits are high, in the mg L^{-1} range.[21] These

limitations have largely prevented the use of SP-ICP-MS for the analysis of carbon containing particles.[22]

As an alternative to the monitoring of carbon for the analysis of carbon containing particles by SP-ICP-MS, several authors have used metal impurities as analytical tracers. Yttrium was used as tracer for the analysis of carbon nanotubes,[23–25] whereas lanthanum was selected by Flores *et al.*,[26] for the analysis of carbon black.

The aim of this part of the thesis was to explore the possibilities of applying single particle ICP-MS for the detection of plastic particles by monitoring carbon isotopes, as well as to develop and validate a method for the analysis of samples containing such types of particles. Since SP-ICP-MS is an atomic spectrometry technique, this information has to be complemented with morphological and molecular composition information obtained by other techniques.

1.2. Experimental

1.2.1. Instrumentation

1.2.1.1. Inductively coupled plasma mass spectrometry (ICP-MS)

A PerkinElmer NexION 2000B ICP mass spectrometer (Toronto, Canada) was used throughout. The sample introduction system consisted of an Asperon™ linear pass spray chamber (PerkinElmer, Toronto, Canada), equipped with a flow focusing nebulizer (Ingeniatrics, Sevilla, Spain). Default instrumental and data acquisition parameters are listed in Table 1.1. Argon of 99.999% purity was used if not specified otherwise. Data were processed with Syngistix Nano Application version 2.5 and Origin 2019b.

Table 1.1. Default instrumental and data acquisition parameters for SP-ICP-MS.

Instrumental parameters	
RF power	1600 W
Argon gas flow rate	
Plasma	15 L min^{-1}
Auxiliary	1.2 L min^{-1}
Nebuliser	1.0 L min^{-1}
Make-up	0.2 L min^{-1}
Sample flow rate	16 µL min^{-1}
Data acquisition parameters	
Dwell time	100 / 200 µs
Readings per replicate	600,000 / 300,000
Total acquisition time	300 s / 60 s
Isotope monitored	^{13}C

1.2.1.2. Optical microscopy

A Zeiss optical microscope (Jena, Germany) was used for visualisation of plastic microparticles in selected samples.

1.2.1.3. Field emission scanning electron microscopy (FESEM)

A Carl Zeiss MERLIN™ field emission scanning electron microscope (Nano Technology Systems, Jena, Germany) was used for visualisation of microplastics. The microscope was equipped with an INCA 350 X-ray energy dispersive (EDX) system (Oxford Instruments, Abingdon, UK) for elemental analysis.

1.2.1.4. Attenuated total reflectance Fourier transform infrared spectroscopy (ATR-FTIR)

A Spectrum 100 attenuated total reflectance Fourier transform spectrometer from Perkin Elmer (Toronto, Canada) was used for identification of the polymeric composition of plastics and microplastics.

1.2.2. Standards

Diluted suspension of polystyrene (PS) microparticles and gold nanoparticles were prepared form commercially available suspensions. Two suspensions obtained from BCR (Geel, Belgium) of reference latex spheres of 2.0 μm and 4.8 μm nominal diameter (RM165 and RM166) were used.[27] The spheres were made of polystyrene cross-linked with divinyl benzene and stabilised with a non-ionic surfactant. The certified mean diameter for RM165 and RM166 were 2.223 ± 0.013 and 4.821 ± 0.019 μm, respectively, with a very narrow distribution (99% of the spheres within ± 2% of the mean diameter). Although the number concentration of the suspensions is not certified, the BCR report shows that the suspensions have a concentration of 3.23×10^{8} L^{-1} and 2.90×10^{5} L^{-1} for RM165 and RM166, respectively.[27] Suspensions of polystyrene microparticles with nominal diameters of 1 μm, 2 μm and 3 μm (certified diameters of 1.04 ± 0.03 μm, 1.98 ± 0.03 μm and 3.03 ± 0.09 μm, respectively) were purchased from Sigma (St. Louis, MO). Suspensions of 2 μm, 4 μm and 5 μm polystyrene microparticles (certified diameters of 2.020 ± 0.015 μm, 4.000 ± 0.043 μm and 5.000 ± 0.043 μm, respectively), were purchased from Thermo (Waltham, MA).

A suspension of gold nanoparticles (PEG-carboxyl surface 0.8 kDa) of 47.8 ± 1.8 nm diameter from NanoComposix (San Diego, CA) was used. All the dilutions, were prepared in ultrapure water (Milli-Q Advantage, Molsheim, France) by accurately weighing (± 0.1 mg) aliquots of the stock suspensions after 1 min sonication (Ultrasonic Cleaner Bath CE-5700 A, 42 KHz, 50 W). Particle suspensions were not stabilised by adding a surfactant, because the latter resulted in increasing the dissolved carbon content and hence, the size detection limits.

A carbon standard made of tartaric acid in 0.2% (*v/v*) HNO_3 (Inorganic Ventures, Christiansburg, VA) were used to prepare aqueous carbon solutions by dilution with 0.2% (*v/v*) HNO_3.

1.2.3. Consumer products

Two types of consumer products were selected for their analysis: personal care products containing plastic particles as exfoliants and plastic tea bags. Three types of personal care products were selected: one exfoliating hair conditioner, PCP1, and two exfoliating facial cleansers, PCP2 and PCP3. These products were purchased from local supermarkets and websites. Regarding tea bags, three brands of tea, packaged in individual plastic bags, were selected. They were purchased from local supermarkets.

1.2.4. Sample preparation procedures

1.2.4.1. SP-ICP-MS analysis

For the detection of microplastics in personal care products, 0.5 g of product was accurately weighed into glass vials. The vials was then filled with 250 ml of water and probe-sonicated for 15 min. Once the suspension was prepared, it was filtered through a 10 μm pore size Isopore^{TM} polycarbonate membranes (Merck, Darmstadt, Germany) to remove large particles. After filtration the suspensions were diluted conveniently for SP-ICP-MS analysis.

For the study of microplastic release from tea bags, the plastic tea bags were cut with steel scissors and the leaves removed. The empty bags were washed thoroughly with water and air-dried to remove any remaining tea leaves. For sample preparation, two empty tea bags were taken and placed in a glass beaker. A volume of 10 mL of water heated to 100 ºC was added to the beaker and left to brew for 5 min. After brewing, the resulting suspension was transferred to clean glass vials for analysis by SP-ICP-MS. Analysis were performed in triplicate, method blanks were also analysed (in duplicate).

1.2.4.2. Optical microscopy

For the visualisation of microplastics in personal care products by optical microscopy, 0.2 g of the product was dispersed in 100 mL of water and

subsequently filtered through a 1 μm polycarbonate filter. The filter was washed and dried overnight at 65 °C in an oven. Images of the filters were taken using a Carl Zeiss optical microscope (Jena, Germany) at x20 magnification.

1.2.4.3. FESEM analysis

The preparation of the tea samples for analysis by FESEM consisted of subjecting the bags to the process described in Section 1.2.4.1. A 200 μL aliqot of the resulting suspension was taken and filtered on 0.05 μm polycarbonate membranes (Poretics™, GVS, Sanford, ME). Afterwards, filters were dried at 60 ºC in an oven for 15 min. After drying, filters were glued to the measurement supports with carbon tape. Before analysis, filters were coated with gold to increase their conductivity with a Leica EM SCD500 (Leica Microsystem, Vienna, Austria).

1.2.4.4. ATR-FTIR analysis

In the case of personal care samples, microplastics were isolated by centrifugation in a low-density solvent. Methanol was selected (density 0.792 g cm^{-3}) for the separation of the expected polystyrene microparticles (density 0.95 g cm^{-3}). The preparation was carried out by suspending 1 g of product in 100 mL of methanol and centrifuged at 5000 rpm for 25 min (Heraeus Multifuge X1R, Thermo Fisher Scientific). The solid collected at the bottom of the centrifugation tube was washed twice with methanol and dried overnight at 60 °C in an oven. The resulting solid was analysed directly by ATR-FTIR (Spectrum 100, Perkin Elmer).

In the case of tea bags, the sample preparation consisted of removing the tea and then washing the bag with water to remove any residue. The filters were dried using compressed air and directly analysed by ATR-FTIR.

1.3. Results and discussion

1.3.1. Carbon determination by ICP-MS

Different substances were reported for the preparation of dissolved carbon standards, such as potassium acid phthalate,[14] citric acid,[17,21] and oxalic acid.[28] In this work, a commercial standard made of tartaric acid in 0.2% (*v/v*) HNO_3 was used.

The next step was selecting the isotope to be measured. Carbon has two stable isotopes, ^{12}C and ^{13}C, with abundances of 98.90% and 1.10%, respectively. The background signals obtained for ultrapure water were between 80,000-100,000 cps, while the signal for a carbon solution of 1 mg L^{-1} was around 1000 cps. In the case of ^{12}C, the background signals obtained for ultrapure water were around 10,000,000 cps. This high background signal made impossible the use of ^{12}C for measurement, as it was well above the working range of the pulse counting detector. Therefore, ^{13}C was selected. Note that SP-ICP-MS measurements must be performed in pulse counting mode to obtain reading frequencies of 100 Hz or higher.

After the selection of the measurement isotope, the possibility of controlling the background present in the samples was considered. Nischwitz *et al.*,[29] reported the use of glass vials instead of plastic ones, as well as the combination of acidification and argon purging as two strategies to reduce background levels down to 30%. While the use of glassware is a key factor in controlling plastic contamination, purging was not considered appropriate as a routine treatment for the removal of dissolved carbon dioxide, because after a short period of time atmospheric CO_2 was readily reabsorbed. The use of ultrapure argon (99.9999%) for reducing the background signals was also checked. The concentrations of carbon species present in ultrapure argon are $C_nH_m \leq 0.2$ mg L^{-1}, CO $\leq$ 1 mg L^{-1} and $CO_2 \leq$ 1 mg L^{-1}. It was found that the use of this type of argon resulted in a 25% reduction of background levels, with respect to the standard high purity argon (99.999%). However, it was decided not to use ultrapure argon, as the background reduction did not lead to a significant

improvement of the detection of the smallest particles because of the cubic dependence of signal and particle diameter, just achieving a reduction of ca. 2% in size.

Under the conditions described above, the sensitivity of carbon was not statistically different in water and nitric acid (0.2%), 1015 cps (mg L^{-1})$^{-1}$ for ^{13}C, the background equivalent concentration (BEC) was 43 mg L^{-1} and the detection limits (3σ) 0.8 mg L^{-1}. The precision, measured with a solution of 10 mg L^{-1}, was 4.6%.

1.3.2. Nebulisation of plastic microparticle suspensions in ICP-MS

A typical nebulisation system used in SP-ICP-MS consists of a cyclonic spray chamber in combination with a concentric nebuliser. In this type of system, dissolved species and nanoparticles, particles with sizes between 1 nm and 100 nm, achieve transport efficiencies over 2%. However, when this system is used for the transport of larger particles, in the micrometer range, the transport efficiency drops below 0.1%,[30] which negatively affect the detection capability of the system in relation to particle concentrations.

To improve the transport efficiencies for microparticles, it was decided to investigate the use of a linear pass spray chamber (Asperon™), which was originally designed for the introduction of intact cells, with sizes in the micrometer range, into the ICP-MS.[30] This type of spray chamber is normally used in conjunctionwith high efficiency concentric micronebulisers, operating at microliters per minute. However, in this work it was replaced by a flow focusing nebuliser (Ingeniatrics, Sevilla, Spain), which showed increased robustness and no clogging due to the introduction of large rigid microparticles. The Asperon™ system (Figure 1.3) has two gas flows to optimise, the nebulisation and the make-up flows. The nebulisation gas is introduced through the nebuliser and controls the formation of the primary aerosol, the nebulisation process and hence the transport efficiency. The make-up flow is introduced tangentially through two inlets at the head of the chamber with the aim of preventing cells from colliding

with the chamber walls. It also allows the control of the residence time of the particles within the plasma, and hence their volatilisation and atomisation, as well as the ionisation of analyte, regardless of the nebulisation gas flow rate.

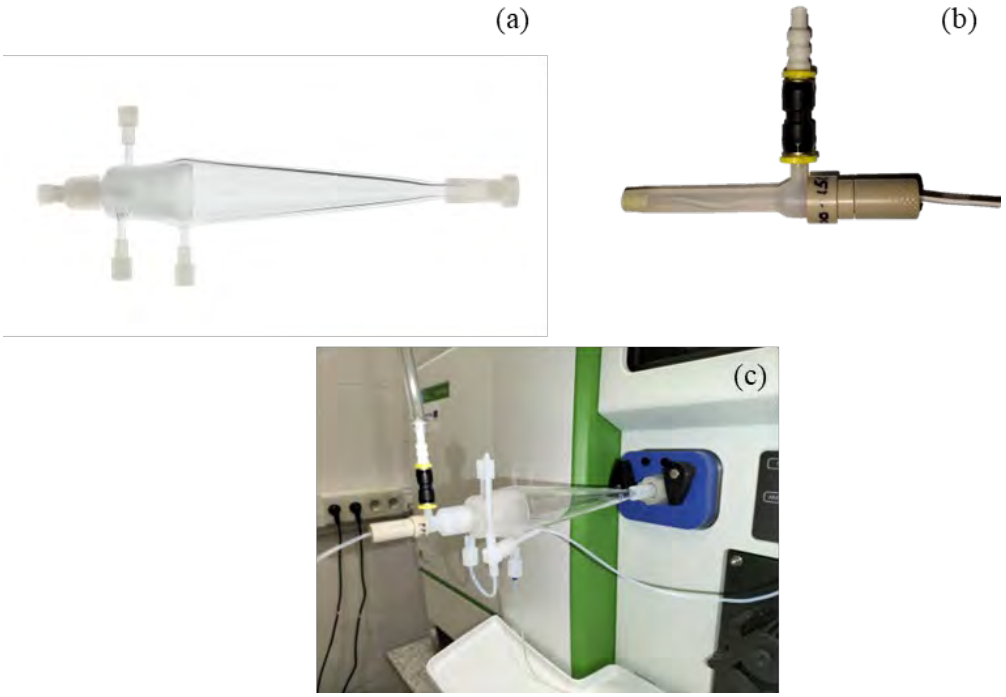

Figure 1.3. Asperon™ system used in ICP-MS. (a) Linear pass-through spray chamber (Perkin Elmer), (b) flow focusing nebuliser (Ingeniatrics) and (c) Asperon™ system coupled to ICP-MS.

The effect of nebulisation and make-up gas flow rates on the nebulisation and volatilisation/atomisation of plastic microparticles (MPs) was studied by introducing a polystyrene microparticle suspension of 2.22 µm at five different make-up gas flow rates (0, 0.2, 0.4, 0.6 and 0.8 L min^{-1}) at nebulisation gas-flow rates in the range of 0.2 - 1.5 L min^{-1}. At each combination of gas flow rates, the number of particles detected, and the mean intensity of the particle events were measured in single particle mode, by using a dwell time of 100 µs. The data obtained is plotted in Figure 1.4.

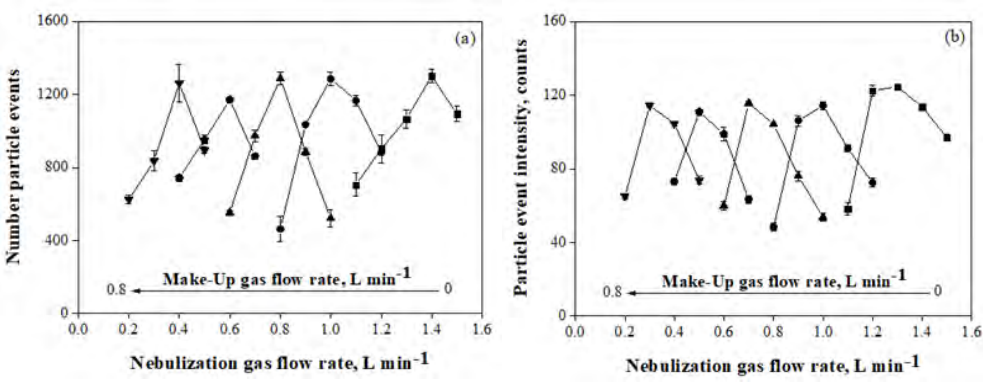

F*igure 1.4. Effect of the nebulisation gas flow rate at different make-up gas flow rates on (a) the number of particles events detected and (b) their mean intensity. Polystyrene microparticles of 2.22 µm diameter. Make-up gas flow rates (L min-1): (■) 0.0; (●) 0.2; (▲) 0.4; (⬟) 0.6; (▼) 0.8.*

As it can be seen in Figure 1.4, a similar behaviour was obtained with the nebulisation system used for different combinations of nebulisation and make-up gas flow rates. The highest number of particles detected, and the maximum particle event intensities were obtained in all cases when the total gas flow rate (the sum of the make-up and the nebulisation gas flow rates) were set between 1.1 - 1.2 L min^{-1}. This behaviour suggests that the total flow rate is responsible of the efficient transport of the microparticles through the nebulisation system, as well as of their volatilisation/atomisation in the plasma. Although various combinations of gas flow rates could be used, it was decided to use the combination of make-up gas flow of 0.2 L min^{-1} and nebulisation gas flow of 1.0 L min^{-1}.

Once the combination of gas flow rates was selected, the transport efficiency was calculated. This calculation was carried out with 50 nm AuNPs, 2.22 µm MPs (BCR) and 4.82 µm MPs (BCR), by applying the number concentration method.[7] The efficiencies obtained for the AuNPs were 28.2 ± 0.4%, 29.9 ± 0.9%, for 2.22 µm MPs and 12.5 ± 0.6% for 4.82 µm MPs. These results confirm the similar nebulisation of nanoparticles (and hence dissolved

species) and microparticles up to 2 - 3 µm, whereas for larger microparticles number concentrations will be underestimated.

1.3.3. Detection of plastic microparticles by SP-ICP-MS and size detection limits

Carbon is an element with high background levels,[22] that will affect the baseline in SP-ICP-MS and hence the detection capability of carbon-containing particles. For a specific background intensity count rate, the count level of the corresponding baseline (Y_B) is controlled by the dwell time used, being proportional to it. The associated noise (σ_B) is equal to the square root of the baseline mean intensity ($\sigma_B = \sqrt{Y_B}$) when a secondary electron multiplier detector is used, because of its Poisson behavior.[4]

On the other hand, when particle events are measured using microsecond dwell times, they are recorded as transient signals, whose heights decrease with dwell time.[31] Since the detection of particle events measured with microsecond dwell times is not only limited by the baseline noise, but also by the height of the recorded transient signals, the detectability of particles is negatively affected by reducing the dwell times when particle events are recorded as transient signals.[32] To select the optimal dwell time, 2.22 µm MPs were analysed at different dwell times (50 µs, 100 µs and 200 µs).

Longer dwell times were not considered because when particle events are recorded as pulses (1-reading particle events), the size detection limits increase with dwell times due to the unique dependence on the baseline noise.[32] The selection of the optimal dwell time was based on the ability to obtain a peak height large enough to be detected above the baseline. The heights obtained for each dwell time were 15 ± 7, 26 ± 12 and 43 ± 19 counts, respectively. With these results, it was finally decided to select 200 µs as the dwell time for measurement. In addition, at this dwell time, 2 - 3 readings per event were recorded, which allowed a correct identification and integration by the data processing software. Figure 1.5 shows the peaks obtained for each dwell time.

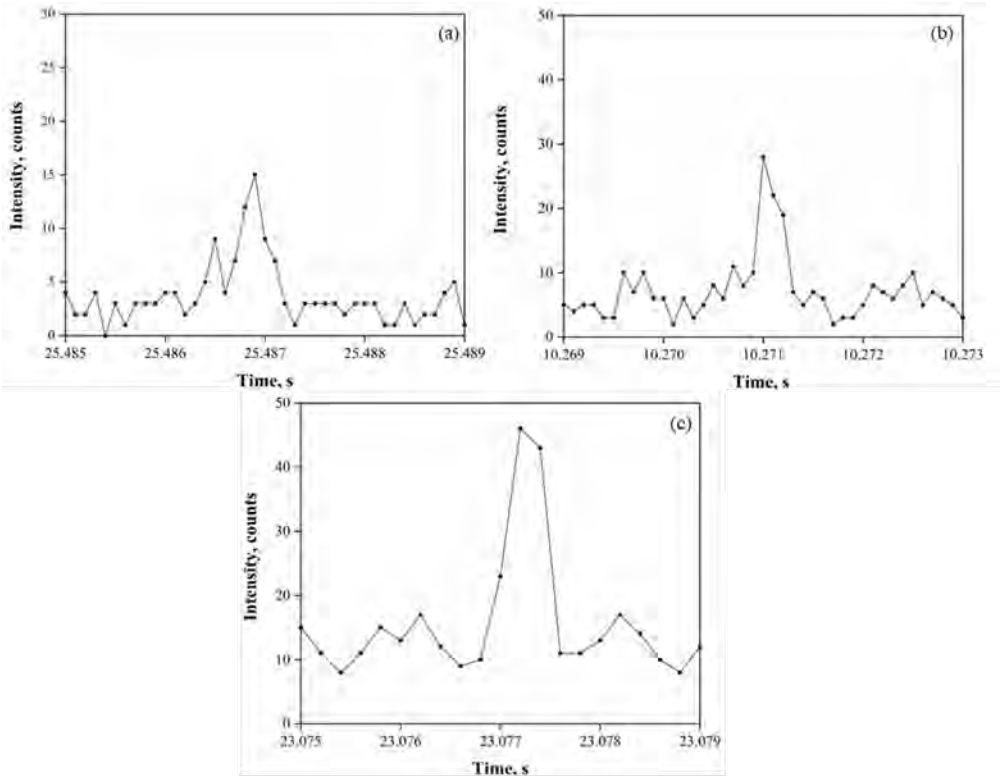

Figure 1.5. Particle event recorded with a dwell time of 50 µs (a), 100 µs (b) and 200 µs (c). Polystyrene microparticles of 2.22 µm diameter.

Once the dwell time was selected, the experimental size limits of detection (LOD_{size}) were calculated from the following expression:

$$LOD_{size} = \left(\frac{5\sigma_B}{K_h}\right)^{1/3} \quad (1.10)$$

where σ_B is the standard deviation of the baseline and K_h the response factor of the net height intensity response of a transient signal (S_{Pmax}) with respect to the cubic diameter (d) of the corresponding particle ($S_{Pmax} = K_h d^3$). The response factor K_h was calculated using the 2.22 µm MPs. The size detection limit for PS microparticles was 1.2 µm for a dwell time of 200 µs and monitoring ^{13}C. Subsequently, the average width of the polystyrene microparticle events was

determined by SP-ICP-MS in the range of 2 to 5 µm using the parameters in Table 1.1. This allowed us to observe that all the microparticle events had an average width of 800 µs (Figure 1.6). These widths were larger than those obtained by 50 nm AuNPs, which were 500 µs in average.[2]

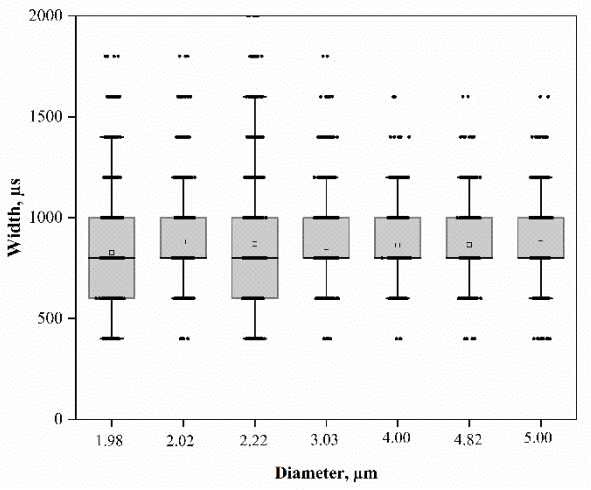

Figure 1.6. Box-and-whisker plot of the widths of particle events recorded from polystyrene microparticles (2 - 5 µm) by SP-ICP-MS.

1.3.4. Determination of plastic microparticle diameter

SP-ICP-MS provides direct information on the elemental mass of the detected particles. Therefore, additional information on the shape, composition and density of the particles is needed to obtain size information. Thus, in the case of spherical and solid particles, the diameter of an individual particle (*d*) can be calculated using the following expression:

$$d = \left(\frac{S_P}{K_d}\right)^{1/3} = \left(\frac{S_P}{\frac{1}{6}\pi\rho F_P K_{ICPMS} K_M}\right)^{1/3} \quad (1.11)$$

where S_p is the net intensity of each particle event, K_d is the slope obtained from a size calibration (net signal intensity vs. particle diameter cubed), ρ the density

and F_P the mass fraction of the element in the particle. K_{ICPMS} is the detection efficiency, which represents the ratio of the number of ions detected versus the number of analyte atoms of the measured isotope introduced into the ICP; and $K_M(= AN_{Av}/M_M)$ is a factor related to the element measured, where A is the atomic abundance of the isotope considered. N_{Av} the Avogadro number and M_M the atomic mass of the element. Although, diameters can be determined by using a calibration with particle size standards of the same chemical composition to obtain the K_d empirically, they can also be estimated from a calibration with a dissolved standard of the element monitored, once the analyte transport efficiency and the sample flow rate are known (Section 1.1.3).

In order to check the good agreement between the measured diameter and the certified values of the different available materials, PS plastic microparticles standards (1 - 5 µm) were analysed by SP-ICP-MS by using the instrumental conditions summarised in Table 1.1. For the calculation of the diameter, the Syngistix Nano application was used. A carbon mass fraction of 0.9231 and a density of 1.04 g cm^{-3} for the spherical PS microparticles were considered, using a calibration with dissolved carbon standards, the measured sample flow rate and the transport efficiency calculated by the frequency method. The results obtained (Table 1.2) showed good agreement between the measured and the certified values for the different PS size standards studied, except for the 1 µm microparticles which were below the size detection limit. These results also confirmed that the carbon in the plastic microparticles was atomised and ionised with the same efficiency as the dissolved carbon. This behaviour was confirmed by plotting the mean intensity of particle events vs. the cubed diameter of PS microparticles of 1 - 5 µm available (Figure 1.7). This plot showed that the microparticles had in this case a linear behaviour up to 5 µm. This confirmed that PS microparticles of at least up to 5 µm volatilised and atomised in the plasma with similar efficiency, allowing an unbiased determination of the size of the plastic microparticles.

Table 1.2. Mean and most-frequent diameter of standard polystyrene microparticles. Mean ± standard deviation (n = 3).

Certified diameter (µm)	Mean diameter (µm)	Bias %	Most frequent diameter (µm)	Bias %
1.04 ± 0.03	1.69 ± 0.07	+63	1.46 ± 0.05	+40
1.98 ± 0.03	1.83 ± 0.01	-7	1.84 ± 0.01	-7
2.02 ± 0.02	1.93 ± 0.01	-5	1.92 ± 0.04	-4
2.22 ± 0.01	2.10 ± 0.02	-6	2.10 ± 0.02	-6
3.03 ± 0.09	2.74 ± 0.01	-10	2.76 ± 0.01	-9
4.00 ± 0.04	3.56 ± 0.06	-10	3.65 ± 0.04	-9
4.82 ± 0.02	4.32 ± 0.02	-10	4.18 ± 0.02	-13
5.00 ± 0.04	4.55 ± 0.05	-9	4.58 ± 0.02	-8

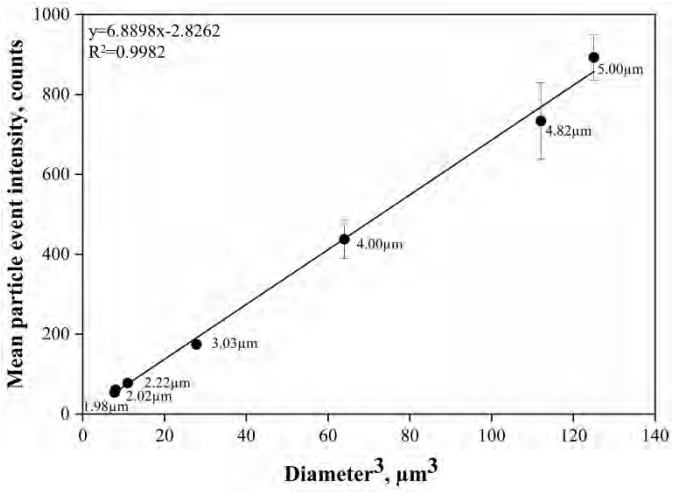

Figure 1.7. Plot of the mean intensity of particle events vs. the cubed diameter of the particles.

In spite of the fact that the mean sizes of the PS microparticles were in good agreement with the certified sizes, the size distribution showed a significant broadening. This situation can be seen in Figure 1.8, which corresponds to the 2.22 µm MPs. By comparing the size distribution obtained from these microparticles by SP-ICP-MS with the distribution from the BCR RM165

report,[27] 10-fold broadening is observed with respect to the original size distribution of the microparticles. This type of broadening in the size distributions measured by SP-ICP-MS was reported elsewhere,[33,34] being more significant for micro[33] than for nanoparticles.[34]

Although the counting statistics contribute to the broadening, variations in the injection position of the particles in the plasma turn out to be especially relevant.[35] The reason may be that particles injected off-axis into the plasma follow different paths and evaporate at different positions, leading to a different transmission of their ion clouds to the mass spectrometer, and thus producing different signals.

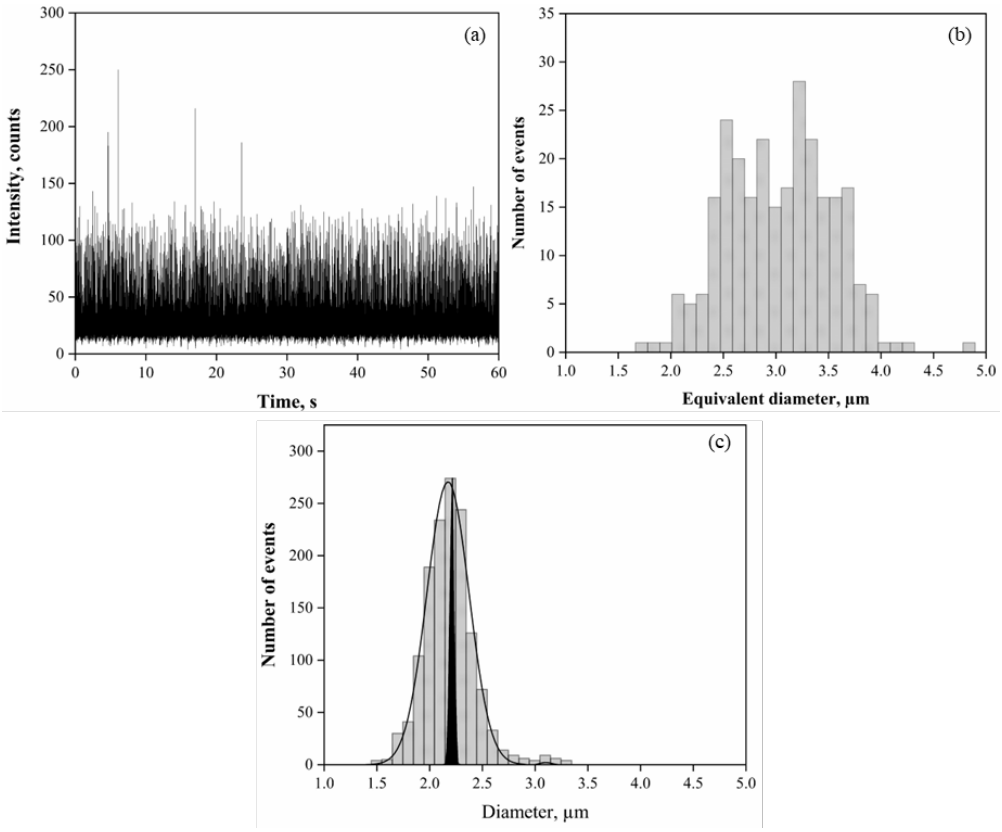

Figure 1.8. (a) Time scan, (b) particle event intensity histogram and (c) size histogram of 2.22 µm polystyrene microparticles (BCR RM165). Reported size distribution of BCR RM165 plot in black in (c).

1.3.5. Transport efficiency determination

Transport efficiency is routinely determined in SP-ICP-MS by following the frequency and the particle size methods developed by Pace *et al*., [7] The former is based on the availability of a number concentration standard (or alternatively, a particle size standard with known composition and certified elemental concentration), while the particle size method requires a particle size standard and dissolved standards of the element to be measured. Moreover, the particle size method requires that the element from the particles and the dissolved standards behave in the plasma in the same way.[7] In this work, both methods were applied although differences were observed in their application to microparticles.

In Section 1.3.2, the frequency method was applied for the calculation of transport efficiencies. Lower transport efficiencies were obtained for larger microparticles (12.5 ± 0.6% for 4.82 μm MPs) compared to smaller ones (29.9 ± 0.9%, for 2.22 μm MPs), which were nebulised in a similar way than nanoparticles or dissolved species. However, when the particle size method was applied, similar transport efficiencies were obtained for both microparticle sizes (25.9 ± 3.4% and 28.1 ± 0.6%, respectively). The difference between both methods for the larger particles indicated that the behaviour in the ICP of carbon in solution and in plastic microparticles were the same, and particles were fully volatilised and atomised, despite they were nebulised with a lower efficiency. Thus, the frequency method by using a number concentration nanoparticle (e.g., 50 nm Au nanoparticles) or a 2 - 3 μm microplastic standard is recommended for general purpose. Working with monodispersed microparticles of larger sizes, determination of the transport efficiency by using a microplastic standard of the expected size and the frequency method would also be recommended.

1.3.6. Determination of plastic microparticle number concentration and detection limits

SP-ICP-MS is based on the fact that the peaks detected correspond to individual particles. Under such conditions, the number of particle events detected is proportional to the number concentration of particles in the sample. However, when the concentration of particles is too high, the probability of recording two or more particle as a single event increase,[31] which affects the linear behaviour of the numerical concentration calibration.

For studying this behaviour, 3 µm MPs suspensions at different concentrations (2.11×10^7, 2.03×10^8, 2.04×10^9 and 6.00×10^9 L^{-1}) were analysed under the conditions specified in Table 1.1. The plotting (Figure 1.9) of the number of particle events versus particle number concentration for each suspension allowed the confirmation of the loss of linearity. Thus, linear behaviour was observed up to concentrations of 2.0×10^9 L^{-1}.

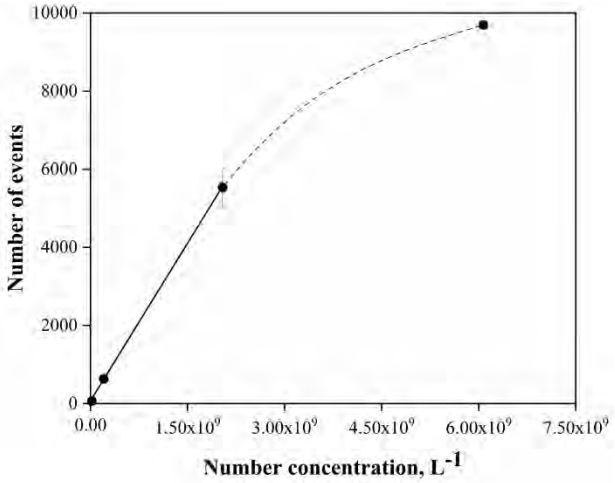

Figure 1.9. Number of events vs. microparticle number concentration. Polystyrene microparticles of 3 µm diameter.

Concerning the calculation of the number concentration, monodisperse samples with particle sizes below 2 - 3 µm allow an unbiased calculation of the number concentration, making use of the experimental working conditions developed. However, the number concentration will be underestimated in samples

containing polydisperse particles over 2 - 3 µm, as explained in Section 1.3.2, because the transport efficiency of particles larger than 3 µm is lower than for smaller particles.

The calculation of the number concentration detection limits can be done using the following expression (1.12):

$$LOD_{number} = \frac{3}{\eta_{neb} Q_{sam} t_i} \quad (1.12)$$

where η_{neb} is the analyte transport efficiency, Q_{sam} the sample introduction flow rate and t_i the acquisition time. This expression refers to the minimum achievable detection limit when no particle events are detected; otherwise, more complex expressions have to be considered.[32] After optimisation of the measurement conditions (Table 1.1) and using the nebulisation systems described in the experimental part, a transport efficiency of 40% was achieved with the 2.22 µm MPs. Using an acquisition time of 60 s, the number concentration detection limit was 5×10^5 L^{-1}. This limit can be reduced by increasing the acquisition time used. By increasing the acquisition time to 300 s and keeping the rest of the parameters, the detection limit was decreased by 5 times (1×10^5 L^{-1}).

1.3.7. Performance of SP-ICP-MS for the analysis of microplastics

The method developed for the analysis of plastic microparticles shows several limitations related to the size of the particles that can be detected and the different transport efficiency attainable for particles of different sizes. In relation with size, the detection of particles below ca. 1 µm is limited by the sensitivity of ICP-MS for carbon, but it is the carbon background that is the most serious limitation. On the other hand, plastic microparticles up to 5 µm were quantitatively volatilised and atomised, as it is shown in Figure 1.7, although larger particles (e.g., up to ca. 10 µm,) may follow a similar trend. Note that particles larger than 2 - 3 µm are nebulised with lower efficiency that dissolved

species, and their number concentration would be underestimated unless adequate correction are included.

Due to all these facts, the method developed can be applied for quantitative analysis in specific studies (e.g., transport, ecotoxicity...) involving monodisperse plastic microparticles with known size, once the transport efficiency for such size was determined by using the corresponding size standard. However, when analysing unknown samples, with plastic particles typically covering a broad range of sizes (e.g., from nano to micrometres and beyond), the SP-ICP-MS method developed can be applied as a screening method allowing a fast detection of the presence of microplastics and providing semiquantitative information about their size and number concentration. This later approach was used for the case studies discussed below.

1.3.8. Case studies

1.3.8.1. Detection of microplastics in personal care products

Some personal care products such as scrubs may contain plastic microparticles in their composition. These microparticles, with sizes in the μm-mm range and typically made of polyethylene, are intentionally added to the product composition and they have to be considered as primary microplastics. Thus, after application of the product and the subsequent rinse, the final destination of the microparticles is the wastewater and, eventually, the environment. Because of this, many countries banned their use.[36]

The analysis of personal care products was carried out, to test the capability of the developed analytical method. Three different scrubs were analysed, PCP1 scrub hair conditioner, PCP2 and PCP3 facial scrub cleansers (Section 1.2.3). Sample preparation was carried out as shown in Section 1.2.4.1. Samples were filtered through 10 μm pore size membranes before analysis by SP-ICP-MS to avoid clogging the nebuliser with larger particles. Two controls, water, and procedure blanks were also analysed. The water control sample was analysed

to determine whether the water used contained plastic microparticles or whether the introduction system could release any plastic microparticle. The procedure control sample consisted in submitting water to the sample preparation process to determine if the procedure introduced plastic microparticles. All samples were analysed using the conditions given in Table 1.1 using an acquisition time of 60 s. The time scans and size distributions obtained for each of the samples are shown in Figure 1.10.

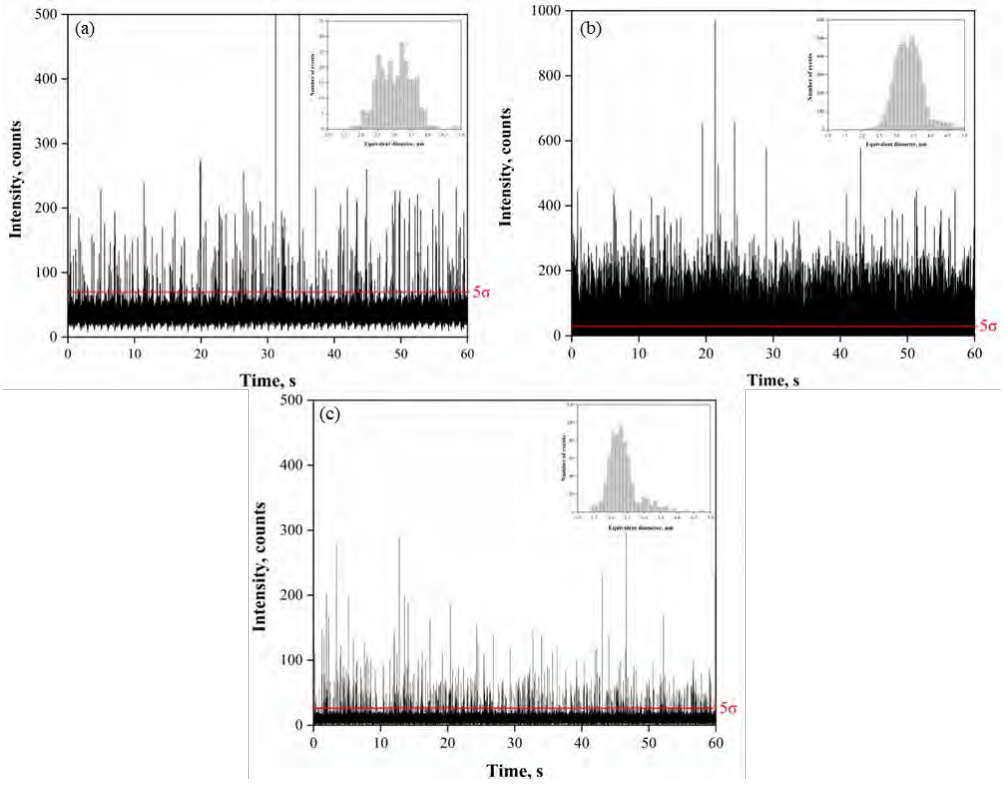

Figure 1.10. SP-ICP-MS time scans corresponding to suspensions of personal care products containing microplastics as scrub agents. The time scans correspond to (a) PCP1 scrub hair conditioner, (b) PCP2 and (c) PCP3 facial scrub cleansers. The size distributions are shown in the insets.

In addition, Table 1.3 shows the most frequent and mean diameters of the particles detected, as well as the number of particles detected in the suspensions analysed and the particle content in the original products. As it can be seen in Table 1.3, both the most frequent and average diameters are about 2 - 3 μm. This

is because particles larger than 2 - 3 μm are underestimated as they are nebulised with lower efficiencies. This situation was discussed previously in Section 1.3.2.

Table 1.3. Microplastic sizes and contents detected in personal care products. Acquisition time: 60 s. Mean ± standard deviation (n = 3).

Personal care product	Most frequent equivalent diameter (μm)	Mean equivalent diameter (μm)	Particle events	Particle content (g^{-1})
Water	-	-	0 ± 0	-
Procedure blank	-	-	3 ± 1	-
PCP1	2.92 ± 0.08	2.89 ± 0.02	263 ± 23	$361x10^5 \pm 20x10^5$
PCP2	3.03 ± 0.01	3.08 ± 0.01	4542 ± 128	$311x10^9 \pm 10x10^9$
PCP3	2.07 ± 0.04	2.11 ± 0.01	615 ± 27	$440x10^8 \pm 50x10^8$

The results obtained confirm the presence of microplastics in all cosmetics, however these results should be considered as semi-quantitative. Regarding to the scans obtained, the scan of sample PCP1 (Figure 1.10(a)) showed a higher baseline compared to the other two products. This was because samples PCP2 and PCP3 were diluted 500 times due to their higher content of microplastics, while PCP1 was not diluted. The water control showed no particulate matter, while in the case of the procedure blank, 3 ± 1 particles were detected. Although some particles were detected due to the processing of the samples, they were not considered especially relevant because they did not represent a major fraction of the particle events detected in the samples. Regarding to the samples, PCP2 showed the highest particle content ($3x10^{11}$ g^{-1}) compared to PCP1 ($3x10^7$ g^{-1}) and PCP3 ($4x10^{10}$ g^{-1}).

Reporting size information in Table 1.3 and Figure 1.10 requires knowing the composition shape and density of the particles detected (Equation 1.11), to provide the size as equivalent size. In this case, the mass of carbon present in the particles is determined, which can be converted to an equivalent diameter once

the composition, mass fraction and density of the polymer are known, and assuming a spherical shape. Particles in the products showed irregular shapes (Figure 1.11), as verified after visualisation of the samples by optical microscopy (Section 1.2.4.2).

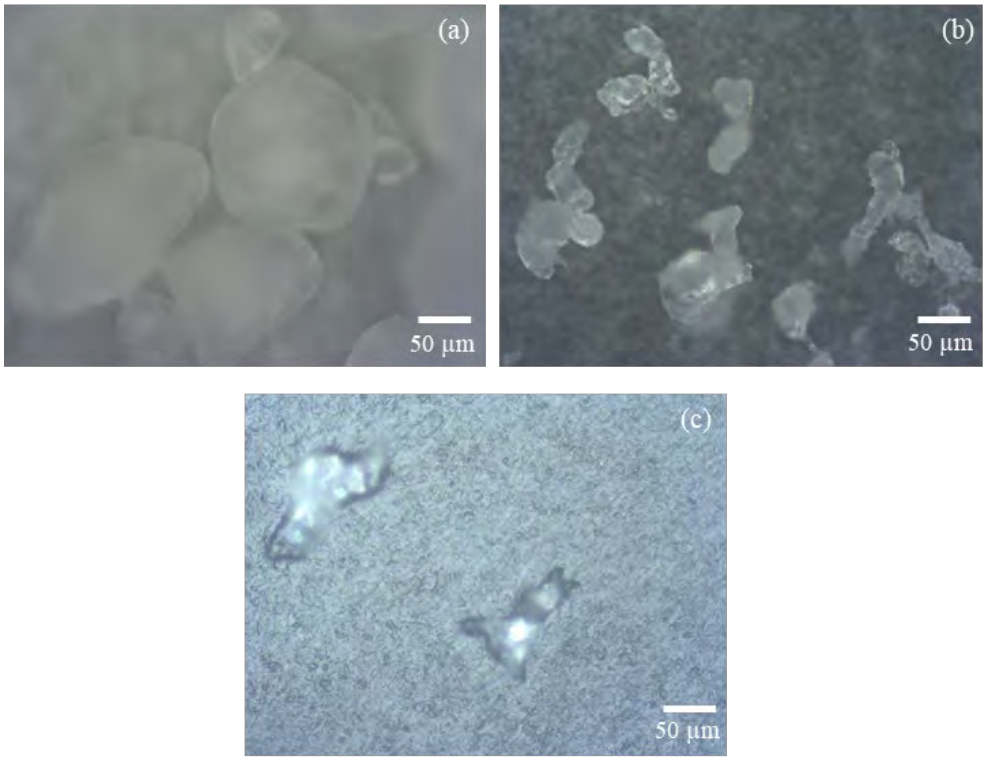

Figure 1.11. Optical microscope images (x20) of microplastics from products. The images correspond to (a) PCP1, (b) PCP2 and (c) PCP3.

Regarding to the chemical composition of the microplastics detected, it was obtained by the analysis of isolated particles by ATR-FTIR, following the procedure outlined in Section 1.2.4.4. This allowed to learn that the particles of PCP1 and PCP2 were polyethylene (F_P: 0.856, ρ: 0.95 g cm^{-3}). No information on PCP3 could be obtained because the sample was insoluble in methanol. The spectra obtained for each sample are shown in Figure 1.12.

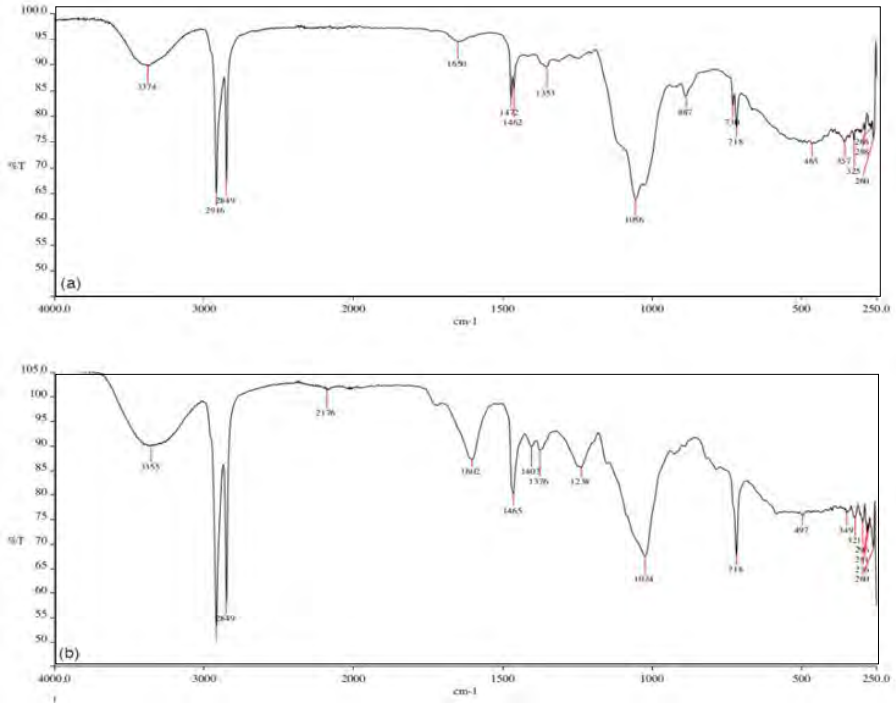

Figure 1.12. *ATR-FT-IR spectra of microparticles isolated from personal care products (a) PCP1 and (b) PCP2.*

1.3.8.2. Release of microplastics from teabags

Although bags containing tea leaves are typically made of cellulose, other materials such as biopolymers are now used in their manufacture. The use of these bags may lead to the release of microplastics during the brewing process, which will be ingested by the consumer. Recently, Hernandez *et al.*,[37] reported the release of nano- and microplastics from plastic teabags during a conventional brewing process as a source of human exposure to such particles.

Therefore, the capability of SP-ICP-MS for the detection of microplastics released from plastic teabags as secondary microparticles from a bulk material was checked. For the analysis, 3 different brands of tea were selected: Teabag A, Teabag B and Teabag C (Section 1.2.3). Sample preparation was carried out as described in Section 1.2.4.1. Samples were introduced into the ICP-MS without any previous filtration. Two controls, water and procedure blanks, were also

analysed. The water control was analysed to determine if the water used contained plastic microparticles. The procedure control consisted of subjecting water to the sample preparation process to determine if the procedure introduced plastic microparticles. All samples were analysed using the conditions given in Table 1.1 for 300 s, because of the lower concentration of microparticles. The time scans and size distributions obtained for each of the samples are shown in Figure 1.13.

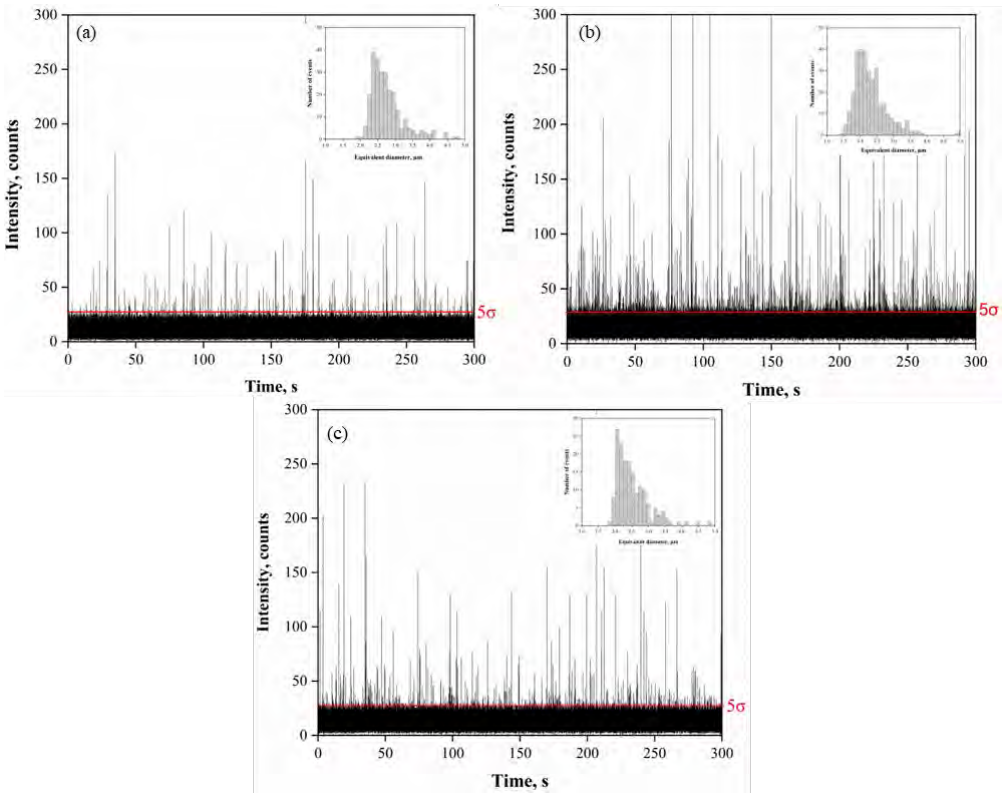

Figure 1.13. SP-ICP-MS time scans corresponding to microplastics released from plastic teabags under conventional brewing. The time scans correspond to (a) teabag A, (b) teabag B and (c) teabag C. The size distributions are shown in the insets.

Table 1.4 shows the most frequent and mean diameters of the particles detected, the number of particles detected in the suspensions analysed and the number of particles released per teabag. Initially, an acquisition time of 1 min was used. However, this time did not allow the detection of more than 100 events, which corresponds to the limit of quantification under zero-blank conditions for

any counting measurement.[38] Therefore, it was decided to increase the acquisition time to 5 min, so that more than 100 events could be recorded.

Table 1.4. Size and number of plastic microparticles released from plastic teabags under conventional brewing. Acquisition time: 5 min. Mean ± standard deviation (n = 3).

Teabags	Most frequent equivalent diameter (µm)	Mean equivalent diameter (µm)	Particle event	Number of particles released per teabag
Water	-	-	1 ± 1	-
Procedure blank	-	-	1 ± 1	-
Teabag A	2.41 ± 0.01	2.70 ± 0.06	141 ± 20	$220x10^2 \pm 30x10^2$
Teabag B	2.01 ± 0.09	2.18 ± 0.05	350 ± 27	$551x10^2 \pm 40x10^2$
Teabag C	2.03 ± 0.08	2.26 ± 0.04	124 ± 16	$191x10^2 \pm 20x10^2$

The results show that in all samples the equivalent mean diameter was around 2-3 µm. This is due to the limitation of the method discussed in Section 1.3.2. In spite of this, plastic microparticles of up to ca. 5 µm were detected in all samples, as it can be seen in the distributions in Figure 1.13. The results in Table 1.4 demonstrate that, under standard laboratory conditions, the environmental contamination and cross contamination from plastic microparticles can be properly handled. In terms of the number of released microplastics, 10,000 particles per teabag in the range of 1 - 5 µm were detected. Note that these values could not be directly compared with those reported by Hernandez *et al.*,[37] because the size range obtained in our results was narrower.

Concerning the sizes reported in Table 1.4 and Figure 1.13, the diameters are provided as equivalent diameters as it was explained in Section 1.3.8.1. In this case the released particles were analysed by scanning electron microscopy (Section 1.2.4.3), observing the irregular shapes (Figure 1.14). The teabags were analysed for the chemical composition with ATR-FTIR as explained in Section

1.2.4.4. The spectra obtained for Teabags A and Teabags B corresponded to polylactic acid and for Teabag C corresponded to polyethylene terephthalate. The spectra obtained for each sample are given in Figure 1.15. As in the case of the microplastics detected in the personal care products, their chemical composition and density were considered for the calculation of the size of particles (polylactic acid, F_P: 0.500, ρ: 1.26 g cm^{-3} polyethylene terephthalate, F_P: 0.625, ρ: 1.34 g cm $^{-3}$).

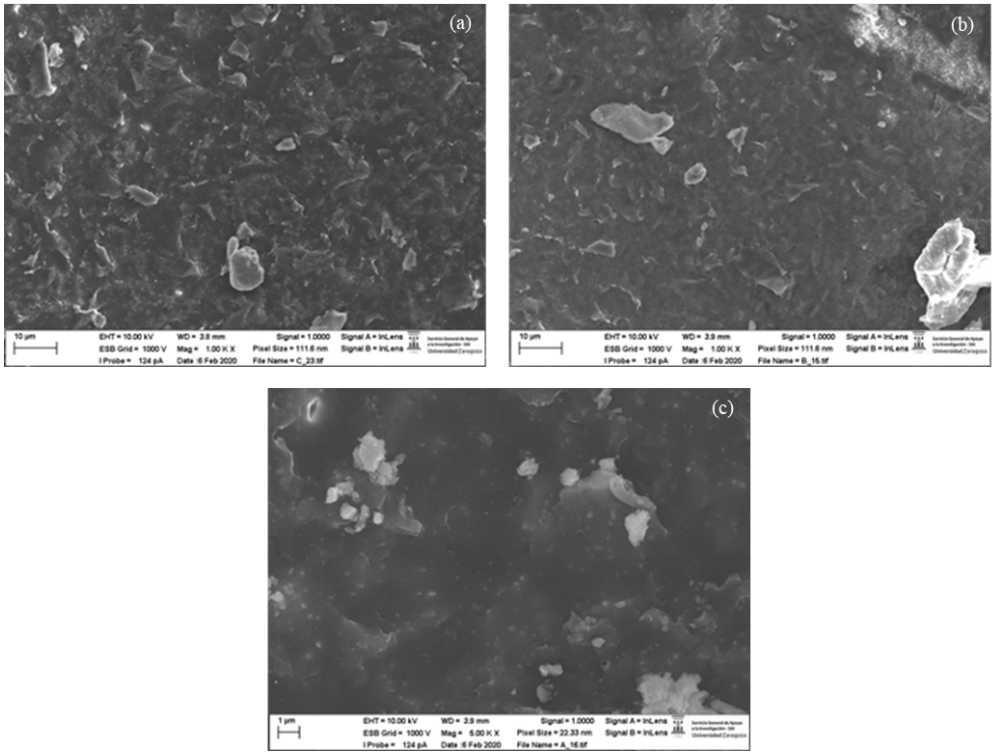

Figure 1.14. FESEM images of the samples of microparticles released from teabags. The images correspond to (a)teabag A, (b) teabag B and (c) teabag C.

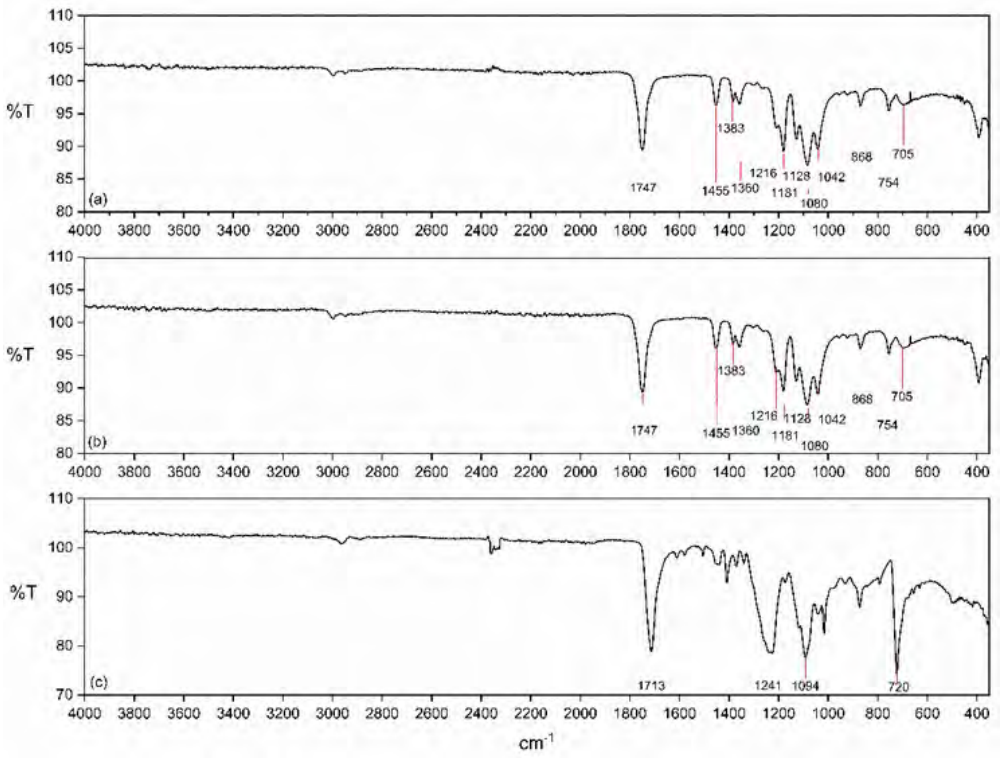

Figure 1.15. *ATR-FT-IR spectra of microplastics released from teabags. (a) Teabag A, (b) teabag B and (c) teabag C.*

1.4. Conclusions

SP-ICP-MS has been demonstrated to be a suitable technique for detection and size characterisation of plastic microparticles by monitoring ^{13}C. The developed method allowed the detection of microparticles with sizes over ca. 1 µm, despite the inherent limitations of carbon detection by ICP-MS. The upper detection limit was conditioned by the efficient nebulisation of large particles. Concerning to the number concentrations determined, they are conditioned by the efficiency of nebulisation and transport of the microparticles, which should be independent of their size. In the case of the nebulisation system used, transport efficiencies around 40% were achieved for microparticles of up to 3 µm, but this efficiency decreased for larger particles. Because of this, in the case of analysing real samples containing microparticles of different sizes, the larger microparticles

will be underestimated. A number concentration detection limit of hundreds of particles per millilitre was achieved, and it can be further reduced by increasing the acquisition time.

For monodisperse microparticles, a wide size distribution was observed, revealing that the measurement process contributes to the broadening of the original size distribution, most probably due to different pathways followed by the microparticles in the plasma, which affect their individual volatilisation, atomisation and ionisation behaviours, but not the average process.

As discussed above, the range of particle sizes that can be quantitatively determined is restricted to ca. 1 - 3 µm. For this reason and considering that plastic particles in most real samples cover a size continuum from nanometres up to millimetres, the method developed is suitable rather as a fast-screening tool, prior to more specific and demanding analyses (e.g., microRaman, microFT-IR, pirolysis GC-MS...). On the other hand, the method developed can be applied for quantitative analysis in studies involving monodisperse plastic microparticles with known size (in the range of ca. 1 - 10 µm), once the transport efficiency for the selected size was determined by using the corresponding size standard. This is the case of toxicological and ecotoxicological studies, as well as fate and transport laboratory-studies, involving specific types of microplastics.

1.5 References

1. Degueldre, C. & Favarger, P.-Y. Colloid analysis by single particle inductively coupled plasma-mass spectroscopy: a feasibility study. Colloids and Surfaces A: Physicochemical and Engineering Aspects, 217, 137–142 (2003).

2. Laborda, F., Gimenez-Ingalaturre, A. C., Bolea, E. & Castillo, J. R. About detectability and limits of detection in single particle inductively coupled plasma mass spectrometry. Spectrochimica Acta Part B: Atomic Spectroscopy, 169, 105883 (2020).

3. Bolea, E., Jimenez, M. S., Perez-Arantegui, J., Vidal, J. C., Bakir, M., Ben-Jeddou, K., Gimenez-Ingalaturre, A. C., Ojeda, D., Trujillo, C. & Laborda, F. Analytical applications of single particle inductively coupled plasma mass spectrometry: A comprehensive and critical review. Analytical Methods, 13, 2742–2795 (2021).

4. Laborda, F., Gimenez-Ingalaturre, A. C., Bolea, E. & Castillo, J. R. Single particle inductively coupled plasma mass spectrometry as screening tool for detection of particles. Spectrochimica Acta Part B: Atomic Spectroscopy, 159, 105654 (2019).

5. Dan, Y., Ma, X., Zhang, W., Liu, K., Stephan, C. & Shi, H. Single particle ICP-MS method development for the determination of plant uptake and accumulation of CeO2 nanoparticles. Analytical and Bioanalytical Chemistry, 408, 5157–5167 (2016).

6. Dan, Y., Shi, H., Stephan, C. & Liang, X. Rapid analysis of titanium dioxide nanoparticles in sunscreens using single particle inductively coupled plasma–mass spectrometry. Microchemical Journal, 122, 119–126 (2015).

7. Pace, H. E., Rogers, N. J., Jarolimek, C., Coleman, V. A., Higgins, C. P. & Ranville, J. F. Determining Transport Efficiency for the Purpose of Counting and Sizing Nanoparticles via Single Particle Inductively Coupled Plasma Mass Spectrometry. Analytical Chemistry, 83, 9361–9369 (2011).

8. Loeschner, K., Brabrand, M. S. J., Sloth, J. J. & Larsen, E. H. Use of alkaline or enzymatic sample pretreatment prior to characterization of gold nanoparticles in animal tissue by single-particle ICPMS. Analytical and Bioanalytical Chemistry, 406, 3845–51 (2014).

9. Hadioui, M., Peyrot, C. & Wilkinson, K. J. Improvements to Single Particle ICPMS by the Online Coupling of Ion Exchange Resins. Analytical Chemistry, 86, 4668–4674 (2014).

10. Laborda, F., Gimenez-Ingalaturre, A. C. & Bolea, E. in Comprehensive Analytical Chemistry, 93, 35–67 (Elsevier B.V., 2021).

11. Laborda, F., Trujillo, C. & Lobinski, R. Technical note: Unlocking Carbon-13 with Single Particle ICP-MS : Feasibility Study for Microplastic Detection. PerkinElmer (2022).

12. Cuello-Nuñez, S., Abad-Álvaro, I., Bartczak, D., del Castillo Busto, M. E., Ramsay, D. A., Pellegrino, F. & Goenaga-Infante, H. The accurate determination of number concentration of inorganic nanoparticles using spICP-MS with the dynamic mass flow approach. Journal of Analytical Atomic Spectrometry, 35, 1832–1839 (2020).

13. Santamaria-Fernandez, R. Precise and traceable carbon isotope ratio measurements by multicollector ICP-MS: what next? Analytical and Bioanalytical Chemistry, 397, 973–978 (2010).

14. Vogl, J. & Heumann, K. G. Development of an ICP−IDMS Method for Dissolved Organic Carbon Determinations and Its Application to Chromatographic Fractions of Heavy Metal Complexes with Humic Substances. Analytical Chemistry, 70, 2038–2043 (1998).

15. Smith, C., Jensen, B. P., Wilson, I. D., Abou-Shakra, F. & Crowther, D. High-performance liquid chromatography/inductively coupled plasma mass spectrometry and tandem mass spectrometry for the detection of carbon-containing compounds. Rapid Communications in Mass Spectrometry, 18, 1487–1492 (2004).

16. Stolpe, B., Hassellöv, M., Andersson, K. & Turner, D. R. High resolution ICPMS as an on-line detector for flow field-flow fractionation; multi-element determination of colloidal size distributions in a natural water sample. Analytica Chimica Acta, 535, 109–121 (2005).

17. Nischwitz, V., Gottselig, N., Missong, A., Meyn, T. & Klumpp, E. Field flow fractionation online with ICP-MS as novel approach for the quantification of fine particulate carbon in stream water samples and soil extracts. Journal of Analytical Atomic Spectrometry, 31, 1858–1868 (2016).

18. Frick, D. A. & Günther, D. Fundamental studies on the ablation behaviour of carbon in LA-ICP-MS with respect to the suitability as internal standard. Journal of Analytical Atomic Spectrometry, 27, 1294–1303 (2012).

19. Deiting, D., Börno, F., Hanning, S., Kreyenschmidt, M., Seidl, T. & Otto, M. Investigation on the suitability of ablated carbon as an internal standard in laser ablation ICP-MS of polymers. Journal of Analytical Atomic Spectrometry, 31, 1605–1611 (2016).

20. Li, F., Armstrong, D. W. & Houk, R. Behavior of bacteria in the inductively coupled plasma: Atomization and production of atomic ions for mass spectrometry. Analytical Chemistry, 77, 1407–1413 (2005).

21. Riisom, M., Gammelgaard, B., Lambert, I. H. & Stürup, S. Development and validation of an ICP-MS method for quantification of total carbon and platinum in cell samples and comparison of open-vessel and microwave-assisted acid digestion methods. Journal of Pharmaceutical and Biomedical Analysis, 158, 144–150 (2018).

22. Bolea-Fernandez, E., Rua-Ibarz, A., Velimirovic, M., Tirez, K. & Vanhaecke, F. Detection of microplastics using inductively coupled plasma-mass spectrometry (ICP-MS) operated in single-event mode. Journal of Analytical Atomic Spectrometry, 35, 455–460 (2020).

23. Reed, R. B., Goodwin, D. G., Marsh, K. L., Capracotta, S. S., Higgins, C. P., Fairbrother, D. H. & Ranville, J. F. Detection of single walled carbon nanotubes by monitoring embedded metals. Environmental Science: Processes & Impacts, 15, 204–13 (2013).

24. Lankone, R. S., Wang, J., Ranville, J. F. & Fairbrother, D. H. Photodegradation of polymer-CNT nanocomposites: effect of CNT loading and CNT release characteristics. Environmental Science: Nano, 4, 967–982 (2017).

25. Wang, J., Lankone, R. S., Reed, R. B., Fairbrother, D. H. & Ranville, J. F. Analysis of single-walled carbon nanotubes using spICP-MS with microsecond dwell time. NanoImpact, 1, 65–72 (2016).

26. Flores, K., Rand, L. N., Valdes, C., Castillo, A., Cantu, J. M., Parsons, J. G., Westerhoff, P. & Gardea-Torresdey, J. L. Targeting Metal Impurities for the Detection and Quantification of Carbon Black Particles in Water via spICP-MS. Environmental Science & Technology, 56, 13719–13727 (2022).

27. R. Thom, H. M. and E. C. The Certification of Monodispersed Latex Spheres in Aqueous Suspensions with Nominal Diameter 2.0 Mm, 4.8 Mm and 9.6 Mm (RM 165, 166 and 167). BCR certificates (1985).

28. Amaral, C. D. B., Amais, R. S., Fialho, L. L., Schiavo, D., Nogueira, A. R. A. & Nóbrega, J. A. Determination of carbon in digested samples and amino acids by inductively coupled plasma tandem mass spectrometry. Microchemical Journal, 122, 29–32 (2015).

29. Heroult, J., Nischwitz, V., Bartczak, D. & Goenaga-Infante, H. The potential of asymmetric flow field-flow fractionation hyphenated to multiple detectors for the quantification and size estimation of silica nanoparticles in a food matrix. Analytical and Bioanalytical Chemistry, 406, 3919–3927 (2014).

30. Perkin Elmer Inc. Patented Asperon Single Cell Spray Chamber Delivering Intact Individual Cells to the ICP-MS Plasma. PerkinElmer (2017).

31. Abad-Álvaro, I., Peña-Vázquez, E., Bolea, E., Bermejo-Barrera, P., Castillo, J. R. & Laborda, F. Evaluation of number concentration quantification by single-particle inductively coupled plasma mass spectrometry: microsecond vs. millisecond dwell times. Analytical and Bioanalytical Chemistry, 408, 5089-5097 (2016).

32. Laborda, F., Gimenez-Ingalaturre, A. C., Bolea, E. & Castillo, J. R. About detectability and limits of detection in single particle inductively coupled plasma mass spectrometry. Spectrochimica Acta Part B: Atomic Spectroscopy, 169, 105883 (2020).

33. Olesik, J. W. & Gray, P. J. Considerations for measurement of individual nanoparticles or microparticles by ICP-MS: determination of the number of particles and the analyte mass in each particle. Journal of Analytical Atomic Spectrometry, 1143–1155 (2012).

34. Laborda, F., Jiménez-Lamana, J., Bolea, E. & Castillo, J. R. Critical considerations for the determination of nanoparticle number concentrations, size and number size distributions by single particle ICP-MS. Journal of Analytical Atomic Spectrometry, 28, 1220–1232 (2013).

35. Aghaei, M. & Bogaerts, A. Particle transport through an inductively coupled plasma torch: Elemental droplet evaporation. Journal of Analytical Atomic Spectrometry, 31, 631–641 (2016).

36. Guerranti, C., Martellini, T., Perra, G., Scopetani, C. & Cincinelli, A. Microplastics in cosmetics: Environmental issues and needs for global bans. Environmental Toxicology and Pharmacology, 68, 75–79 (2019).

37. Hernandez, L. M., Xu, E. G., Larsson, H. C. E., Tahara, R., Maisuria, V. B. & Tufenkji, N. Plastic Teabags Release Billions of Microparticles and Nanoparticles into Tea. Environmental Science & Technology, 53, 12300–12310 (2019).

38. Lide, D. R. Limits for Qualitative Detection and Quantitative Determination. A Century of Excellence in measurements, standards and technology. NIST (2018).

2. Detection of microplastics in river water samples

2.1. Introduction

2.1.1. The “plastic-cycle”: the origin of nano- and microplastics in river water

Nanoplastics and microplastics can circulate in the environment, resulting in the so-called “plastic cycle”. This cycle is currently made up of four “environmental compartments”: terrestrial, freshwater, seawater and atmospheric. These compartments are interconnected, with indistinct and permeable boundaries. The interactions between them are influenced by different weather and environmental conditions.

Therefore, the presence or absence of plastics in the different compartments will vary greatly in time and space. Plastics are essentially transported from land to seawater. However, they can be washed back onto land by high tides or storms. The same situation occurs with freshwaters, which can return or take plastics from land when flooding occurs. The water cycle itself can influence on the transport of plastics from seawater to land or freshwater due to the evaporation of water in the seas and its subsequent deposition as rain.[1–5] Figure 2.1 shows the different compartments of the “plastics cycle” and the movements that can take place between them.

The presence of plastic particles (macro, micro and nanoplastics) in the environment facilitates their consumption by animals, either by mistaking them for food or by consuming them together with food. This allows plastics to enter the food chain. The presence of microplastics (MPs) was already been confirmed in a number of animals in their natural environments, such as bivalves,[6] fish,[7] shellfish,[7] crabs[8] and tufted ducks,[9] among others. Today, MPs can also be found in other products for human consumption such as sea salt[10–12] or drinking water.[13,14] This situation has resulted in humans being exposed to the presence of these particles daily. Several studies showed the presence of MPs in human faeces[15] and in human placenta.[16]

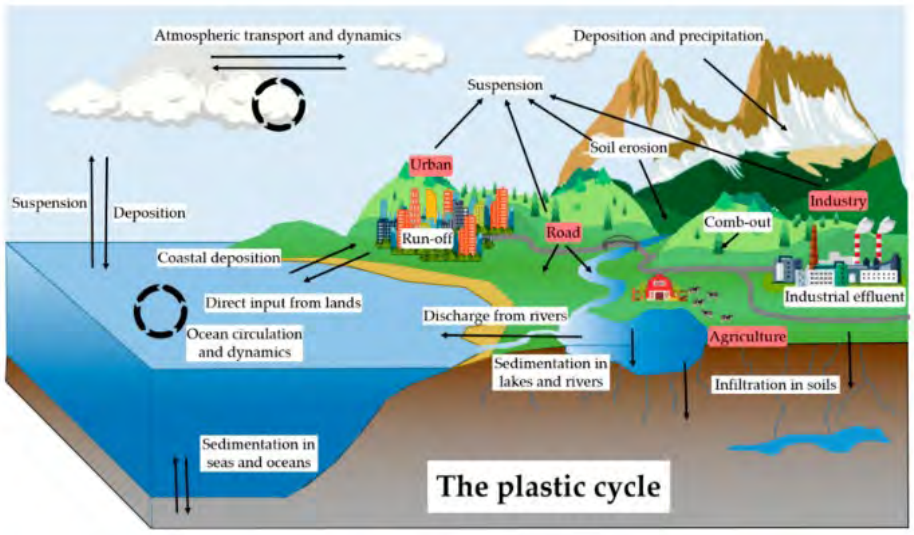

Figure 2.1. "Plastic cycle" model. Red boxes represent sources and white boxes represent transport factors and mechanisms. Arrows represent transport pathways.[5]

2.1.2. The presence of plastics in rivers: a transport route for microplastics?

Rivers accumulate an important part of the plastics produced in urban areas derived from wastewater and play a prominent role in the "plastic cycle" as transporter of MPs. Wastewater treatment plants (WWTP) can remove around 99% of the plastics present in wastewater. However, despite this, it is estimated that around 10^{10} particles per day are released into rivers by these plants.[17] It should also be noted that around 80% of the world wastewater is released untreated into rivers. It is therefore necessary to consider rivers as a dynamic reservoir of MPs. [18]

Once plastics reach the rivers, due to their physical-chemical properties, they tend to concentrate more often on the river surface. These concentrations can be modified by the action of seasonal changes, which affect river flow (droughts, rainfall, or floods, among others).[18] The presence of large cities and industrial areas close to rivers, favours the presence of large amounts of MPs, leading to

different studies in various rivers in Asia and Europe to know the current situation. Table 2.1 summarises studies carried about the topic, including the techniques used for the analysis, the type of plastics detected, the concentration of MPs present and their size. Among the rivers studied were the Citarum river, which is considered the most polluted river on the planet; the Yangtze River, the longest river in Asia, or the Elbe River, which is one of the main rivers in Central Europe. The results obtained from these studies show that plastic pollution in rivers is becoming an emerging problem, which needs a thorough investigation.

Europe adopted actions to address this situation through the "European strategy for plastics in a circular economy" in 2018. In addition, the Directive 2019/90441[19]prohibits the commercialization of single-use plastic products from products such as straws, cups and similar. On the other hand, China also decided to implement several actions, such as the “Law of the P.R.China on the Prevention and Control of Environmental Pollution by Solid Wastes in April 2020.[20] Also, Canada joined these strategies with the "Single-use Plastics Prohibition Regulations" (SOR/2022-138),[21] as well as United Kingdom through the law 2020/971 for restriction of single-use plastic straws, cotton buds and drink stirrers.[22]

The aim of research discussed in this chapter is to evaluate the application of SP-ICP-MS as screening technique for the detection of microplastics in river waters as the first step prior to their analysis by other techniques (e.g., Raman spectroscopy, FTIR, GC-MS). The methodology developed in the previous chapter was adapted to the features of river water samples. The developed method was applied to the analysis of a number of samples from river basins in the north and south of Pyrenees to obtain a first insight into the microplastic pollution of these areas.

Table 2.1. Summary of studies related to the occurrence of microplastics in rivers.

River	Country	Technique	Type of plastic	Size	Plastic concentration	Ref.
Citarum	Indonesia	Optical microscopy FTIR μFTIR	PET PS Cellophane Nylon PP PE	<300 μm - >1000 μm	3.35 ± 0.54 m^{-3}	23
Ticino	Italy	Optical microscopy μFTIR	LDPE PET PP	>20 μm	$3.40\times10^{11}\pm1.1\times10^{11}$ MPs	24
Biała Czarna Hańcza	Poland	Optical microscopy	–	>0.04-4 mm	10.83 ± 3.96 L^{-1} 10.29 ± 3.90 L^{-1}	25
Yangtze	China	Optical microscopy μRaman	PP PE PA PS PVC PET PC	>0.11 mm	1.27 ± 0.83 L^{-1}	26
Thames	United Kingdom	Optical microscopy FTIR	Rubber PVC PE	<0.5mm - 5mm	51 ± 10 L^{-1}	27
Northern Dvina	Rusia	visual analysis FTIR	PE PP EEA	>0.5mm	$0.6–1.4\times10^{4}$ Km^{-2}	28
Seine	France	Optical microscopy μFTIR	PP PE PES	32-2528 μm	15.5 ± 4.9 L^{-1}	29
Lis	Portugal	Optical microscopy FTIR μFTIR	PP PVC PC Nylon	14-4726 μm	234 ± 398 m^{-3}	30
Elbe Mulde	Germany	Optical microscopy Pyr-GC-MS	PE PP PS	>50 μm	15 ± 2 m^{-3} 0.33-1.19 mg m^{-3}	31
Garone	France	Optical microscopy ATR-FTIR	PE PP PS	700 μm - 5 mm	0.15 ± 0.46 m^{-3}	32

2.2. Experimental

2.2.1. Instrumentation

2.2.1.1. Inductively coupled plasma mass spectrometry (ICP-MS)

A PerkinElmer NexION 2000B ICP mass spectrometer (Toronto, Canada) was used throughout. The sample introduction system consisted of an Asperon™ linear pass spray chamber (PerkinElmer, Toronto, Canada), equipped with a flow focusing nebulizer (Ingeniatrics, Sevilla, Spain) and an autosampler µDx Single Cell Autosampler (Elemental Scientific, Omaha, NE) which allows flow rates in the µL min^{-1} range to be continuously fed to an ICP-MS through a syringe pump. Default instrumental and data acquisition parameters are listed in Table 2.2. Argon of 99.999% purity was used. Data were processed with Syngistix Nano Application version 2.5 and Origin 2019b.

Table 2.2. Default instrumental and data acquisition parameters for SP-ICP-MS.

Instrumental parameters	
RF power	1600 W
Argon gas flow rate	
Plasma	15 L min^{-1}
Auxiliary	1.2 L min^{-1}
Nebulizer	1.0 L min^{-1}
Make-up	0.2 L min^{-1}
Sample flow rate	10 µL min^{-1}
Data acquisition parameters	
Dwell time	200 µs
Readings per replicate	300 000 / 2 400 000
Total acquisition time	60 s / 480 s
Isotope monitored	^{13}C

2.2.1.2. Raman microscopy

A confocal Raman microscope WITec Alpha 300+ equipped with an integrated microscope (Oxford Instruments, Abingdon, UK) was used. The objective used for sample visualization and spectral acquisition was x100 (Oxford Instruments, Abingdon, UK). Raman scattering was excited with a 532-nm laser diode (Oxford Instruments, Abingdon, UK). The laser power used was 3.21 or 6.81 mW depending of the sample. The spectra were obtained using 3 s of acquisition time and 25 collections for each spot of the samples analysed.

2.2.1.3. Raman Database

The processing of the spectra obtained from the Raman analysis was carried out using two Raman databases. The KnowItAll™ database of Wiley (Hoboken, NJ) and the PublicSpectra™ database, a free online database.

2.2.1.4. Field Emission Scanning Electron Microscopy (FESEM)

A field emission scanning electron microscope Carl Zeiss MERLIN™ (Nano Technology Systems, Jena, Germany) was used for visualization of samples. The microscope was equipped with an INCA 350 X-ray energy dispersive (EDX) system (Oxford Instruments, Abingdon, UK) for elemental analysis.

2.2.2. Standards

A suspension obtained from BCR (Geel, Belgium) of reference latex spheres of 2.0 μm nominal diameter (RM165) made of polystyrene cross-linked with divinylbenzene and stabilised with a non-ionic surfactant was used. RM165 have a certified diameter of 2.223 ± 0.013 μm and an approximate numerical concentration of $3.23 \times 108\ L^{-1}$. A suspension of polystyrene microparticles with a nominal diameter of 3 μm from Sigma (Saint Louis, MO), with a certified diameter of 3.03 ± 0.09 μm, was also used. All dilutions were prepared in ultrapure water (Milli-Q Advantage, Molsheim, France) by accurately weighing (± 0.1 mg) aliquots of the stock suspensions after 1 min sonication (Ultrasonic Cleaner Bath CE-5700 A, 42 KHz, 50 W). Particle suspensions were not stabilized by adding

surfactants, not to increase their dissolved carbon content and hence the size detection limits.

Tartaric acid in 0.2% (*v/v*) HNO_3 (Inorganic Ventures, Christiansburg, EEUU) were used to prepare aqueous carbon solutions by dilution in 0.2% (*v/v*) HNO_3.

The bacteria used belonged to the *Escherichia coli* J62 strain. $AgNO_3$ (Sigma, Saint Louis, MO) was used to prepare the silver labelled bacteria suspension.

2.2.3. River water samples

River water samples were collected from rivers in France (Occitania and Nouvelle-Aquitaine) and in Spain (Aragon, Navarra, La Rioja, and Catalonia). The geographical location of the sampling points is shown in Figure 2.2 (Spain) and Figure 2.3 (France) and listed in Table 2.3.[33]

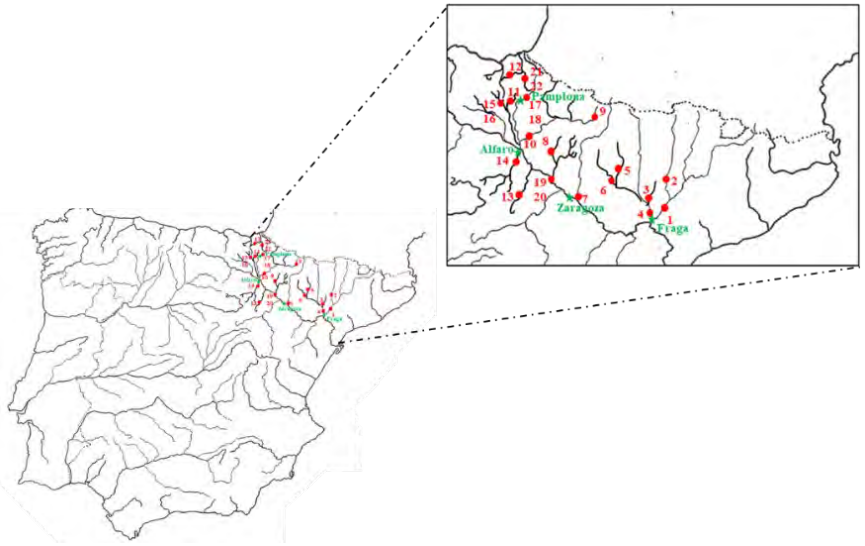

Figure 2.2. Geographical distribution of sampling points in Spanish rivers.

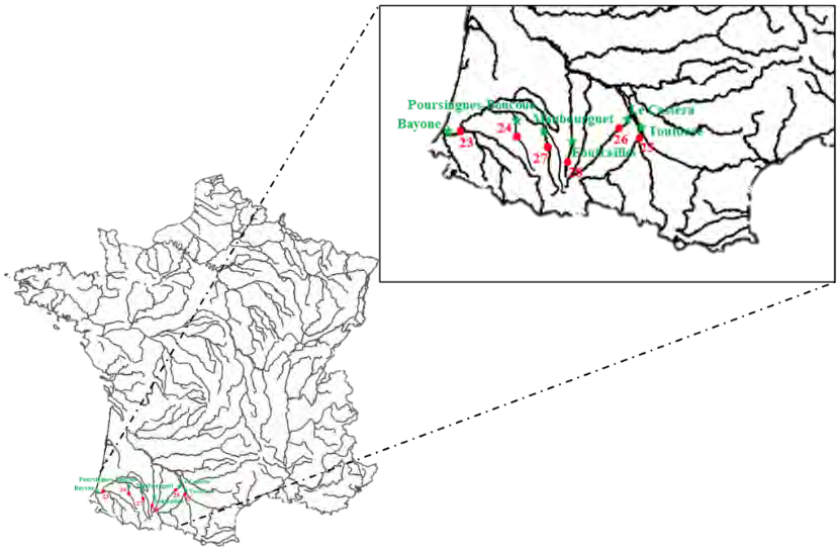

Figure 2.3. Geographical distribution of sampling points in French rivers.

Table 2.3. List of rivers studied and locations of the sampling points.

Sample identification	River	Location
RW01	Segre	Torres de Segre
RW02	Noguera Ribagorzana	Corbins
RW03	Clamor Amarga	Zaidín
RW04	Cinca	Fraga
RW05	Alcanadre	Sariñena
RW06	Flumen	Albalatillo
RW07	Gállego	San Mateo de Gállego
RW08	Arba de Ríquel	Ejea de los Caballeros
RW09	Aragon Subordan	Javierregay
RW10	Aragón	Caparroso
RW11	Irantzu	Estella
RW12	Arakil	Irañeta
RW13	Queiles	Novallas
RW14	Alhama	Alfaro
RW15	Ega	Estella (upstream)
RW16	Ega	Estella (dowstream)
RW17	Ega	Pamplona (upstream)
RW18	Arga	Pamplona (dowstream)
RW19	Ebro	Tudela (upstream)
RW20	Ebro	Tudela (dowstream)
RW21	Biadasoa	Bera de Bidasoa (upstream)
RW22	Biadasoa	Bera de Bidasoa (dowstream)
RW23	Adour	Bayonne
RW24	Gabas	Poursiugues-Boucoue
RW25	Garonne	Toulouse
RW26	Save	Le Castéra
RW27	Echez	Maubourguet
RW28	Baïse	Fontrailles

2.2.4. Procedures

2.2.4.1. Sampling and storage of river water

Samples were collected during the months of May to June 2021. Samples were taken in 500 mL glass bottles, to avoid plastic contamination. Afterwards, samples were stored at 4 ºC.[34]

2.2.4.2. Analysis by SP-ICP-MS

An aliquot of 15 mL of river water sample was transferred to 20 mL glass vials, after manual shaking of the 500 mL obtained in Section 2.2.4.1. In all cases prior to analysis by SP-ICP-MS the 20 mL vials were shaken.

2.2.4.3. Pre-treatment of river water samples

Two different acidification pre-treatment procedures were applied to the river water samples. One consisted of the addition of different volumes of HNO_3 followed by heating. For this purpose, 0.2, 1, 10 and 50 % (*v/v*) HNO_3 were studied by adding 6, 30, 300 and 1500 µL of 69% HNO_3 to 2.99, 2.97, 2.7 and 1.5 mL of river water, respectively. The samples were heated for 5 min at 100ºC in a heating plate (IKA® RH basic, Staufen, Germany). In the other procedure, a volume of HNO_3 was added to the sample to reach the HNO_3 concentration of 10% (*v/v*) and stirred for 24 h without heating. For sample preparation, 300 µL of 69% HNO_3 was added to 2.7 mL of sample in a glass vial, which was stirred for 24 h at 150 rpm in a Rotamax120 (Heildoph, Schawabach, Germany).

2.2.4.4. Raman microscopy analysis

2 mL of river water were filtered on alumina filters of 0.1 µm pore size (Anodisc™ 25, Cytiva, Amersham, UK) in a glass filtration system to avoid plastic contamination. Afterwards, filters were dried at 60 ºC in an oven for 15 min. After drying, filters were deposited on a glass slide and stored until analysis avoiding particle contamination.

2.2.4.5. Raman spectrum treatment

The information about the composition of the analysed particles was obtained by comparing the spectra obtained with the spectra present in the databases used (Section 2.2.1.3). Both databases have a numerical parameter to evaluate the degree of agreement of the analysed spectra with the spectra available in the database. In the case of KnowItAll™, this is the High-Quality Index (HQI), a parameter provided by the software based on the correlation coefficient between the test spectrum and each spectrum in the library, with a range between 0 and 100. PublicSpectra™ uses a percentage of correlation.

2.2.4.6. FESEM analysis

A 2 mL aliquot of river water was filtered on an alumina filter of 0.1 µm pore size (Anodisc™ 25, Cytiva, Amersham, UK) in a glass filtration system to avoid plastic contamination. Afterwards, filters were dried at 60 ºC in an oven for 15 min. After drying, filters were glued to the measurement support with carbon tape. Before analysis, filters were coated with gold to increase their conductivity with a Leica EM SCD500 (Leica Microsystem, Vienna, Austria).

2.2.4.7. Bacteria suspensions

The bacterial suspensions used were prepared from a suspension of the bacterial strain *E.coli* J62 at a concentration of 5.40 x 10^9 CFU mL^{-1} exposed to 0.5 mg L^{-1} $AgNO_3$ during 24 h.

2.3. Results and discussion

2.3.1. Pre-treatment of river water samples

River water contains different forms of carbon, with around 60% present as inorganic carbon, while the rest corresponds to organic carbon, although this distribution could change depending on the river.[35] Inorganic carbon is mainly present as dissolved carbonates (HCO_3^- and CO_3^{2-}), although the presence of particulate carbonates ($CaCO_3$, $MgCO_3$...) or black carbon (soot) cannot be

discarded. The hydrogen carbonate present in river waters originates from the action of the carbon dioxide dissolved in the waters on calcareous minerals from the river basin. Black carbon particles are due to the incomplete combustion of fossil fuels and biomass, appearing in the river waters due to the aerial deposition of these particles on the rivers and transport by run-off waters from the riverbanks.[36,37]

Organic carbon present in rivers includes different substances (proteins, carbohydrates, carboxylic acids, humic and fulvic acids...) grouped together as dissolved organic carbon (DOM), although particulate forms may be also present. In both cases the origin of this organic matter is the degradation of adjacent vegetation and other organisms. On the other hand, microorganisms (bacteria, microalgae...) are also considered as carbon containing particles naturally present in rivers.[38,39] Also, the human contribution due to the discharge of non-treated wastewaters in rivers cannot be neglected.[40,41] The presence of these different forms of carbon in river waters can pose a problem for the detection of microplastics. Firstly, the presence of DOM and dissolved carbonates will have an effect on the increase in the baseline, reducing the detectability of smaller microplastics. On the other hand, microorganisms, insoluble carbonates and black carbon can be misidentified as microplastics because of their carbon content. Therefore, it is necessary to apply some kind of pre-treatment to remove these forms of carbon from the river water samples.

The rivers studied flow through basins which are largely made up of marl, gypsum, limestone, shale and siltstone. Marl and limestone are rocks rich in calcium carbonate ($CaCO_3$), magnesium carbonate ($MgCO_3$) and other types of carbonates. This situation indicates that the waters under study will contain relevant concentrations of inorganic dissolved carbon and the presence of particulate carbonates should not be discarded.[42–52] In this respect, the proportion of carbon in alkaline earth carbonates is low (0.3 - 0.4), which means that only particles larger than ca. 20 µm should theoretically be detected by SP-ICP-MS.

However, particles of this size nebulise with very low efficiency in ICP-MS, which makes their detection very unlikely.

Considering that the main source of dissolved carbon in the samples is carbonate species, a pre-treatment based on the use of nitric acid was selected. Upon acidification, carbonate species are transformed into carbon dioxide and partially released from the solution. Alkaline earth carbonates would also dissolve if present. Due to the oxidant properties of nitric acid, the oxidation of natural organic matter to carbon dioxide would also be promoted, as well as of microorganisms, that would be digested by the acid.

The acid pre-treatment selected was evaluated with 2.22 µm MPs to evaluate their recovery. For this purpose, 2.22 µm MPs were subjected to the two pre-treatments described in Section 2.2.4.3. All samples were analysed by SP-ICP-MS as explained in Section 2.2.1.1. Samples with HNO_3 contents above 10% were diluted before analysis to reduce the concentration of the acid introduced into the instrument. Table 2.4 shows the results obtained from the 2.22 µm MPs subjected to acid pre-treatments. The recovery was calculated as the ratio between the number of particle events measured in suspensions with and without pre-treatment.

The 2.22 µm MPs subjected to pre-treatments using nitric acid concentrations of 10% or lower showed recoveries of 60 - 70%, with no relevant differences due to heating at 100ºC for 5 min, whereas the use of 50% nitric acid reduced recoveries to less than 30%. On the other hand, the pre-treatments had no effect significant effect on the mean size of the particles. When using a pre-treatment with 10% nitric acid, recoveries of ca. 65% were obtained with and without heating. It was decided to select a pre-treatment using 10% nitric acid at room temperature for 24 h.

Once the effect of the acid pre-treatment on the recovery of 2.22 µm MPs was studied, the effect of the river water matrix on the particle recovery and on the removal of dissolved carbonates/organic matter was investigated. For this purpose, a river water sample with a low content of particles was selected (RW07)

and spiked with plastic microparticles (2.22 µm and 3 µm). All the samples were analysed without dilution for 60 s (acquisition time).

Table 2.4. Recovery of microparticles subjected to pre-treatments with nitric acid. Plastic microparticles: 2.22 µm PS (BCR). Mean ± standard deviation (n = 3).

Sample	HNO_3 (% *v/v*)	Baseline intensity (counts)	Mean size (µm)	Number of events	Particle concentration (L^{-1})	Particle recovery (%)
Water	-	8 ± 1	-	1 ± 1	$46x10^2 \pm 12x10^2$	-
2.22 µm MPs	-	14 ± 1	2.12 ± 0.02	1553 ± 50	$313x10^4 \pm 10x10^4$	-
with heating (100ºC 5 min)						
Procedure blank	0.2	6 ± 1	-	4 ± 2	-	-
2.22 µm MPs	0.2	13 ± 2	2.12 ± 0.03	937 ± 90	$189x10^6 \pm 12x10^6$	60
Procedure blank	1	6 ± 1	-	3 ± 1	-	-
2.22 µm MPs	1	14 ± 3	2.12 ± 0.02	1079 ± 84	$218x10^6 \pm 13x10^6$	69
Procedure blank	10	6 ± 1	-	2 ± 2	-	
2.22 µm MPs	10	13 ± 1	2.12 ± 0.02	1026 ± 102	$207x10^6 \pm 9x10^6$	66
Procedure blank	50	6 ± 1	-	1 ± 1	-	
2.22 µm MPs	50	8 ± 2	2.04 ± 0.02	427 ± 23	$86x10^6 \pm 17x10^6$	27
without heating (room temperature, 24h)						
Procedure blank	10	7 ± 2	-	2 ± 1	-	-
2.22 µm MPs	10	13 ± 0	2.20 ± 0.01	1026 ± 21	$220x10^6 \pm 5x10^6$	65

Table 2.5 shows the results obtained from the pre-treatment with 10% nitric acid 24 h at room temperature on river water RW07. As it can be seen, the pre-treatment contributed to decrease the baseline ca. 50%, from 23 to 11 counts, close to the background level of water. This effect can be clearly seen in the time scans from the samples in Figures 2.4(a) and 2.4(b).

This decrease of baseline intensity allowed the reduction of the LOD_{size} from 2.05 µm to 1.42 µm, thus increasing the measurement range. When the sample was spiked with 2.22 µm MPs, the baseline was increased due the high concentration of surfactant in the BCR standard, apparently increasing the LOD_{size}. In any case, a similar reduction of the baseline, from 38 ± 6 to 18 ± 1 counts, was also observed. Regarding the recovery of the spiked particles, recoveries of 66% were achieved for an untreated sample, whereas 76% was obtained for at sample subjected to acid pre-treatment.

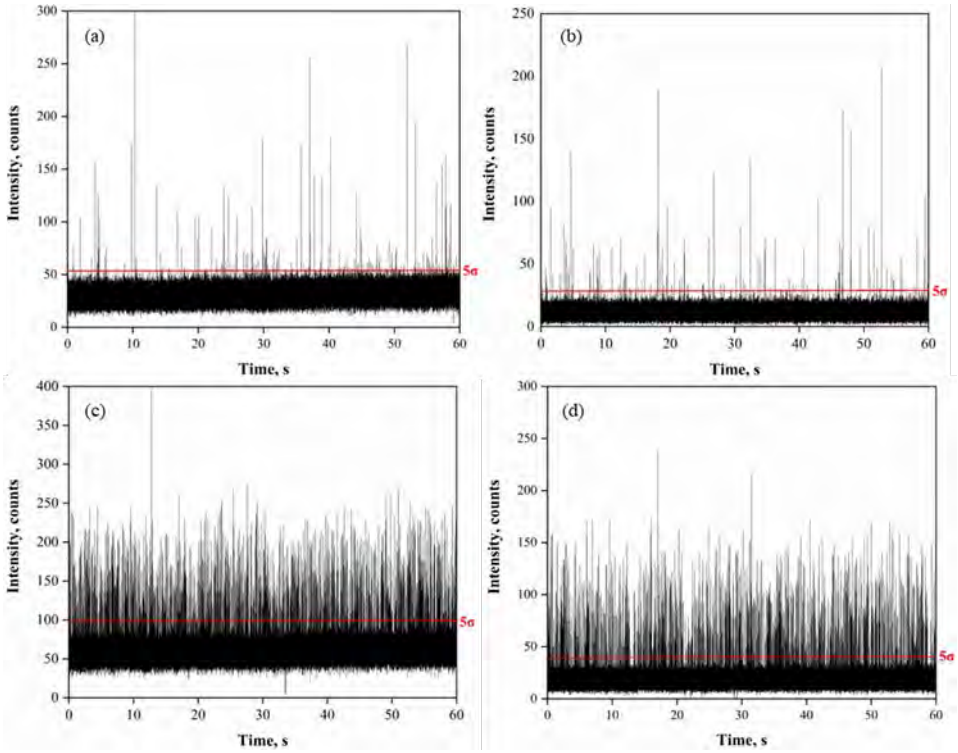

Figure 2.4. SP-ICP-MS time scans corresponding to the original sample RW07 (a) and (b), and spiked with 2.22 µm MPs (c) and (d). In (b) and (d), samples were subjected to acid pre-treatment with 10% nitric acid at room temperature for 24 h. The red line marks the 5σ threshold applied for each sample.

Table 2.5. Baseline reduction and particle recovery of river water samples subjected to pre-treatment with 10% nitric acid. Plastic microparticles: 2.22 µm MPs and 3 µm. River water sample: RW07. Mean ± standard deviation (n = 3). Recovery tests were carried out in duplicate.

Sample	HNO_3 (% *v/v*)	Baseline intensity (counts)	LOD_{size} (µm)	Mean size (µm)	Number of events	Particle concentration (L^{-1})	Particle recovery (%)
Water	-	8 ± 1	-	-	3 ± 1	-	-
Procedure blank	10	7 ± 1	1.29	-	1 ± 1	-	-
RW07	-	23 ± 5	2.05	1.70 ± 0.01	34 ± 3	$26x10^5 \pm 1x10^5$	-
RW07	10	11 ± 0	1.42	2.20 ± 0.01	19 ± 2	$17x10^5 \pm 2x10^5$	-
2.22 µm MPs	-	14 ± 1	-	2.12 ± 0.02	1553 ± 50	$313x10^6 \pm 10x10^6$	-
RW07 + 2.22 µm MPs	-	38 ± 6	2.47	2.54 ± 0.03	1059 ± 49	$227x10^6 \pm 11x10^6$	66
RW07 + 2.22 µm MPs	10	18 ± 1	1.58	2.23 ± 0.01	1216 ± 24	$261x10^6 \pm 5x10^6$	76
3 µm MPs	-	9 ± 0	-	3.41 ± 0.03	1028 ± 100	$220x10^6 \pm 21x10^6$	-
RW07+ 3 µm MPs	-	34 ± 2	2.21	3.41 ± 0.02	655 ± 39	$169x10^6 \pm 19x10^6$	65
RW07+ 3 µm MPs	10	11 ± 0	1.46	3.15 ± 0.03	641 ± 49	$130x10^6 \pm 2x10^6$	64

The observations in Table 2.5 for the 2.22 µm MPs are also valid for the 3 µm MPs. As in the previous case, when applying the pre-treatment on the RW07 with 3 µm MPs, a decrease in the baseline was observed, from 34 ± 2 to 11 ± 0 counts. This situation can be clearly seen in the time scans of the different samples in Figure 2.5. This allowed a LOD_{size} of 1.46 µm to be obtained. The particle recovery was around 65 - 64% and 65 - 62% for the case of RW07 with 3 µm MPs without and after pre-treatment, respectively.

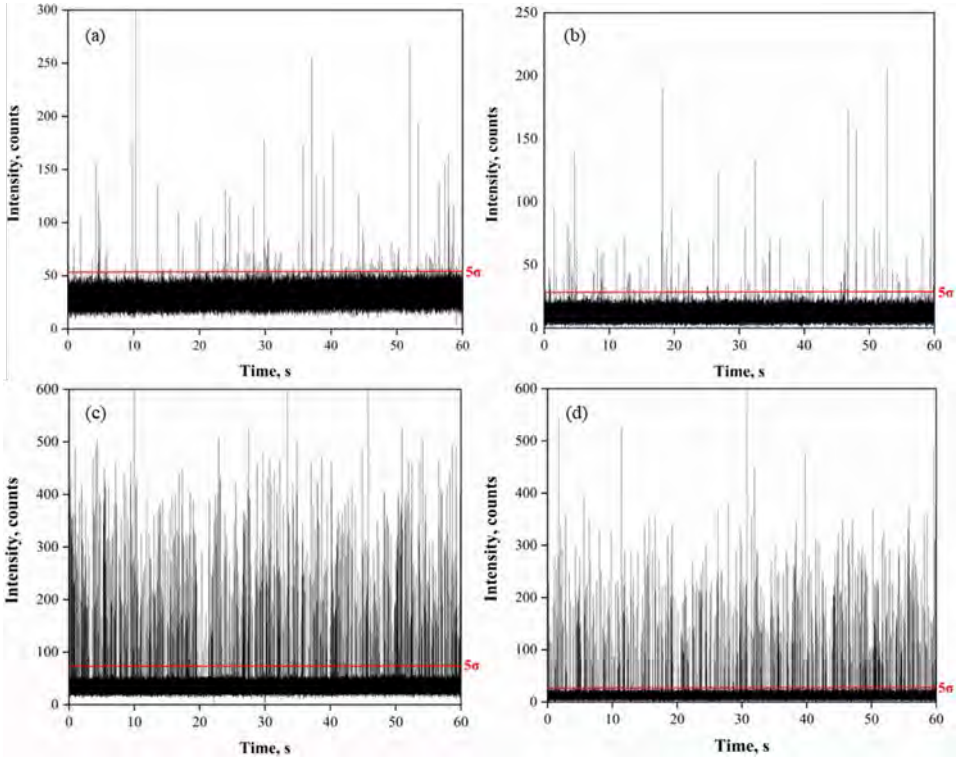

Figure 2.5. SP-ICP-MS time scans corresponding to the original sample RW07 (a) and (b), and spiked with 3 µm MPs (c) and (d). In (b) and (d) samples were subjected to pre-treatment with 10% nitric acid for 24 h. The red line marks the threshold applied for each sample.

The presence of micro-organisms in river water cannot be excluded. Although it was not the rule, the FESEM image in Figure 2.6 shows the presence of bacteria in one of the river water samples analysed. Therefore, the potential detection of microorganisms as carbon containing microparticles was studied. For this purpose, a bacteria suspension exposed to $AgNO_3$ for internal labelling (Section 2.2.4.7) was used. The bacteria were subjected to the acid treatment with 10% nitric acid for 24 h at room temperature and analysed by SP-ICP-MS monitoring ^{13}C and ^{107}Ag. Whereas ^{13}C allows to check if the bacteria themselves could be detected through their carbon content, ^{107}Ag can confirm the presence of intact bacteria in the case of not having been detected by ^{13}C.

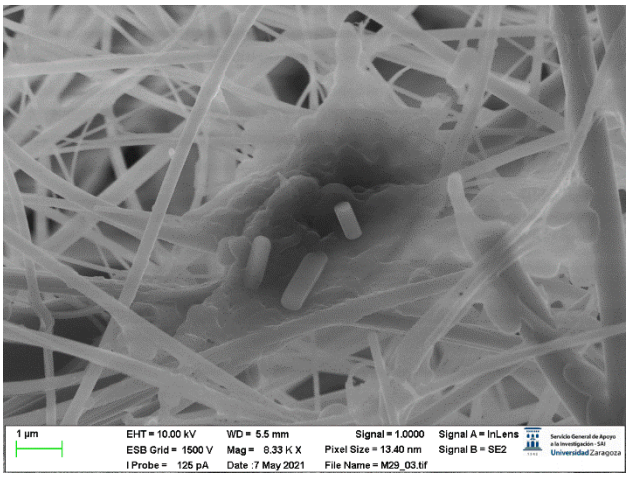

Figure 2.6. FESEM image of bacteria form river water filtered on glass fibre.

Table 2.6 summarises the results of the acidic treatment on *E.coli* suspensions. Suspensions containing 1 x 10^8 CFU mL^{-1} analysed by SP-ICP-MS monitoring ^{107}Ag showed 10281 ± 101 events, whereas fewer than 50 events were recorded using ^{13}C. Regarding the effect of the acid pre-treatment, the number of events detected by ^{107}Ag was 93 ± 8, whereas by monitoring ^{13}C, it decreased from 44 ± 6 to 31 ± 6. The results obtained shows that individual bacteria were hardly detected by ^{13}C, and the recorded events could be bacteria clusters. On the other hand, ^{107}Ag measurements confirm the capacity of the pre-treatment to eliminate > 99% of bacteria, although the remaining events could be due to bacteria clusters. Figure 2.7 shows the time scans of the bacteria analysed by monitoring ^{13}C and ^{107}Ag.

Table 2.6. Results of the acidic treatment on E.coli suspensions analysed by monitoring ^{13}C and ^{107}Ag.

Isotope monitored	**HNO_3 (%*v/v*)**	**Number of events**	**Cell concentration (L^{-1})**
^{107}Ag	-	10281 ± 101	$129x10^4 \pm 1x10^4$
^{107}Ag	10	93 ± 8	$116x10^2 \pm 10x10^2$
^{13}C	-	44 ± 6	$73x10^2 \pm 10x10^2$
^{13}C	10	31 ± 6	$60x10^2 \pm 21x10^2$

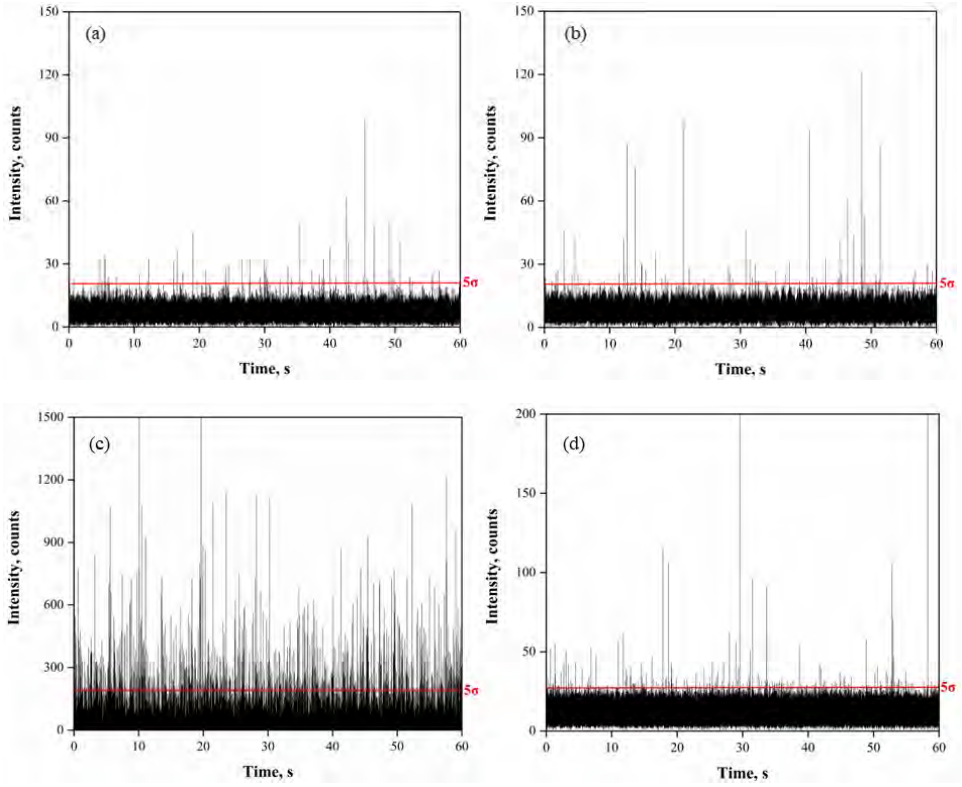

Figure 2.7. SP-ICP-MS time scan obtained from the bacteria suspensions monitoring ^{13}C, (a) and (b), and ^{107}Ag, (c) and (d); without (a) and (c) and with pre-treatment (b) and (d).

2.3.2. Analysis of river water samples by SP-ICP-MS

Table 2.7 shows the results obtained for the direct analysis of the river water samples using the instrumental conditions and procedures described in Sections 2.2.1.1 and 2.2.4.2, respectively. No dilution of the samples was performed. An acquisition time of 60 s was selected. The aim of this analysis was to obtain preliminary information about the presence of carbon containing particles in the samples. All river waters showed higher baseline intensities in comparison with water. This led to an increase in the size detection limits, affecting to the number of particles detected, as well as their size range. Under the measurement conditions the LOD_{size} was 1.25 µm and 3 ± 2 particle events were detected in water.

Table 2.7. Preliminary results of the analysis of river waters by SP-ICP-MS. Total acquisition time: 60 s. Mean ± standard deviation (n = 3).

Sample	Baseline intensity (counts)	BEC (mg L^{-1})	LOD_{size} (µm)	Mean size (µm)	Number of events	Particle concentration (L^{-1})
Water	4 ± 1	15	1.25	-	3 ± 2	-
RW01	14 ± 2	52	1.44	1.37 ± 0.16	38 ± 10	$295x10^4 \pm 32 x10^4$
RW02	13 ± 3	48	1.44	1.56 ± 0.14	40 ± 12	$310x10^4 \pm 25x10^4$
RW03	19 ± 3	71	1.53	2.24 ± 0.16	28 ± 8	$217x10^4 \pm 21x10^4$
RW04	16 ± 2	48	1.48	1.92 ± 0.10	10 ± 3	$109x10^4 \pm 12x10^4$
RW05	17 ± 3	63	1.49	2.12 ± 0.09	28 ± 7	$217x10^4 \pm 15x10^4$
RW06	20 ± 2	75	1.55	1.71 ± 0.19	22 ± 5	$171x10^4 \pm 20x10^4$
RW07	24 ± 3	90	1.63	2.51 ± 0.14	17 ± 6	$132x10^4 \pm 19x10^4$
RW08	18 ± 3	67	1.54	2.28 ± 0.13	15 ± 4	$116x10^4 \pm 26x10^4$
RW09	12 ± 2	45	1.41	2.30 ± 0.13	16 ± 4	$124x10^4 \pm 15x10^4$
RW10	15 ± 1	56	1.47	2.14 ± 0.18	19 ± 8	$147x10^4 \pm 10x10^4$
RW11	12 ± 3	45	1.39	2.30 ± 0.18	13 ± 3	$101x10^4 \pm 9x10^4$
RW12	14 ± 2	52	1.45	2.05 ± 0.08	17 ± 4	$132x10^4 \pm 9x10^4$
RW13	19 ± 2	71	1.51	2.24 ± 0.20	10 ± 5	$78x10^4 \pm 7x10^4$
RW14	16 ± 2	60	1.47	2.38 ± 0.20	27 ± 6	$209x10^4 \pm 19x10^4$
RW15	15 ± 1	56	1.46	2.34 ± 0.02	24 ± 4	$186 x10^4 \pm 13x10^4$
RW16	19 ± 2	71	1.52	1.80 ± 0.16	6 ± 2	$47x10^4 \pm 5x10^4$
RW17	14 ± 2	52	1.46	1.60 ± 0.12	20 ± 4	$155x10^4 \pm 20x10^4$
RW18	15 ± 1	56	1.48	1.60 ± 0.14	19 ± 3	$147x10^4 \pm 27x10^4$
RW19	14 ± 2	52	1.47	2.10 ± 0.15	16 ± 2	$124x10^4 \pm 30x10^4$
RW20	16 ± 2	60	1.49	2.20 ± 0.10	12 ± 2	$93x10^4 \pm 20x10$
RW21	10 ± 2	37	1.35	1.68 ± 0.10	20 ± 3	$155x10^4 \pm 32x10^4$
RW22	8 ± 2	30	1.31	2.21 ± 0.11	18 ± 4	$140x10^4 \pm 16x10^4$
RW23	9 ± 1	34	1.37	1.41 ± 0.18	42 ± 11	$326x10^4 \pm 42x10^4$
RW24	10 ± 3	37	1.37	1.78 ± 0.16	27 ± 10	$209x10^4 \pm 21x10^4$
RW25	7 ± 2	26	1.31	2.01 ± 0.14	43 ± 9	$334x10^4 \pm 44x10^4$
RW26	16 ± 2	60	1.50	2.07 ± 0.09	11 ± 3	$85x10^4 \pm 6x10^4$
RW27	9 ± 1	34	1.35	2.23 ± 0.22	29 ± 6	$225x10^4 \pm 30x10^4$
RW28	8 ± 1	30	1.32	1.52 ± 0.17	16 ± 5	$124x10^4 \pm 10x10^4$

The criterion considered for the detection of particles according to their size was based on 5 times the baseline standard deviation.[53,54] It was applied indistinctly to the calculation of the critical value (or limit of decision), used for processing of the SP-ICP-MS data, and of the size detection limit, used as a figure of merit.[53,54] However, the detection of particles over the critical value, requires a different criterion based on counting statistics.[55] If no particles are detected from a blank, the critical value (X_C^{number}) is 0 and the minimum detection value can be rounded to 3 particle events. If particles are detected in the blank, the expression for α = β = 0.05 and paired measurement (blank subtracted) should be used:[54]

$$S_{C,N} = 2.33\sigma_{N,B} \tag{2.1}$$

where $\sigma_{N,B}$ corresponds to the standard deviation of the number of events detected in the blank.

Whereas the application of the number concentration critical value allows the confirmation of the presence of particles over the size critical value, reporting number concentration results requires recording particle events over a limit of quantification. Under ideal counting conditions where no particles are detected in a blank, the limit of quantification requires counting 100 particles. In such a case, the number concentration limit of quantification is defined by Equation 2.2:[53]

$$LOQ_{number} = \frac{100}{\eta Q_{sam} t_i} \tag{2.2}$$

More complex expressions have been developed for non-ideal blanks number of events, but they will not be considered here.

The net number concentration critical value, calculated from the water blank (3 ± 2) and rounded up, was 5 events. As particle events shown in Table 2.7 correspond to gross counting, the applied critical value was 8 events. In view of the results summarised in Table 2.7, all samples except RW16 would contain carbon bearing particles, although the concentrations shown cannot be considered reliable, as they were below the limit of quantification (LOQ), which was 1.6 x 10^7 L^{-1}.

In a next step, the samples with the highest number of events recorded were selected for a more in-depth analysis (RW01, RW02, RW03, RW05, RW14, RW23, RW24, RW25 and RW27). The selected samples were analysed by SP-ICP-MS without dilution at a total acquisition time of 480 s, the maximum allowable time due to limitations of data storage of the ICP mass spectrometer. Under these conditions, the detection capability of particles increased by a factor of 8, with the aim of exceeding the minimum number of 100 events that allows the quantification of the number concentrations. Moreover, the samples were also analysed after applying the acid pre-treatment discussed in Section 2.2.4.3 to evaluate the reduction of baseline intensities to increase the LOD_{size} as explained in Section 2.3.1. The results are shown in Table 2.8. The results are shown in Table 2.8. In this case, some of the river water samples analysed (marked in bold in Table 2.8), presented a particle concentration higher than the LOQ obtained for this case, which was set at 2.1 x 10^6 L^{-1}.

Samples analysed directly without pre-treatment showed baseline intensities ranging from 18 up to 57 counts, corresponding to BECs from 60 to 190 mg L^{-1}. These results are not directly comparable with those in Table 2.7 because the latter had been obtained previously under conditions of lower sensitivity of the instrument.

Table 2.8. Results from selected river waters analysed by SP-ICP-MS without and with acid pre-treatment (10% HNO_3, 24 h). Total acquisition time: 480 s. Mean ± standard deviation (n = 3).

Sample	Baseline intensity (counts)	BEC (mg L^{-1})	LOD_{size} (µm)	Mean size (µm)	Number of events	Particle concentration (L^{-1})
Water	6 ± 2	26.67	1.26	-	3 ± 2	-
RW01	45 ± 1	150.01	1.72	1.85 ± 0.04	88 ± 10	$188x10^4 \pm 21x10^4$
RW02	41 ± 2	136.67	1.70	1.80 ± 0.09	84 ± 11	$180x10^4 \pm 24x10^4$
RW03	57 ± 2	190.10	1.84	2.36 ± 0.14	45 ± 15	$96x10^4 \pm 31x10^4$
RW05	50 ± 3	166.67	1.82	2.18 ± 0.09	41 ± 16	$88x10^4 \pm 34x10^4$
RW14	46 ± 2	153.33	1.75	2.37 ± 0.10	230 ± 21	**$490x10^4 \pm 45x10^4$**
RW23	30 ± 1	100.05	1.62	1.93 ± 0.02	110 ± 4	**$249x10^4 \pm 9x10^4$**
RW24	18 ± 1	60.10	1.48	2.04 ± 0.01	119 ± 10	**$253x10^4 \pm 21x10^4$**
RW25	27 ± 1	90.20	1.58	1.94 ± 0.04	95 ± 8	$182x10^4 \pm 17x10^4$
RW27	20 ± 2	66.67	1.50	2.13 ± 0.02	91 ± 18	$194x10^4 \pm 39x10^4$
Procedure blank	7 ± 1	23.33	1.25	1.01 ± 0.09	2 ± 2	$28x10^3 \pm 26x10^3$
RW01+10%HNO_3	7 ± 1	23.33	1.28	1.89 ± 0.09	50 ± 8	$106x10^4 \pm 18x10^4$
RW02+10%HNO_3	7 ± 1	23.33	1.26	1.90 ± 0.07	46 ± 5	$97x10^4 \pm 11x10^4$
RW03+10%HNO_3	9 ± 1	30.12	1.33	1.89 ± 0.03	256 ± 37	**$554x10^4 \pm 78x10^4$**
RW05+10%HNO_3	9 ± 1	30.12	1.31	1.86 ± 0.01	214 ± 49	**$470x10^4 \pm 70x10^4$**
RW14+10%HNO_3	8 ± 1	26.67	1.32	1.87 ± 0.07	164 ± 40	**$349x10^4 \pm 84x10^4$**
RW23+10%HNO_3	7 ± 2	23.33	1.25	2.01 ± 0.03	107 ± 11	**$227x10^4 \pm 15x10^4$**
RW24+10%HNO_3	7 ± 1	23.33	1.27	1.85 ± 0.02	104 ± 11	**$221x10^4 \pm 23x10^4$**
RW25+10%HNO_3	6 ± 1	20.00	1.24	1.97 ± 0.04	120 ± 19	**$277x10^4 \pm 37x10^4$**
RW27+10%HNO_3	7 ± 1	23.33	1.27	1.84 ± 0.03	93 ± 10	$197x10^4 \pm 22x10^4$

Under such conditions, size detection limits were affected by the increase in baseline noise, raising from 1.26 up to 1.84 µm. Whereas this increase in size detection limits can be considered not significant from the point of view sizing, it is relevant from the point of view of the number of particles detected. As it can be

seen, even by increasing the total acquisition time, more than 100 particle events were recorded only in three samples (RW14, RW23 and RW24). When the acid pre-treatment was applied, the baselines of all the samples were reduced below 10 counts, reaching in some cases the baseline of the procedure blank (RW01, RW02, RW23, RW24 and RW27). Under such conditions, the best available size detection limits were achieved (ca. 1.25 μm) and hence the best overall detection capability of the technique. Figure 2.8 shows graphically the effect of the pre-treatment of the river water samples and the decrease in the baseline after its application. The positive effect of reducing the baseline intensity is clearly seen in samples RW03 and RW05, in which the number of particles detected increased 5 times after the application of the pre-treatment. In other cases, the number of particles events detected remained similar (RW14, RW23, RW24, RW25, RW27), within a range of ± 25%, whereas samples RW01 and RW02, showed a 50% reduction in the number of events previously detected in the untreated samples. These lower recoveries may be due to the characteristics of the river waters or the particles detected. In any case the recovery studies performed with the PS microparticle standard should be considered an approximation to the problem, because the nature and stabilization of the particles in the river waters samples is not the same in the standards, which are stabilized by different amounts of surfactants.

In any case, the results shown in Table 2.8 confirm the presence of carbon containing particles in all the samples. From a quantitative point of view, the number concentrations reported for samples RW03, RW05, RW14, RW23, RW24 and RW25, analysed after acid pre-treatment, as well as those from samples RW14, RW23 and RW24, analysed directly, could be considered valid, as they were calculated from the detection of more than 100 events, the minimum limit of quantifications in the counting process. However, considering that just microparticles in a narrow size range were detected by the SP-ICP-MS method developed, these number concentrations should be considered as semi-quantitative minimum values.

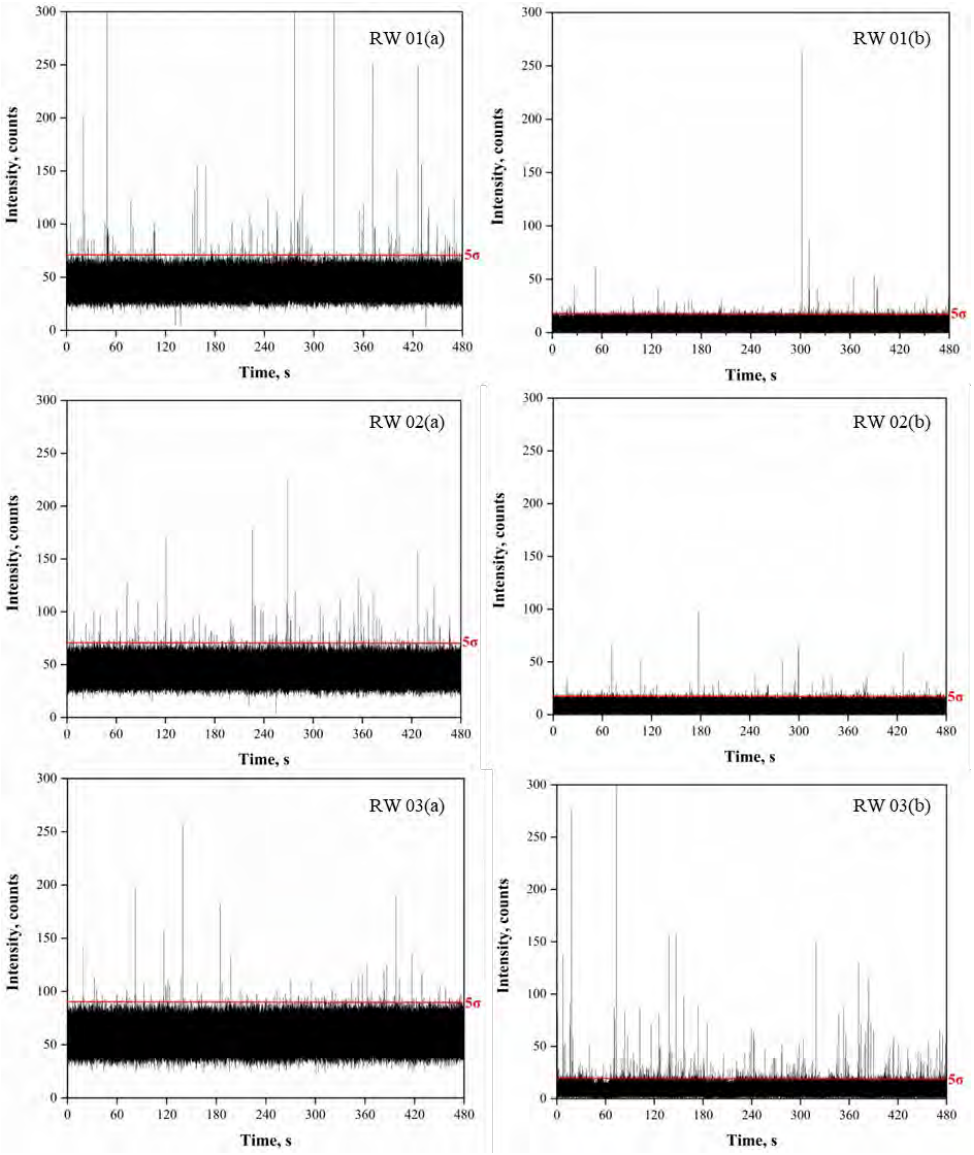

Figure 2.8. Time scans of river water samples analysed by SP-ICP-MS. (a) Direct analyses of untreated river waters samples and (b) after acid pre-treatment.

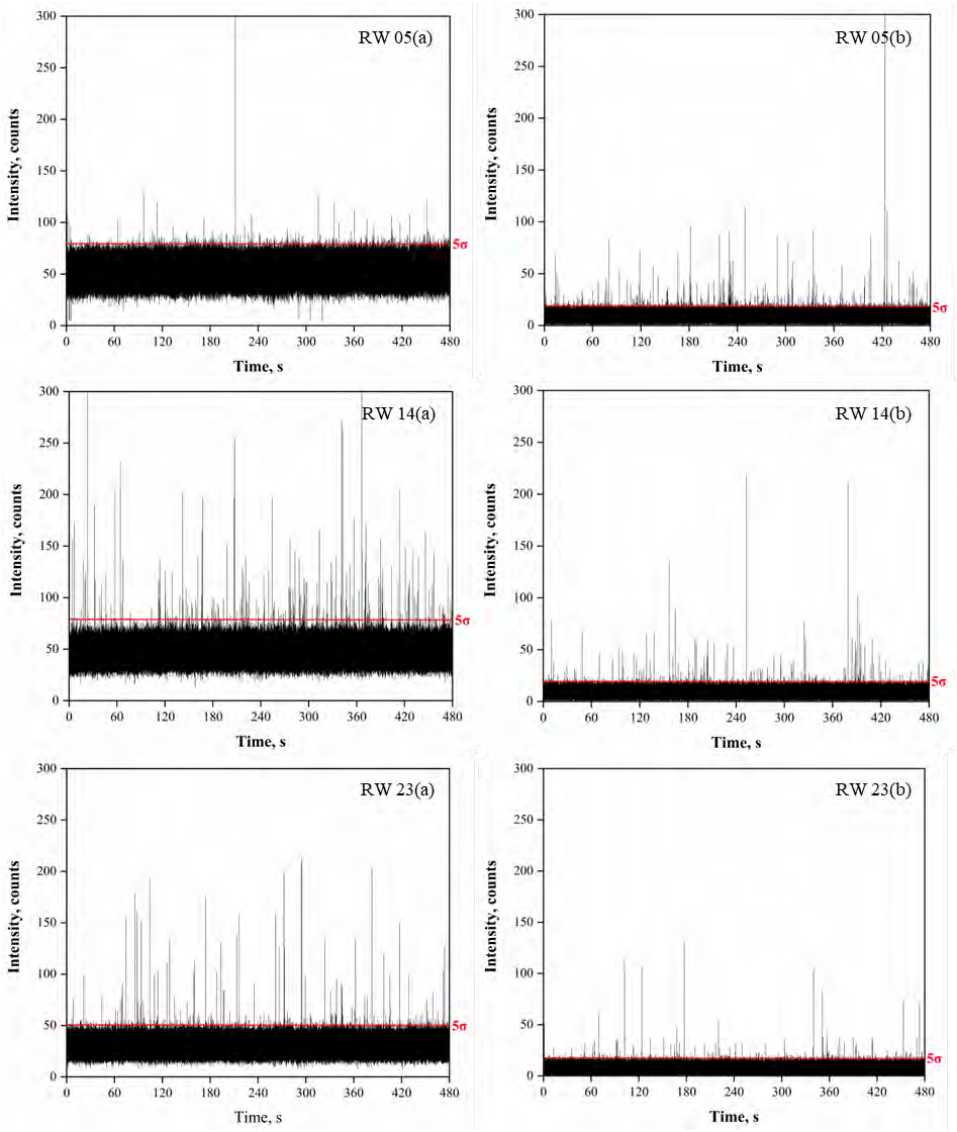

Figure 2.8 (cont.). Time scans of river water samples analysed by SP-ICP-MS. (a) Direct analyses of untreated river waters samples and (b) after acid pre-treatment.

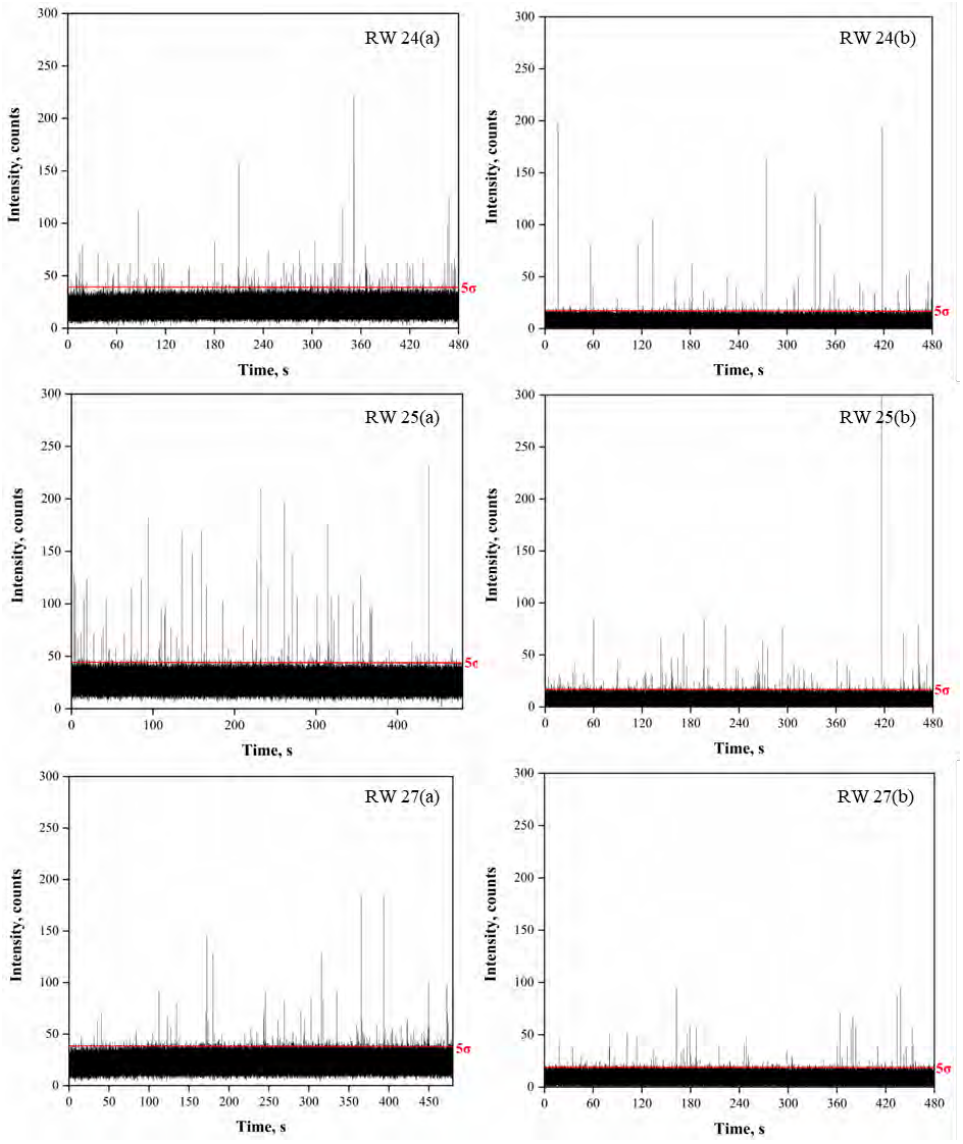

Figure 2.8 (cont.). Time scans of river water samples analysed by SP-ICP-MS. (a) Direct analyses of untreated river waters samples and (b) after acid pre-treatment.

2.3.3. Analysis of river water samples by electron and Raman microscopy

The analysis by SP-ICP-MS only confirmed the presence of carbon containing particles in the samples analysed. Because SP-ICP-MS has been used as screening technique, the identification of these carbon containing particles as microplastics requires the use of more a selective technique, capable of providing information about the specific chemical composition, on the particle-by-particle basis. FESEM in combination with EDX was selected to obtain information about the morphology of carbon containing particles, whereas Raman microscopy [56] was used to confirm the presence of microplastics.

2.3.3.1. FESEM-EDX

Three river water samples with the highest number of events detected in SP-ICP-MS (RW02, RW03 and RW25) were chosen to visualize particle according to their composition by FESEM.

River waters have a disparity of particles, whether carbonates or clays among other natural particles. This makes it even more difficult to identify a particle as a plastic. Therefore, to be able to identify a particle as a potential plastic using FESEM, it was necessary to have the information available provided through the elemental spectra obtained by EDX. Plastics just with a hydrocarbon backbone (e.g., PE, PP, PS, PIB) will show a high intensity carbon peak (K-line), whereas those with functional groups containing oxygen (e.g., PET, Nylon) or any other heteroatom (e.g., PVC, PVF, PAN) will show additional peaks corresponding to those elements.[57] In any case, the use of EDX for plastic identification cannot be considered conclusive, since a black carbon particle from combustion process would produce a spectrum with a K-line only.

Sample preparation was carried out as described in Section 2.2.4.6. Figure 2.9 shows some of the particles visualised by FESEM in the river water samples, which could be considered as potential plastic particles due to the presence of carbon and/or oxygen in their EDX spectra.

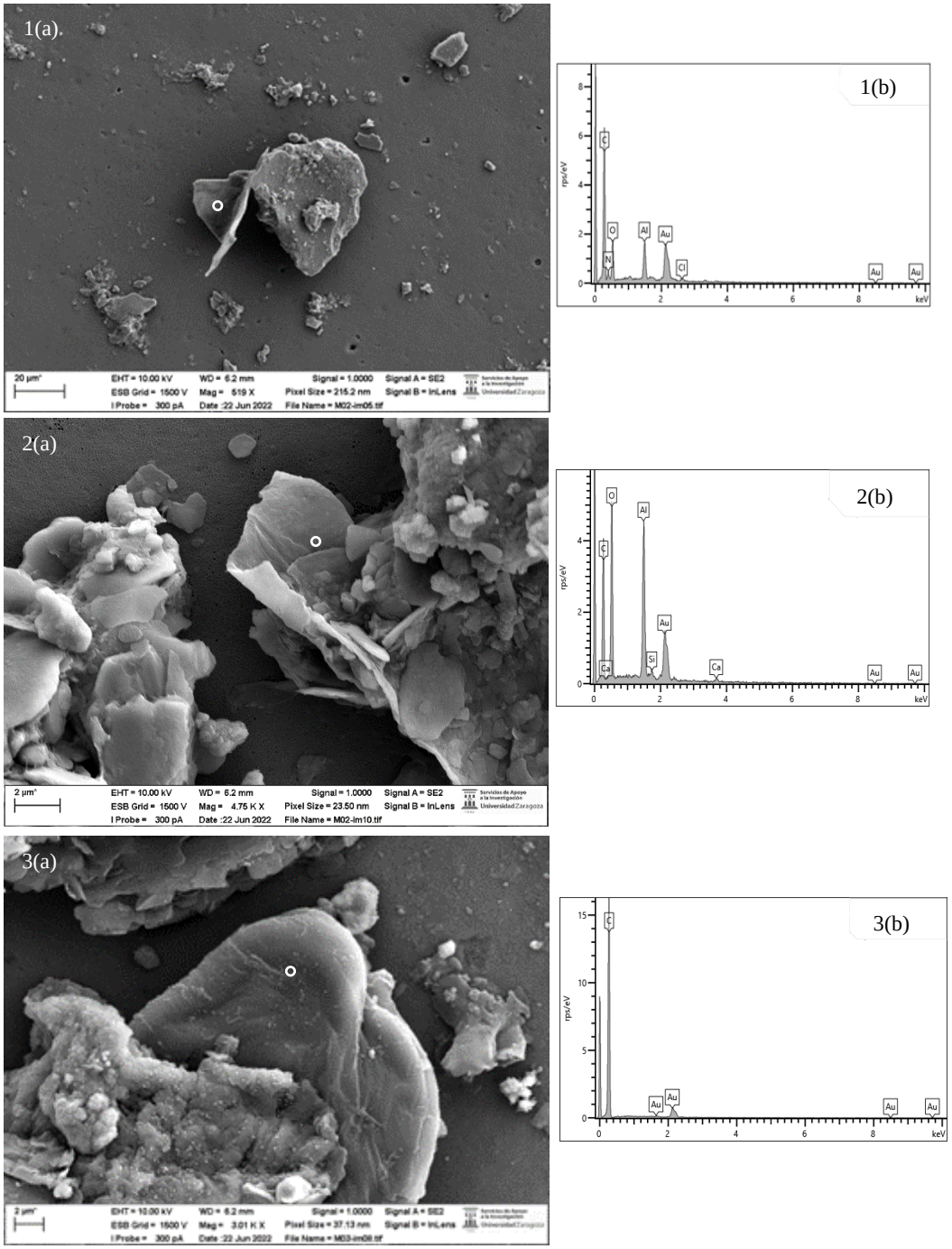

Figure 2.9. FESEM images and EDX spectra corresponding to the particles visualised in the river water samples. (a) FESEM image and (b) EDX spectrum.

The particles observed by FESEM (Figure 2.9) are mostly grouped together, a situation which makes their visualisation and analysis difficult, as the possible spectra to be obtained will be influenced by the elements of the neighbouring particles. Concerning the potential plastic particles visualised in Figure 2.9, they showed in all cases irregular shapes. This situation makes sense because the particles obtained by the degradation of macroplastics do not tend to present spherical shapes.[58] The sizes of the visualised particles (Figure 2.9), were approximately 28 µm, 5 µm and 19 µm, for 1(a), 2(a) and 3(a), respectively.

All the spectra obtained by EDX for all the particles analysed, showed the presence of Au and Al, because of the coating applied and the alumina filter used, respectively. All the spectra obtained for the particles in Figure 2.9, showed a significant carbon peak, although in the case of 3(b) no other element was recorded. In the case of spectrum 1(b), the presence of carbon and oxygen only is seen indicating another type of particle. In spectrum 2(b), as in the previous case, the peaks of carbon and oxygen are observed, accompanied by small peaks corresponding to calcium. The presence of the latter spectrum casts doubt on whether this particle is a plastic and or a carbonate.

Consequently, in order to verify whether particles visualised by FESEM correspond to plastic particles or not, it is necessary to apply a technique providing information about the chemical structure. For this purpose, Raman microscopy was used.

2.3.3.2. Raman microscopy

River waters samples containing higher number concentration of particles detected by SP-ICP-MS were selected for Raman microscopy analysis (RW1, RW2, RW3, RW23 and RW25). Sample preparation was carried out as described in Section 2.2.4.4. About 20 particles from each filter were selected by visual inspection and the individual Raman spectra were recorded. The spectra were greatly influenced by a high level of background, in some cases by the fluorescence of the particles and by the degradation of some particles after the

laser irradiation. Figure 2.10 shows images of some of the particles in the river water samples analysed by Raman microscopy.

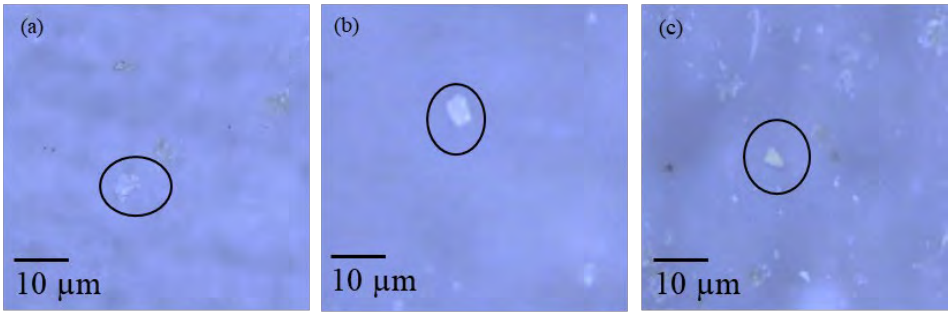

Figure 2.10. Images obtained with Raman microscopy from river waters samples. (a) Particle analysed RW01, (b) particle analysed RW02 and (c) particle analysed RW03. The black circles marked to the particles analysed by Raman spectrocopy.

The spectra obtained were analysed using the Raman database KnowItAll™ and the PublicSpectra™ (Section 2.2.4.5) to obtain the most probable composition of the particle. Table 2.9 shows the results obtained for plastic particles. At the same time, Figure 2.11 shows the spectra of these particles obtained from the Raman microscopy analysis and the spectra from the databases to be compared. The results presented show some differences, this situation is due to the spectra recorded in each of the databases. Table 2.10 summarises the composition of all the particles analysed.

*Table 2.9. Composition of plastic particles detected after processing the spectra (KnowItAll™ and PublicSpectra™) obtained by Raman microscopy. * Non-viable database proposals.*

	KnowitAll™		PublicSpectra™	
Sample	**Composition**	**HQI**	**Composition**	**Correlation %**
RW01_08	Polylactic acid	76.2	Polylactic acid	60.4
RW01_10	PMMA	73.9	Nylon	72.1
RW01_11	Polylactic acid	64.7	Polylactic acid	69.7
RW01_12	Polylactic acid	65.3	Polylactic acid	72.2
RW01_13	PMMA	65.1	Nylon	82.5
RW02_01	HDPE	90.6	-*	
RW02_13	Polylactic acid	66.4	Polylactic acid	48.0
RW02_19	HDPE	91.4	Nylon	92.9
RW03_05	PVA	73.1	PMMA	62.4
RW03_07	Polylactic acid	78.4	Polylactic acid	83.6
RW03_09	PE	90.9	PE	93.2
RW23_04	PVA	66.8	Melamine resin	56.7
RW23_05	PE	85.2	PMP	96.1
RW23_15	PP	89.5	PMP	97.1
RW23_20	PP	87.7	PMP	93.1
RW25_08	PMMA	87.9	-*	

The number of plastic particles determined in each of the river water samples varies depending on the sample. The number of plastic particles analysed in the samples of RW01, RW02, RW03, RW23 and RW25 was 5, 3, 3, 4 and 1, respectively. This makes it possible to evaluate the average percentage of plastic particles analysed in the river water to be ca. 15%. Within this percentage, mainly plastic particles of polylactic acid, PMMA, HDPE, PE, PVA and PP were found. The remaining percentage of particles (85%) consisted of wool fibre, cellulose, and various minerals (quartz, silica, pyrophyllite, muscovite, zeolite and malaquite, among others) and other types of particles.

*Table 2.10. Composition of non-plastic particles detected after processing the spectra (KnowItAll™ and PublicSpectra™) obtained by Raman microscopy. *Non-viable database proposals.*

	KnowitAll™		PublicSpectra™	
Sample	**Composition**	**HQI**	**Composition**	**Correlation %**
RW01_01	Wool Fiber	77.1	-*	
RW01_02	Zeolite	69.5	-*	
RW01_03	Quartz	65.2	Quartz	59.3
RW01_04	Zeolite	62.8	-*	
RW01_05	Cellulose	71.6	Cellulose	64.9
RW01_06	Zeolite	81.0	-*	
RW01_07	Zeolite	72.4	-*	
RW01_09	Cellulose	72.1	Cellulose	74.1
RW01_14	Quartz	61.2	Quartz	57.2
RW01_15	Cellulose	81.2	-*	
RW01_16	Wool Fiber	90.3	-*	
RW01_17	Quartz	68.1	-*	
RW01_18	Cellulose	80.6		71.6
RW01_19	Cellulose	80.3	Cellulose	72.9
RW01_20	Cellulose	51.2	Cellulose	45.3
RW02_02	Zeolite	68.5	Quartz	44.2
RW02_03	Zeolite	76.3	-*	
RW02_04	Malaquite	62.1	Quartz	57.4
RW02_05	Malaquite	62.1	Glass	53.8
RW02_06	Malaquite	69.6	Glass	51.2
RW02_07	Malaquite	60.0	-*	
RW02_08	Zeolite	77.6	Glass	32.7
RW02_09	Muscovite	73.1	Quartz	38.6
RW02_10	Quartz	88.1	Quartz	41.4
RW02_11	Zeolite	77.0	Cellulose	31.5
RW02_12	Malaquite	67.4	-*	
RW02_14	Zeolite	59.7	-*	
RW02_15	Zeolite	58.7	-*	
RW02_16	Cellulose	80.6	Cellulose	31.5

*Table 2.10 (cont). Composition of non-plastic particles detected after processing the spectra (KnowItAll™ and PublicSpectra™) obtained by micro-Raman. * Non-viable database proposals.*

	KnowitAll™		PublicSpectra™	
Sample	**Composition**	**HQI**	**Composition**	**Correlation %**
RW02_17	Malaquite	64.59	-*	
RW02_18	Malaquite	68.4	Quartz	42.10
RW02_20	Malaquite	79.13	Glass	58.58
RW03_01	Zeolite	81.68	-*	
RW03_02	Zeolite	79.12	-*	
RW03_03	Zeolite	78.06	Quartz	50.9
RW03_04	Zeolite	80.32	Quartz	51.5
RW03_06	Zeolite	81.47	-*	
RW03_08	Quartz	68.94	Quartz	80.36
RW03_10	Zeolite	79.82	-*	
RW03_11	Muscovite	81.11	-*	
RW03_12	Muscovite	70.98	-*	
RW03_13	Zeolite	83.04	-*	
RW03_14	Quartz	58.74	-*	
RW03_15	Zeolite	76.45	-*	
RW03_16	Zeolite	79.40	Cellulose	46.84
RW03_17	Quartz	59.61	-*	
RW03_18	Zeolite	65.67	Cellulose	68.5
RW03_19	Quartz	50.02	Quartz	27.5
RW03_20	Zeolite	74.38	-*	
RW23_01	Pirophilite	77.01	Quartz	55.32
RW23_02	Malaquite	75.36	Glass	57.48
RW23_03	Hair	77.91	-*	
RW23_06	Dolomite	57.06	-* -*	
RW23_07	Zeolite	73.67	-*	
RW23_08	Muscovite	73.36	-*	
RW23_09	Zeolite	67.32	Glass	35.41
RW23_10	Zeolite	64.49	Quartz	50.99

*Table 2.10 (cont). Composition of non-plastic particles detected after processing the spectra (KnowItAll™ and PublicSpectra™) obtained by Raman microscopy. * Non-viable database proposals.*

	KnowitAll™		PublicSpectra™	
Sample	**Composition**	**HQI**	**Composition**	**Correlation %**
RW23_11	Muscovite	81.1	Glass	
RW23_12	Zeolite	62.9	-*	
RW23_13	Dolomite	62.7	-*	
RW23_14	Zeolite	73.8	-*	
RW23_16	Zeolite	77.6	-*	
RW23_17	Zeolite	61.7	Quartz	52.0
RW23_18	Zeolite	68.4	Quartz	38.2
RW23_19	Zirconium Oxide	65.0	Glass	53.3
RW25_01	Quartz	72.4	Quartz	33.7
RW25_02	Quartz	91.8	Quartz	41.1
RW25_03	Dolomite	78.6	Quartz	64.8
RW25_04	Zeolite	70.4	-*	
RW25_05	Zirconium Oxide	67.9	Glass	33.3
RW25_06	Muscovite	78.5	-*	
RW25_07	Zeolite	57.3	-*	
RW25_09	Zeolite	65.7	-*	
RW25_10	Pirophilite	79.4	Quartz	40.0
RW25_11	Zeolite	74.9	-*	
RW25_12	Muscovite	86.3	Quartz	39.8
RW25_13	Zeolite	60.7	-*	
RW25_14	Muscovita	76.3	Glass	36.2
RW25_15	Muscovita	78.5	Quartz	45.8
RW25_16	Muscovita	70.8	Quartz	36.5
RW25_17	Zeolite	71.6	-*	
RW25_18	Pirophilite	80.8	Quartz	37.4
RW25_19	Biotite	69.4	Quartz	42.1
RW25_20	Muscovita	81.3	Quartz	52.1

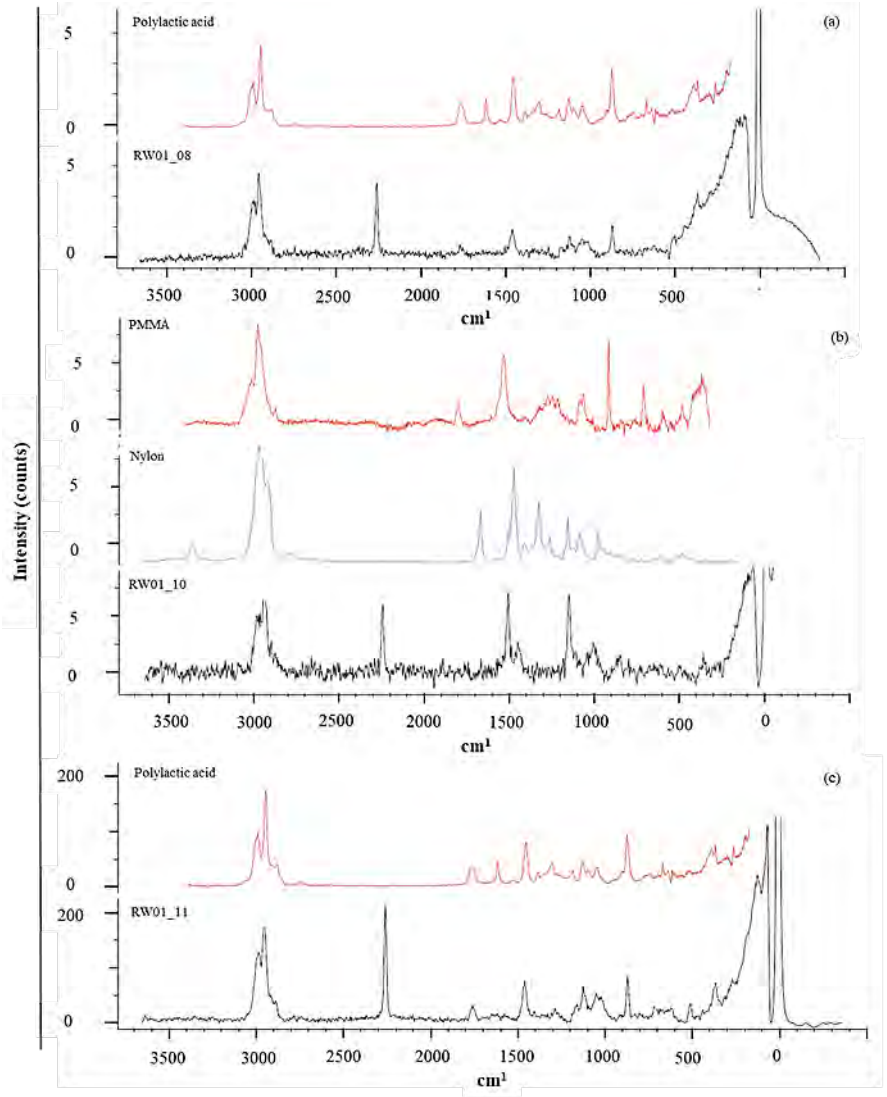

Figure 2.11. Raman spectra of the plastic particles presented in Table 2.9. In black, spectra obtained from the analysis of the river water particles. In red, and blue, spectra of the most probable compositions provided by the databases (KnowItAll™ and PublicSpectra™, respectively).

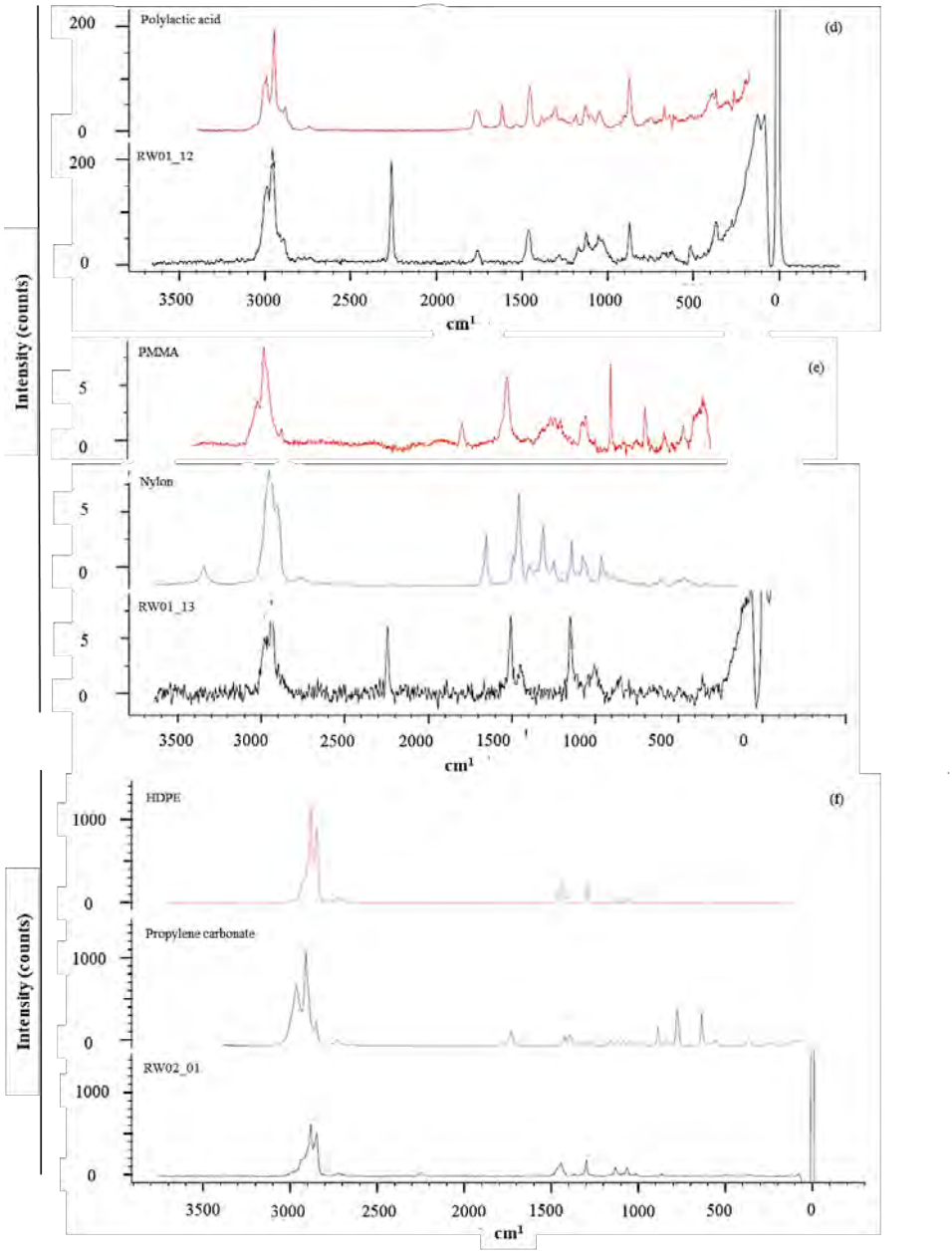

Figure 2.11 (cont). Raman spectra of the plastic particles presented in Table 2.9. In black, spectra obtained from the analysis of the river water particles. In red, and blue, spectra of the most probable compositions provided by the databases (KnowItAll™ and PublicSpectra™, respectively).

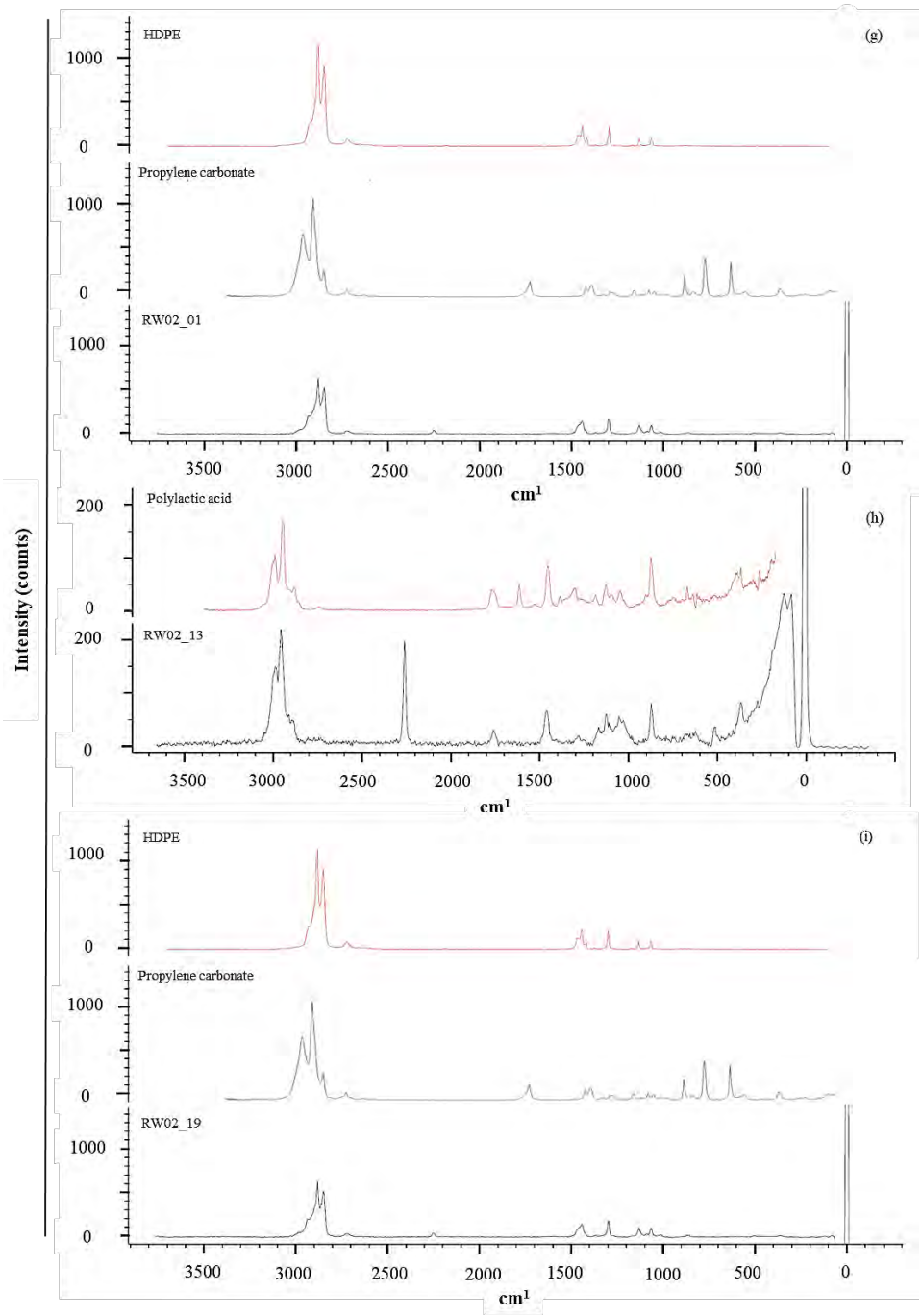

Figure 2.11 (cont). Raman spectra of the plastic particles presented in Table 2.9. In black, spectra obtained from the analysis of the river water particles. In red, and blue, spectra of the most probable compositions provided by the databases (KnowItAll™ and PublicSpectra™, respectively).

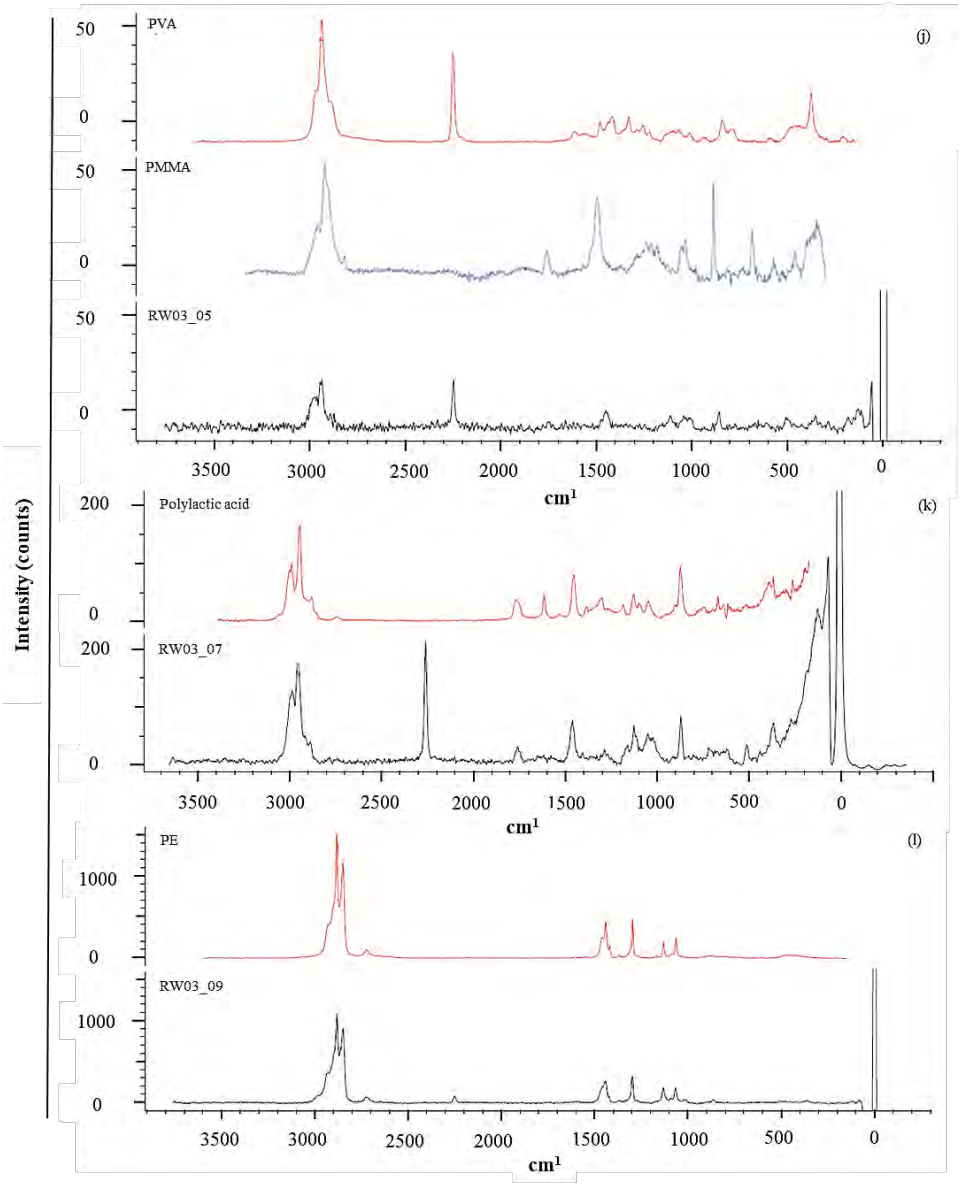

Figure 2.11 (cont). Raman spectra of the plastic particles presented in Table 2.9. In black, spectra obtained from the analysis of the river water particles. In red, and blue, spectra of the most probable compositions provided by the databases (KnowItAll™ and PublicSpectra™, respectively).

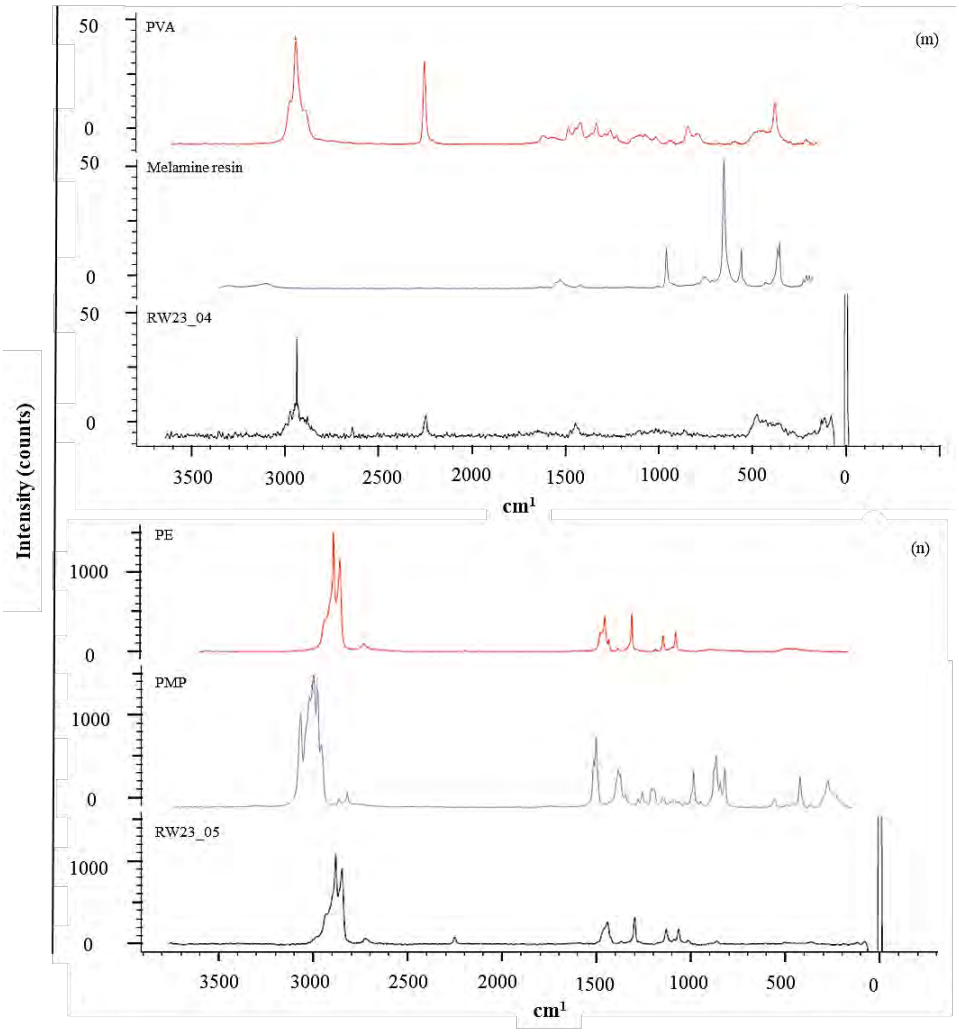

Figure 2.11 (cont). Raman spectra of the plastic particles presented in Table 2.9. In black, spectra obtained from the analysis of the river water particles. In red, and blue, spectra of the most probable compositions provided by the databases (KnowItAll™ and PublicSpectra™, respectively).

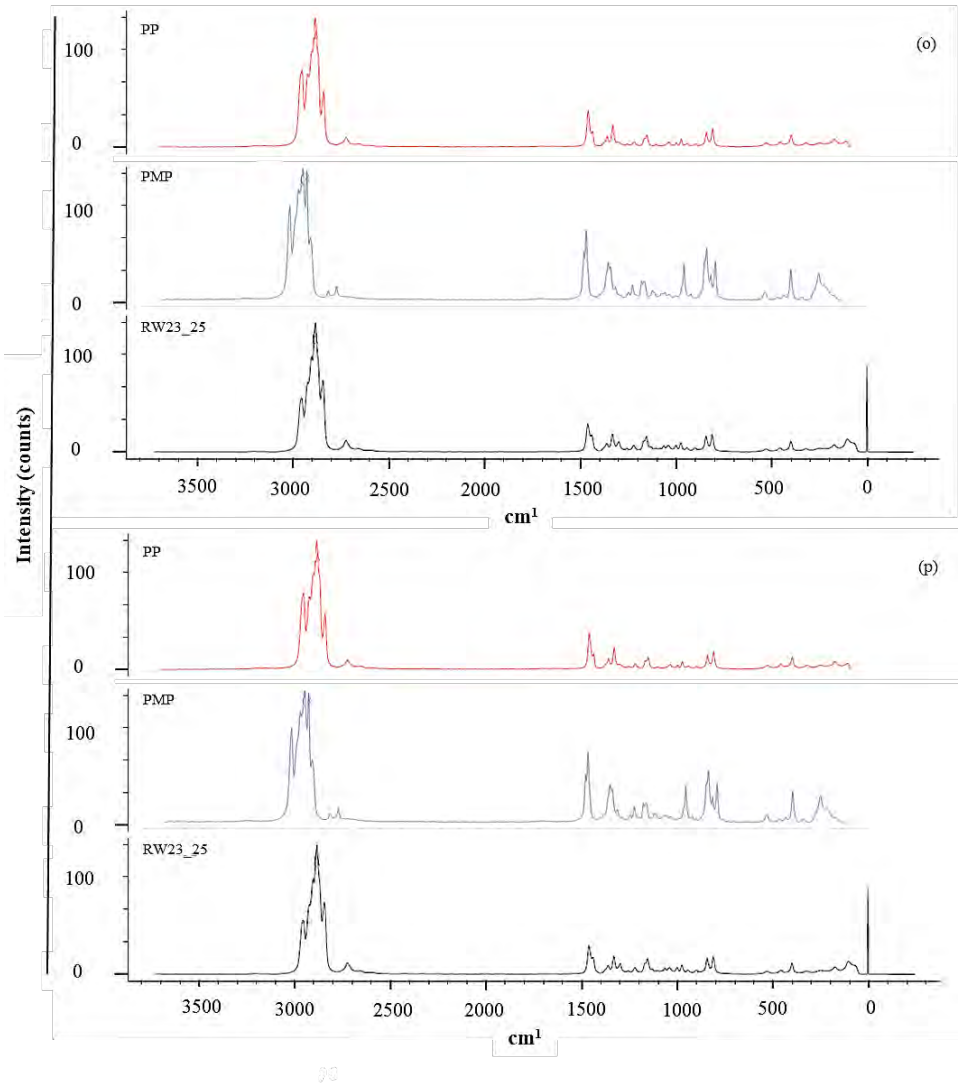

Figure 2.11 (cont). Raman spectra of the plastic particles presented in Table 2.9. In black, spectra obtained from the analysis of the river water particles. In red, and blue, spectra of the most probable compositions provided by the databases (KnowItAll™ and PublicSpectra™, respectively).

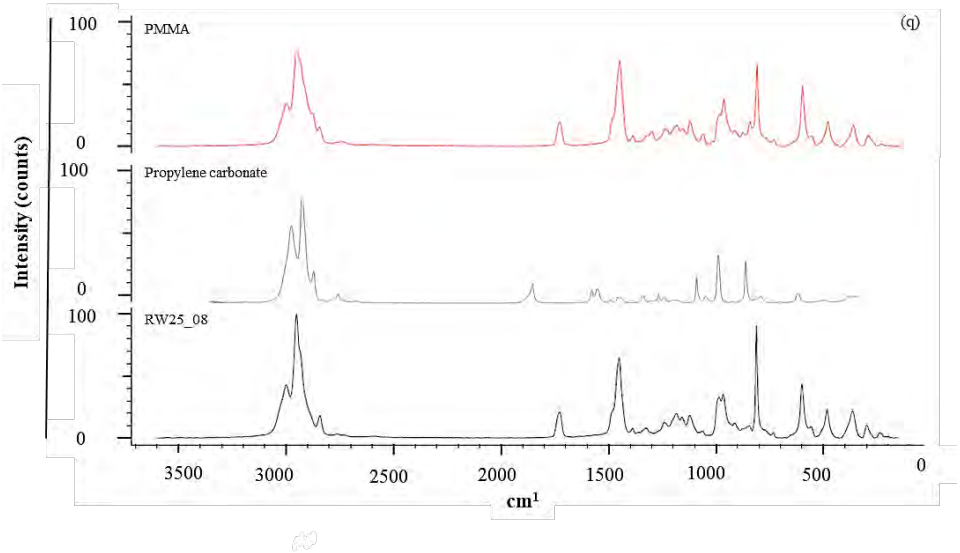

Figure 2.11. Raman spectra of the plastic particles presented in Table 2.9. In black, spectra obtained from the analysis of the river water particles. In red, and blue, spectra of the most probable compositions provided by the databases (KnowItAll™ and PublicSpectra™, respectively).

The presence of plastic particles in water may be due to their different origins. Polylactic acid is used in many consumers goods industry (food packaging or hygiene products among others)[59,60] and in agriculture.[60,61] The use of this type of biopolymers is on the rise, among other reasons, due to the European directive 2019/904,[19] which prohibits the introduction of single-use plastic products on the market. On the other hand, PMMA is used fibre optics and protection among others uses. In the case of HDPE, it is used to produce containers, buckets, signage, sprockets, water and sewer pipes. PVA is used as a polymeric adhesive. As well PP and PE were also detected, these ones are used in consumer goods.[62]

2.4. Conclusions

The application of SP-ICP-MS to the detection of plastic particles in environmental samples, such as river water is a novelty. Indeed, the techniques routinely used in this type of samples are based on the use of microscopy (FTIR, Raman or optical) and gas chromatography in combination with mass spectrometry. Moreover, particle detection focuses on the search for particles of larger sizes than those detected by SP-ICP-MS. The use of SP-ICP-MS as a technique for the detection of plastic microparticles in environmental samples opens the possibility of lowering the particle size range, while reducing the analysis time.

SP-ICP-MS used for rapid screening of samples for microplastics in combination with Raman microscopy and/or GC-MS techniques can be a suitable analytical platform for the monitoring of plastic pollution in the environment. SP-ICP-MS by itself allows semi-quantitative data to be obtained. The application of an acid pre-treatment improves the detectability of the plastic microparticles present in the samples due to the reduction of their dissolved carbon content and, consequently, allows a decrease of the LOD_{size} to values close to those obtained for ultrapure water. The presence of other carbon-containing particles, such as carbonates or micro-organisms, would not be detected by SP-ICP-MS due to their low carbon content, and would require much larger particles than those efficiently nebulised in ICP-MS. In any case, the nitric acid pre-treatment would contribute to the dissolution of carbonate microparticles and the degradation of microorganisms. Only black carbon microparticles, originating from atmospheric emissions, would be detected by SP-ICP-MS.

In this study, the presence of plastic microparticles was detected in all the river water samples analysed and the SP-ICP-MS results were validated using Raman microscopy and FESEM. The fact of detecting particles at all sampling points out, indicates pollution, with no differences between the rivers of the northern and southern side of the Pyrenees.

2.5. References

1. Su, L., Xiong, X., Zhang, Y., Wu, C., Xu, X., Sun, C. & Shi, H. Global transportation of plastics and microplastics: A critical review of pathways and influences. Science of the Total Environment, 831, 154884 (2022).

2. Petersen, F. & Hubbart, J. A. The occurrence and transport of microplastics: The state of the science. Science of The Total Environment, 758, 143936 (2021).

3. Hoellein, T. J. & Rochman, C. M. The "plastic cycle": a watershed-scale model of plastic pools and fluxes. Frontiers in Ecology ant the Environment, 19, 176–183 (2021).

4. Horton, A. A. & Dixon, S. J. Microplastics: An introduction to environmental transport processes. Wiley Interdisciplinary Reviews: Water, 5, 1268 (2018).

5. Bianco, A. & Passananti, M. Atmospheric Micro and Nanoplastics: An Enormous Microscopic Problem. Sustainability, 12, 7327 (2020).

6. Li, J., Yang, D., Li, L., Jabeen, K. & Shi, H. Microplastics in commercial bivalves from China. Environmental Pollution, 207, 190–195 (2015).

7. Rochman, C. M., Tahir, A., Williams, S. L., Baxa, D. v., Lam, R., Miller, J. T., Teh, F. C., Werorilangi, S. & Teh, S. J. Anthropogenic debris in seafood: Plastic debris and fibers from textiles in fish and bivalves sold for human consumption. Scientific Reports, 5, 1–10 (2015).

8. Waite, H. R., Donnelly, M. J. & Walters, L. J. Quantity and types of microplastics in the organic tissues of the eastern oyster Crassostrea virginica and Atlantic mud crab Panopeus herbstii from a Florida estuary. Marine Pollution Bulletin, 129, 179–185 (2018).

9. Nakao, S., Ozaki, A., Yamazaki, K., Masumoto, K., Nakatani, T. & Sakiyama, T. Microplastics contamination in tidelands of the Osaka Bay area in western Japan. Water and Environment Journal, 34, 474–488 (2019).

10. Renzi, M. & Blašković, A. Litter & microplastics features in table salts from marine origin: Italian versus Croatian brands. Marine Pollution Bulletin, 135, 62–68 (2018).

11. Kim, J.-S., Lee, H.-J., Kim, S.-K. & Kim, H.-J. Global Pattern of Microplastics (MPs) in Commercial Food-Grade Salts: Sea Salt as an Indicator of Seawater MP Pollution. Environmental Science & Technology, 52, 12819–12828 (2018).

12. Karami, A., Golieskardi, A., Keong Choo, C., Larat, V., Galloway, T. S. & Salamatinia, B. The presence of microplastics in commercial salts from different countries. Scientific Reports, 7, 1–11 (2017).

13. Winkler, A., Santo, N., Ortenzi, M. A., Bolzoni, E., Bacchetta, R. & Tremolada, P. Does mechanical stress cause microplastic release from plastic water bottles? Water Research, 166, 115082 (2019).

14. Zuccarello, P., Ferrante, M., Cristaldi, A., Copat, C., Grasso, A., Sangregorio, D., Fiore, M. & Oliveri Conti, G. Reply for comment on "Exposure to microplastics (<10 μm) associated to plastic bottles mineral water consumption: The first quantitative study by Zuccarello et al. [Water Research 157 (2019) 365–371]". Water Research, 166, 115077 (2019).

15. Schwabl, P., Köppel, S., Königshofer, P., Bucsics, T., Trauner, M., Reiberger, T. & Liebmann, B. Detection of Various Microplastics in Human Stool. Annals of Internal Medicine, 171, 453–457 (2019).

16. Ragusa, A., Svelato, A., Santacroce, C., Catalano, P., Notarstefano, V., Carnevali, O., Papa, F., Rongioletti, M. C. A., Baiocco, F., Draghi, S., D'Amore, E., Rinaldo, D., Matta, M. & Giorgini, E. Plasticenta: First evidence of microplastics in human placenta. Environment International, 146, 106274 (2021).

17. Enfrin, M., Dumée, L. F. & Lee, J. Nano/microplastics in water and wastewater treatment processes – Origin, impact and potential solutions. Water Research, 161, 621–638 (2019).

18. D'Avignon, G., Gregory-Eaves, I. & Ricciardi, A. Microplastics in lakes and rivers: an issue of emerging significance to limnology. Environmental Reviews, 30, 228–244 (2022).

19. European Council. Directive (Eu) 2019/904 of the European Parliament and of the Council of 5 June 2019 on the reduction of the impact of certain plastic products on the environment. 1–19 (2019).

20. Liu, J., Yang, Y., An, L., Liu, Q. & Ding, J. The Value of China's Legislation on Plastic Pollution Prevention in 2020. Bulletin of Environmental Contamination and Toxicology, 108, 601–608 (2022).

21. Codification, C. Single-use Plastics Prohibition Regulations Règlement interdisant les plastiques à usage unique. Canada Gazette Part II, V, (2022).

22. Environmental Protection, E. The Environmental Protection (Plastic Straws, Cotton Buds and Stirrers) (England) Regulations 2020. UK Draft Legislation 62, (2020).

23. Cordova, M. R., Nurhati, I. S., Shiomoto, A., Hatanaka, K., Saville, R. & Riani, E. Spatiotemporal macro debris and microplastic variations linked to domestic waste and textile industry in the supercritical Citarum River, Indonesia. Marine Pollution Bulltin, 175, 113338 (2022).

24. Winkler, A., Antonioli, D., Masseroni, A., Chiarcos, R., Laus, M. & Tremolada, P. Following the fate of microplastic in four abiotic and biotic matrices along the Ticino River (North Italy). Science of the Total Environment, 823, 153638 (2022).

25. Pol, W., Żmijewska, A., Stasińska, E. & Zieliński, P. Spatial-Temporal Distribution of microplastics in lowland rivers flowing through two cities (Ne-Poland). Water, Air & Soil Pollution, 233, 140 (2022).

26. Yuan, W., Christie-Oleza, J. A., Xu, E. G., Li, J., Zhang, H., Wang, W., Lin, L., Zhang, W. & Yang, Y. Environmental fate of microplastics in the world's third-largest river: Basin-wide investigation and microplastic community analysis. Water Research, 210, 118002 (2022).

27. Devereux, R., Westhead, E. K., Jayaratne, R. & Newport, D. Microplastic abundance in the Thames River during the New Year period. Marine Pollution Bulletin, 177, 113534 (2022).

28. Zhdanov, I., Lokhov, A., Belesov, A., Kozhevnikov, A., Pakhomova, S., Berezina, A., Frolova, N., Kotova, E., Leshchev, A., Wang, X., Zavialov, P. & Yakushev, E. Assessment of seasonal variability of input of microplastics from the Northern Dvina River to the Arctic Ocean. Marine Pollution Bulletin, 175, 113370 (2022).

29. Treilles, R., Gasperi, J., Tramoy, R., Dris, R., Gallard, A., Partibane, C. & Tassin, B. Microplastic and microfiber fluxes in the Seine River: Flood events versus dry periods. Science of the Total Environment, 805, (2022).

30. Sá, B., Pais, J., Antunes, J., Pequeno, J., Pires, A. & Sobral, P. Seasonal Abundance and Distribution Patterns of Microplastics in the Lis River, Portugal. Sustainability, 14, 1–18 (2022).

31. Laermanns, H., Reifferscheid, G., Kruse, J., Földi, C., Dierkes, G., Schaefer, D., Scherer, C., Bogner, C. & Stock, F. Microplastic in Water and Sediments at the Confluence of the Elbe and Mulde Rivers in Germany. Frontiers in Environmental Science, 9, 1–11 (2021).

32. de Carvalho, A. R., Garcia, F., Riem-Galliano, L., Tudesque, L., Albignac, M., ter Halle, A. & Cucherousset, J. Urbanization and hydrological conditions drive the spatial and temporal variability of microplastic pollution in the Garonne River. Science of the Total Environment, 769, (2021).

33. Water and Environmental Health Research Group (University of Zaragoza) in collaboration with IPREM CNRS. Tecnologías innovadoras para diagnóstico, prevención y eliminación de contaminantes emergentes (antibióticos) de las aguas del territorio POCTEFA (Programa Interreg-POCTEFA 2014-2020). (2020).

34. Moles, S., Gozzo, S., Ormad, M. P., Mosteo, R., Gómez, J., Laborda, F. & Szpunar, J. Long-Term Study of Antibiotic Presence in Ebro River Basin (Spain): Identification of the Emission Sources. Water, 14, 1–16 (2022).

35. Gwenaël Abril, H. E. B. D. M. F. V. B. Carbonate dissolution in the turbid and eutrophic Loire estuary. Marine Ecology Progress Series, 259, 129–138 (2003).

36. Ali, S. S., Elsamahy, T., Koutra, E., Kornaros, M., El-Sheekh, M., Abdelkarim, E. A., Zhu, D. & Sun, J. Degradation of conventional plastic wastes in the environment: A review on current status of knowledge and future perspectives of disposal. Science of The Total Environment, 771, 144719 (2021).

37. Li, P., Lai, Y., Li, Q., Dong, L., Tan, Z., Yu, S., Chen, Y., Sharma, V. K., Liu, J. & Jiang, G. Total Organic Carbon as a Quantitative Index of Micro- and Nano-Plastic Pollution. Analytical Chemistry, 94, 740–747 (2022).

38. López, A. D. F., Fabiani, M., Lassalle, V. L., Spetter, C. V. & Severini, M. D. F. Critical review of the characteristics, interactions, and toxicity of micro/nanomaterials pollutants in aquatic environments. Marine Pollution Bulltin, 174, 113276 (2022).

39. Yu, Y., Mo, W. Y. & Luukkonen, T. Adsorption behaviour and interaction of organic micropollutants with nano and microplastics – A review. Science of the Total Environment, 797, 149140 (2021).

40. Butman, D. E., Wilson, H. F., Barnes, R. T., Xenopoulos, M. A. & Raymond, P. A. Increased mobilization of aged carbon to rivers by human disturbance. Nature Geoscience, 8, 112–116 (2015).

41. Wohl, E., Hall, R. O., Lininger, K. B., Sutfin, N. A. & Walters, D. M. Carbon dynamics of river corridors and the effects of human alterations. Ecological Monographs, 87, 379–409 (2017).

42. Territorial, D. Plan hidrológico del río Ebro desde el río Martín hasta su desembocadura. (2008).

43. Confederación Hidrográfica del Ebro (CHE). Plan hidrológico del río Gállego. (2007).

44. Confederación Hidrográfica del Ebro (CHE). Plan hidrológico del río Noguera Ribargorzana. (2007).

45. Confederación Hidrográfica del Ebro (CHE). Plan hidrológico del río Aragón. (2008).

46. Confederación Hidrográfica del Ebro (CHE). Plan hidrológico del río Ega. (2008).

47. Confederación Hidrográfica del Ebro (CHE). Plan hidrológico del río Arga. (2008).

48. Confederación Hidrográfica del Ebro (CHE). Plan hidrológico del río Garona. (2008).

49. Confederación Hidrográfica del Ebro (CHE). Plan hidrológico del río Alcanadre. (2008).

50. Confederación Hidrográfica del Ebro (CHE). Plan hidrológico del río Cinca. (2008).

51. Confederación Hidrográfica del Ebro (CHE). Plan hidrológico del río Segre. (2008).

52. Confederación Hidrográfica del Ebro (CHE). Plan hidrológico del río Arba. (2008).

53. Laborda, F., Gimenez-Ingalaturre, A. C., Bolea, E. & Castillo, J. R. About detectability and limits of detection in single particle inductively coupled plasma mass spectrometry. Spectrochimica Acta Part B: Atomic Spectroscopy, 169, 105883 (2020).

54. Laborda, F., Gimenez-Ingalaturre, A. C., Bolea, E. & Castillo, J. R. Single particle inductively coupled plasma mass spectrometry as screening tool for detection of particles. Spectrochimica Acta Part B: Atomic Spectroscopy, 159, 105654 (2019).

55. Currie, L. A. Limits for Qualitative Detection and Quantitative Determination Application to Radiochemistry. Analytical Chemistry, 40, 586–593 (1968).

56. Lu, J., Xue, Q., Bai, H. & Wang, N. Design of a confocal micro-Raman spectroscopy system and research on microplastics detection. Applied Optics, 60, 8375 (2021).

57. Steve Lampman. Characterization and failure analysis of plastics. (2003).

58. Tong, H., Zhong, X., Duan, Z., Yi, X., Cheng, F., Xu, W. & Yang, X. Micro- and nanoplastics released from biodegradable and conventional plastics during degradation: Formation, aging factors, and toxicity. Science of the Total Environment, 833, 155275 (2022).

59. Azevedo, A. G., Barros, C., Miranda, S., Machado, A. V., Castro, O., Silva, B., Saraiva, M., Silva, A. S., Pastrana, L., Carneiro, O. S. & Cerqueira, M. A. Active Flexible Films for Food Packaging: A Review. Polymers, 14, 2442 (2022).

60. Ranakoti, L., Gangil, B., Mishra, S. K., Singh, T., Sharma, S., Ilyas, R. A. & El-Khatib, S. Critical Review on Polylactic Acid: Properties, Structure, Processing, Biocomposites, and Nanocomposites. Materials, 15, 4312 (2022).

61. Wanner, P. Plastic in agricultural soils – A global risk for groundwater systems and drinking water supplies? – A review. Chemosphere, 264, 128453 (2021).

62. Andrady, A.L. & Neal, M.A. Applications and societal benefits of plastics. Philosophical Transactions of the Royal Society B: Biological Sciences, 364, 1977–1984 (2009).

3. Adsorption of emerging pollutants on plastic particles

3.1. Introduction

3.1.1. Plastic particles as a Trojan horse for emerging pollutants

The presence of nano- and microplastics in the environment, due to their abundance and size, is a threat due to their potential ecotoxicity but also because of their capacity to act as vectors of pollutants for their uptake by aquatic organisms, a phenomenon known as "Trojan horse" effect.[1–5] Plastics can act as vectors of endogenous and exogenous pollutants in the environment. Endogenous pollutants are substances released from the plastics themselves, whereas exogenous pollutants are substances already present in the environment.

Plastics contain additives added to provide or reinforce the inherent properties of the plastics. Among the most frequently added additives to plastics are phthalates (plasticizers), bisphenol A (plasticizers; antioxidant; stabilizer), nonylphenols (plasticizers; antioxidant; surfactants) and flame retardants (reduce the rate of combustion). In general, these substances are not chemically bound to the polymer matrix, so they can be released and absorbed by other organisms or other plastics.[4]

The group of exogenous substances includes substances such as heavy metals,[6,7] persistent organic pollutants (POPs)[8] or pharmaceutical products.[9,10] Within the group of heavy metals that are found in the environment and that show the greatest affinity for plastics are cadmium, lead, bromine, iron oxides, copper, zinc, cobalt, nickel, and arsenic.[6,7,11] In the case of POPs, the pollutants most frequently present are polycyclic aromatic hydrocarbons (PAHs), polychlorinated biphenyls (PCBs) and pesticides.[2,3,8,11] In the group of pharmaceutical products, substances such as antibiotics (amoxicillin, sulfadiazine or tetracycline),[9,10] analgesics (paracetamol)[12] or gadolinium-based contrast agents,[13] can be found among others.

3.1.2. Plastics and health risk

The presence of plastics has already been reported in most trophic levels, such as zooplankton, marine fauna, soil fauna, terrestrial animals, and even humans.[14,15] Living organisms are exposed to plastics by various routes such as inhalation, dermal contact, and ingestion, being the latter one of the most important routes.[16]

When ingesting plastics, most living organisms eliminate them through defecation. Currently it is estimated that a human being consumes around 39,000 - 52,000 plastic particles per year.[16] However, sometimes plastics can pass through the intestinal wall and be translocated to other tissues. In addition, when the plastic is ingested, it remains in the stomach for a period, during which the presence of gastrointestinal fluids can favour the desorption of the attached contaminants and promote their bioavailability to living organisms.[1–5] Due to these issues, the potential health risks due to plastics are mainly focused on oxidative stress, metabolic disorders, immunity disruption, neurotoxicity, reproductive toxicity, and carcinogenicity.[16,17]

3.1.3. Factors influencing the sorption of pollutants by microplastics

The sorption by nano- and microplastics of different pollutants is largely due to the properties of nano- and microplastics, the characteristics of the pollutants and the environmental conditions in which both substances are found.

In the case of nano- and microplastics, the factors that influence sorption are the type of polymer, particle size and degree of ageing, among others. The various polymers manufactured have different characteristics related to surface charge, surface area or the presence of functional groups, which will influence the degree of sorption of contaminants. At the same time, the reduction of particle size favours the increase of sorption rates, as the area to volume ratio related to surface area increases. This is one of the parameters to be considered when determining the extent of the risk. It is also necessary to consider the degree of ageing of the plastics, as plastics show an increase in the concentration of some

polycyclic aromatic hydrocarbons (PAHs) on microplastics as well as an increase in the formation of functional groups.[4,18–20]

About the characteristics of the pollutants that will affect sorption, the presence of functional groups, hydrophobicity and concentration are the most important. Plastics are hydrophobic particles, which favours the sorption of organic pollutants, but the presence of oxygen-containing functional groups decreases this fact. On the other hand, increasing the concentration of the pollutant favours the sorption rate.[4,18–20]

The medium in which both the plastic and the pollutant are found will be a decisive factor in sorption. pH of the medium plays an important role in the interaction of both substances, as it can promote or suppress electrostatic repulsion, promote the dissociation of neutral molecules or favour adsorption. The presence of dissolved organic matter (DOM) in turn can modify the surface properties of plastics, such as the stability of the dispersion. The effect of salinity will depend on the degree of electrostatic interaction or the ion exchange mechanism of the sorption process. [4,18–20]

3.1.4. Interaction between plastics and pollutants

The interaction between plastics and pollutants takes place through the sorption process. In the sorption process, chemical species present in a fluid phase (air or water, among others) adhere to a solid phase (surface or bulk) such as plastics. Sorption includes both absorption and adsorption.

Absorption occurs by chemical action between a contaminant and the plastic (sorbent), where molecules penetrate and are retained within the plastic due to the action of Van der Waals forces. Absorption is usually dependent on the hydrophobicity of the sorbent chemistry, the properties of the solid phase and the surface to volume ratio of the solids. In the case of adsorption, the contaminants remain at the interface between the liquid and the solid phase. In this case, adsorption occurs due to the action of ionic interactions, Van der Waals forces and

steric or covalent bonds. In general, most of the interactions between organic pollutants and plastics are mainly adsorption based. [4,18,20]

3.1.5 Gadolinium-based contrast agents (GBCAs)

Gadolinium-based contrast agents (GBCAs) have been used in magnetic resonance imaging (MRI) for over 30 years. It is estimated that 10 million of doses are administered annually in the world. The use of these substances is due to the paramagnetic properties of gadolinium (Gd^{3+}) when chelated.[21,22] There are several types of GBCAs which can be divided into linear and macrocyclic depending on their chemical structures. Linear GBCAs are characterised by a polyamino-carboxylic acid molecule that surrounds Gd^{3+} partially, while macrocyclic contrast agents have a polyamino ring that fully surrounds Gd^{3+}. They are classified according to their electric charge as ionic and non-ionic (Table 3.1). [23]

Table 3.1. Classification of some of the most used GBCAs classified according to their chemical structure and charge.[24]

Brand Name	Chemical Name	Structure
Magnevist®	Gadopentetate	Linear-ionic
MultiHance®	Gadobenate	Linear-ionic
Omniscan®	Gadodiamide	Linear-nonionic
Dotarem Clariscan®	Gadoterate	Macrocyclic-ionic
ProHance®	Gadoteridol	Macrocyclic-nonionic
Gadavist®	Gadobutrol	Macrocyclic-nonionic
Eovist®	Gadoxetate	Linear-ionic

In general, these products are administered intravenous injection and excreted via the kidneys without major problems. However, several studies have shown that they can accumulate in various tissues (bone,[25] skin,[26] liver [27] and brain[28]). Different studies have confirmed this fact, but no clear clinical evidence of adverse effects is available. Nevertheless, some international medical agencies, such as the European Medicines Agency,[29] have banned the use of some contrast

agents, in particular linear ones, because they have a greater capacity to be retained in the brain.

The aim of the research described in this chapter was to study the adsorption on plastic particles of emerging pollutants, such as GBCAs under different environmental conditions. For this purpose, different GBCAs and model and environmental nanoplastics have been evaluated. Moreover, nanoplastics and natural colloids were compared as adsorbents of GBCAs. The experimental design considered a wide range of environmental conditions, including ionic strength and pH of the media.

3.2. Experimental

3.2.1. Instrumentation

An Agilent 7900 ICP-MS (Tokyo, Japan) was used for the quantification of Gd. ^{157}Gd was monitored for this purpose. Default instrumental and data acquisition parameters are listed in Table 3.1.

Table 3.1. Default instrumental and data acquisition parameters for ICP-MS.

Instrumental parameters	
RF power	1550W
Argon gas flow rate	
Plasma	1.5 L min^{-1}
Auxiliary	0.9 L min^{-1}
Nebuliser	1.10 L min^{-1}
Sample flow rate	0.3 mL min^{-1}
Isotope monitored	^{157}Gd

Dynamic light scattering (DLS) was used to determine the size of ENPTs in the initial suspension. Vasco Flex model of nanoparticle size analyser (Cordouan Technology, Pessac, France) was used to perform the measurements.

An ICP-OES iCAP 6500 (Thermo, Walthman, MA) was used for the analysis of the natural colloid suspension obtained in the Section 3.2.3.1.

A Cary 630 FTIR Spectrometer (Agilent, Tokyo, Japan) was used for the identification of plastics.

3.2.2 Standards

Dotarem® (net charge -1) 0.5 mmol mL^{-1} (Guerbet, Villepinte, France), Omniscan® (net charge 0) 0.5 mmol mL^{-1} (GE Healthcare, Cork, Ireland) and Multihance® (net charge -2) 0.5 mmol mL^{-1}(Bracco Diagnostics Inc, Singen, Germany) were the gadolinium-based products selected for the essays. Gadolinium (Gd^{3+}) solutions were prepared from a standards stock solution of 1000 mg L^{-1} (Sigma, St. Louis, MO). 65% HNO_3 (Merck, Darmstadt, Germany).

Sodium borate decahydrate ($Na_2[B_4O_5(OH)_4]\cdot 8H_2O$), magnesium chloride ($MgCl_2$), calcium chloride ($CaCl_2$), sodium bicarbonate ($NaHCO_3$), sodium chloride (NaCl), sodium sulphate (Na_2SO_4), potassium chloride (KCl) and potassium bromide (KBr), used for the preparation of the media were purchased from Sigma (St. Louis, MO). Ultrapure water was obtained from a Milli-Q system (Molsheim, France).

The ICP-Ms calibration standard was prepared from the 100 mg L^{-1} rare earth elements standard (Ce, Er, Gd, La, Nd, Sm, Tb, Tm, Yb, Dy, Eu, Ho, Lu, Pr, Sc, Th, U, Y) from Inorganic Ventures (Christiansburg, VA). 0.5 mg L^{-1} Tl standard (Sigma, St. Louis, MO) was used as the stock solution of internal standard. For the control of the oxides, Ba, Ce and Nd standards (Sigma, St. Louis, MO) were used. All the dilutions were made with 2% (*v/v*) HNO_3.

3.2.3. Procedures

3.2.3.1. Adsorbent preparation

Model nanoplastics (NPTs). The NPTs used (PS22) were made of polystyrene (PS) and were synthesised without the presence of additives (surfactants, bactericides, or metals). The synthesis, described elsewhere,[30] was carried out by a soap-free emulsion copolymerisation process using APS as initiator. The NPTs dispersed in water were purified by centrifugation and the aggregates were removed by filtration.

Environmental nanoplastics (ENPTs). The elaboration of ENPTs was based on the protocol developed by El Hadri *et al.*[31] from plastics collected on beaches of the French Atlantic coast. The preparation of the nanoplastics started with the reduction of the size of the collected plastics (size > 1 mm). This step was carried out using a blade grinder, and resulted in a primary powder. The next step consisted in the fragmentation of this primary powder by means of a planetary ball mill Pulverisette 7 (Fritsch, Idar-Oberstein, Germany). The grinding process was based on 10 grinding steps, each consisting of 3 min of grinding and 6 min of rest, with a speed of 450 rpm. This process was repeated 6 times. The first grinding step was carried out under dry conditions, the subsequent steps were carried out using ethanol (2 mL) as dispersant. Once the steps were completed, the suspension obtained was dried to remove ethanol. Subsequently, water was added to the powder to obtain the nanoparticle suspension. The amount of water to be added depended on the amount of powder obtained. The water suspension was sonicated for 5 min and filtered through filter paper of >1 μm. This process was repeated at least 10 times until an off-white suspension was obtained.

Natural colloids. The sediments used to obtain the colloids were collected in the Gallocanta lagoon, Spain. The protocol developed by Navratilova *et al.*[32] was followed for the colloid extraction. For the extraction of the initial colloids, it was first necessary to perform a wet sieving (< 63 μm), to remove larger particles. The product obtained was collected and frozen for subsequent lyophilisation (CRIOS, Cryotec, Saint-Gély-du-Fesc, France). After lyophilisation, 4 g of

sediment was suspended in 40 mL of water. This suspension was shaken for 21 h and then centrifuged at 3233 rpm for 50 min (Eppendorf 5804R, Hamburg, Germany). After centrifugation, the supernatant was removed and replaced with water and then vortexed for 30 s, followed by 10 min of sonication, and finally shaken for 24 h. Then, it was centrifuged again for 6 min at 1957 rpm, after which the supernatant was removed and replaced by water. For the final extraction of the colloids, the process of agitation (30 s vortex, 10 min sonication and 1h agitation) and centrifugation (6 min at 1957 rpm) was carried out 16 times, the supernatant being removed after each centrifugation and collected in a glass container. The supernatant was kept refrigerated.

3.2.3.2. Preparation of the test media

Three different media were used for the experiments (Carbonate-borate buffer, sea water and hard water). Carbonate-borate buffer solution contained $NaHCO_3$ at 0.3 mM and $Na_2[B_4O_5(OH)_4]$ $8H_2O$ (Borax) at 0.8 mM (IS = 0.004 M). Hard water (HW) solution contained $MgCl_2$ at 6.2 mM, $CaCl_2$ at 266 mM and $NaHCO_3$ at 267 mM (IS = 1.08 M). Sea water (SW) was prepared with NaCl, $MgCl_2$, Na_2SO_4, $CaCl_2$, KCl, $NaHCO_3$ and KBr at concentration of 419 mM, 54.6 mM, 28.8 mM, 10.4 mM, 9.33 mM, 2.41 mM, and 0.878 mM (IS = 0.7 M), respectively. All media were prepared in water.

3.2.3.3. Characterization of adsorbents

The NPT PS22 had a particle size of 333 ± 40 nm, a raspberry shape, particle surface functionality of 57 COOH groups per nm^2 and particle surface area of 348 191 nm^2. Their characterization was described carried elsewhere.[33]

The particle size of ENPTs were measured by DLS. The values ranged from 100 to 500 nm. The concentration of ENPT suspension was 34 ± 1 mg L^{-1}. It was measured by weight differences after freeze-drying. The composition of the nanoplastics was polypropylene, low-density polyethylene (LDPE) and high-density polyethylene (HDPE). They were determined by analysis of the macroplastics used to obtain the nanoplastics using a FTIR.

The particle size of the colloids was measured by DLS. It ranged from 115 to 846 nm. The concentration of the suspension was 2119 ± 20 mg L^{-1}. It was measured by weight differences after freeze-drying. The concentrations of the major components present in the final colloid suspension were 188 ± 3, 59 ± 2, 3364 ± 2, 121 ± 1, 60 ± 5, 2 ± 0.1, 41 ± 2 and 214 ± 9 mg L^{-1} for Ca, Fe, K, Mg, Na, P, S and Si, respectively. They were measured by ICP-OES iCAP 6500 (Thermo, Walthman, MA).

3.2.3.4. Adsorption experiments

Gd species interactions with nano objects were investigated in seven experiments summarized in Table 3.2. Each experiment required up to a maximum of 14 conditions, three replicates being carried out for each condition. The first set of experiment focused on the model NPTs at a fixed Gd species concentration (i) to get a preliminary view of the interactions with the different Gd species, at pHs 5 and 9 (Experiment 1); (ii) to describe the time require to reach adsorption equilibrium (Experiment 2) and (iii) to investigate the role of ionic strength in the media (Experiment 3). The concentration of NPTs (1.04 x 10^{12} L^{-1}) and Gd (10 - 1000 µg L^{-1}) selected were based on various literature reports in which the concentrations of plastic particles were between 1.50 x 10^{2} - 2.34 x 10^{14} L^{-1}. [34–38] In the case of Gd, the concentrations present in the environment are lower (0.06 - 188 ng L^{-1})[13,39–47] than the ones used in the experiments. Subsequent experiments were designed to draw adsorption isotherms in seawater after 48 h keeping only Gd^{3+} and Dotarem® as adsorbing species. Isotherms were acquired by varying the adsorbent concentration (ENPTs in experiment 5 and experiment 6) or the adsorbent type (NTP in experiment 4, ENTPs in experiment 5 and natural colloids in experiment 7). Dotarem® was selected in experiments 3, 4, 5, 6 and 7 because it is the main GBCAs used in Europe, whereas MultiHance® has a more limited use, and the use of Omniscan® has been discontinued in Europe.

Each sample was prepared by adding the media in a glass vial, followed by the gadolinium solution and, finally, adding the adsorbent, with a final volume

of 5 mL. pH of the samples was adjusted with 0.1 M HCl or 0.6 M NaOH. The samples were then incubated at 20 ºC with a 40 rpm speed shaking (Grant, Cambridgeshire, UK).

*Table 3.2. Adsorption experiments: Summary of experiments and conditions used. * Conditions used exclusively for the carbonate-borate buffer. Ncond, refers to the number of conditions used during each of the experiments.*

	Type of adsorbent	**Adsorbent concentration**	**Gd species**	**GBCAs concentration**	**Time**	**Media**	**pH**	**N_{cond}**
Exp.**1** pH and Gd species	PS22	20 mg L^{-1}	Dotarem® Omniscan® Multihance® Gd^{3+}	1000 µg L^{-1}	168 h	Carbonate-borate buffer	5 9	8
Exp.2 Time Kinetic	PS22	20 mg L^{-1}	Omniscan® Gd^{3+}	1000 µg L^{-1}	30 s -168 h	Carbonate-borate buffer	5	14
Exp.3 Media influence	PS22	20 mg L^{-1}	*Omniscan®/Dotarem® Gd^{3+}	100 µg L	48h/*168 h	Carbonate-borate buffer Hard Water Seawater	*5/7	9
Exp.4 PS22 Isotherm	PS22	20 mg L^{-1}	Dotarem® Gd^{3+}	10-300 µg L^{-1}	48 h	Seawater	7	8
Exp.5 High ENPTs isotherm	ENPTs	600 µg L^{-1}	Dotarem® Gd^{3+}	10-1000 µg L^{-1}	48 h	Seawater	7	8
Exp.6 Low ENPTs isotherm	ENPTs	10 µg L^{-1}	Dotarem® Gd^{3+}	10-300 µg L^{-1}	48 h	Seawater	7	8
Exp.7 Colloids isotherm	Colloids	20 mg L^{-1}	Dotarem® Gd^{3+}	10-300 µg L^{-1}	48 h	Seawater	7	8

3.2.3.5. Gadolinium determination

3.2.3.5.1. Ultrafiltration

At the end of each experiment, suspensions were subjected to ultrafiltration. For this purpose, 1 mL of each of the incubated samples was centrifuged at 4200 rpm for 15 min (Eppendorf 5804R, Hamburg, Germany) using acid clean Amicon Ultra-4 10K centrifugal filters (Merck Millipore, Burlington, VT). After centrifugation, the re fractions retained by the filter (Gd_{Ret}) and the filtrate fraction (Gd_{UF}) were weighed. To reduce possible losses of Gd in the ultrafilter, both parts of the filter were washed with 2% (*v/v*) HNO_3 and sonicated for 5 min. The volumes added for cleaning were subsequently collected and added to the corresponding fractions of the samples (retentate and filtrate), being weighed again.

3.2.3.5.2. Sample analysis

For the analysis by ICP-MS (Section 3.2.1) of the bulk, retentate and filtrate obtained in Section 3.2.3.5.1, were subsequently diluted with 2% (*v/v*) HNO3. Attention was paid to possible interferences due to oxides (CeOH and PrO). For this purpose, equation 3.1 was used when calculating Gd concentrations:

$$[^{157}Gd]_{Final} = [^{157}Gd] - \frac{[^{157}Gd]}{[^{140}Ce]} * 100 * [^{157}Gd] - [^{141}Pr] * 0.03 - [Blank_{HNO3}] \quad (3.1)$$

where $[^{157}Gd]$ corresponds to the initial Gd concentration obtained, [^{140}Ce] corresponds to the initial concentration, $[^{141}Pr]$ corresponds to the initial concentration, and $[Blank_{HNO3}]$ corresponds to the average of the HNO_3 blanks measured.

The associated limits of quantification and detection are presented in the Table 3.3.

Table 3.3. Gadolinium limits of detection and quantification obtained in each of the media used. (n = 20)

	Buffer	**Hard water**	**Seawater**
LOQ	0.018 μg L^{-1}	0.014 μg L^{-1}	0.050 μg L^{-1}
LOD	0.0006 μg L^{-1}	0.005 μg L^{-1}	0.016 μg L^{-1}

3.2.3.5.3. Isotherm modelling

Adsorption is generally represented using isotherms. These can be based on various models, being those of Langmuir and Freundlich the most widely used for plastics. Langmuir model assumes that the surface of an adsorbent is uniform, there is no interaction between the adsorbents and adsorption only occurs on the outer surface of the adsorbent (monolayer adsorption). Freundlich's, on the other hand, assumes a multilayer adsorption in a heterogeneous surface without saturation.[7,48] The isotherms were fitted using the non-linear Langmuir and Freundlich models. However, since linearity was not obtained with Langmuir, Freundlich was chosen as the model used.

The Langmuir isotherm corresponds to:

$$[Gd]_{ads} = \frac{[Gd]_{non-ads}\ S_T\ K_{ads}}{1+K_{ads}\ [Gd]_{Non-ads}} \quad (3.2)$$

The Freundlich isotherm corresponds to:

$$[Gd]_{ads} = S_T\ K_{ads}\ \ [Gd]_{Non-ads}{}^{1/n} \quad (3.3)$$

where S_T corresponds to the total sites of adsorption, K_{ads} is the Langmuir/Freundlich constant, and n is the non-linearity coefficient. Regarding to the $[Gd]_{Non-ads}$, it was estimated from equation (3.4), assuming no nanoparticles pass through the filter:

$$[Gd]_{Non-ads} = [Gd]_{UF} \quad (3.4)$$

while the adsorbed Gd was calculated according to equation (3.5):

$$[Gd]_{ads} = \frac{([Gd]_{Ret} - [Gd]_{UF})V_{Ret}}{Vtotal} \quad (3.5)$$

where $[Gd]_{Ret}$ is the concentration of the retentate fraction (i.e., retained by the ultrafilter), $[Gd]_{UF}$ is the concentration of the ultrafiltrate fraction, V_{Ret} is the associated volume (corresponds to ~0.09 mL, weighed, of the 1 ml used in centrifugation) and V_{Total} corresponds to 1 mL.

To verify the ultrafiltration recovery, the mass budget error (MBE) was calculated according to the following equation:

$$MBE = \frac{[Gd]_{UF}V_{UF} + [Gd]_{Ret}V_{Ret} - [Gd]_{Total}V_{Total}}{[Gd]_{Total}V_{Total}} x\ 100 \quad (3.6)$$

where the V_{UF} correspond to the associated volume (corresponds to ~0.91 mL, weighted, of the 1 mL used in centrifugation) and $[Gd]_{Total}$ is the total concentration before filtration.

Formula 3.6 was applied to all the samples analysed and was used as a method to remove nonconforming samples. Therefore, samples with an MBE >10% were discarded, which was the case for 23 samples out of 284 analysed.

3.3. Results and discussion

3.3.1. Preliminary experiments

The adsorption of contaminants on plastics can be affected by various factors. They are related to the intrinsic properties of the plastic particles (polarity, crystallinity, functional groups, size or ageing) and to the properties of the contaminants (hydrophobicity or dissociated forms). In addition, there is an effect of environmental factors (temperature, pH or salinity) on the adsorption capacity.[49] Therefore, several test conditions were investigated to study their effect on the interaction between Gd species and NPTs.

3.3.1.1. Effect of pH on the adsorption of Gd species

pH of the medium and the type of Gd species has an influence on the adsorption of the latter on the nanoplastics. For this reason, the adsorption of the different Gd species at two different pH values (5 and 9) in the same medium (carbonate-borate buffer) was studied. The studies were carried out with the same concentrations of NPTs (20 mg L^{-1}) and Gd species (1000 μg L^{-1}) for a period of 168 h (Section 3.2.3.4).

In order to know the behaviour of the Gd species at different pHs (5 and 9) in the media without adsorbent presence, the adsorption study without adding the NPTs was made. Figure 3.1 shows the results obtained.

The results shown in Figure 3.1 demonstrate the stability of all Gd species in aqueous solution, except for Gd^{3+} at pH 9. At this pH, Gd^{3+} precipitates almost completely, a situation not observed at pH 5, where Gd^{3+} remains in solution. This can be explained by the solubility product ($1.8x10^{-23}$ mol L^{-1}). It indicates hydroxide precipitation at pH > 6, with the saturation at a Gd^{3+} concentration of 620 μg L^{-1} at pH 7 and at Gd^{3+} 0.6 ng L^{-1} at pH 9.

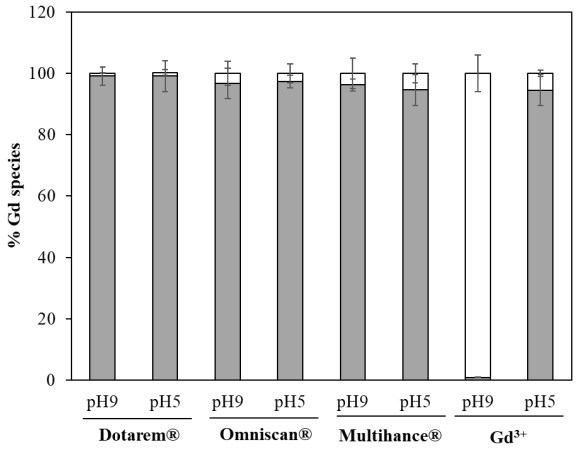

Figure 3.1. Adsorption of the Gd species without the presence of NPTs (Gd species (1000 µg L^{-1}) in carbonate-borate buffer at pH 5 and 9 for 16 8h). The grey area of the bars corresponds to the percentage of Gd species non-adsorbed while the white area corresponds to the percentage Gd species adsorbed. Mean ± standard deviation (n = 3).

The adsorption studies carried out in the presence of NPTs are shown in Figure 3.2. In contrary with the study without NPTs, Gd^{3+} shows a high adsorption at pH 9, which could indicate a strong interaction of Gd^{3+} with NPTs. However, this adsorption can be due to the precipitation of Gd^{3+} as previously discussed for Figure 3.1. In the case of the other Gd species, they showed a lower affinity for NPTs in comparison to Gd^{3+} (Gd^{3+} > MultiHance® > Omniscan® ~ Dotarem®). This can be explained by the electrostatic interaction between the negative NPTs surface charge (zeta potential of -46 mV at pH 7) due to the carboxylic groups and Gd^{3+}. On the other hand, MultiHance® showed the strongest interaction compared to the rest of GBCAs even though this complex has the most negative net charge (-2 v -1 for Dotarem® and 0 for Omniscan®). In turn, the interaction of MultiHance® can be influenced by its linear-ionic structure, with the presence of an aromatic ring, which favours its specificity and stability.

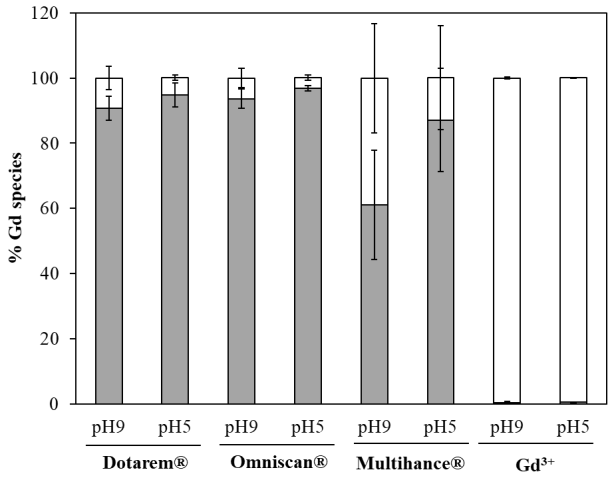

Figure 3.2. Adsorption of the Gd species on NPTs (Gd species (1000 µg L^{-1}) and NPTs (20 mg L^{-1}) in carbonate-borate buffer at pH 5 and 9 for 168 h). The grey area of the bars corresponds to the percentage of Gd species non-adsorbed while the white area corresponds to the percentage Gd species adsorbed. Mean ± standard deviation (n = 3).

The adsorption affinity as a function of pH (5 or 9) suggests higher adsorption at pH 5 than at pH 9 (Figure 3.1 and Figure 3.2, respectively), in particular for MultiHance®. Two reasons for that can be envisaged: one is, that the higher protonation of NPT surface can decrease the intensity of the electrostatic repulsion of the complexes. The other one can be, that the lower stability of complexes in acidic conditions favours a Gd release in its cationic form that adsorbs on the NPT surface. Due to the problems at pH 9 for Gd^{3+}, it was decided to use pH 5 for the adsorption studies. Regarding the Gd species to be used, although MultiHance® has a higher adsorption, it was decided to use Dotarem® and/or Omniscan® in following experiments. This was because MultiHance® has a very limited use and Dotarem® is one of the most use GBCAs.

3.3.1.2. Evaluation of SP-ICP-MS as a tool for adsorption studies

SP-ICP-MS has become a well-established technique for the detection, size characterisation and quantification of inorganic nanoparticles. This opens the possibility of using SP-ICP-MS for measuring Gd in adsorption studies to obtain

direct information about the adsorption of Gd species on NPTs. As an example, the samples following the adsorption of Omniscan® on NPTs at pH9 were analysed by SP-ICP-MS. ^{157}Gd isotope was measured, dwell time was 100 µs and acquisition time 60 s. A time scan is shown in Figure 3.3

Figure 3.3 shows that the mass of Gd adsorbed on the individual particles was not high enough to detect the NPTs containing Gd. Therefore, the option of using SP-ICP-MS was discarded and the Gd adsorption was studied indirectly after separation of the NPTs by ultrafiltration.

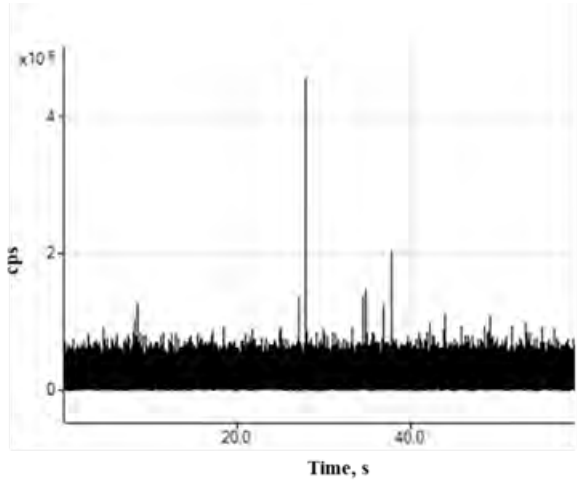

Figure 3.3. Time scans corresponding to Omniscan® obtained from the SP-ICP-MS analysis of the samples of Section 3.3.1.1 at pH 9.

3.3.1.3. Effect of the contact time on adsorption

The adsorbent and adsorbate require a contact time for interaction and subsequent saturation or equilibrium to occur. The time required for this interaction is highly dependent on the substances used.

Initially, in the pH effect study, a relatively high contact time (168 h) was selected in the aim to ensure the interaction between the NPTs and the Gd species. However, to know how fast the interaction between the Gd species (Gd^{3+} and Omniscan®) and the NPTs was, it was decided to carry out an adsorption study at different contact times (30 s, 5 min, 30 min, 2h, 18 h, 48 h and 168 h) at pH 5 in

carbonate-borate buffer (Section 3.2.3.4). Figure 3.4 shows the adsorption results obtained for each of the Gd species.

Figure 3.4 shows a fast adsorption, with the equilibrium reached in less than 30 s between NPTs and Gd^{3+} (~100% adsorption) or Omniscan® (5 % adsorption) at pH 5, then a steady state was maintained during at least one week. The time required to reach equilibrium vary widely in the literature reports.[7,50–52] However, most studies show that both the type of plastic and metal used will have a significant influence on the interaction, Holmes *et al.*[7] observed that the adsorption behaviour over time of Co^{2+}, Cd^{2+}, Cr^{3+} and Pb^{2+} varied. For Co^{2+} and Cd^{2+}, here was a rapid adsorption of the metal observed and a subsequent equilibrium while in the case of Cr^{3+} and Pb^{2+}, this adsorption and its approach to equilibrium were much slower (40 h). As a function of the type of plastic used, depending on whether or not it was weathered, equilibrium was be reached in 2 h or 10 h, respectively.[52]

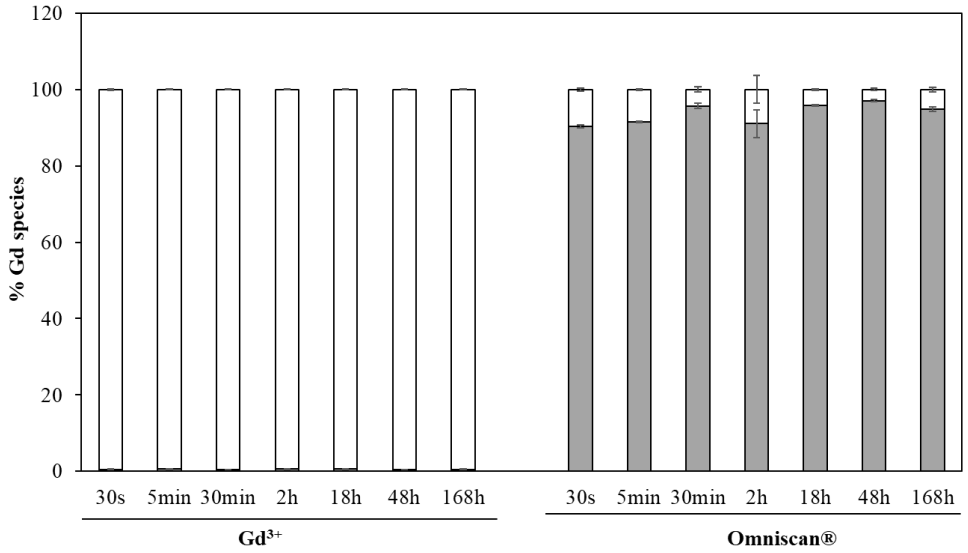

Figure 3.4. Adsorption of the Gd species with NPTs (Gd species (1000 µg L^{-1}) and NPTs (20 mg L^{-1}) in carbonate-borate buffer at pH 5 at different contact times. The grey area of the bars corresponds to the percentage of Gd species non-adsorbed while the white area corresponds to the percentage Gd species adsorbed. Mean ± standard deviation (n = 3).

A time of 48 h was selected as the contact time for the subsequent studies. This is because for both Gd^{3+} and Omniscan®, no changes in adsorption were observed after this time.

3.3.1.4. Effect of the test medium on adsorption

The medium in which the interaction between adsorbent and adsorbate takes place is another condition that strongly influences the interaction between both, playing an important role in the interaction mechanism.

It is therefore likely that the adsorption between NPTs and Gd species will be influenced by the contact medium. Therefore, it was decided to compare the adsorption between three different media: carbonate-borate buffer, hardwater and seawater. These media were selected as each has a different ionic strength. The carbonate-borate buffer study was carried out with Omniscan® at pH 5 and a contact time of 168 h. However, the seawater and hardwater studies were carried out with Dotarem® at pH 7 and a contact time of 48 h. The change in the Gd species used was due to the need to study those still in use (the use of Omiscan® is banned in Europe) Regarding the pH, this was set at 7 in view of the natural pH of seawater, which is between 7.5 - 8.5. The concentrations of NPTs (20 mg L^{-1}) and Gd species (100 µg L^{-1}) were the same in all the studies (Section 3.2.3.4). Figure 3.5 shows the differences in adsorption between the different Gd species with respect to the test media.

Figure 3.5 shows a critical effect of the ionic strength on adsorption capacity of the NPTs with a significant adsorption at a low ionic strength, ~100 % adsorption for Gd^{3+} and 30% adsorption for Dotarem® in the carbonate-borate buffer (IS = 0.004 M). Conversely, at a higher ionic strength, it was significantly reduced, below 10%. This situation was observed for various ions such as Pb^{2+}, Cd^{2+}, Zn^{2+} and Cu^{2+},[6] and suggests an important Gd release from nanoplastics across the salinity gradient, such as that in estuarine environment. The adsorption difference between HW matrix (IS = 1.08 M) and SW (IS = 0.7 M) is negligeable as shown in Figure 3.5. No major differences were observed when comparing the adsorption of Dotarem® and Gd^{3+} on NPTs (pH 7) on HW and SW.

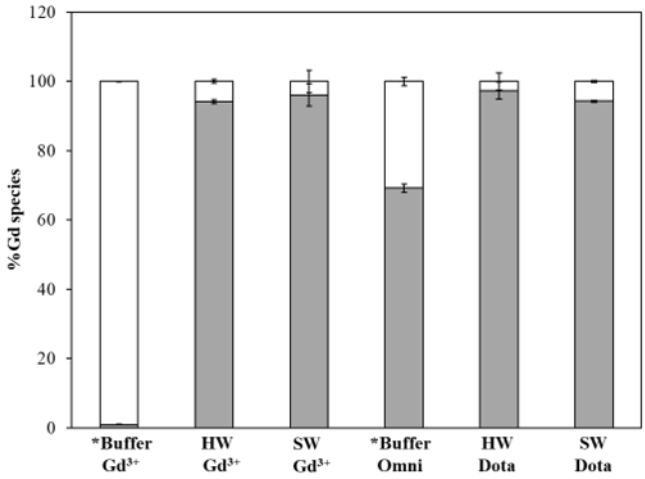

*Figure 3.5. Adsorption of Gd^{3+} (20 mg L^{-1}) and Dotarem® (100 µg L^{-1}) on NPTs at pH 5/7 in carbonate/borate buffer, hardwater (HW) and seawater (SW) media during 168 h/48 h. The grey area of the bars corresponds to the % of Gd species not adsorbed while the white area corresponds to the % Gd species adsorbed. * Conditions used exclusively for the carbonate-borate buffer (pH 5, Omniscan®, 168 h).*

3.3.2. Adsorption isotherms in seawater

Adsorption isotherms are models used to describe the behaviour of adsorbents and adsorbate as a function of properties such as pH, ionic strength or temperature. In general, they are used to predict the amounts of adsorbate that can be adsorbed on a solid surface and to determine whether the adsorption mechanism is based on linear monolayer coverage (Langmuir) or multilayer adsorption (Freundlich).[49]

In this case, four experiments were carried out (Experiments. 4, 5, 6 and 7, Table 3.2), to obtain the corresponding adsorption isotherms. All experiments were carried out in seawater, at pH 7, with a contact time of 48 h and using Gd^{3+} and Dotarem® as Gd species. However, they differed in terms of the type of adsorbent and its concentration, as well as in the concentration of the Gd species.

NPTs (20 mg L^{-1}), ENPTs (600 µg $L^{-1}$and 10 µg L^{-1}) and natural colloids (20 mg L^{-1}) were used as adsorbents.

3.3.2.1. Application of Freundlich isotherms

A fit was carried out using the Langmuir and Freundlich non-linear models on the isotherms obtained from the experiments described in Section 3.3.2. After the application of both models, it was observed that the Freundlich model fitted better than the Langmuir model the data obtained. Figures 3.6 - 3.9 show the adsorption isotherm corresponding to NPTs (Experiment 4), ENPTs (Experiment 5), ENPTs (Experiment 6) and natural colloids (Experiment 7) with the two fits as an example, respectively.

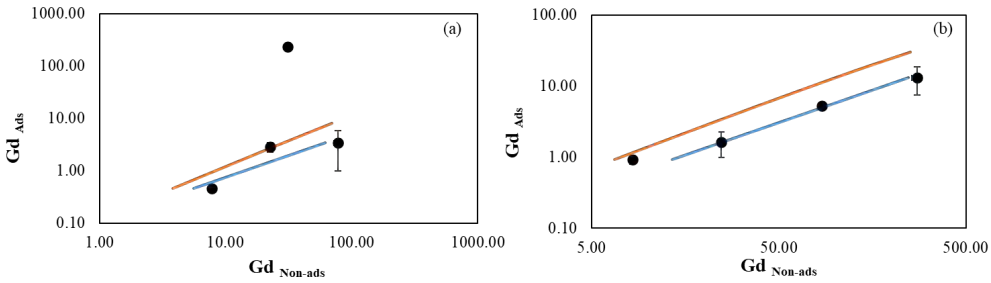

Figure 3.6. Adsorption isotherms of NPTs (20 mg L^{-1}) with Gd species (10 - 300 µg L^{-1}) in seawater at pH 7 for 48 h. (a) Gd^{3+} isotherm and (b) Dotarem® isotherm. The Langmuir adjustment is shown in orange and the Freundlich adjustment in blue.

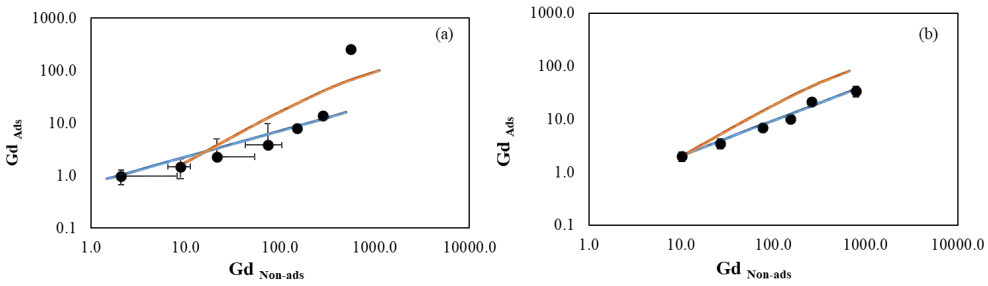

Figure 3.7. Adsorption isotherms of ENPTs (600 µg L^{-1}) with Gd species (10 - 1000 µg L^{-1}) in seawater at pH 7 for 48 h. (a) Gd^{3+} isotherm and (b) Dotarem® isotherm. The Langmuir adjustment is shown in orange and the Freundlich adjustment in blue.

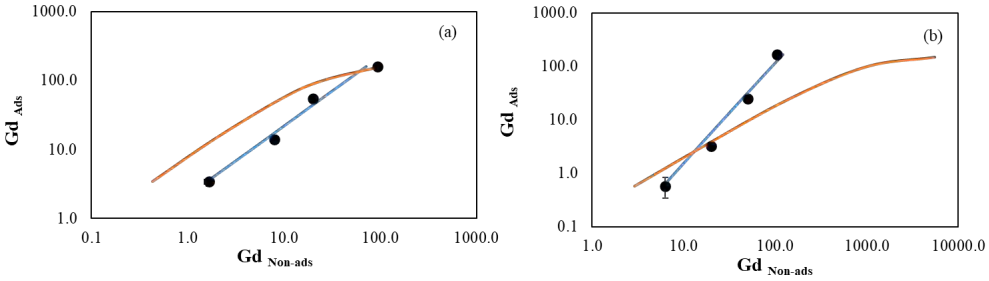

Figure 3.8. Adsorption isotherms of colloids (20 mg L-1) with Gd species (10-300 µg L^{-1}) in seawater at pH 7 for 48 h. (a) Gd^{3+} isotherm and (b) Dotarem® isotherm. The Langmuir adjustment is shown in orange and the Freundlich adjustment in blue.

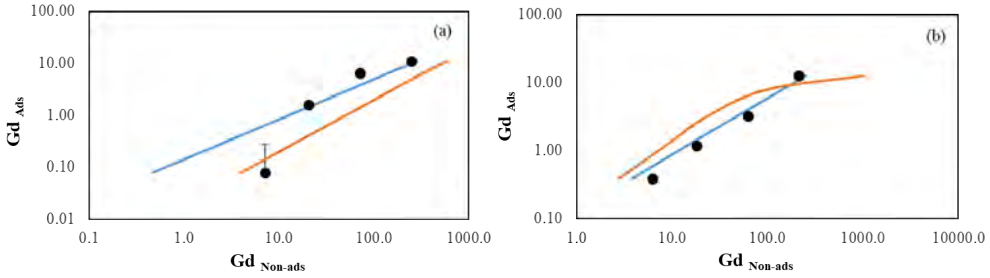

Figure 3.9. Adsorption isotherms of colloids (20 mg L^{-1}) with Gd species (10 - 300 µg L^{-1}) in seawater at pH 7 for 48 h. (a) Gd^{3+} isotherm and (b) Dotarem® isotherm. The Langmuir adjustment is shown in orange and the Freundlich adjustment in blue.

The Freundlich isotherm was the best fit to the data sets obtained, with a correlation coefficient R^2 always near to 0.970. This coefficient indicates that the Freundlich model is suitable for describing the adsorption processes. Note that the data point from the higher concentration of Gd^{3+} (300 μg L^{-1}) was suppressed, because of its possible precipitation at high salinity. The excellent fitting by Freundlich isotherm, in comparison with Langmuir isotherm underlines the lack of saturation behaviour, probably due to the large number of adsorption sites available. Table 3.4 shows the Freundlich constants obtained for each of the experiments carried out, as well as the correlation coefficient R^2 and the n coefficient, derived from the regression analysis.

Table 3.4. Constants defining the adsorption of Gd^{3+} and Dotarem® on the different adsorbents NPTs (Experiment 4), ENPTs (Experiment 5 and Experiment 6) and natural colloids (Experiment 7) according to the Freundlich model. Mean ± standard deviation (n = 3).

	Gd^{3+}			**Dotarem®**		
	K_{ads}	n	R^2	K_{ads}	n	R^2
Experiment 4 NPT Isotherm	0.05±0.02	1.2	0.999	0.04±0.01	1.1	0.999
Experiment 5 High ENPTs isotherm	0.205±0.07	1.7	0.993	0.22±0.09	1.5	0.983
Experiment 6 Low ENPTs isotherm	1.06±0.19	0.9	0.999	0.01±0.01	0.5	0.969
Experiment 7 Natural colloid isotherm	0.08±0.01	1.3	0.991	0.06±0.01	0.9	0.997

3.3.2.2. Comparison of the adsorption isotherms

The isotherms obtained from the studies carried out (Section 3.3.2) show clear differences in adsorption between the different adsorbents NPTs (Experiment 4), ENPTs (Experiment 5 and 6) and colloids (Experiment 7), and with regard to the Gd species (Gd^{3+} and Dotarem®). The isotherm curves obtained for each experiment are shown in Figure 3.10.

In the isotherm obtained for NPTs (Experiment 4: NTPs concentration of 20 mg L^{-1}, Gd species of 10 - 300 μg L^{-1}, which corresponds to Figure 3.10.(a)), all the points of Gd^{3+} and Dotarem®, except for the Gd^{3+} point of 100 μg L^{-1}, demonstrated an adsorption close to 10% as predicted by the theoretical model of Freundlich (Table 3.4).The lack of significant differences between the adsorptions of Gd^{3+} and Dotarem® indicates that the charge of the species has almost no influence on the adsorption behaviour in sea water. Surprisingly, a similar behaviour was observed when natural colloids (Experiment 7: colloid concentration of 20 mg L^{-1}, Gd species of 10-300 μg L^{-1}) were used instead of NPTs (Figure 3.10. (b) and Figure 3.10. (a), respectively), where the adsorption of Gd^{3+} and Dotarem® was also below 10 %. This may be related to the strong influence of the ionic strength, minimizing the role of the surface chemistry, or to the presence of carboxylic groups as main absorption sites at the surface of both adsorbants (NPTs and natural colloids).[53]

Similarly, for ENTPs (Experiments 5: ENTPs concentration of 600 μg L^{-1}, Gd species of 10-1000 μg L^{-1}, Figure 3.10.(d)), the adsorption was around 10%, but with a slightly higher Freundlich coefficient (*n* of 1.7 and 1.5, for Gd^{3+} and Dotarem® respectively). This higher *n* value could be related to the steric hindrance produced by previously adsorbed species, probably because of the 20-fold lower concentration of the adsorbent.

At a lower ENPTs concentration (Experiment 6: ENTPs concentration of 10 μg L^{-1}, Gd species of 10-300 μg L^{-1}) the adsorption was remarkably higher (> 50%) despite a 60-fold lower ENPT concentration (Figure 3.10. (c)). This is in contradiction with the Freundlich isotherm theory since the adsorption must be proportional to the number of adsorption sites (eq. 3.3) and, hence, to the adsorbent concentration. This paradox can be explained if the colloidal behaviour of ENPTs in sea water is considered. At higher concentrations a homoaggregation process may take place, as it was shown in other studies,[53–55] especially in the presence of high concentration of salts. The homoaggregation of ENPTs at higher concentrations implies the reduction of the number of sites, while at lower

concentrations NPTs are well dispersed and more active surface, and hence more sites, are available for the Gd species. On the other hand, the isotherm obtained at low ENPTs concentration and Dotarem® suggests a Freundlich isotherm with a *n* value significantly lower than 1, which would be in contradiction with all the existent adsorption models. This result would suggest the breaking of the Gd complex and the subsequent release of Gd^{3+}, resulting in an increase of Gd^{3+} free, and then available, as the Dotarem® concentration increases higher than the predicted by the model.

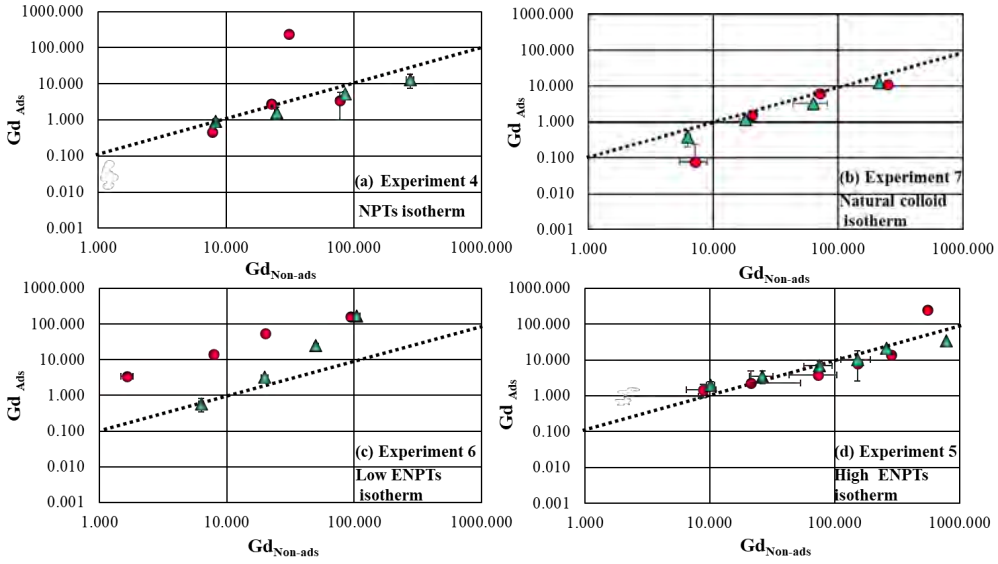

Figure 3.10. Adsorption isotherms obtained for NPTs (a), natural colloids (b), low ENPTs (c) and high ENPTs (d). The red circles correspond to the data obtained for Gd^{3+} and the green triangles correspond to the data obtained for Dotarem®. The line represented in each of the isotherms marks the point where the 10% adsorption point is reached.

3.4. Conclusions

Nanoplastics can act as a Trojan horse of other emerging pollutants, such as pharmaceuticals. They were shown here shown to have affinity for different Gd species, the affinity which is strongly influenced by several factors. They include

environmental factors, such as pH, ionic strength and contact time, and those related to the structure and stability of the Gd species. Studies at different pH values demonstrated the effect of pH on Gd^{3+} precipitation, which became evident at pH 9. In the case of ionic strength, adsorption of the species was favoured in media with lower ionic strengths. The contact times required for adsorption were relatively short, allowing adsorption stability to be achieved at 48 h. The structure of the Gd species was a key factor for their adsorption, being lower for Gd complexes, such as Dotarem®, Omniscan® and MultiHance®, compared to Gd^{3+}.

It is known that nanoplastics undergo several alterations in the environment which influence their adsorption capacity and their ability to act as competitors of other adsorbents. It was observed here that the adsorption of Gd species on environmental nanoplastics was favoured at low concentrations in comparison with model nanoplastics in high salinity media, due to the occurrence of homoaggregation at higher concentrations that contributes to the reduction of the number of available adsorption sites. Regarding the adsorption of GBCAs on natural colloids, it was similar to that obtained by model and environmental nanoplastics at high concentrations, but lower to the adsorption on environmental nanoplastics at low concentrations.

The results obtained highlight the role of nanoplastics as vectors for gadolinium-based contrast agents in natural waters, in line with other emerging pollutants studied in the literature,[12,56–60] as well as the ability of nanoplastics to compete with natural colloids in the adsorption and transport of these pollutants in natural environments.

3.5 References

1. Zhang, M. & Xu, L. Transport of micro- and nanoplastics in the environment: Trojan-Horse effect for organic contaminants. Critical Reviews in Environmental Science and Technology, 52, 810–846 (2022).

2. Hu, L., Zhao, Y. & Xu, H. Trojan horse in the intestine: A review on the biotoxicity of microplastics combined environmental contaminants. Journal of Hazardous Materials, 439, 129652 (2022)

3. Naasz, S., Altenburger, R. & Kühnel, D. Environmental mixtures of nanomaterials and chemicals: The Trojan-horse phenomenon and its relevance for ecotoxicity. Science of the Total Environment, 635, 1170–1181 (2018)

4. Yu, Y., Mo, W. Y. & Luukkonen, T. Adsorption behaviour and interaction of organic micropollutants with nano and microplastics: A review. Science of the Total Environment ,797, 14940 (2021)

5. Atugoda, T., Vithanage, M., Wijesekara, H., Bolan, N., Sarmah, A. K., Bank, M. S., You, S. & Ok, Y. S. Interactions between microplastics, pharmaceuticals and personal care products: Implications for vector transport. Environmental International, 149, 106367 (2021).

6. Yu, F., Yang, C., Zhu, Z., Bai, X. & Ma, J. Adsorption behavior of organic pollutants and metals on micro/nanoplastics in the aquatic environment. Science of the Total Environment, 694, 133643 (2019).

7. Holmes, L. A., Turner, A. & Thompson, R. C. Adsorption of trace metals to plastic resin pellets in the marine environment. Environmental Pollution, 160, 42–48 (2012).

8. Bakir, A., Rowland, S. J. & Thompson, R. C. Competitive sorption of persistent organic pollutants onto microplastics in the marine environment. Marine Pollution Bulletin, 64, 2782–2789 (2012).

9. Li, J., Zhang, K. & Zhang, H. Adsorption of antibiotics on microplastics. Environmental Pollution, 237, 460–467 (2018).

10. Guo, X. & Wang, J. Sorption of antibiotics onto aged microplastics in freshwater and seawater. Marine Pollution Bulletin, 149, 110511 (2019).

11. Reynaud, S., Aynard, A., Grassl, B. & Gigault, J. Nanoplastics: From model materials to colloidal fate. Current Opinion in Colloid & Interface Science, 57, 101528 (2022).

12. Godoy, V., Martín-Lara, M. A., Calero, M. & Blázquez, G. The relevance of interaction of chemicals/pollutants and microplastic samples as route for transporting contaminants. Process Safety and Environmental Protection, 138, 312–323 (2020).

13. Kulaksız, S. & Bau, M. Contrasting behaviour of anthropogenic gadolinium and natural rare earth elements in estuaries and the gadolinium input into the North Sea. Earth and Planetary Science Letters, 260, 361–371 (2007).

14. Ragusa, A., Svelato, A., Santacroce, C., Catalano, P., Notarstefano, V., Carnevali, O., Papa, F., Rongioletti, M. C. A., Baiocco, F., Draghi, S., D'Amore, E., Rinaldo, D., Matta, M. & Giorgini, E. Plasticenta: First evidence of microplastics in human placenta. Environmental International, 146, 106274 (2021)

15. Yan, Z., Liu, Y., Zhang, T., Zhang, F., Ren, H. & Zhang, Y. Analysis of Microplastics in Human Feces Reveals a Correlation between Fecal Microplastics and Inflammatory Bowel Disease Status. Environmental Science & Technology, 56, 414–421 (2022).

16. Rahman, A., Sarkar, A., Yadav, O. P., Achari, G. & Slobodnik, J. Potential human health risks due to environmental exposure to nano- and microplastics and knowledge gaps: A scoping review. Science of the Total Environment 757, 143872 (2021)

17. Molina, E. & Benedé, S. Is There Evidence of Health Risks from Exposure to Micro- and Nanoplastics in Foods? Frontiers in Nutrition, 9, 10094 (2022)

18. Wang, F., Zhang, M., Sha, W., Wang, Y., Hao, H., Dou, Y. & Li, Y. Sorption behavior and mechanisms of organic contaminants to nano and microplastics. Molecules, 25(8), 1827 (2020).

19. Atugoda, T., Vithanage, M., Wijesekara, H., Bolan, N., Sarmah, A. K., Bank, M. S., You, S. & Ok, Y. S. Interactions between microplastics, pharmaceuticals and personal care products: Implications for vector transport. Environmental International, 149, 106367 (2021)

20. Fred-Ahmadu, O. H., Bhagwat, G., Oluyoye, I., Benson, N. U., Ayejuyo, O. O. & Palanisami, T. Interaction of chemical contaminants with microplastics: Principles and perspectives. Science of The Total Environment, 706, 135978 (2020).

21. Liu, M. Lifecycle of Gadolinium-Based Contrast Agents. Journal of Magnetic Resonance Imaging, 53, 1295–1299 (2021).

22. Day, P., Erdahl, S., Eckdahl, S., Bornhorst, J. & Jannetto, P. J. Gadolinium-based contrast agents: A clinically significant analytical interference in inductively coupled plasma mass spectrometry elemental analysis. Annals of Clinical Biochemistry, 56, 638–645 (2019).

23. Pasquini, L., Napolitano, A., Visconti, E., Longo, D., Romano, A., Tomà, P. & Espagnet, M. C. R. Gadolinium-Based Contrast Agent-Related Toxicities. CNS Drugs, 32, 229–240 (2018).

24. Xiao, Y. D., Paudel, R., Liu, J., Ma, C., Zhang, Z. S. & Zhou, S. K. MRI contrast agents: Classification and application (Review). International Journal of Molecular Medicine, 38, 1319–1326 (2016).

25. Lord, M. L., Chettle, D. R., Gräfe, J. L., Noseworthy, M. D. & McNeill, F. E. Observed deposition of gadolinium in bone using a new noninvasive in vivo biomedical device: Results of a small pilot feasibility study. Radiology, 287, 96–103 (2018).

26. Roberts, D. R., Lindhorst, S. M., Welsh, C. T., Maravilla, K. R., Herring, M. N., Braun, K. A., Thiers, B. H. & Davis, W. C. High levels of gadolinium deposition in the skin of a patient with normal renal function. Investigative Radiology, 51, 280–289 (2016).

27. Mercantepe, T., Tümkaya, L., Çeliker, F. B., Topal Suzan, Z., Çinar, S., Akyildiz, K., Mercantepe, F. & Yilmaz, A. Effects of gadolinium-based MRI contrast agents on liver tissue. Journal of Magnetic Resonance Imaging, 48, 1367–1374 (2018).

28. Kanda, T., Ishii, K., Kawaguchi, H., Kitajima, K. & Takenaka, D. High signal intensity in the dentate nucleus and globus pallidus on unenhanced T1-weighted MR images: Relationship with increasing cumulative dose of a gadoliniumbased contrast material. Radiology, 270, 834–841 (2014).

29. Medicines Agency, E. EMA's final opinion confirms restrictions on use of linear gadolinium agents in body scans Recommendations conclude EMA's scientific review of gadolinium deposition in brain and other tissues. (2017)

30. Pessoni, L., Veclin, C., el Hadri, H., Cugnet, C., Davranche, M., Pierson-Wickmann, A. C., Gigault, J., Grassl, B. & Reynaud, S. Soap- and metal-free polystyrene latex particles as a nanoplastic model. Environmental Science: Nano, 6, 2253–2258 (2019).

31. El Hadri, H., Gigault, J., Maxit, B., Grassl, B. & Reynaud, S. Nanoplastic from mechanically degraded primary and secondary microplastics for environmental assessments. NanoImpact, 17, 100206 (2020).

32. Navratilova, J., Praetorius, A., Gondikas, A., Fabienke, W., von der Kammer, F. & Hofmann, T. Detection of engineered copper nanoparticles in soil using single particle ICP-MS. International Journal of Environmental Research and Public Health, 12, 15756–15768 (2015).

33. Jiménez-Lamana, J., Marigliano, L., Allouche, J., Grassl, B., Szpunar, J. & Reynaud, S. A Novel Strategy for the Detection and Quantification of Nanoplastics by Single Particle Inductively Coupled Plasma Mass Spectrometry (ICP-MS). Analytical Chemistry, 92, 11664–11672 (2020).

34. Cordova, M. R., Nurhati, I. S., Shiomoto, A., Hatanaka, K., Saville, R. & Riani, E. Spatiotemporal macro debris and microplastic variations linked to domestic waste and textile industry in the supercritical Citarum River, Indonesia. Marine Pollution Bulletin, 175, 113338 (2022).

35. Winkler, A., Antonioli, D., Masseroni, A., Chiarcos, R., Laus, M. & Tremolada, P. Following the fate of microplastic in four abiotic and biotic matrices along the Ticino River (North Italy). Science of the Total Environment, 823, 153638 (2022).

36. Yuan, W., Christie-Oleza, J. A., Xu, E. G., Li, J., Zhang, H., Wang, W., Lin, L., Zhang, W. & Yang, Y. Environmental fate of microplastics in the world's third-largest river: Basin-wide investigation and microplastic community analysis. Water Research, 210, 118002 (2022).

37. Zhdanov, I., Lokhov, A., Belesov, A., Kozhevnikov, A., Pakhomova, S., Berezina, A., Frolova, N., Kotova, E., Leshchev, A., Wang, X., Zavialov, P. & Yakushev, E. Assessment of seasonal variability of input of microplastics from the Northern Dvina River to the Arctic Ocean. Marine Pollution Bulletin, 175, 113370 (2022).

38. Sá, B., Pais, J., Antunes, J., Pequeno, J., Pires, A. & Sobral, P. Seasonal Abundance and Distribution Patterns of Microplastics in the Lis River, Portugal. Sustainability,14, 1–18 (2022).

39. Okabayashi, S., Kawane, L., Mrabawani, N. Y., Iwai, T., Narukawa, T., Tsuboi, M. & Chiba, K. Speciation analysis of Gadolinium-based contrast agents using aqueous eluent-hydrophilic interaction liquid chromatography hyphenated with inductively coupled plasma-mass spectrometry. Talanta, 222, 121531 (2021).

40. Lawrence, M. G. & Ort, C. Comment on 'Speciation analysis of gadolinium chelates in hospital effluents and wastewater treatment plant sewage by a novel HILIC/ICP-MS method'. Environmental Science & Technology, 43, 5547–5548 (2009).

41. Rabiet, M., Brissaud, F., Seidel, J. L., Pistre, S. & Elbaz-Poulichet, F. Positive gadolinium anomalies in wastewater treatment plant effluents and aquatic environment in the Hérault watershed (South France). Chemosphere, 75, 1057–1064 (2009).

42. Zabrecky, J. M., Liu, X. M., Wu, Q. & Cao, C. Evidence of anthropogenic gadolinium in triangle area waters, north Carolina, USA. Water, 13, 1–9 (2021).

43. Han, R., Wang, Z., Shen, Y., Wu, Q., Liu, X., Cao, C., Gao, S. & Zhang, J. Anthropogenic Gd in urban river water: A case study in Guiyang, SW China. Elementa, 9, 1–13 (2021).

44. Schmidt, K., Bau, M., Merschel, G. & Tepe, N. Anthropogenic gadolinium in tap water and in tap water-based beverages from fast-food franchises in six major cities in Germany. Science of the Total Environment, 687, 1401–1408 (2019).

45. Morteani, G., Möller, P., Fuganti, A. & Paces, T. Input and fate of anthropogenic estrogens and gadolinium in surface water and sewage plants in the hydrological basin of Prague (Czech Republic). Environmental Geochemistry and Health, 28, 257–264 (2006).

46. Kulaksiz, S. & Bau, M. Anthropogenic gadolinium as a microcontaminant in tap water used as drinking water in urban areas and megacities. Applied Geochemistry, 26, 1877–1885 (2011).

47. Kulaksiz, S. & Bau, M. Rare earth elements in the Rhine River, Germany: First case of anthropogenic lanthanum as a dissolved microcontaminant in the hydrosphere. Environmental International, 37, 973–979 (2011).

48. Sun, H., Gao, B., Tian, Y., Yin, X., Yu, C., Wang, Y. & Ma, L. Q. Kaolinite and Lead in Saturated Porous Media: Facilitated and Impeded Transport. Journal of Environmental Engineering, 136, 1305–1308 (2010).

49. Fu, L., Li, J., Wang, G., Luan, Y. & Dai, W. Adsorption behavior of organic pollutants on microplastics. Ecotoxicology and Environmental Safety, 217, 112207 (2021)

50. Ahechti, M., Benomar, M., el Alami, M. & Mendiguchía, C. Metal adsorption by microplastics in aquatic environments under controlled conditions: exposure time, pH and salinity. International Journal of Environmental Analytical Chemistry, 102, 1118–1125 (2022).

51. Liu, S., Huang, J. H., Zhang, W., Shi, L. X., Yi, K. X., Zhang, C. Y., Pang, H. L., Li, J. N. & Li, S. Z. Investigation of the adsorption behavior of Pb(II) onto natural-aged microplastics as affected by salt ions. Journal of Hazardous Materials, 431, (2022).

52. Huang, X., Zemlyanov, D. Y., Diaz-Amaya, S., Salehi, M., Stanciu, L. & Whelton, A. J. Competitive heavy metal adsorption onto new and aged polyethylene under various drinking water conditions. Journal of Hazardous Materials, 385, 121585 (2020).

53. Dong, S., Cai, W., Xia, J., Sheng, L., Wang, W. & Liu, H. Aggregation kinetics of fragmental PET nanoplastics in aqueous environment:

Complex roles of electrolytes, pH and humic acid. Environmental Pollution, 268, (2021).

54. Alimi, O. S., Farner Budarz, J., Hernandez, L. M. & Tufenkji, N. Microplastics and Nanoplastics in Aquatic Environments: Aggregation, Deposition, and Enhanced Contaminant Transport. Environmental Science & Technology, 52, 1704–1724 (2018)

55. Liu, L., Song, J., Zhang, M. & Jiang, W. Aggregation and Deposition Kinetics of Polystyrene Microplastics and Nanoplastics in Aquatic Environment. Bulletin of Environmental Contamination and Toxicology, 107, 741–747 (2021).

56. Santana-Viera, S., Montesdeoca-Esponda, S., Torres-Padrón, M. E., Sosa-Ferrera, Z. & Santana-Rodríguez, J. J. An assessment of the concentration of pharmaceuticals adsorbed on microplastics. Chemosphere, 266, 129007 (2021).

57. Wardrop, P., Shimeta, J., Nugegoda, D., Morrison, P. D., Miranda, A., Tang, M. & Clarke, B. O. Chemical Pollutants Sorbed to Ingested Microbeads from Personal Care Products Accumulate in Fish. Environmental Science & Technology, 50, 4037–4044 (2016).

58. Wojnowska-Baryła, I., Bernat, K. & Zaborowska, M. Plastic Waste Degradation in Landfill Conditions: The Problem with Microplastics, and Their Direct and Indirect Environmental Effects. International Journal of Environmental Research and Public Health, 19, 13223 (2022).

59. Beloe, C. J., Browne, M. A. & Johnston, E. L. Plastic Debris as a Vector for Bacterial Disease: An Interdisciplinary Systematic Review. Environmental Science & Technology, 56, 2950–2958 (2022).

60. Moura, D. S., Pestana, C. J., Moffat, C. F., Hui, J., Irvine, J. T. S., Edwards, C. & Lawton, L. A. Adsorption of cyanotoxins on polypropylene and polyethylene terephthalate: Microplastics as vector of eight microcystin analogues. Environmental Pollution, 303, 119135 (2022).

CONCLUSIONS

The monitoring of the C-13 isotope by SP-ICP-MS turned out to be an attractive basis for analytical methodology allowing the detection of plastic particles at concentrations down to hundreds of particles per millilitre, with sizes larger than 1 µm and reaching an upper range of around 5 - 6 µm. This working range in size was conditioned by the inherent limitations for detection of carbon in ICP-MS, but also by the transport efficiency of large particles with pneumatic nebulisation systems. The nebulisation efficiency was found to be around 40% for particles up to ca. 3 µm, decreasing for larger particles, and hence underestimating their concentration. Due to these limitations, SP-ICP-MS should not be used for the quantitative determination of polydisperse microplastics, although it can be used as a rapid screening technique for the detection of plastic particles.

The feasibility of the methodology developed was demonstrated for the analysis of different consumer products. Primary microplastics intentionally added to personal care products used for scrubbing was successfully detected in a number of commercial products. On the other hand, the release of secondary microplastics from teabags submitted to conventional brewing was also confirmed.

The SP-ICP-MS methodology developed allowed the probing of environmental waters from Spanish and French rivers for the presence of microplastics. The application of an acid pre-treatment to the samples improved the detectability of plastics microparticles, as well as the selectivity of the method. The analysis by SP-ICP-MS of the river waters showed the presence of carbon-containing particles in all the samples analysed. The subsequent analysis of the selected samples by Raman microscopy confirmed the presence of plastic particles. Hence, SP-ICP-MS can be used a suitable screening technique for the discrimination of samples containing microplastics, which should then be analysed by Raman or FT-IR microscopy, techniques that require longer analysis

times. In any case, the results obtained in Spanish and French rivers confirm the microplastic pollution on the environment.

The presence of plastic particles in the environment makes it necessary to understand their role as vector for emerging pollutants. For this reason, gadolinium-based contrast agents were selected to study their adsorption on model and environmental nanoplastics and compared to that of ionic gadolinium. It was confirmed that parameters such as pH, concentration, contact time or medium influenced the adsorption of these gadolinium species, which follow Freundlich isotherms.

Moreover, adsorption studies of these Gd species with natural colloids were also carried out. The results obtained highlight the role of nanoplastics as vectors for gadolinium-based contrast agents in natural waters, in line with other emerging pollutants, as well as the ability of nanoplastics to compete with natural colloids in the adsorption and transport of these pollutants in natural environments.

ANNEXES

In compliance with the cotutelle signed between La Universidad de Zaragoza (UNIZAR) and l´Université de Pau et des Pays de l'Adour (UPPA) through the call PI-PRD/2018-001, the parts of the thesis corresponding to the abstract, introduction and conclusions are presented in Spanish and French.

RESUMEN

Hoy en día, el plástico es un material muy utilizado en muchos sectores. Como consecuencia, gran parte del plástico acaba como residuo en el medio ambiente, lo que lo convierte en un problema global. Se calcula que alrededor del 80% de los plásticos producidos se vierten en el medio ambiente. Algunos de estos plásticos acaban como nanoplásticos y microplásticos en los sistemas acuáticos. La presencia de estos plásticos es problemática por su tamaño y su capacidad para adsorber y transportar contaminantes emergentes, y facilitar así su ingestión por los organismos vivos. La comprensión de los efectos de los microplásticos y nanoplásticos sigue siendo limitada, en gran parte debido a la falta de métodos sólidos para su detección y cuantificación.

En este contexto, el objetivo de esta tesis doctoral fue desarrollar un método analítico para la detección, caracterización del tamaño y cuantificación de micropartículas de plástico mediante ICP-MS operando en modo de partícula única con tiempos de residencia en el rango de los microsegundos. Este método ha permitido detectar partículas de poliestireno de hasta 1,2 µm de tamaño mediante trazado isotópico de ^{13}C y se ha utilizado para analizar microplásticos en productos de cuidado personal y los liberados por los envases de alimentos. También se ha desarrollado una plataforma analítica para el análisis de muestras medioambientales, como el agua de los ríos, que combina ICP-MS de partícula única, microscopía electrónica de barrido de emisión de campo y espectroscopía Raman. Gracias a esta plataforma, pudimos determinar la presencia y la identidad química de micropartículas de plástico en las muestras de agua de río analizadas. También estudiamos la capacidad de adsorción de los nanoplásticos ambientales para contaminantes emergentes, como los agentes de contraste a base de gadolinio, y su capacidad para actuar como competidores de los coloides naturales. Se demostró la capacidad de los nanoplásticos para actuar como portadores de contaminantes emergentes en condiciones ambientales.

1. Los plásticos hoy

Los plásticos son polímeros orgánicos de alto peso molecular y cadena larga producidos a partir de materias primas fósiles, como el petróleo o el gas. Se dividen en dos grupos: termoplásticos y termoestables.[1,2] Entre los primeros, que pueden fundirse al calentarse y endurecerse al enfriarse, figuran el polietileno (PE), el polipropileno (PP), el cloruro de polivinilo (PVC), el tereftalato de polietileno (PET) y el poliestireno (PS). El segundo grupo, que sufre transformaciones químicas al calentarse, creando una red tridimensional, incluye el poliuretano (PUR), el poliéster insaturado, las resinas epoxi y la resina de melamina.[3]

El primer plástico sintético, la baquelita, fabricado en 1907 por Leo Hendrik Baekeland, inició una nueva era en la ciencia de los materiales.[1,4] Desde principios del siglo XX, el uso de plásticos en el mundo ha aumentado exponencialmente. En la actualidad, los plásticos más utilizados son el polietileno, el polipropileno, el cloruro de polivinilo, el tereftalato de polietileno, el poliuretano y el poliestireno.[3,5] Su producción mundial pasó en 2018 de 359 millones de toneladas a 368 millones en 2019 y va en aumento.[3] Entre los países con mayor producción de plásticos, China tuvo una cuota del 31% de la producción mundial en 2019.[3]

Más de 8 millones de toneladas de plásticos se vierten cada año en el ecosistema marino.[6] Se acumulan en los giros oceánicos de determinadas zonas del planeta. Una de las más conocidas es la Gran Mancha de Basura del Pacífico (GPGP) en el Pacífico Norte, que ocupa alrededor de 1,6 millones de km^2.[7]

Los plásticos se utilizan de diversas formas en productos de consumo, cosméticos o alimentos, lo que puede dar lugar a la presencia de microplásticos y nanoplásticos disponibles para el consumo humano. Se ha informado de su liberación en envases de comida para llevar8 y botellas de plástico.[9–11] También se encontraron microplásticos y nanoplásticos en productos alimentarios de consumo, como la leche,[12] sal[13–17] o té.[18] En consecuencia, los plásticos pueden

entrar en la cadena alimentaria de distintos organismos.

2. Microplásticos y nanoplásticos: estado de la cuestión

En la actualidad no se dispone de una definición normalizada de microplásticos y nanoplásticos. En muchos casos, las clasificaciones utilizadas dificultan la comparación de los resultados obtenidos en diferentes estudios. [19] La Figura 1 muestra una representación de la clasificación de los plásticos en diferentes estudios. La principal diferencia entre estas definiciones está relacionada con el tamaño de las partículas.

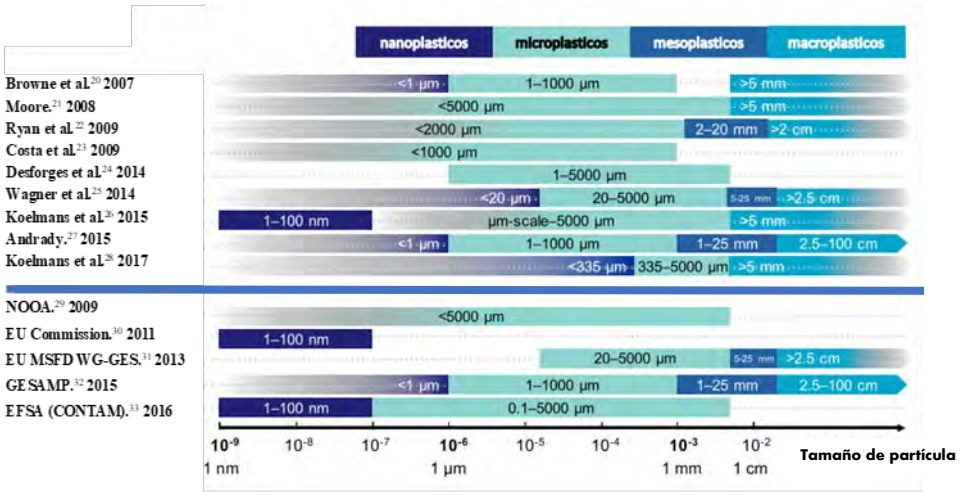

Figura 1. Ejemplos de diferencias en la categorización de los residuos plásticos según su tamaño, tal como se aplican (y/o definen) en la literatura científica y en los informes institucionales. Cabe señalar que no se trata de una lista exhaustiva de todas las clases de tamaño utilizadas.[19]

Los plásticos se dividen, según su tamaño, en cuatro grandes grupos: macroplásticos, mesoplásticos, microplásticos y nanoplásticos. En general, se entiende por macroplásticos los plásticos con tamaños comprendidos entre 5[20,21,26,28] y 2.5 mm.[22,25,27,31,32] El tamaño de los mesoplásticos es de 1 y 25 mm,[22,25,27,31,32] pero a menudo no se consideran una clase aparte. En el caso de los plásticos denominados microplásticos, el rango de tamaño de las partículas

varía en diferentes estudios: 1-5000 µm,[24,25,28,31] 0.1-5000 µm[21,22,26,33] or 1-1000 µm.[20,23,27,32] Frias *et al*.,[4] definió los microplásticos como "cualquier partícula sólida sintética o matriz polimérica, de forma regular o irregular y con un tamaño comprendido entre 1 µm y 5 mm, de origen primario o secundario de fabricación, que son insolubles en agua". En el caso de los nanoplásticos, sus rangos de tamaño tienden a marcarse entre 1-100 nm o por debajo de 1 µm. Gigault *et al.*,[34] definió los nanoplásticos como "partículas de un tamaño comprendido entre 1 y 1.000 nm resultantes de la degradación de objetos plásticos industriales y que pueden presentar un comportamiento coloidal".

2.1. Formación de los nanoplásticos y microplásticos

La formación de microplásticos y nanoplásticos a partir de macroplásticos y mesoplásticos requiere la acción de diversos procesos, que no sólo modificarán el tamaño de las partículas, sino también las características de su superficie. Estos procesos incluyen la degradación mecánica, la fotodegradación, la degradación térmica y la biodegradación.[35,36]

2.1.1. Degradación mecánica

La degradación mecánica se basa en la degradación de los plásticos debido a su rotura por fuerzas externas. La degradación se produce cuando las fuerzas aplican una tensión excesiva sobre el plástico, lo que provoca la ruptura de las cadenas moleculares y la formación de un par de radicales libres. En presencia de oxígeno, estos radicales pueden formar radicales peroxídicos. Los radicales producidos debido a la tensión se originan en la parte principal de la columna vertebral del plástico en la región sometida a tensión.[37–39] Estas fuerzas externas pueden deberse a la fricción entre el plástico con otro material. Un ejemplo de esta degradación mecánica es la abrasión entre el neumático y la carretera, que conlleva el desprendimiento de fragmentos de la superficie del neumático como consecuencia de la fricción.[38] En el medio ambiente, las fricciones pueden deberse a la acción de las olas del mar, la congelación, el

viento, la arena, los choques con rocas o las actividades humanas (por ejemplo, el cultivo del suelo y la rotación de cultivos). [39,40]

2.1.2. Fotodegradación

La fotodegradación es la degradación de los plásticos debida a la acción de la luz (luz visible, infrarroja y UV). La fracción UV de la luz es la que más afecta a los plásticos, en particular las radiaciones UVB (290 - 315 nm) y UVA (315 - 400 nm).[38,40] Este proceso de degradación tiene lugar en la capa exterior de los plásticos y puede alcanzar una profundidad de µm, dependiendo del tipo de plástico.[40]

El proceso de fotodegradación se basa en tres pasos: iniciación, propagación y terminación. En la etapa de iniciación, la energía UV rompe los enlaces químicos de las cadenas poliméricas y favorece la formación de radicales libres. El paso de propagación se basa en una serie de reacciones comunes a todos los polímeros con un esqueleto de carbono. Estas reacciones conducen a la generación de especies de hidroperóxidos que favorecen las reacciones posteriores que conducen a la autooxidación. La etapa de terminación se produce cuando los radicales libres son absorbidos para crear productos inertes. Este paso se alcanza de forma natural por reacción con los estabilizantes del plástico[5,37–39,41] Para poder continuar este proceso, debe aplicarse otra capa no oxidada. La figura 2 muestra el proceso de fotodegradación.

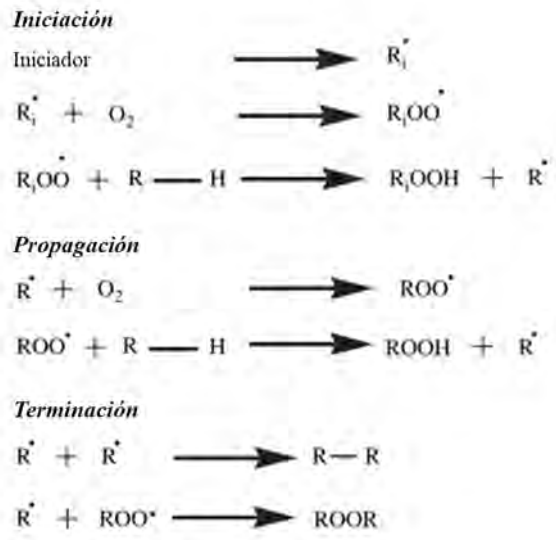

Figura 2. Diagrama del proceso de fotodegradación Diagrama del proceso de fotodegradación, mostrando las 3 etapas del proceso: Iniciación, propagación y terminación.[37]

2.1.3. Degradación térmica

La degradación térmica se basa en la degradación de los plásticos debido a las altas temperaturas. La degradación depende de las características de los aditivos antioxidantes de los polímeros, que determinan la temperatura a la que tendrá lugar el proceso.[37,38]

El proceso de degradación comienza cuando el polímero tiene suficiente calor para superar la barrera energética, de modo que se pueden generar radicales libres a partir de las cadenas poliméricas. Los radicales libres pueden reaccionar con el oxígeno para producir hidroperóxidos, que a su vez pueden escindirse para formar radicales libres hidroxilos y radicales alcoxis. La primera parte del proceso es como en la fotodegradación. Esta reacción se autopropagará a lo largo del polímero hasta que se interrumpa el suministro de energía o cuando se formen productos inertes debido a la colisión de dos radicales.[5,37,38] En el medio ambiente, este tipo de degradación se produce en entornos en los que los plásticos están expuestos a la luz solar directa.[38]

2.1.4. Biodegradación

La biodegradación se basa en la degradación de los plásticos debido a la transformación bioquímica por parte de microorganismos. El grado de biodegradación está controlado por las características fisicoquímicas del polímero (superficie, peso molecular, estructura química, elasticidad...). Los microbios implicados en la biodegradación incluyen bacterias, hongos, algas y protozoos. Este tipo de degradación puede producirse a varios niveles estructurales (molecular, macromolecular, microscópico y macroscópico).[36,37,39,41,42] Esta degradación está fuertemente influenciada por el tipo de plástico, que puede ser hidrolizable o no hidrolizable, dependiendo de la presencia o ausencia de grupos éster o amida. Los plásticos no hidrolizables son el PE, el PP y el PVC, ya que tienen una estructura similar a la lignina, lo que dificulta su degradación.[38,40]

El proceso de degradación implica tres etapas: biofragmentación, asimilación y mineralización (Figura 3).

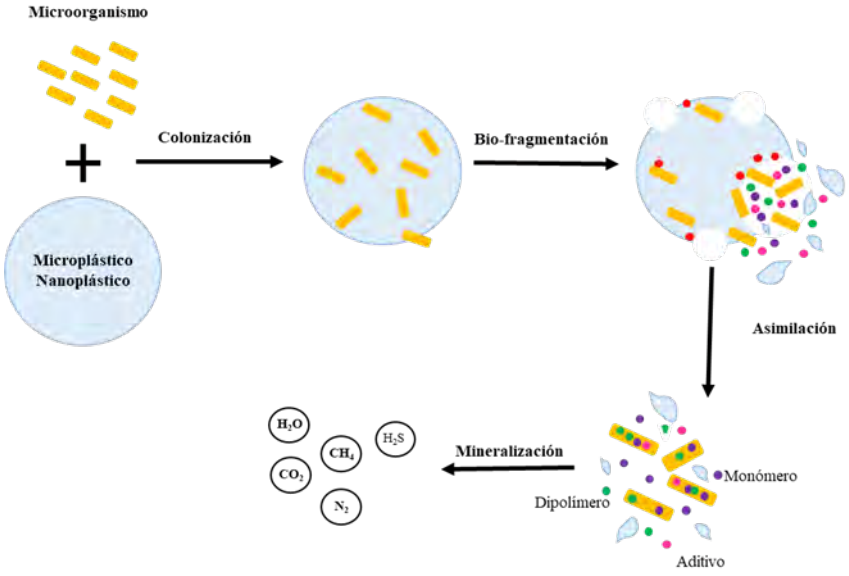

Figura 3. Diagrama que representa la biodegradación llevada a cabo por microorganismos, mostrando las 3 etapas: biofragmentación, asimilación y mineralización. [40]

La biofragmentación se produce tras la adhesión de un microorganismo a la superficie del polímero y/o su penetración en los poros del mismo. Las sustancias extracelulares liberadas actúan sobre el esqueleto de carbono del polímero, produciendo oligómeros, dímeros y monómeros, que pueden atravesar la membrana semipermeable del microorganismo, en un proceso conocido como asimilación. Estos compuestos absorbidos se transforman en CO_2, H_2O, CH_4, H_2S y N_2 por diferentes vías metabólicas.[5,36–41]

3. Principales técnicas analíticas para la detección, caracterización y cuantificación de nanoplásticos y microplásticos

La exposición de los seres humanos a los nano y microplásticos requiere técnicas que permitan su detección, caracterización y cuantificación en una amplia variedad de muestras. En la actualidad, no existe una única técnica que permita determinar la composición, la forma, el tamaño y la concentración de estas partículas. Por ello, en general, la caracterización de estos nano y microplásticos se realiza a dos niveles, el físico y el químico. La caracterización física suele referirse a la descripción de un material según su tamaño de partícula, distribución del tamaño de partícula (PSD), forma y área superficial. El estado de aglomeración/agregación puede incluirse aquí, ya que puede evaluarse por el tamaño de las partículas. La caracterización química de una partícula incluye su composición elemental y/o molecular, una fórmula química con una estequiometría específica, el estado químico de los elementos y la estructura-conformación molecular, siempre que sea posible.[43]

3.1. Microscopia

Las técnicas de microscopía se utilizan ampliamente para obtener información sobre el tamaño, la forma, el estado de agregación y las propiedades superficiales de los plásticos. Incluyen la microscopía óptica, la microscopía electrónica y la microscopía de fuerza atómica.

La microscopía óptica suele utilizarse para realizar el primer examen de una muestra. Al ser una técnica sencilla y barata, puede realizarse en el lugar de muestreo. Sin embargo, presenta algunos inconvenientes relacionados con su incapacidad para distinguir los plásticos de otras partículas. El tamaño mínimo que se puede visualizar es de unos 10 μm.[44,45]

La microscopía electrónica es una de las técnicas más utilizadas para el análisis de nanomateriales, pero para el análisis de plásticos tiende a utilizarse como técnica complementaria. Pueden utilizarse dos tipos de microscopía electrónica: Microscopía Electrónica de Barrido (SEM) y Microscopía Electrónica de Transmisión (TEM). Para identificar y cuantificar los elementos, la SEM y la TEM suelen combinarse con la espectroscopia de rayos X por dispersión de energía (EDX).[46,47] Estas técnicas son caras, los tiempos de análisis son largos y la preparación de las muestras laboriosa.

SEM utiliza un haz de electrones de alta intensidad para irradiar la muestra, la interacción entre el haz y la muestra produce electrones secundarios que se utilizan para obtener la imagen. El límite de detección del tamaño de las partículas es de unos 3 nm.[44,45,47–49] TEM detecta el haz de electrones de transmisión a través de la muestra que requiere altas tensiones de aceleración de electrones y secciones transversales de muestra ultrafinas.[44,45,47,50] Aunque esta técnica tiene un límite de detección de tamaño de 1 nm,[44] su uso en plásticos se ve dificultado por el bajo contraste debido a las débiles interacciones elásticas de los plásticos con los electrones.[47]

En la microscopía de fuerza atómica (AFM), la imagen de la muestra se forma pasando sobre la muestra una pequeña punta de material conductor muy rígido que se fija al extremo del voladizo. Para la formación de la imagen, se registra la desviación de la punta a través de la muestra, causada por interacciones electrostáticas o de van der Waals.[47] Esta técnica proporciona imágenes con una alta resolución en torno a 0,3 nm e imágenes en 3D de la estructura de la superficie. Además, permite investigar la superficie de polímeros no conductores. Pueden surgir problemas por daños en la punta debidos a la

interacción con la muestra. En algunos casos, pueden desprenderse fragmentos que, en el caso de polímeros adhesivos, pueden producir imágenes incorrectas.[44,45,47,50]

3.2. Técnicas de dispersión de luz

Varias técnicas se basan en la aplicación de la dispersión de luz láser sobre las partículas para obtener información sobre el tamaño de las partículas, su distribución (PSD) o su estado de agregación. Las técnicas más utilizadas para el análisis de plásticos son la dispersión de luz dinámica (DLS), el análisis de seguimiento de nanopartículas (NTA) y la dispersión de luz multiángulo (MALS).

La técnica DLS se basa en la medición de las fluctuaciones de intensidad de un haz láser sobre la muestra debidas al movimiento browniano de las partículas presentes. Concretamente, la DLS permite determinar el diámetro hidrodinámico (d_h), PSD y el estado de agregación de la partícula. Por otro lado, presenta problemas cuando se utiliza para muestras con partículas grandes, con alta polidispersidad y en matrices complejas. Su rango de tamaño de trabajo se fija entre 10 nm y 3 µm a concentraciones de mg L^{-1}.[44–46]

El análisis de seguimiento de nanopartículas (NTA), al igual que el DLS, se basa en la medición del movimiento browniano de las partículas. Sin embargo, en este caso, se aplica un microscopio y una cámara digital para registrar y transformar el movimiento utilizando la viscosidad y la temperatura del medio para obtener información sobre las partículas. Al igual que en la DLS, es posible obtener información sobre (d_h) y PSD, así como la concentración numérica. La NTA funciona mejor con muestras polidispersas y complejas, pero es más difícil de utilizar que la DLS. Esta técnica puede utilizarse con partículas de tamaños comprendidos entre 10 y 1000 nm, mientras que el intervalo de concentración de trabajo es de 10^9 - 10^{12} L^{-1}. [44,46,51]

MALS, también conocida como dispersión de luz estática (SLS), permite medir las propiedades físicas derivadas de la dependencia angular de la luz dispersada por las partículas. La dispersión proporciona información sobre el tamaño de las partículas y el radio de giro (d_g) . El rango de trabajo está entre 10 - 1000 nm. El principal problema de MALS es que requiere muestras más limpias que DLS.[44–46,50]

Todas estas técnicas de dispersión pueden acoplarse en línea a técnicas de separación como el fraccionamiento asimétrico de flujo-campo (AF4), evitando los problemas derivados de la polidispersidad y la presencia de partículas interferentes.[44–46]

3.3. Técnicas espectroscópicas

Las técnicas espectroscópicas se utilizan para la identificación química de las partículas presentes en las muestras. Entre estas técnicas, las más utilizadas son la espectroscopia infrarroja por transformada de Fourier (FTIR) y la espectroscopia Raman.

FTIR se basa en la irradiación de la muestra con luz infrarroja (rango de números de onda 400 - 4000 cm^{-1} para el IR medio) que, dependiendo de la estructura molecular de la muestra, es absorbida y posteriormente medida, ya sea en modo de reflexión o de transmisión. Esta técnica permite un análisis directo y no destructivo y proporciona información adicional sobre la meteorización fisicoquímica de los plásticos. Sin embargo, esta técnica tiene limitaciones relacionadas con el límite inferior de tamaño a analizar, que se fija en unos 20 µm. Cuando es necesario analizar muestras con tamaños de partícula más pequeños (< 10 µm), es necesario utilizar la espectroscopia infrarroja con microtransformación de Fourier (µFTIR), que se basa en el acoplamiento de FTIR con microscopía. Utilizando µFTIR no sólo podemos obtener información sobre la composición de las partículas, sino también realizar su cuantificación.

Sin embargo, para su uso se requieren muestras secas y es menos sensible en comparación con la espectroscopia Raman.[44,45,47–50,52]

La espectroscopia Raman se basa en los movimientos vibratorios de las moléculas provocados por la radiación láser de una partícula, que causa la reemisión de luz a longitudes de onda características de grupos atómicos específicos. Los espectros obtenidos corresponden a la estructura química de las partículas analizadas, actuando como una huella dactilar de la partícula. En comparación con el FTIR, la espectroscopia Raman ofrece una mejor resolución espacial, una mayor sensibilidad a los grupos funcionales no polares y una menor interferencia causada por el agua. Micro-Raman (µRaman) permite analizar partículas de hasta 0,5 µm.

El principal problema de la espectroscopia Raman es el riesgo de degradación de los polímeros debido a las altas temperaturas provocadas por el láser.[44,47–49]

3.4. Técnicas termoanalíticas

Las técnicas termoanalíticas permiten identificar los tipos de plásticos mediante la degradación de las partículas y el análisis de los productos de degradación por técnicas cromatográficas. Los cromatogramas (pirogramas) obtenidos permiten la identificación simultánea de diferentes polímeros y aditivos orgánicos asociados. Sin embargo, se echa en falta información sobre el tamaño o la forma de las partículas. Entre las técnicas termoanalíticas más utilizadas se encuentran la espectrometría de masas por cromatografía de gases de pirólisis (Py-GC-MS) y la termoextracción y desorción (TED-GC-MS).[44,45,48,50]

En Py-GC-MS, la muestra se degrada térmicamente en una atmósfera inerte y los fragmentos de pirólisis de la estructura polimérica pueden separarse mediante cromatografía de gases y caracterizarse por espectrometría de masas. El análisis requiere una pequeña cantidad de muestra seca (ng - µg) y puede

utilizarse para identificar simultáneamente tipos de polímeros y aditivos plásticos orgánicos asociados.[44,45,48,50]

El TED-GC-MS combina una extracción térmica de los productos del análisis termogravimétrico en un absorbedor en fase sólida, que posteriormente se desorben térmicamente en espectrometría de masas por cromatografía de gases para permitir la identificación del polímero. El método requiere cantidades de muestra de miligramos y no requiere preconcentración ni selección de partículas. Los tiempos de medición son más cortos que los de Py-GC-MS.[44,45,48,50]

4. Objetivos

La presencia de microplásticos y nanoplásticos en el medio ambiente puede producir varios efectos directos inherentes a su propia naturaleza, pero también una serie de efectos indirectos relacionados con su capacidad para adsorber y transportar distintos tipos de contaminantes, magnificando sus efectos potenciales sobre los organismos vivos. Por ello, es necesario disponer de información sobre su presencia, distribución y efectos en el medio ambiente. Aunque el número de estudios sobre estos temas ha aumentado en los últimos años, todavía son muy limitados, en gran parte debido a la falta de métodos analíticos para detectar, caracterizar y cuantificar los micro y nanoplásticos en diferentes sistemas.

Los objetivos de esta tesis fueron:

- Desarrollo de una metodología analítica basada en ICP-MS de partícula única para la detección de partículas de plástico mediante trazado isotópico de carbono, así como su validación para el análisis de muestras que contengan este tipo de partículas.
- Investigación de la presencia de microplásticos en productos de consumo y muestras medioambientales.

- Estudio del papel de los micro/nanoplásticos como vectores de otros contaminantes emergentes.

Tras una introducción general, la tesis se ha estructurado en tres capítulos diferentes, en cada uno de los cuales se abordan los antecedentes científicos, las condiciones experimentales, los resultados y la discusión correspondiente a los retos mencionados. El primer capítulo se centra en el desarrollo de una metodología basada en SP-ICP-MS para el análisis de partículas plásticas. El segundo capítulo se centra en la aplicación de la metodología previamente desarrollada para la detección de microplásticos en aguas fluviales mediante análisis de cribado. El tercer capítulo se centra en el estudio del comportamiento adsorbente de los plásticos en presencia de contaminantes emergentes como los agentes de contraste basados en gadolinio. Por último, el manuscrito de tesis termina con una conclusión.

La información presentada en el primer capítulo se publicó en Talanta *(Laborda, F., Trujillo, C. & Lobinski, R. Analysis of microplastics in consumer products by single particle-inductively coupled plasma mass spectrometry using the carbon-13 isotope. Talanta* ***221,*** *121486 (2021))* y una nota técnica (*Laborda, F., Trujillo, C. & Lobinski, R. Unlocking Carbon-13 with Single Particle ICP-MS: Feasibility Study for Microplastic Detection. Perkin Elmer (2022)*). Los resultados presentados en los capítulos dos y tres están en proceso de preparación para su publicación.

5. References

1. Chalmin, P. Field Actions Science Reports The history of plastics: from the Capitol to the Tarpeian Rock. Field Actions Science Reports, 19, 5–11 (2019).

2. Su, L., Xiong, X., Zhang, Y., Wu, C., Xu, X., Sun, C. & Shi, H. Global transportation of plastics and microplastics: A critical review of pathways and influences. Science of the Total Environment, 831, 154884 (2022).

3. PlasticsEurope. Plastics – the Facts 2020. PlasticEurope (2020).

4. Frias, J. & Nash, R. Microplastics: Finding a consensus on the definition. Marine Pollution Bulletin, 138, 145–147 (2019).

5. Ali, S. S., Elsamahy, T., Koutra, E., Kornaros, M., El-Sheekh, M., Abdelkarim, E. A., Zhu, D. & Sun, J. Degradation of conventional plastic wastes in the environment: A review on current status of knowledge and future perspectives of disposal. Science of The Total Environment 771, 144719 (2021).

6. Naik, R. K., Naik, M. M., D'Costa, P. M. & Shaikh, F. Microplastics in ballast water as an emerging source and vector for harmful chemicals, antibiotics, metals, bacterial pathogens and HAB species: A potential risk to the marine environment and human health. Marine Pollution Bulletin, 149, 110525 (2019).

7. Lebreton, L., Slat, B., Ferrari, F., Sainte-Rose, B., Aitken, J., Marthouse, R., Hajbane, S., Cunsolo, S., Schwarz, A., Levivier, A., Noble, K., Debeljak, P., Maral, H., Schoeneich-Argent, R., Brambini, R. & Reisser, J. Evidence that the Great Pacific Garbage Patch is rapidly accumulating plastic. Scientific Reports, 8, 4666 (2018).

8. Du, F., Cai, H., Zhang, Q., Chen, Q. & Shi, H. Microplastics in take-out food containers. Journal of Hazardous Materials, 399, 122969 (2020).

9. Winkler, A., Santo, N., Ortenzi, M. A., Bolzoni, E., Bacchetta, R. & Tremolada, P. Does mechanical stress cause microplastic release from plastic water bottles?. Water Research, 166, 115082 (2019).

10. Mason, S. A., Welch, V. G. & Neratko, J. Synthetic Polymer Contamination in Bottled Water. Frontiers in Chemistry, 6 (407) (2018).

11. Robertson, I. Aplication note: FT-IR Microscopic Analysis of Microplastics in Bottled Water. PerkinElmer (2018).

12. Kutralam-Muniasamy, G., Pérez-Guevara, F., Elizalde-Martínez, I. & Shruti, V. C. Branded milks – Are they immune from microplastics contamination?. Science of The Total Environment ,714, 136823 (2020).

13. Kim, J.-S., Lee, H.-J., Kim, S.-K. & Kim, H.-J. Global Pattern of Microplastics (MPs) in Commercial Food-Grade Salts: Sea Salt as an Indicator of Seawater MP Pollution. Environmental Science & Technology, 52, 12819–12828 (2018).

14. Yang, D., Shi, H., Li, L., Li, J., Jabeen, K. & Kolandhasamy, P. Microplastic Pollution in Table Salts from China. Environmental Science & Technology, 49, 13622–13627 (2015).

15. Seth, C. K. & Shriwastav, A. Contamination of Indian sea salts with microplastics and a potential prevention strategy. Environmental Science and Pollution Research, 25, 30122–30131 (2018).

16. Iñiguez, M. E., Conesa, J. A. & Fullana, A. Microplastics in Spanish Table Salt. Scientific Reports, 7, 8620 (2017).

17. Peixoto, D., Pinheiro, C., Amorim, J., Oliva-Teles, L., Guilhermino, L. & Vieira, M. N. Microplastic pollution in commercial salt for human consumption: A review. Estuarine, Coastal and Shelf Science, 219, 161–168 (2019).

18. Hernandez, L. M., Xu, E. G., Larsson, H. C. E., Tahara, R., Maisuria, V. B. & Tufenkji, N. Plastic Teabags Release Billions of Microparticles and Nanoparticles into Tea. Environmental Science & Technology, 53, 12300–12310 (2019).

19. Hartmann, N. B., Hüffer, T., Thompson, R. C., Hassellöv, M., Verschoor, A., Daugaard, A. E., Rist, S., Karlsson, T., Brennholt, N., Cole, M., Herrling, M. P., Hess, M. C., Ivleva, N. P., Lusher, A. L. & Wagner, M. Are We Speaking the Same Language? Recommendations for a Definition and Categorization Framework for Plastic Debris. Environmental Science & Technology, 53, 1039–1047 (2019).

20. Browne, M., Galloway, T., & Thompson, R. Microplastics-an emerging contaminant of potential concern?. Integrated Environmental Assessment and Management, 3 (4), 458–458 (2008).

21. Moore, C. J. Synthetic polymers in the marine environment: A rapidly increasing, long-term threat. Environmental Research, 108, 131–139 (2008).

22. Ryan, P. G., Moore, C. J., van Franeker, J. A. & Moloney, C. L. Monitoring the abundance of plastic debris in the marine environment. Philosophical Transactions of the Royal Society B: Biological Sciences, 364, 1999–2012 (2009).

23. Costa, M. F., Ivar Do Sul, J. A., Silva-Cavalcanti, J. S., Araújo, M. C. B., Spengler, Â. & Tourinho, P. S. On the importance of size of plastic fragments and pellets on the strandline: A snapshot of a Brazilian beach. Environmental Monitoring and Assessment, 168, 299–304 (2010).

24. Desforges, J.P.W., Galbraith, M., Dangerfield, N. & Ross, P.S. Widespread distribution of microplastics in subsurface seawater in the NE Pacific Ocean. Marine Pollution Bulletin, 79, 94–99 (2014).

25. Wagner, M., Scherer, C., Alvarez-Muñoz, D., Brennholt, N., Bourrain, X., Buchinger, S., Fries, E., Grosbois, C., Klasmeier, J., Marti, T., Rodriguez-Mozaz, S., Urbatzka, R., Vethaak, A. D., Winther-Nielsen, M. & Reifferscheid, G. Microplastics in freshwater ecosystems: what we know and what we need to know. Environmental Science Europe, 26, 12 (2014).

26. In: Bergmann, M., Gutow, L. & Klages, M. (Eds.). Marine Anthropogenic Litter. Springer (2015).

27. Andrady, A. L. Plastics and Environmental Sustainability. Wiley (2015)

28. Koelmans, A. A., Kooi, M., Law, K. L. & Van Sebille, E. All is not lost: deriving a top-down mass budget of plastic at sea. Environmental Research Letters, 12 (11), 114028 (2017).

29. Arthur, C., Baker, J. & Bamford, H. Proceedings of the International Research Workshop on the Occurrence , Effects , and Fate of Microplastic Marine Debris. (2009).

30. Commission, T., European, T. & Joint, C. Commission recommendations. Nursing Standard, 24, 6–6 (2010).

31. European Commission. Guidance on Monitoring of Marine Litter in European Seas. (2013).

32. GESAMP. Sources, fate and effects of microplastics in the marine environment:A global assessment. (2015).

33. EFSA Panel. Presence of microplastics and nanoplastics in food, with particular focus on seafood. EFSA Journal, 14, (2016).

34. Gigault, J., Halle, A. ter, Baudrimont, M., Pascal, P. Y., Gauffre, F., Phi, T. L., El Hadri, H., Grassl, B. & Reynaud, S. Current opinion: What is a nanoplastic? Environmental Pollution 235, 1030–1034 (2018).

35. Wang, T., Wang, L., Chen, Q., Kalogerakis, N., Ji, R. & Ma, Y. Interactions between microplastics and organic pollutants: Effects on toxicity, bioaccumulation, degradation, and transport. Science of the Total Environment, 748, 142427 (2020).

36. Manzoor, S., Naqash, N., Rashid, G. & Singh, R. Plastic Material Degradation and Formation of Microplastic in the Environment: A Review. Materials Today: Proceedings, 56, 3254–3260 (2022).

37. Singh, B. & Sharma, N. Mechanistic implications of plastic degradation. Polymer Degradation and Stability, 93, 561–584 (2008).

38. Zhang, K., Hamidian, A. H., Tubić, A., Zhang, Y., Fang, J. K. H., Wu, C. & Lam, P. K. S. Understanding plastic degradation and microplastic formation in the environment: A review. Environmental Pollution, 274, 116554 (2021).

39. Bacha, A.-U.-R., Nabi, I. & Zhang, L. Mechanisms and the Engineering Approaches for the Degradation of Microplastics. ACS ES&T Engineering, 1 (11), 1481–1501 (2021).

40. Duan, J., Bolan, N., Li, Y., Ding, S., Atugoda, T., Vithanage, M., Sarkar, B., Tsang, D. C. W. & Kirkham, M. B. Weathering of microplastics and interaction with other coexisting constituents in terrestrial and aquatic environments. Water Research, 196, 117011 (2021).

41. Du, H., Xie, Y. & Wang, J. Microplastic degradation methods and corresponding degradation mechanism: Research status and future perspectives. Journal of Hazardous Materials, 418, 126377 (2021).

42. Yang, H., Chen, G. & Wang, J. Microplastics in the marine environment: Sources, fates, impacts and microbial degradation. Toxics, 9, 1–19 (2021).

43. Laborda, F. & Bolea, E. Reference Module in Chemistry, Molecular Sciences and Chemical Engineering. Elsevier (2018).

44. Schwaferts, C., Niessner, R., Elsner, M. & Ivleva, N. P. Methods for the analysis of submicrometer- and nanoplastic particles in the environment. TrAC Trends in Analytical Chemistry, 112, 52–65 (2019).

45. Ali, I., Cheng, Q., Ding, T., Yiguang, Q., Yuechao, Z., Sun, H., Peng, C., Naz, I., Li, J. & Liu, J. Micro- and nanoplastics in the environment: Occurrence, detection, characterization and toxicity – A critical review. Journal of Cleaner Production, 313, 127863 (2021).

46. Laborda, F., Bolea, E., Cepriá, G., Gómez, M. T., Jiménez, M. S., Pérez-Arantegui, J. & Castillo, J. R. Detection, characterization and quantification of inorganic engineered nanomaterials: A review of techniques and methodological approaches for the analysis of complex samples. Analytica Chimica Acta, 904, 10–32 (2016).

47. Mariano, S., Tacconi, S., Fidaleo, M., Rossi, M. & Dini, L. Micro and Nanoplastics Identification: Classic Methods and Innovative Detection Techniques. Frontiers in Toxicology, 3, 1–17 (2021).

48. Silva, A. B., Bastos, A. S., Justino, C. I. L., da Costa, J. P., Duarte, A. C. & Rocha-Santos, T. A. P. Microplastics in the environment: Challenges in analytical chemistry - A review. Analytica Chimica Acta,1017, 1–19 (2018).

49. Tirkey, A. & Upadhyay, L. S. B. Microplastics: An overview on separation, identification and characterization of microplastics. Marine Pollution Bulletin, 170, 112604 (2021).

50. Ivleva, N. P. Chemical Analysis of Microplastics and Nanoplastics: Challenges, Advanced Methods, and Perspectives. Chemical Reviews, 121, 11886–11936 (2021).

51. Lambert, S. & Wagner, M. Characterisation of nanoplastics during the degradation of polystyrene. Chemosphere, 145, 265–268 (2016).

52. Ateia, M., Ersan, G., Alalm, M. G., Boffito, D. C. & Karanfil, T. Emerging investigator series: microplastic sources, fate, toxicity, detection, and interactions with micropollutants in aquatic ecosystems – a review of reviews. Environmental Science: Processes & Impacts, 24, 172–195 (2022).

CONCLUSIONES

El seguimiento del isótopo C-13 mediante Single Particle-ICP-MS resultó ser una metodología analítica óptima para la detección de partículas de plástico a concentraciones de hasta cientos de partículas por mililitro, con tamaños superiores a 1 µm y alcanzando un rango superior de alrededor de 5 - 6 µm. Este rango de trabajo en tamaño estaba condicionado por las limitaciones inherentes para la detección de carbono en ICP-MS, pero también por la eficiencia de transporte de partículas grandes en los sistemas de nebulización neumática. Por otro lado, se observó que la eficiencia de nebulización se situó en torno al 40% para partículas de hasta 3 µm aproximadamente, disminuyendo para partículas más grandes y, por tanto, subestimando su concentración. Debido a estas limitaciones, SP-ICP-MS no debe ser utilizado para la determinación cuantitativa de microplásticos polidispersos, sin embargo, presenta gran utilidad como técnica de cribado rápido para la detección de partículas plásticas.

La viabilidad de la metodología desarrollada para el análisis de distintos productos de consumo fue demostrada. Ello se consiguió a través de la detección exitosa de microplásticos primarios añadidos intencionadamente a productos de cuidado personal utilizados a modo de exfoliantes. Además de por la confirmación de la presencia de microplásticos secundarios liberados de bolsas de té sometidas a un proceso de infusión convencional.

La metodología SP-ICP-MS desarrollada, también fue utilizada para explorar las aguas ambientales de ríos españoles y franceses a fin de detectar la presencia de microplásticos. La aplicación de un pretratamiento ácido a las muestras mejoró la detectabilidad de micropartículas plásticas, así como la selectividad del método. Todas las aguas fluviales analizadas mediante SP-ICP-MS mostraron la presencia de partículas que contenían carbono. Posteriormente, unas muestras seleccionadas fueron analizadas mediante microscopia Raman lo que confirmo la presencia de partículas plásticas en las mismas. Por tanto, la SP-ICP-MS puede ser utilizada como una técnica adecuada de cribado para la discriminación de muestras que contengan microplásticos, las cuales

posteriormente deberían ser analizadas mediante microscopía Raman o FT-IR, técnicas que requieren tiempos de análisis más largos. En cualquier caso, los resultados obtenidos en los ríos españoles y franceses confirman la contaminación por microplásticos en el medio ambiente.

El hecho de confirmar la presencia de partículas plásticas en el medio ambiente hace necesario comprender papel de estas como vectores de contaminantes emergentes. Por este motivo, se llevo a cabo el estudio de adsorción de los agentes de contraste basados en gadolinio sobre nanoplásticos modelo y medioambientales, y la comparación con la adsorción del gadolinio iónico. Estos estudios adsorción, ajustados al modelo de Freundlich, confirmaron que parámetros como el pH, la concentración, el tiempo de contacto o el medio influían en la adsorción de estas especies de gadolinio.

Por otro lado, también se llevó a cabo la adsorción de estas especies de Gd sobre coloides naturales. Los resultados obtenidos manifestaron el papel de los nanoplásticos en aguas naturales como vectores de los agentes de contraste basados en gadolinio, resultados en línea con otros contaminantes emergentes. Además, también se demostró la capacidad de los nanoplásticos para competir con los coloides naturales en la adsorción y transporte de estos contaminantes en ambientes naturales.

RÉSUMÉ

Aujourd'hui, le plastique est un matériau largement utilisé dans de nombreux secteurs. Par conséquent, une grande partie du plastique finit en déchets dans l'environnement, ce qui en fait un problème mondial. On estime qu'environ 80 % des plastiques produits sont rejetés dans l'environnement. Certains de ces plastiques se retrouvent sous forme de nanoplastiques et de microplastiques dans les systèmes aquatiques. La présence de ces plastiques pose des problèmes en raison de leur taille et de leur capacité à adsorber et transporter les polluants émergents, et donc à faciliter leur ingestion par les organismes vivants. La compréhension des effets des micro- et nanoplastiques est encore limitée, en grande partie à cause du manque de méthodes robustes pour leur détection et leur quantification.

Dans ce contexte, cette thèse de doctorat a eu pour objectif le développement d'une méthode analytique pour la détection, la caractérisation de la taille et la quantification des microparticules de plastique par ICP-MS fonctionnant en mode particule unique avec des temps de séjour de l'ordre de la microseconde. Cette méthode a permis la détection de particules de polystyrène d'une taille allant jusqu'à 1,2 µm par traçage isotopique ^{13}C et a été utilisée pour analyser les microplastiques dans les produits de soins personnels et ceux libérés par les emballages alimentaires. Une plateforme analytique a également été développée pour l'analyse d'échantillons environnementaux, tels que l'eau de rivière, en combinant l'ICP-MS à particule unique, la microscopie électronique à balayage à émission de champ et la spectroscopie Raman. L'utilisation de cette plateforme nous a permis de déterminer la présence et l'identité chimique des microparticules de plastique dans les échantillons d'eau de rivière analysés. Nous avons également étudié la capacité d'adsorption des nanoplastiques environnementaux pour les polluants émergents, tels que les agents de contraste à base de gadolinium, et leur capacité à agir comme concurrents des colloïdes naturels. La capacité des nanoplastiques à agir comme des vecteurs de polluants émergents dans des conditions environnementales a été démontrée.

1. Les plastiques aujourd'hui

Les plastiques sont des polymères organiques à longue chaîne de poids moléculaire élevé produits à partir de matières premières fossiles, telles que le pétrole ou le gaz. Ils sont divisés en deux groupes, les thermoplastiques et les thermodurcissables.[1,2] Les premiers, qui peuvent fondre lorsqu'ils sont chauffés et durcir lorsqu'ils sont refroidis, comprennent le polyéthylène (PE), le polypropylène (PP), le chlorure de polyvinyle (PVC), le polyéthylène téréphtalate (PET) et le polystyrène (PS). Le deuxième groupe, qui subit des transformations chimiques lorsqu'il est chauffé, créant un réseau tridimensionnel, comprend le polyuréthane (PUR), le polyester insaturé, les résines époxy et la résine mélamine.[3]

Le premier plastique synthétique, la bakélite, fabriqué en 1907 par Leo Hendrik Baekeland, a inauguré une nouvelle ère dans la science des matériaux. Depuis le début du 20e siècle, l'utilisation des plastiques dans le monde a augmenté de façon exponentielle. Actuellement, les plastiques les plus utilisés sont le polyéthylène, le polypropylène, le chlorure de polyvinyle, le polyéthylène téréphtalate, le polyuréthane et le polystyrène. Leur production mondiale est passée en 2018 de 359 millions de tonnes à 368 millions de tonnes en 2019 et est en augmentation. Parmi les pays ayant la plus grande production de plastiques, la Chine représentait 31% de la production mondiale en 2019.[3]

Plus de 8 millions de tonnes de plastiques sont rejetées chaque année dans l'écosystème marin. Ils s'accumulent dans les gyres océaniques dans certaines régions du globe. L'un des plus connus est le Great Pacific garbage patch (GPGP) dans le Pacifique Nord, qui occupe environ 1,6 million de km^2.[7]

Les plastiques sont utilisés sous diverses formes dans les produits de consommation, les cosmétiques ou les aliments, ce qui peut entraîner la présence de microplastiques et de nanoplastiques disponibles pour la consommation humaine. Leur libération a été signalée à partir de contenants de nourriture à emporter et de bouteilles en plastique. Des microplastiques et des nanoplastiques ont également été trouvés dans des produits alimentaires de consommation, tels

que le lait,[12] le sel[13-17] ou les thés.[18] Par conséquent, les plastiques peuvent entrer dans la chaîne alimentaire de différents organismes.

2. Microplastiques et nanoplastiques: état de l'art

Aucune définition normalisée n'est actuellement disponible pour les microplastiques et les nanoplastiques. Dans de nombreux cas, les classifications utilisées rendent difficile la comparaison des résultats obtenus dans différentes études.[19] La Figure 1 montre une représentation de la classification des plastiques dans différentes études. La principale différence entre ces définitions est liée à la taille des particules.

Les plastiques sont divisés, en fonction de leur taille, en quatre grands groupes: macroplastiques, mésoplastiques, microplastiques et nanoplastiques. En général, les macroplastiques sont compris comme des plastiques de tailles comprises entre 5[20,21,26,28] et 2,5 mm.[22,25,27,31,32] La taille des mésoplastiques est de 1 et 25 mm,[22,25,27,31,32] mais ils ne sont souvent pas considérés comme une classe distincte. Dans le cas des plastiques appelés microplastiques, la gamme de tailles de particules variait selon les études: 1-5000 μm,[24,25,28,31] 0,1-5000 μm[21,22,26,33] ou 1-1000 μm.[20,23,37,32] Frias *et al.,*[4] ont défini les microplastiques comme « toute particule solide synthétique ou matrice polymère, de forme régulière ou irrégulière et de taille allant de 1 μm à 5 mm, d'origine primaire ou secondaire, qui sont insolubles dans l'eau ». Dans le cas des nanoplastiques, leurs gammes de tailles ont tendance à être marquées entre 1 et 100 nm ou moins de 1 μm. Gigault et *al.,*[34] ont défini les nanoplastiques comme « des particules d'une taille allant de 1 à 1000 nm résultant de la dégradation d'objets plastiques industriels et pouvant présenter un comportement colloïdal ».

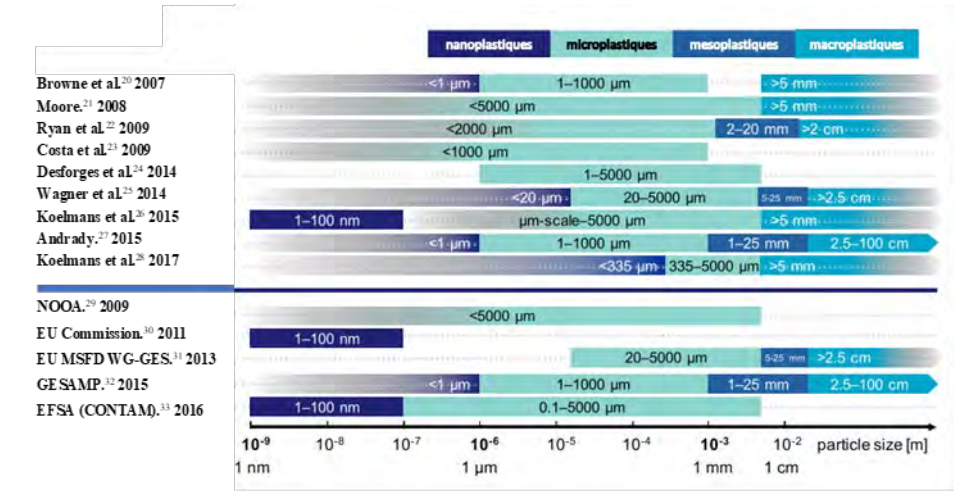

Figure 1. Exemples de différences dans la catégorisation des débris plastiques en fonction de leur taille, telles qu'appliquées (et/ou définies) dans la littérature scientifique et dans les rapports institutionnels. Il convient de noter qu'il ne s'agit pas d'un aperçu exhaustif de toutes les classes de taille utilisées.[19]

2.1. Formation de nanoplastiques et de microplastiques

La formation de micro et nanoplastiques à partir de macro et mésoplastiques nécessite l'action de divers processus, qui modifieront non seulement la taille des particules, mais aussi les caractéristiques de surface. Ces processus comprennent la dégradation mécanique, la photodégradation, la dégradation thermique et la biodégradation.[35,36]

2.1.1. Dégradation mécanique

La dégradation mécanique est basée sur la dégradation des plastiques due à leur dégradation par des forces externes. La dégradation se produit lorsque les forces appliquent une contrainte excessive sur le plastique, ce qui entraîne la rupture des chaînes moléculaires et la formation d'une paire de radicaux libres. En présence d'oxygène, ces radicaux peuvent former des radicaux peroxy. Les radicaux produits en raison de la contrainte proviennent de la partie principale du plastique dans la région stressée. Ces forces externes peuvent être dues au frottement entre le plastique et un autre matériau. Un exemple de cette dégradation

mécanique est l'abrasion entre le pneu et la route, qui entraîne la libération de fragments de la surface du pneu à la suite du frottement. Dans l'environnement, les frictions peuvent être causées par l'action des vagues de la mer, le gel, le vent, le sable, les collisions avec des roches ou par les activités humaines (p. ex., la culture du sol et la rotation des cultures).[39,40]

2.1.2. Photodégradation

La photodégradation est la dégradation des plastiques due à l'action de la lumière (visible, infrarouge et UV). La fraction UV de la lumière a le plus grand effet sur les plastiques, en particulier les rayons UVB (290 - 315 nm) et UVA (315-400 nm). [38,40] Ce processus de dégradation a lieu dans la couche externe des plastiques et peut atteindre une profondeur de μm, selon le type de plastique. [40]

Le processus de photodégradation repose sur trois étapes : initiation, propagation et terminaison. Dans l'étape d'initiation, l'énergie UV brise les liaisons chimiques des chaînes polymères et favorise la formation de radicaux libres. L'étape de propagation est basée sur une série de réactions communes à tous les polymères à base de carbone. Ces réactions conduisent à la génération d'espèces d'hydroperoxydes qui favorisent les réactions ultérieures conduisant à l'auto-oxydation. L'étape de terminaison se produit lorsque les radicaux libres sont absorbés pour créer des produits inertes. Cette étape est atteinte naturellement par réaction avec des stabilisants dans le plastique. Afin de pouvoir poursuivre ce processus, une autre couche non oxydée doit l'être. [5,37–39,41] La Figure 2 illustre le processus de photodégradation.

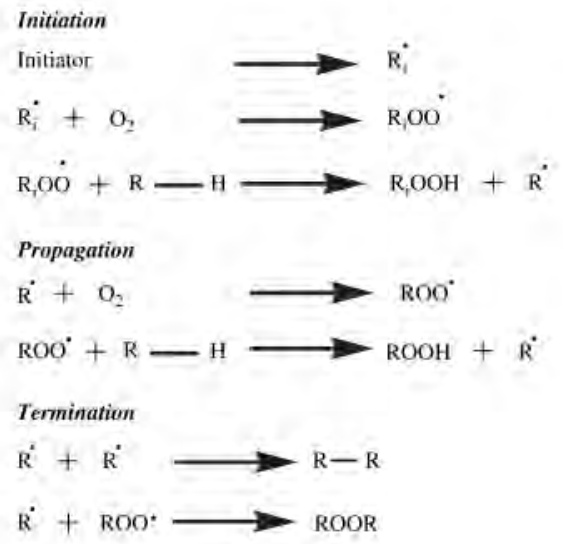

Figure 2. Schéma du processus de photodégradation, montrant les 3 étapes du processus : Initiation, propagation et terminion.[37]

2.1.3. Dégradation thermique

La dégradation thermique est basée sur la dégradation des plastiques due aux températures élevées. La dégradation dépend des caractéristiques des additifs antioxydants dans les polymères, qui déterminent la température à laquelle le processus aura lieu.[37,38]

Le processus de dégradation commence lorsque le polymère a suffisamment de chaleur pour surmonter la barrière énergétique, de sorte que des radicaux libres peuvent être générés à partir des chaînes polymères. Les radicaux libres peuvent réagir avec l'oxygène pour produire des hydroperoxydes, qui peuvent ensuite se cliver pour former des radicaux libres hydroxyles et des radicaux alcoxy. La première partie du processus est comme dans la photodégradation. Cette réaction se propagera d'elle-même le long du polymère jusqu'à ce que l'alimentation en énergie soit interrompue ou lorsque des produits inertes se forment en raison de la collision de deux radicaux.[5,37,38] Dans l'environnement, ce type de dégradation se produit dans des environnements où les plastiques sont exposés à la lumière directe du soleil. [38]

2.1. 4. Biodégradation

La biodégradation est basée sur la dégradation des plastiques due à la transformation biochimique par des micro-organismes. Le degré de biodégradation est contrôlé par les caractéristiques physico-chimiques du polymère (surface, poids moléculaire, structure chimique, élasticité...). Les microbes impliqués dans la biodégradation comprennent les bactéries, les champignons, les algues et les protozoaires. Ce type de dégradation peut se produire à différents niveaux structurels (moléculaire, macromoléculaire, microscopique et macroscopique).[36,37,39,41,42] Cette dégradation est fortement influencée par le type de plastique, qui peut être hydrolysable ou non hydrolysable, selon la présence ou l'absence de groupes ester ou amide. Les plastiques non hydrolysables comprennent le PE, le PP et le PVC, car ils ont une structure semblable à celle de la lignine, ce qui rend leur dégradation difficile.[38,40]

Le processus de dégradation comporte trois étapes : la biofragmentation, l'assimilation et la minéralisation (Figure 3).

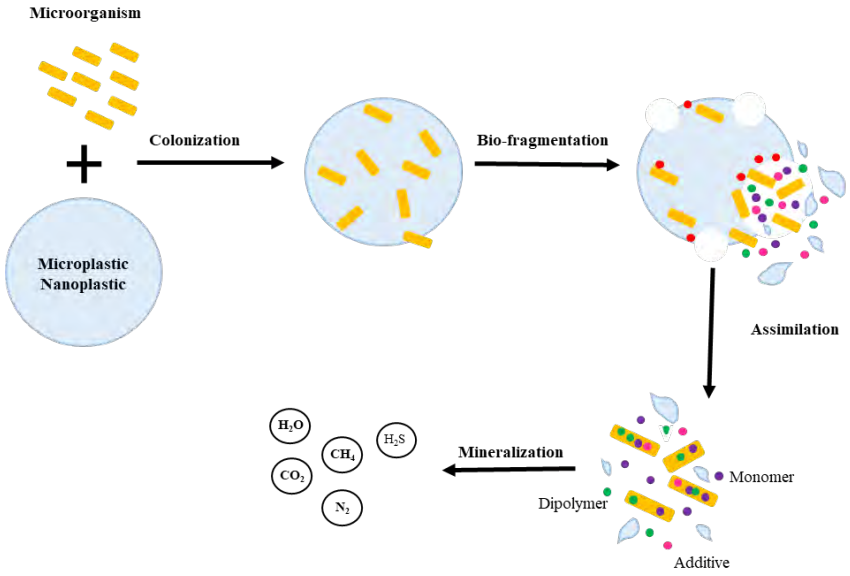

Figure 3. Schéma représentant la biodégradation réalisée par les micro-organismes, montrant les 3 étapes : bio-fragmentation, assimilation et minéralisation. [40]

La biofragmentation est produite à la suite de l'adhésion d'un microorganisme à la surface du polymère et/ou de sa pénétration dans les pores du polymère. Les substances extracellulaires libérées agissent sur le squelette carboné du polymère, produisant des oligomères, des dimères et des monomères, qui peuvent traverser la membrane semi-perméable du microorganisme, dans un processus connu sous le nom d'assimilation. Ces composés absorbés sont transformé en CO_2, H_2Oh, CH_4, H_2S et N_2 par différents métaboliques Voies.[5,36–41]

3. Principales techniques techniques de détection, de caractérisation et de quantification des nanoplastiques et des microplastiques

L'exposition des humains aux nano- et microplastiques nécessite des techniques permettant leur détection, leur caractérisation et leur quantification dans une grande variété d'échantillons. Actuellement, il n'existe pas de technique unique qui nous permette de déterminer la composition, la forme, la taille et la concentration de ces particules. Par conséquent, en général, la caractérisation de ces nano et microplastiques est effectuée à deux niveaux, le physique et le chimique. La caractérisation physique fait généralement référence à la description d'un matériau en fonction de sa taille de particule, de sa distribution granulométrique (PSD), de sa forme et de sa surface. L'état d'agglomération/agrégation peut être inclus ici, car il peut être évalué par la taille des particules. Une caractérisation chimique d'une particule comprend sa composition élémentaire et/ou moléculaire, une formule chimique avec une stœchiométrie spécifique, l'état chimique des éléments et la structure-conformation moléculaire, dans la mesure du possible.[43]

3.1. Microscopie

Les techniques de microscopie sont largement utilisées pour obtenir des informations sur la taille, la forme, l'état d'agrégation et les propriétés de surface

des plastiques. Ils comprennent la microscopie optique, la microscopie électronique et la microscopie à force atomique.

La microscopie optique est souvent utilisée pour effectuer le premier examen d'un échantillon. Parce qu'il s'agit d'une technique simple et peu coûteuse, elle peut être réalisée sur le site d'échantillonnage. Cependant, il présente quelques inconvénients liés à son incapacité à distinguer les plastiques des autres particules. La taille minimale à visualiser est d'environ 10 μm.[44,45]

La microscopie électronique est l'une des techniques les plus utilisées pour l'analyse des nanomatériaux, mais pour l'analyse des plastiques, elle tend à être utilisée comme technique complémentaire. Deux types de microscopie électronique peuvent être utilisés : la microscopie électronique à balayage (SEM) et la microscopie électronique à transmission (TEM). Afin d'identifier et de quantifier les éléments, le MEB et le MET ont tendance à être combinés à la spectroscopie à rayons X à dispersion d'énergie (EDX).[46,47] Ces techniques sont coûteuses, les temps d'analyse sont longs et la préparation des échantillons laborieuse.

Le SEM utilise un faisceau d'électrons de haute intensité pour irradier l'échantillon, l'interaction entre le faisceau et l'échantillon produit des électrons secondaires qui sont utilisés pour obtenir l'image. La limite de détection granulométrique est d'environ 3 nm. [44,45,47–49] TEM détecte le faisceau d'électrons de transmission à travers l'échantillon nécessitant des tensions d'accélération électronique élevées et des sections transversales ultra-minces de l'échantillon. [44,45,47,50] Bien que cette technique ait une limite de détection de taille de 1 nm, [44] son utilisation pour les plastiques est entravée par le faible contraste dû aux faibles interactions élastiques des plastiques avec les électrons.[47]

En microscopie à force atomique (AFM), l'image de l'échantillon est formée en passant sur l'échantillon une petite pointe de matériau conducteur très rigide qui est fixée à l'extrémité du porte-à-faux. Pour la formation de l'image, la déviation de la pointe à travers l'échantillon, qui est causée par des interactions électrostatiques ou de van der Waals, est enregistrée.[47] Cette technique fournit des

images avec une haute résolution environ 0,3 nm et images 3D de la structure de surface. De plus, il permet d'étudier la surface des polymères non conducteurs. Les problèmes peuvent être causés par des dommages à la pointe dus à l'interaction avec l'échantillon. Dans certains cas, des fragments peuvent être libérés, ce qui, dans le cas des polymères adhésifs, peut produire des images incorrectes.[44,45,47,50]

3.2. Techniques de catterage de la lumière

Plusieurs techniques sont basées sur l'application de la diffusion laser de la lumière sur les particules pour obtenir des informations sur la taille des particules, la distribution granulométrique (PSD) ou l'état d'agrégation. Les techniques les plus utilisées pour l'analyse des plastiques sont la diffusion dynamique de la lumière (DLS), l'analyse de suivi des nanoparticules (NTA) et la diffusion de la lumière multi-angles (MALS).

La technique DLS est basée sur la mesure des fluctuations d'intensité d'un faisceau laser sur l'échantillon dues au mouvement brownien des particules présentes. Plus précisément, DLS permet de déterminer le diamètre hydrodynamique (d_h) PSD et PSD et l'état d'aggravation de la particule. D'autre part, il présente des problèmes lorsqu'il est utilisé pour des échantillons avec de grosses particules, avec une polydispersité élevée et dans des matrices complexes. Sa plage de dimensions de travail est fixée entre 10 nm et 3 μm à des concentrations de mg L^{-1}.[44–46]

L'analyse de suivi des nanoparticules, comme DLS, est basée sur la mesure du mouvement brownien des particules. Cependant, dans ce cas, un microscope et une caméra numérique sont appliqués pour enregistrer et transformer le mouvement en utilisant la viscosité et la température du milieu pour obtenir des informations sur les particules. Comme dans DLS, il est possible d'obtenir des informations sur (et PSD ainsi que la concentration en d_h)nombre. Le NTA fonctionne mieux sur les échantillons polydispersés et complexes, mais

il est plus difficile à utiliser que le DLS. Cette technique peut être utilisée pour des particules de taille comprise entre 10 et 1000 nm alors que la plage de concentration de travail est de 10^9 á 10^{12} L^{-1}.[44,46,51]

MALS, également connu sous le nom de diffusion statique de la lumière (SLS), fournit la mesure des propriétés physiques dérivées de la dépendance angulaire de la lumière diffusée par les particules. La diffusion fournit des informations sur la taille des particules et le rayon de giration (d_g). Laplage de travail est comprise entre 10 et 1000 nm. Le principal problème de MALS est qu'il nécessite des échantillons plus propres que DLS.[44–46,50]

Toutes ces techniques de diffusion peuvent être couplées en ligne à des techniques de séparation telles que le fractionnement asymétrique par champ d'écoulement (AF4), évitantainsi les problèmes liés à la polydispersité et à la présence de particules interférentes.[44–46]

3.3. Techniques spectroscopiques

Les techniques spectroscopiques sont utilisées pour l'identification chimique des particules présentes dans les échantillons. Parmi ces techniques, les plus utilisées sont la spectroscopie infrarouge à transformée de Fourier (FTIR) et la spectroscopie Raman.

Le FTIR est basé sur l'irradiation de l'échantillon par la lumière infrarouge (gamme de numéros d'onde 400-4000 cm^{-1} pour l'IR moyen) qui, en fonction de la structure moléculaire de l'échantillon, est absorbée puis mesurée, soit en mode de réflexion, soit en mode de transmission. Cette technique permet une analyse directe et non destructive et fournit des informations supplémentaires sur l'altération physico-chimique des plastiques. Cependant, cette technique présente des limites liées à la limite inférieure de taille à analyser, qui est fixée à environ 20 μm. Lorsque des échantillons avec des particules de plus petite taille (<10 μm) doivent être analysés, il est nécessaire d'utiliser la spectroscopie

infrarouge à micro-transformée de Fourier (μFTIR), qui est basée sur le couplage du FTIR avec la microscopie. En utilisant μFTIR, nous pouvons non seulement obtenir des informations sur la composition des particules, mais aussi effectuer une quantification des particules. Cependant, des échantillons secs sont nécessaires pour son utilisation et il est moins sensible par rapport à la spectroscopie Raman.[44,45,47–50,52]

La spectroscopie Raman est basée sur les mouvements vibratoires des molécules provoqués par le rayonnement laser d'une particule, qui provoque la réémission de lumière à des longueurs d'onde caractéristiques de groupes atomiques spécifiques. Les spectres obtenus correspondent à la structure chimique des particules analysées, agissant comme une empreinte digitale de la particule. En comparaison avec FTIR, la spectroscopie Raman offre une meilleure résolution spatiale, une meilleure sensibilité aux groupes fonctionnels et une interférence plus faible causée par l'eau. Micro-Raman (μRaman) permet l'analyse de particules jusqu'à 0,5 μm.

Le principal problème de la spectroscopie Raman est le risque de dégradation des polymères en raison des températures élevées causées par le laser.[44,47–49]

3.4. Techniques thermo-analytiques

Les techniques thermoanalytiques permettent l'identification des types de plastiques par la dégradation des particules et l'analyse des produits de dégradation par des techniques chromatographiques. Les chromatogrammes (pyrogrammes) obtenus permettent l'identification simultanée de différents polymères et additifs organiques associés. Cependant, les informations sur la taille ou la forme des particules sont manquantes. Parmi les techniques thermoanalytiques les plus utilisées figurent la spectrométrie de masse par chromatographie en phase gazeuse par pyrolyse (Py-GC-MS) et la thermo-extraction et désorption (TED-GC-MS).[44,45,48,50]

Dans Py-GC-MS, l'échantillon est dégradé thermiquement dans une atmosphère inerte et les fragments de pyrolyse de la structure du polymère peuvent être séparés par chromatographie en phase gazeuse et caractérisés par spectrométrie de masse. L'analyse nécessite une petite quantité d'échantillon sec (ng - μg) et peut être utilisée pour identifier simultanément les types de polymères et les additifs plastiques organiques associés.[44,45,48,50]

TED-GC-MS combine une extraction thermique des produits de l'analyse thermogravimétrique sur un adsorbeur en phase solide, qui sont ensuite désorbés thermiquement en spectrométrie de masse chromatographique en phase gazeuse pour permettre l'identification du polymère. La méthode nécessite des quantités d'échantillons de milligrammes et ne nécessite pas de préconcentration ou de sélection de particules. Les temps de mesure sont plus courts que ceux de Py-GC-MS.[44,45,48,50]

4.Les objectifs

La présence de micro- et nanoplastiques dans l'environnement peut produire plusieurs effets directs inhérents à leur nature même, mais aussi une série d'effets indirects liés à leur capacité à adsorber et à transporter différents types de polluants, amplifiant leurs effets potentiels sur les organismes vivants. Par conséquent, des informations sur leur présence, leur répartition et leurs effets dans l'environnement sont nécessaires. Bien que le nombre d'études sur ces sujets ait augmenté ces dernières années, elles sont encore très limitées, en grande partie en raison du manque de méthodes analytiques pour détecter, caractériser et quantifier les micro et nanoplastiques dans différents systèmes.

Les objectifs de cette thèse étaient les suivants :

- Le développement d'une méthodologie analytique basée sur ICP-MS à particule unique pour la détection de particules plastiques par traçage isotopique du carbone, ainsi que sa validation pour l'analyse d'échantillons contenant ce type de particules.

- Enquête sur la présence de microplastiques dans les produits de consommation et les échantillons environnementaux
- Une étude du rôle des micro/nanoplastiques en tant que vecteurs d'autres polluants émergents.

Après une introduction générale, la thèse a été structurée en trois chapitres différents, dans lesquels chaque chapitre traite du contexte scientifique, des conditions expérimentales, des résultats et de la discussion correspondant aux défis mentionnés ci-dessus. Le premier chapitre est consacré au développement d'une méthodologie basée sur SP-ICP-MS pour l'analyse des particules plastiques. Le deuxième chapitre se concentre sur l'application de la méthodologie précédemment développée pour la détection des microplastiques dans l'eau des rivières par l'analyse de criblage. Le troisième chapitre se concentre sur l'étude de la performance adsorbante des plastiques en présence de polluants émergents tels que les agents de contraste à base de gadolinium. Enfin, le manuscrit de thèse se termine par une conclusion.

Les informations présentées dans le premier chapitre ont été publiées dans Talent (*Laborda, F., Trujillo, C. & Lobinski, R. Analysis of microplastics in consumer products by single particle-inductively coupled plasma mass spectrometry using the carbon-13 isotope. Talanta, 221, 121486 (2021))* et dans une note technique (*Laborda, F., Trujillo, C. & Lobinski, R. Unlocking Carbon-13 with Single Particle ICP-MS: Feasibility Study for Microplastic Detection. Perkin Elmer (2022)*). Les résultats présentés dans les chapitres deux et trois sont en cours de préparation en vue de leur publication.

5. References

1. Chalmin, P. Field Actions Science Reports The history of plastics: from the Capitol to the Tarpeian Rock. Field Actions Science Reports, 19, 5–11 (2019).

2. Su, L., Xiong, X., Zhang, Y., Wu, C., Xu, X., Sun, C. & Shi, H. Global transportation of plastics and microplastics: A critical review of pathways and influences. Science of the Total Environment, 831, 154884 (2022).

3. PlasticsEurope. Plastics – the Facts 2020. PlasticEurope (2020).

4. Frias, J. & Nash, R. Microplastics: Finding a consensus on the definition. Marine Pollution Bulletin, 138, 145–147 (2019).

5. Ali, S. S., Elsamahy, T., Koutra, E., Kornaros, M., El-Sheekh, M., Abdelkarim, E. A., Zhu, D. & Sun, J. Degradation of conventional plastic wastes in the environment: A review on current status of knowledge and future perspectives of disposal. Science of The Total Environment 771, 144719 (2021).

6. Naik, R. K., Naik, M. M., D'Costa, P. M. & Shaikh, F. Microplastics in ballast water as an emerging source and vector for harmful chemicals, antibiotics, metals, bacterial pathogens and HAB species: A potential risk to the marine environment and human health. Marine Pollution Bulletin, 149, 110525 (2019).

7. Lebreton, L., Slat, B., Ferrari, F., Sainte-Rose, B., Aitken, J., Marthouse, R., Hajbane, S., Cunsolo, S., Schwarz, A., Levivier, A., Noble, K., Debeljak, P., Maral, H., Schoeneich-Argent, R., Brambini, R. & Reisser, J. Evidence that the Great Pacific Garbage Patch is rapidly accumulating plastic. Scientific Reports, 8, 4666 (2018).

8. Du, F., Cai, H., Zhang, Q., Chen, Q. & Shi, H. Microplastics in take-out food containers. Journal of Hazardous Materials, 399, 122969 (2020).

9. Winkler, A., Santo, N., Ortenzi, M. A., Bolzoni, E., Bacchetta, R. & Tremolada, P. Does mechanical stress cause microplastic release from plastic water bottles?. Water Research, 166, 115082 (2019).

10. Mason, S. A., Welch, V. G. & Neratko, J. Synthetic Polymer Contamination in Bottled Water. Frontiers in Chemistry, 6 (407) (2018).

11. Robertson, I. Aplication note: FT-IR Microscopic Analysis of Microplastics in Bottled Water. PerkinElmer (2018).

12. Kutralam-Muniasamy, G., Pérez-Guevara, F., Elizalde-Martínez, I. & Shruti, V. C. Branded milks – Are they immune from microplastics contamination?. Science of The Total Environment ,714, 136823 (2020).

13. Kim, J.-S., Lee, H.-J., Kim, S.-K. & Kim, H.-J. Global Pattern of Microplastics (MPs) in Commercial Food-Grade Salts: Sea Salt as an Indicator of Seawater MP Pollution. Environmental Science & Technology, 52, 12819–12828 (2018).

14. Yang, D., Shi, H., Li, L., Li, J., Jabeen, K. & Kolandhasamy, P. Microplastic Pollution in Table Salts from China. Environmental Science & Technology, 49, 13622–13627 (2015).

15. Seth, C. K. & Shriwastav, A. Contamination of Indian sea salts with microplastics and a potential prevention strategy. Environmental Science and Pollution Research, 25, 30122–30131 (2018).

16. Iñiguez, M. E., Conesa, J. A. & Fullana, A. Microplastics in Spanish Table Salt. Scientific Reports, 7, 8620 (2017).

17. Peixoto, D., Pinheiro, C., Amorim, J., Oliva-Teles, L., Guilhermino, L. & Vieira, M. N. Microplastic pollution in commercial salt for human consumption: A review. Estuarine, Coastal and Shelf Science, 219, 161–168 (2019).

18. Hernandez, L. M., Xu, E. G., Larsson, H. C. E., Tahara, R., Maisuria, V. B. & Tufenkji, N. Plastic Teabags Release Billions of Microparticles and Nanoparticles into Tea. Environmental Science & Technology, 53, 12300–12310 (2019).

19. Hartmann, N. B., Hüffer, T., Thompson, R. C., Hassellöv, M., Verschoor, A., Daugaard, A. E., Rist, S., Karlsson, T., Brennholt, N., Cole, M., Herrling, M. P., Hess, M. C., Ivleva, N. P., Lusher, A. L. & Wagner, M. Are We Speaking the Same Language? Recommendations for a Definition and Categorization Framework for Plastic Debris. Environmental Science & Technology, 53, 1039–1047 (2019).

20. Browne, M., Galloway, T., & Thompson, R. Microplastics-an emerging contaminant of potential concern?. Integrated Environmental Assessment and Management, 3 (4), 458–458 (2008).

21. Moore, C. J. Synthetic polymers in the marine environment: A rapidly increasing, long-term threat. Environmental Research, 108, 131–139 (2008).

22. Ryan, P. G., Moore, C. J., van Franeker, J. A. & Moloney, C. L. Monitoring the abundance of plastic debris in the marine environment. Philosophical Transactions of the Royal Society B: Biological Sciences, 364, 1999–2012 (2009).

23. Costa, M. F., Ivar Do Sul, J. A., Silva-Cavalcanti, J. S., Araújo, M. C. B., Spengler, Â. & Tourinho, P. S. On the importance of size of plastic fragments and pellets on the strandline: A snapshot of a Brazilian beach. Environmental Monitoring and Assessment, 168, 299–304 (2010).

24. Desforges, J.P.W., Galbraith, M., Dangerfield, N. & Ross, P.S. Widespread distribution of microplastics in subsurface seawater in the NE Pacific Ocean. Marine Pollution Bulletin, 79, 94–99 (2014).

25. Wagner, M., Scherer, C., Alvarez-Muñoz, D., Brennholt, N., Bourrain, X., Buchinger, S., Fries, E., Grosbois, C., Klasmeier, J., Marti, T., Rodriguez-Mozaz, S., Urbatzka, R., Vethaak, A. D., Winther-Nielsen, M. & Reifferscheid, G. Microplastics in freshwater ecosystems: what we know and what we need to know. Environmental Science Europe, 26, 12 (2014).

26. In: Bergmann, M., Gutow, L. & Klages, M. (Eds.). Marine Anthropogenic Litter. Springer (2015).

27. Andrady, A. L. Plastics and Environmental Sustainability. Wiley (2015)

28. Koelmans, A. A., Kooi, M., Law, K. L. & Van Sebille, E. All is not lost: deriving a top-down mass budget of plastic at sea. Environmental Research Letters, 12 (11), 114028 (2017).

29. Arthur, C., Baker, J. & Bamford, H. Proceedings of the International Research Workshop on the Occurrence , Effects , and Fate of Microplastic Marine Debris. (2009).

30. Commission, T., European, T. & Joint, C. Commission recommendations. Nursing Standard, 24, 6–6 (2010).

31. European Commission. Guidance on Monitoring of Marine Litter in European Seas. (2013).

32. GESAMP. Sources, fate and effects of microplastics in the marine environment:A global assessment. (2015).

33. EFSA Panel. Presence of microplastics and nanoplastics in food, with particular focus on seafood. EFSA Journal, 14, (2016).

34. Gigault, J., Halle, A. ter, Baudrimont, M., Pascal, P. Y., Gauffre, F., Phi, T. L., El Hadri, H., Grassl, B. & Reynaud, S. Current opinion: What is a nanoplastic? Environmental Pollution 235, 1030–1034 (2018).

35. Wang, T., Wang, L., Chen, Q., Kalogerakis, N., Ji, R. & Ma, Y. Interactions between microplastics and organic pollutants: Effects on toxicity, bioaccumulation, degradation, and transport. Science of the Total Environment, 748, 142427 (2020).

36. Manzoor, S., Naqash, N., Rashid, G. & Singh, R. Plastic Material Degradation and Formation of Microplastic in the Environment: A Review. Materials Today: Proceedings, 56, 3254–3260 (2022).

37. Singh, B. & Sharma, N. Mechanistic implications of plastic degradation. Polymer Degradation and Stability, 93, 561–584 (2008).

38. Zhang, K., Hamidian, A. H., Tubić, A., Zhang, Y., Fang, J. K. H., Wu, C. & Lam, P. K. S. Understanding plastic degradation and microplastic formation in the environment: A review. Environmental Pollution, 274, 116554 (2021).

39. Bacha, A.-U.-R., Nabi, I. & Zhang, L. Mechanisms and the Engineering Approaches for the Degradation of Microplastics. ACS ES&T Engineering, 1 (11), 1481–1501 (2021).

40. Duan, J., Bolan, N., Li, Y., Ding, S., Atugoda, T., Vithanage, M., Sarkar, B., Tsang, D. C. W. & Kirkham, M. B. Weathering of microplastics and interaction with other coexisting constituents in terrestrial and aquatic environments. Water Research, 196, 117011 (2021).

41. Du, H., Xie, Y. & Wang, J. Microplastic degradation methods and corresponding degradation mechanism: Research status and future perspectives. Journal of Hazardous Materials, 418, 126377 (2021).

42. Yang, H., Chen, G. & Wang, J. Microplastics in the marine environment: Sources, fates, impacts and microbial degradation. Toxics, 9, 1–19 (2021).

43. Laborda, F. & Bolea, E. Reference Module in Chemistry, Molecular Sciences and Chemical Engineering. Elsevier (2018).

44. Schwaferts, C., Niessner, R., Elsner, M. & Ivleva, N. P. Methods for the analysis of submicrometer- and nanoplastic particles in the environment. TrAC Trends in Analytical Chemistry, 112, 52–65 (2019).

45. Ali, I., Cheng, Q., Ding, T., Yiguang, Q., Yuechao, Z., Sun, H., Peng, C., Naz, I., Li, J. & Liu, J. Micro- and nanoplastics in the environment: Occurrence, detection, characterization and toxicity – A critical review. Journal of Cleaner Production, 313, 127863 (2021).

46. Laborda, F., Bolea, E., Cepriá, G., Gómez, M. T., Jiménez, M. S., Pérez-Arantegui, J. & Castillo, J. R. Detection, characterization and quantification of inorganic engineered nanomaterials: A review of techniques and methodological approaches for the analysis of complex samples. Analytica Chimica Acta, 904, 10–32 (2016).

47. Mariano, S., Tacconi, S., Fidaleo, M., Rossi, M. & Dini, L. Micro and Nanoplastics Identification: Classic Methods and Innovative Detection Techniques. Frontiers in Toxicology, 3, 1–17 (2021).

48. Silva, A. B., Bastos, A. S., Justino, C. I. L., da Costa, J. P., Duarte, A. C. & Rocha-Santos, T. A. P. Microplastics in the environment: Challenges in analytical chemistry - A review. Analytica Chimica Acta,1017, 1–19 (2018).

49. Tirkey, A. & Upadhyay, L. S. B. Microplastics: An overview on separation, identification and characterization of microplastics. Marine Pollution Bulletin, 170, 112604 (2021).

50. Ivleva, N. P. Chemical Analysis of Microplastics and Nanoplastics: Challenges, Advanced Methods, and Perspectives. Chemical Reviews, 121, 11886–11936 (2021).

51. Lambert, S. & Wagner, M. Characterisation of nanoplastics during the degradation of polystyrene. Chemosphere, 145, 265–268 (2016).

52. Ateia, M., Ersan, G., Alalm, M. G., Boffito, D. C. & Karanfil, T. Emerging investigator series: microplastic sources, fate, toxicity, detection, and interactions with micropollutants in aquatic ecosystems – a review of reviews. Environmental Science: Processes & Impacts, 24, 172–195 (2022).

CONCLUSIONS

La surveillance de l'isotope C-13 par ICP-MS à particule unique s'est avérée être une méthodologie analytique optimale pour la détection de particules de plastique à des concentrations allant jusqu'à des centaines de particules par millilitre, avec des tailles supérieures à 1 µm et atteignant une gamme supérieure d'environ 5 - 6 µm. Cette gamme de taille a été conditionnée par les limites inhérentes à la détection du carbone dans l'ICP-MS, mais aussi par l'efficacité du transport des grandes particules dans les systèmes de nébulisation pneumatique. D'autre part, il a été observé que l'efficacité de l'atomisation était d'environ 40% pour les particules jusqu'à environ 3 µm, diminuant pour les particules plus grandes et sous-estimant ainsi leur concentration. En raison de ces limites, la SP-ICP-MS ne doit pas être utilisée pour la détermination quantitative des microplastiques polydispersés, mais elle est très utile comme technique de dépistage rapide pour la détection des particules de plastique.

La faisabilité de la méthodologie développée pour l'analyse de différents produits de consommation a été démontrée. Ce résultat a été obtenu grâce à la détection réussie de microplastiques primaires ajoutés intentionnellement à des produits de soins personnels utilisés comme exfoliants. En outre, la présence de microplastiques secondaires libérés par les sachets de thé soumis à un processus d'infusion conventionnel a été confirmée.

La méthodologie SP-ICP-MS développée a également été utilisée pour explorer les eaux environnementales de rivières espagnoles et françaises pour la présence de microplastiques. L'application d'un prétraitement acide aux échantillons a amélioré la détectabilité des microparticules de plastique ainsi que la sélectivité de la méthode. Toutes les eaux de rivière analysées par SP-ICP-MS ont montré la présence de particules contenant du carbone. Ensuite, des échantillons sélectionnés ont été analysés par microscopie Raman, ce qui a confirmé la présence de particules de plastique dans les échantillons. Par conséquent, la SP-ICP-MS peut être utilisée comme une technique de dépistage appropriée pour la discrimination des échantillons contenant des microplastiques,

qui doivent ensuite être analysés par microscopie Raman ou FT-IR, des techniques qui nécessitent des temps d'analyse plus longs. En tout cas, les résultats obtenus dans les rivières espagnoles et françaises confirment la contamination par les microplastiques dans l'environnement.

La confirmation de la présence de particules de plastique dans l'environnement rend nécessaire la compréhension de leur rôle de vecteurs de polluants émergents. Pour cette raison, des études d'adsorption d'agents de contraste à base de gadolinium sur des nanoplastiques modèles et environnementaux et une comparaison avec l'adsorption du gadolinium ionique ont été réalisées. Ces études d'adsorption, ajustées au modèle de Freundlich, ont confirmé que des paramètres tels que le pH, la concentration, le temps de contact ou le milieu influençaient l'adsorption de ces espèces de gadolinium.

D'autre part, l'adsorption de ces espèces de Gd sur des colloïdes naturels a également été réalisée. Les résultats obtenus ont montré le rôle des nanoplastiques dans les eaux naturelles en tant que vecteurs d'agents de contraste à base de gadolinium, résultats en phase avec d'autres polluants émergents. En outre, la capacité des nanoplastiques à concurrencer les colloïdes naturels dans l'adsorption et le transport de ces polluants dans les environnements naturels a également été démontrée.

- Laborda, F., Trujillo, C. & Lobinski, R. Analysis of microplastics in consumer products by single particle-inductively coupled plasma mass spectrometry using the carbon-13 isotope. Talanta 221, 121486 (2021).

- Laborda, F., Trujillo, C. & Lobinski, R. Unlocking Carbon-13 with Single Particle ICP-MS : Feasibility Study for Microplastic Detection. Perkin Elmer (2022).

Talanta 221 (2021) 121486

Contents lists available at ScienceDirect

Talanta

journal homepage: www.elsevier.com/locate/talanta

Analysis of microplastics in consumer products by single particle-inductively coupled plasma mass spectrometry using the carbon-13 isotope

Francisco Laborda [a,*], Celia Trujillo [a], Ryszard Lobinski [b]

[a] Group of Analytical Spectroscopy and Sensors (GEAS), Institute of Environmental Sciences (IUCA), University of Zaragoza, Pedro Cerbuna 12, 50009, Zaragoza, Spain
[b] Universite de Pau et des Pays de L'Adour, E2S UPPA, CNRS, IPREM UMR 5254, Helioparc, 64053, Pau, France

ARTICLE INFO

Keywords:
Single particle detection
ICP-MS
Carbon
Microplastics
Cosmetics
Food packagings

ABSTRACT

Single particle inductively coupled plasma mass spectrometry (SP-ICP-MS) has become a well-established technique for the detection, size characterization and quantification of inorganic nanoparticles but its use for the analysis of micro- and nanoparticles composed of carbon has been scarce. Here, the analysis of a microplastic suspensions by ICP-MS operated in single particle mode using microsecond dwell times is comprehensively discussed. The detection of polystyrene microparticles down to 1.2 μm was achieved by monitoring the ^{13}C isotope. Plastic microparticles of up to 5 μm were completely volatized and their components atomized, which allowed the detection of microplastics, their quantification using aqueous dissolved carbon standards, and the measurement of the size-distribution of the detected particles. Limits of detection of 100 particles per milliliter were achieved for an acquisition time of 5 min. The method developed was applied to the screening of microplastics in personal care products and released from food packagings. The chemical identity of the detected microplastics was confirmed by attenuated total reflectance Fourier-transform infrared spectroscopy.

1. Introduction

The use of inductively coupled plasma mass spectrometry (ICP-MS) in single particle mode has allowed the conversion of this powerful technique of trace metal analysis into a particle counting technique capable of providing information on a particle-by-particle basis [1–3]. Detection of individual particles in an ICP-MS instrument is possible during the analysis of very dilute particle suspensions at very high reading frequencies (from 10^2 to 10^5 Hz). The result is a time scan containing a number of particle events, consisting of one or more readings per particle, depending on the frequency selected, over the baseline. The latter depends on the instrumental background and on the presence of dissolved species of the element measured [4]. Under such conditions, the intensity of the particle events is related to the mass of element in the particle. Hence, it can be correlated with the particle size if additional information about the composition, density and shape is available, whereas the number of events depends on the number concentration of particles.

Single particle ICP-MS (SP-ICP-MS) exploits the inherent capacity of ICP-MS to achieve absolute limits of detection at the attogram level, which enables the detection of metallic nanoparticles below 10 nm [5]. This detection capability is affected by a number of factors depending on the particle and the element measured, but also the baseline. The use of short dwell times, in the range of microseconds, contributes to reduce the count level of the baseline and hence its noise, improving the detection of smaller particles.

In terms of elements, carbon is very seldom determined by ICP-MS. It attracted some attention with regard to the measurement of its isotope ratios [6], the monitoring of organic species separated by liquid chromatography [7,8] or field-flow fractionation [9,10], and its use as internal standard in laser ablation ICP-MS [11,12]. The main reasons why carbon is not determined routinely by ICP-MS are the low sensitivity of the element and its high background levels. Carbon sensitivity is limited by its low ionization efficiency (ca. 5%) because of its high ionization potential (11.26 eV), together with its low transmission in the ICP-MS interface due to space charge effects [13]. The baseline is considerable due to the ubiquitous presence of carbon dioxide in air and water. As a result of these limitations, the attainable limits of detection are high, in the range of mg L^{-1} [14].

The above limitations have largely prevented the use of SP-ICP-MS to

* Corresponding author.
E-mail address: flaborda@unizar.es (F. Laborda).

https://doi.org/10.1016/j.talanta.2020.121486
Received 30 April 2020; Received in revised form 22 July 2020; Accepted 29 July 2020
Available online 14 September 2020

the analysis of carbon nano- and microparticles [15]. Regarding the nanoplastics the major problem is insufficient sensitivity. Regarding microplastics, the problems are their efficient nebulization, so that a significant fraction of microparticles reaches the ICP source, and their subsequent complete volatilization and atomization into their elemental components, followed by the ionization of the carbon atoms. Direct introduction of microparticle suspensions in ICP sources were already addressed in the late1980s, when slurry sample introduction was investigated as an alternative to the digestion of difficult samples [16]. Efficient introduction of particles of up to 2–3 μm was achieved with transport efficiencies around 1% by using conventional nebulizers and single or double pass spray chambers [17]. More recently, different nebulization systems for single cell ICP-MS were developed [18] and have become commercially available [19,20]. These systems have been designed to provide high nebulization efficiencies for intact bioparticles (bacteria, cells, algae …) of 1–10 μm diameter, and offer a potential solution for the nebulization of microplastics.

Plastic pollution is a global environmental issue that is leading to policies oriented to the adequate use, waste management and recycling of plastics [21]. One of their aims is reducing the likelihood that plastic products enter the environment and degrade into microparticles, which have been found in seawater, freshwater, sediments, soils and air, as well as along the food chain, involving human exposure [22,23]. Although microplastics at high concentrations have shown to cause physical harm to the environment and living beings, there is still no evidence of widespread risk to human health at present [24]. However, the current understanding of their effects can still be considered scarce because of the lack of robust methods for detection and quantification of microplastics to determine their exposure levels in the environment (water, soils, sediments, biological tissues) [25] and the food chain [26]. Microplastics are currently isolated from soil, sediment and water by density separation and/or microfiltration whereas biological tissues are subjected to different mild digestion procedures [27]. Visual examination by optical microscopy is commonly used for detecting, sorting and counting microplastics over 50 μm. However, identification of the polymers requires the use of spectroscopic techniques, namely Fourier transform infrared (FT-IR) or Raman. The use of these techniques in combination with optical microscopy (FT-IR and Raman microscopies) allows the detection, the chemical and morphological (size and shape) characterization and the number quantification of individual particles down to 10 and 1 μm, respectively [28]. On the other hand, pyrolysis and thermal extraction desorption gas chromatography-mass spectrometry, as well as other thermo-analytical techniques [29], are being used for the chemical identification and mass quantification. Very recently, SP-ICP-MS was proposed for the detection of polystyrene microparticle standards but no applications to real-world samples were reported [15].

The objective of this work was the comprehensive optimization and in-depth discussion of SP-ICP-MS for the detection, size characterization and quantification of microplastics with the aim of developing a method for their analysis in personal care products and the monitoring of their release from food packagings.

2. Material and methods

2.1. Instrumentation

A PerkinElmer NexION 2000B ICP mass spectrometer (Toronto, Canada) was used throughout. The sample introduction system consisted of an Asperon™ linear pass spray chamber (PerkinElmer, Toronto, Canada), equipped with a flow focusing nebulizer (Ingeniatrics, Sevilla, Spain). Default instrumental and data acquisition parameters are listed in Table 1. Argon of 99.999% purity was used unless noted otherwise.

Data acquisition was performed at frequencies up to 20,000 Hz by using dwell times down to 50 μs. Under such conditions, particle events are recorded as transient signals whose intensity is calculated as the sum of the net intensities of the readings along each signal and its height as the maximum net intensity of these reading. Data were processed with Syngistix Nano Application version 2.4 and Origin 2019b.

Table 1
Default instrumental and data acquisition parameters for SP-ICP-MS.

Instrumental parameters	
RF power	1600 W
Argon gas flow rate	
Plasma	15 L min^{-1}
Auxiliary	1.2 L min^{-1}
Nebulizer	1.0 L min^{-1}
Make-up	0.2 L min^{-1}
Sample flow rate	16 μL min^{-1}
Data acquisition parameters	
Dwell time	100/200 μs
Readings per replicate	600,000/300,000
Total acquisition time	60 s
Isotope monitored	^{13}C

2.2. Standards

Dilute suspensions of polystyrene (PS) microparticles and gold nanoparticles were prepared from commercially available suspensions. Two reference latex sphere suspensions of 2.0 and 4.8 μm nominal diameter (RM165 and RM166) were obtained from BCR (Geel, Belgium). The spheres are made of polystyrene cross-linked with divinyl benzene and stabilized with a non-ionic surfactant. The certified mean diameter for RM165 and RM166 were 2.223 ± 0.013 and 4.821 ± 0.019 μm, respectively, with a very narrow distribution (99% of the spheres within ±2% of the mean diameter). Although the number concentration of the suspensions is not certified, 3.23×10^8 and 2.90×10^5 L^{-1} were declared for the respective materials in the BCR report [30]. Polystyrene microparticle suspensions with nominal diameters of 1, 2 and 3 μm (certified diameters: 1.04 ± 0.03, 1.98 ± 0.03 and 3.03 ± 0.09 μm, respectively) were purchased from Sigma (Saint Louis, MO); polystyrene microparticle suspensions of 2, 4 and 5 μm (certified diameters: 2.020 ± 0.015, 4.000 ± 0.043 and 5.000 ± 0.043 μm, respectively) were purchased from Thermo (Waltham, MA). A gold nanoparticle (PEG-carboxil 0.8 kDa surface) suspension of 47.8 ± 1.8 nm diameter was obtained from NanoComposix (San Diego, CA). Dilutions were prepared in ultrapure water (Milli-Q Advantage, Molsheim, France) by accurately weighing (±0.1 mg) aliquots of the stock suspensions after 1 min sonication (Ultrasonic Cleaner Bath CE-5700 A, 42 KHz, 50 W). Suspensions were measured after preparation and they were not stabilized by adding any surfactant, because their organic nature results in increasing the dissolved carbon content and hence the size detection limits. Aqueous carbon solutions were prepared from a standard stock solution of 1001 ± 3 mg L^{-1} prepared from tartaric acid in 0.2% (v/v) HNO_3 (Inorganic Ventures, Christiansburg, VA) by dilution in nitric acid 0.2% (v/v).

2.3. Analysis of consumer products

Two types of consumer products were studied: Personal care products containing plastic particles as exfoliants and plastic teabags. Three different personal care products (one exfoliating hair conditioner, PCP1, and two facial exfoliating cleansers, PCP2 and PCP3) were purchased in local supermarkets and websites. Teas (A, B and C) packaged in individual plastic bags were purchased from local supermarkets.

Microplastic detection in personal care products. 0.5 g of product were accurately weighed in glass vials, filled with 250 mL of ultrapure water and probe sonicated for 15 min. The suspensions were filtered through 10 μm pore size polycarbonate Isopore™ membranes (Merck, Darmstadt, Germany) to remove large particles and diluted conveniently for submitting to SP-ICP-MS analysis. Duplicate method blanks were also

analyzed.

Microplastic release from teabags. The plastic teabags were cut with steel scissors and the leaves removed. The empty bags were thoroughly washed with ultrapure water and air dried. Glass vials containing two empty bags were filled with 10 mL of ultrapure water heated to 100 °C and left to brew for 5 min. After brewing, the resulting suspension was transferred to clean glass vials for analysis by SP-ICP-MS. Analysis were performed in triplicate, duplicate method blanks were also analyzed.

3. Results and discussion

3.1. Carbon determination by ICP-MS

As it has been stated in the Introduction, carbon is not determined routinely by ICP-MS because of its high limits of detection. Stable isotopes of carbon are ^{12}C and ^{13}C with abundances of 98.90 and 1.10%, respectively. Typical sensitivities achieved with the ICP-MS spectrometer used in this work were around 1000 cps per 1 mg L^{-1} of ^{13}C, with background signals for ultrapure water of 80,000–100,000 cps. Consequently, background signals for ^{12}C were around 10 million cps, well over the working range of the pulse count detector. SP-ICP-MS measurements must be performed in pulse counting mode to get reading frequencies of 100 Hz or higher, thus ^{13}C was selected for carbon measurements.

With regard to the control of background, Nischwitz et al. [31] reported the use of glass instead of plastic vials, as well as the combination of acidification and purging with argon as two strategies for reduction of background levels down to 30%. On the other hand, the use of ultrapure argon (99.9999%) was checked, accounting for a 25% reduction of background levels, due to the lower level of organics. Whereas the use of glassware becomes obvious to control organic carbon contamination, the acidification followed by purging was not considered appropriate as a routine treatment for removal of inorganic carbon (dissolved carbon dioxide) from microplastic suspensions. Neither was the routine use of ultrapure argon, because the achievable background reduction did not lead to significant improvements in the detection of smaller particles.

Concerning dissolved carbon standards, several organic compounds have been reported in literature, such as potassium hydrogen phthalate [7], citric acid [10,14] and oxalic acid [32]. Here, tartaric acid was selected and used throughout. The carbon sensitivity was not statistically different in ultrapure water and nitric acid (0.2%), achieving limits of detection (3σ) of 0.8 mg L^{-1} for ^{13}C.

3.2. Nebulization and atomization of plastic microparticle suspensions in ICP-MS

Whereas current nebulization systems achieve transport efficiencies over 2% for dissolved species by using concentric nebulizers and cyclonic spray chambers, the transport of microparticles drops below 0.1% [19]. In an attempt to improve nebulization efficiency and expand size limits of the measurable particles, a linear pass spray chamber, developed elsewhere for the introduction of intact cells into an ICP-MS [19], was investigated for microparticle introduction. This spray chamber is ordinarily used in combination with a high efficiency concentric nebulizer, which was replaced here by a flow focusing nebulizer to avoid potential clogging when large rigid microparticles, such as microplastics, were introduced. The spray chamber uses a dual make-up gas to create a tangential flow to the spray chamber walls, to avoid losses of cells (or particles) onto the walls. In addition, this make-up gas allows to control the residence time of the particles within the plasma, and hence their volatilization and atomization, as well as the ionization of carbon, regardless of the nebulization gas flow rate. Moreover, maximum aerosol transport is ensured by the laminar gas flow within the spray chamber.

Fig. 1 shows the effect of the nebulization gas flow rate at different make-up gas flow rates on the number of particles detected, and their mean intensity for a suspension of PS microparticles of 2.22 μm, measured in single particle mode with a dwell time of 100 μs. Whereas the number of particles detected is related to their transport efficiency, the intensity observed depends on the atomization efficiency of the particles and the ionization efficiency of carbon. As it can be seen, similar behaviors were observed for different combinations of make-up and nebulizer gas flow rates, with the highest number of particles nebulized and the highest intensities per particle at total gas flow rates (make-up + nebulizer gas flow rate) of ca. 1.1–1.2 L min^{-1}. Although other gas flow rate combinations can be used, a make-up gas flow rate of 0.2 L min^{-1} and a nebulizer gas flow rate of 1.0 L min-1, were used unless noted otherwise.

The analyte transport efficiency determined by using the BCR standard of 2.22 μm PS microparticles was 29.9 ± 0.9% at 1.1 and 0.2 L min^{-1} make-up and nebulizer gas flow rates, respectively. The analyte transport efficiency was calculated by applying the number concentration method [33] and it was in fair agreement with the efficiency calculated by using 50 nm Au nanoparticles (28.2 ± 0.4%). On the other hand, the efficiency dropped to 12.5 ± 0.6% for PS microparticles of 4.82 μm, revealing that microparticles at least up to ca. 2–3 μm were nebulized like dissolved species, as well as the dependence of the efficiency of the nebulization system with respect to the size for microparticles over ca. 3–5 μm.

3.3. Detection of plastic microparticles by SP-ICP-MS

Detection of carbon-bearing particles by SP-ICP-MS had not been considered feasible so far because of the high background levels and the low sensitivity of the element [15]. However, for a background with a given count rate, the count level of the corresponding SP-ICP-MS baseline (Y_B) is controlled by the dwell time used, being proportional to it, whereas the associated noise (σ_B) is equal to the squared root of the baseline mean intensity ($\sigma_B = \sqrt{Y_B}$) when secondary electron multiplier detectors are used [34]. Thus, the count level of the baseline, and hence its noise, can be significantly reduced by using very short dwell times. Nevertheless, when particle events are measured by using microsecond dwell times, they are recorded as transient signals, whose heights decrease with dwell time [35]. Since detection of particle events measured at microsecond dwell times is not just limited by the noise of the baseline, but also by the height of the transient signals recorded, the detectability of particles is negatively affected by reducing dwell times when particle events are recorded as transient signals [36].

Experimental size limits of detection (LOD_{size}) were calculated from the following expression:

$$LOD_{size} = \left(\frac{5\sigma_B}{K_h}\right)^{1/3} \quad (1)$$

where σ_B is the standard deviation of the baseline of a blank and K_h the response factor of the net height intensity of a transient signal (S_{Pmax}) with respect to the cubed diameter (d) of the corresponding particle ($S_{Pmax} = K_h d^3$). The response factor K_h was calculated by using the RM165 PS standard of 2.22 μm. Limits of detection down to 1.2 μm for PS microparticles were obtained by using dwell times of 200 μs for ^{13}C. Longer dwell times were not considered because when particle events are recorded as pulses (one-reading recorded transient signals), size limits of detection increase with dwell times due to the single dependence on baseline noise [36]. Microparticles produced transient signals broader than nanoparticles, with median widths of 800 μs for PS microparticles in the range of 2–5 μm (Figure S1 in Supplementary Information) against 500 μs for 50 nm Au nanoparticles. Under these conditions, 2–3 readings per particle event were recorded at dwell times of 200 μs, as it can be seen in Fig. 2, allowing the proper identification and integration by the data processing software.

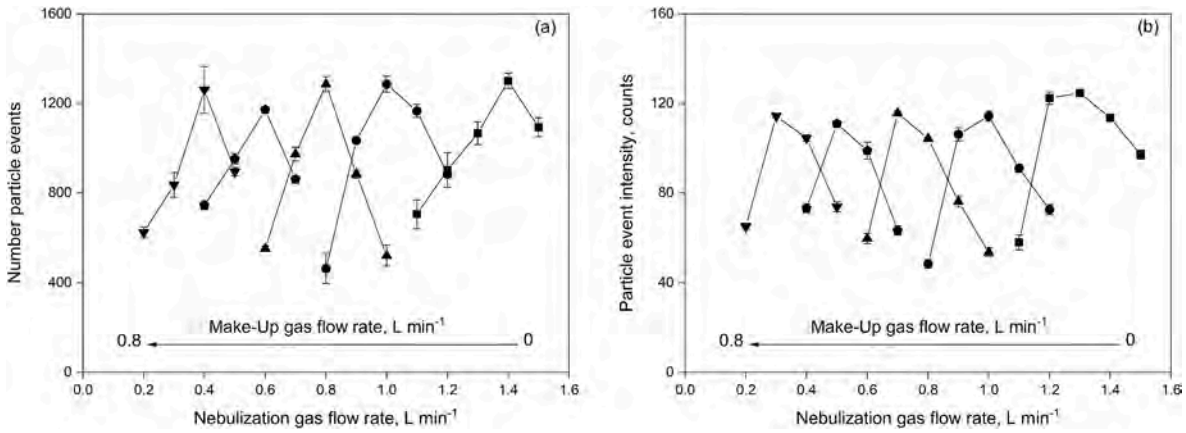

Fig. 1. Effect of the nebulization gas flow rate at different make-up gas flow rates on (a) the number of particles events detected and (b) their mean intensity. Polystyrene microparticles of 2.22 μm diameter. Make-up gas flow rates (L min^{-1}): (■) 0.0; (●) 0.2; (▲) 0.4; (⬟) 0.6; (▼) 0.8.

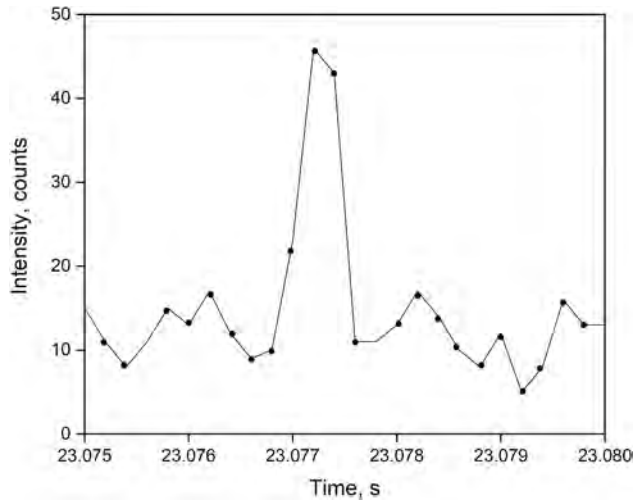

Fig. 2. Particle event recorded with a dwell time of 200 μs. Polystyrene microparticles of 2.22 μm diameter.

3.4. Determination of the plastic microparticle diameter

SP-ICP-MS just provide direct information about the mass of element in the particles detected. Thus, additional information about the shape, composition and density of the particles is needed to obtain size information. In the case of spherical and solid particles, the diameter of a single particle (d) can be calculated by using the following expressions:

$$d = \left(\frac{S_P}{K_d}\right)^{1/3} = \left(\frac{S_P}{\frac{1}{6}\pi\rho F_P K_{ICPMS} K_M}\right)^{1/3} \quad (2)$$

where S_P is the net intensity of each particle event, K_d is the slope obtained from a size calibration (net signal intensity vs. particle diameter cubed), ρ the density and F_P the mass fraction of the element in the particle, K_{ICPMS} is the detection efficiency, which represents the ratio of the number of ions detected versus the number of analyte atoms of the measured isotope introduced into the ICP; and K_M ($= AN_{Av}/M_M$) is a factor related to the element measured, where A is the atomic abundance of the isotope considered, N_{Av} the Avogadro number, and $M_M$the atomic mass of the element. Although diameters can be determined by calibration with particle size standards of the same chemical composition to obtain K_d empirically, they are usually estimated from a calibration with a dissolved standard of the element monitored, the analyte transport efficiency and the sample flow rate (the description of the procedure is included in the Supplementary Information).

The expected linear behavior of the mean intensity of particle events vs. the cubed diameter of the particles was obtained for PS microparticles up to 5 μm (figure S3 a in supplementary information). On the other hand, the logarithmic plot of the mean intensity of particle events vs. particle diameter showed a slope of 2.94 ± 0.07 in agreement with the expected value of 3 (figure S3 b in supplementary information). The behavior observed confirmed that PS microparticles at least up to 5 μm were volatilized and atomized in the plasma with similar efficiency, allowing the unbiased size determination of plastic microparticles.

As it can be seen in Table 2, good agreement with the certified values were obtained for the different PS size standards studied, except for 1 μm microparticles which were below the size detection limit. Diameters where calculated through the Syngistix Nano Application considering a carbon mass fraction of 0.9231 and a density of 1.04 g cm^{-3} for spherical PS microparticles and by using a calibration with dissolved carbon standards, the measured sample flow rate, and the transport efficiency calculated by using the number concentration method. The results obtained also confirmed that carbon from plastic microparticles ionized with the same efficiency than dissolved carbon. With respect to the analyte transport efficiency, it is important to consider the method applied for its determination. Whereas the number concentration method just relies upon the availability of a number concentration standard, the particle size method requires particle size and dissolved standards of the element involved, but also that the ionization efficiency of carbon from the particles and the dissolved standards is equal [33]. As it has been shown above, by using the number concentration method, PS microparticles of 4.82 μm showed lower transport efficiency than 2.22 μm particles, whereas the later ones were nebulized in a similar way than nanoparticles or dissolved species. However, when the particle size method was applied, similar transport efficiencies were obtained for both microparticles (28.1 ± 0.6% and 25.9 ± 3.4%, respectively). The disagreement between both calculation methods for the larger microparticles confirms the similar behavior of dissolved carbon and plastic microparticles in the ICP source but not in the nebulization system for larger microparticles.

Fig. 3 shows a typical time scan with the corresponding particle event intensity histogram and the calculated size distribution for 2.22 μm PS microparticles. Although a good agreement with respect to the determination of the mean size was obtained, the size distribution showed a significant broadening. The size distribution reported for the 2.22 μm PS microparticles [30] is compared with the Gaussian fitted distribution obtained by SP-ICP-MS in Fig. 3c, showing a broadening of ca. 10 times with respect to the original distribution of the microparticles. The broadening of size distributions measured by SP-ICP-MS has

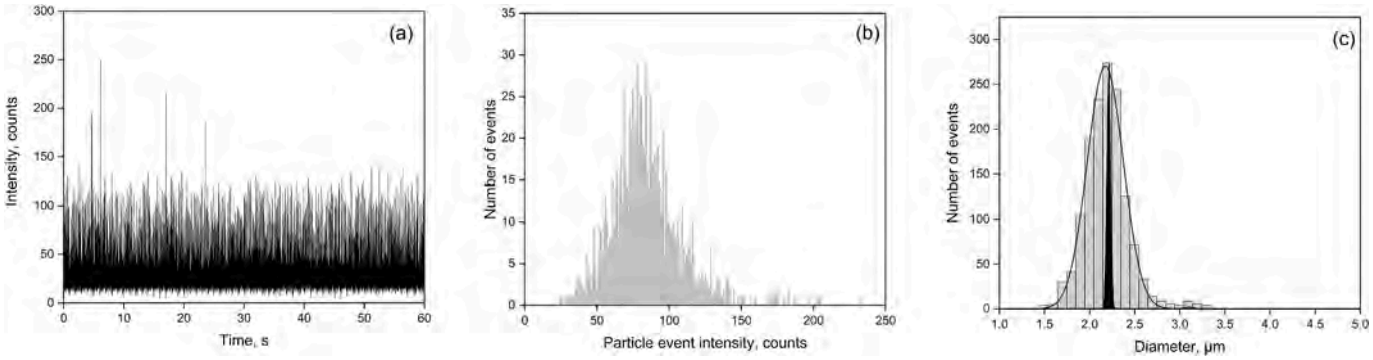

Fig. 3. (a) Time scan, (b) particle event intensity histogram and (c) size histogram of 2.22 μm polystyrene microparticles (BCR RM165). Reported size distribution of BCR RM165 plot in black in (c) [30].

Table 2
Mean and most-frequent diameter of standard polystyrene microparticles (mean ± standard deviation, n = 3).

certified diameter μm	mean diameter μm	recovery %	most frequent diameter μm	recovery %
1.04 ± 0.03	1.69 ± 0.07	163	1.46 ± 0.05	140
1.98 ± 0.03	1.83 ± 0.01	93	1.84 ± 0.01	93
2.02 ± 0.02	1.93 ± 0.01	95	1.92 ± 0.04	96
2.22 ± 0.01	2.10 ± 0.02	94	2.10 ± 0.02	94
3.03 ± 0.09	2.74 ± 0.01	90	2.76 ± 0.01	91
4.00 ± 0.04	3.56 ± 0.06	90	3.65 ± 0.04	91
4.82 ± 0.02	4.32 ± 0.02	90	4.18 ± 0.02	87
5.00 ± 0.04	4.55 ± 0.05	91	4.58 ± 0.02	92

been reported by several authors [37,38], being more significant for micro [37] than for nanoparticles [38]. Although counting statistics contributes to such broadening, variations in the injection position of the particles in the plasma proved to be particularly relevant [39]. The reason is mainly because particles injected off-axis in the plasma follow different paths and evaporate at different positions, leading to a lower transmission of their clouds of ions to the mass spectrometer, and thus, producing smaller signals.

3.5. Determination of the plastic microparticle number concentration

The plot of the number of particle events vs. the particle number concentration for 3-μm PS microparticles (figure S4 in supplementary information) followed a linear behavior up to concentrations of 2.0 × 10^9 L^{-1}, confirming that all the particles introduced into the plasma were detected despite the broad distribution of signals observed for monodisperse microparticles. The loss of linearity is related to the occurrence of particle events corresponding to more than one particle at high number concentrations [35].

Under the experimental conditions of this work, unbiased determination of the number concentration was limited to microparticles below ca. 2–3 μm, which were nebulized similarly to dissolved species and to nanoparticles. The number concentration of larger particles will be underestimated otherwise the results are corrected with the transport efficiency corresponding to the size of the microparticles analyzed. For the same reason, the total number concentration is expected to be underestimated for samples with a broad-size distribution of microparticles over 2–3 μm.

Number concentration limits of detection (LOD_{number}) can be calculated by using the following expression [3]:

$$LOD_{number} = \frac{3}{\eta_{neb} Q_{sam} t_i} \quad (3)$$

where η_{neb} is the analyte transport efficiency, Q_{sam} the sample introduction flow rate and t_i the acquisition time. This expression corresponds to the minimum attainable limit of detection when no particle events are detected in a blank; otherwise, more complex expressions should be considered [36]. By using the nebulization systems described in the Experimental section, under the instrumental conditions of Table 1, analyte transport efficiencies up to 40% were achieved at 16 μL min^{-1}. Thus, best-case limits of detection of 5 × 10^5 L^{-1} could be achieved with acquisition times of 1 min. As it can be seen, the high analyte transport efficiency obtained with the system used requires the use of low sample flow rates. The most suitable way of improving the number concentration limits of detection is the increase in the acquisition time.

3.6. Detection of microplastics by SP-ICP-MS in consumer products

Once the feasibility of SP-ICP-MS for the detection, size

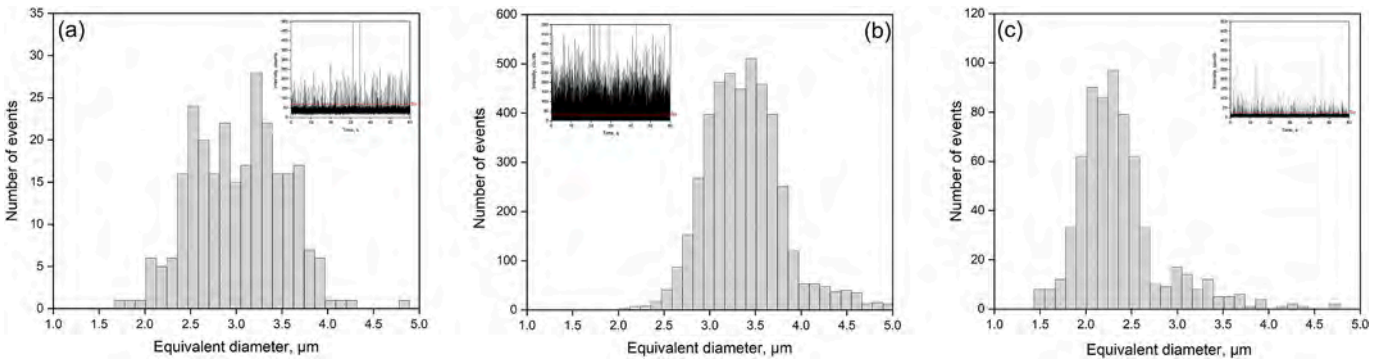

Fig. 4. Size distributions corresponding to suspensions of personal care products containing microplastics as exfoliant agents. (a) PCP1 exfoliating hair conditioner, (b) PCP2 and (c) PCP3 facial exfoliating cleansers. The SP-ICP-MS time scans are shown in the insets.

characterization and quantification of monodispersed polystyrene microparticles was demonstrated, two real situations corresponding to the analysis of samples containing microplastics were addressed as representative case studies. The first case, which is related to the environmental emission of primary microplastics (those added intentionally to consumer products as such) corresponded to the detection of microplastics in personal care products. The second one involved the detection of microplastics released from plastic teabags as secondary microparticles from a bulk material, a direct source of human exposure to microplastics.

3.6.1. Detection of microplastics in personal care products

Plastic microparticles are added to personal care products as abrasive agents in exfoliants. Because they represent a threat to the environment, their use has been banned in some countries, although not worldwide yet [40]. Sizes reported for microplastics in personal care products range from around 10 μm up to more than 1 mm, being mainly made of polyethylene [40]. However, the occurrence of smaller particles cannot be disregarded because isolation and detection methods applied are mostly based on microfiltration and optical microscopy.

Personal care products were diluted in ultrapure water for detection of microplastics to obtain a homogeneous suspension followed by filtration through 10 μm pore size membranes, to avoid clogging of the nebulizer with very large particles. Fig. 4 shows the time scans and size distributions of the suspensions obtained from the personal care products analyzed. Plastic microparticles up to ca. 5 μm were detected in the samples. Table 3 summarizes most frequent and mean diameters of the particles detected, as well as the number of particles detected in the suspensions analyzed and the particle content in the original products. It must be pointed out that the particle content reported corresponds to the particles detected by SP-ICP-MS under the conditions selected, which are limited to particles over ca. 1 and below 10 μm; moreover, particles over 2–3 μm are underestimated because they were nebulized with lower efficiency. Thus, the information presented confirms the presence of microplastics in the low micrometer range but the results must be considered semiquantitative.

The time scan of sample PCP1 (Fig. 4a), corresponding to the hair conditioner, showed a baseline signal higher than the other two products. The reason for it is that the PCP1 suspensions were analyzed directly with no further dilution, whereas PCP2 and PCP3 were diluted 500-fold due to their higher microplastic contents. The increase of the baseline up to 40 counts was due to the presence of dissolved organics from the matrix of the product, whereas typical baseline signal similar to the controls (ca. 10 counts) were obtained for the other samples. In terms of controls, no particles were detected in ultrapure water, whereas 3 ± 1 were detected in the procedural blanks obtained through the whole process (dilution, sonication, filtration). Sizes reported in Fig. 4 and Table 3 are reported as equivalent diameters, because particles in the products showed irregular shapes (Figure S5 in Supplementary Information). They were calculated by assuming spherical shapes and considering the chemical composition and density of the microplastics detected (polyethylene: $F_P = 0.856$, $\rho = 0.95$ g cm^{-3}). The microparticles were also isolated and identified by ATR-FTIR (procedure and spectra in Supplementary Information).

3.6.2. Release of microplastics from teabags

Recently, Hernandez et al. [41] reported the release of nano- and microplastics from plastic teabags during a conventional brewing process as a source of human exposure to such particles. By using scanning electron microscopy, particles in the ranges of 17–1260 nm and 0.5–270 μm were detected, estimating the number of particles released per teabag as 2.3×10^6 micro-sized (>1 μm) and 1.5×10^{10} submicron particles (<1 μm). Fig. 5 shows the size distributions and time scans of the suspensions obtained from the teabags submitted to the brewing process described in the Experimental section. Plastic microparticles up to ca. 5 μm were detected from all the samples.

Table 4 summarized most frequent and mean equivalent diameters of the particles detected, as well as the number of particles release and detected per teabag. As in the case of the analysis of personal care products, the results obtained must be considered as semiquantitative. Due to the low number of particles in the released suspensions, acquisition time had to be extended to 5 min. Under such conditions, more than 100 events were recorded, which corresponds to the limit of quantification under zero-blank conditions for any counting measurement [42]. With respect to the analysis of controls, the results presented in Table 4 were performed in three different sessions, particles were not detected in ultrapure water and procedure controls in two sessions, whereas 3 ± 1 and were 4 ± 1 were detected in the ultrapure water and procedure blank in the other one. It can be concluded that under standard laboratory conditions, the environmental and cross contamination from plastic microparticles can be properly handled.

The release of microplastics in the range of 1–5 μm was over ten thousand particles per teabag. Unfortunately, these values could not be directly compared with those reported by Hernandez et al. [41], because the size range was narrower in this study. With respect to the composition of the teabags, their ATR-FTIR spectra corresponded to polylactic acid (Teabags A and B) and polyethylene terephthalate (Teabag C) (Figure S.8 Supplementary Information). As in the case of the microplastics detected in the personal care products, their chemical composition and density were considered for the calculation of the size of particles (polylactic acid, $F_P = 0.500$, $\rho = 1.26$ g cm^{-3}; polyethylene terephthalate, $F_P = 0.625$, $\rho = 1.34$ g cm^{-3}), which were reported as equivalent diameters of spheres because of the irregular shape of the particles released (Figure S.7 Supplementary Information).

4. Conclusions and outlook

SP-ICP-MS has proved to be a feasible methodology for detection and size characterization of plastic microparticles, although the determination of their chemical composition must rely on other techniques, like Raman or FT-IR spectrometries. The minimum detected sizes were restricted to about 1 μm due to the inherent limitations of carbon detection by ICP-MS, whereas the upper limit of 5–6 μm was conditioned by the working range of the detector. The number concentration information is conditioned by the efficient nebulization and transport of microparticles, which should be independent of the microparticle size. The nebulization system used in this work provided transport efficiencies of 40% for microparticles up to ca. 3 μm, although it showed lower efficiency for larger particles. Under such conditions, the

Table 3
Microplastic sizes and contents detected in personal care products. Acquisition time: 1 min. Mean ± standard deviation (n = 3).

personal care product	most frequent equivalent diameter μm	mean equivalent diameter μm	particle events counted	particle content g^{-1}
ultrapure water control	–	–	0 ± 0	–
procedure control	–	–	3 ± 1	–
PCP1	2.92 ± 0.08	2.89 ± 0.02	263 ± 23	$3.6 \times 10^7 \pm 0.2 \times 10^7$
PCP2	3.03 ± 0.01	3.08 ± 0.01	4542 ± 128	$3.1 \times 10^{11} \pm 0.1 \times 10^{11}$
PCP3	2.07 ± 0.04	2.11 ± 0.01	615 ± 27	$4.4 \times 10^{10} \pm 0.5 \times 10^{10}$

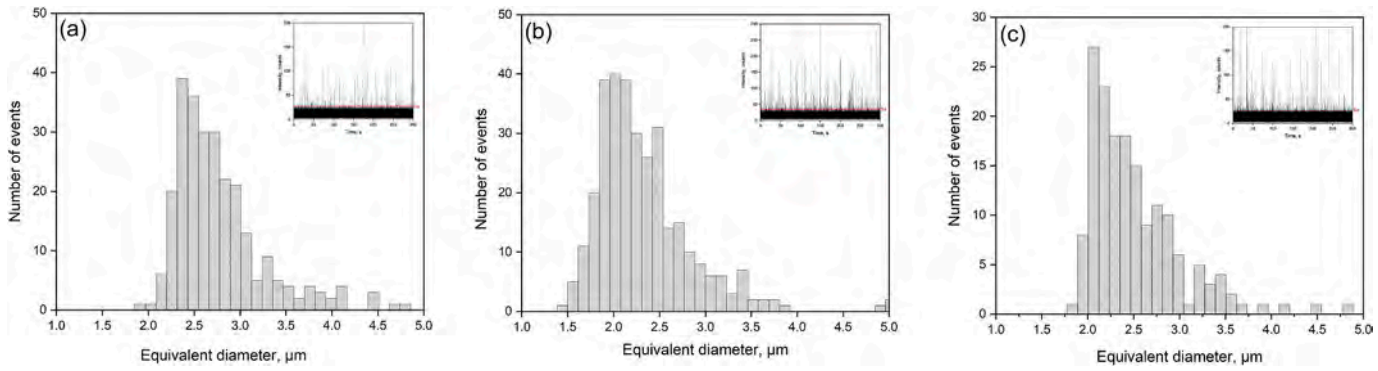

Fig. 5. Size distributions corresponding to microplastics released from plastic teabags under conventional brewing. (a) Teabag A, (b) Teabag B (c) Teabag C. The SP-ICP-MS time scans are shown in the insets.

Table 4
Size and number of plastic microparticles released from plastic teabags under conventional brewing. Acquisition time: 5 min. Mean ± standard deviation (n = 3).

	most frequent equivalent diameter μm	mean equivalent diameter μm	particle events counted	particles released per teabag
ultrapure water control	–	–	1 ± 1	–
procedure control	–	–	1 ± 1	–
Teabag A	2.49 ± 0.01	2.70 ± 0.06	141 ± 20	$2.2 \times 10^4 \pm 0.3 \times 10^4$
Teabag B	2.01 ± 0.09	2.18 ± 0.05	350 ± 27	$5.5 \times 10^4 \pm 0.4 \times 10^4$
Teabag C	2.03 ± 0.08	2.26 ± 0.04	124 ± 16	$1.9 \times 10^4 \pm 0.2 \times 10^4$

measured number concentrations of larger microparticles are underestimated, which is especially important in the analysis of microplastics, which occur as a size continuum in real samples. Finally, monodispersed microparticles reaching the plasma showed broad distributions of responses, revealing that most probably particles followed different paths within the plasma, producing size distributions wider than expected. With respect to the number concentration detection limits achieved, in the range of hundreds of particles per milliliter, these may not be sufficient for the analysis of environmental samples, with concentrations of hundreds of particles per liter have been reported in drinking waters [23]. In spite of these current limitations, the feasibility of SP-ICP-MS as screening method for the rapid detection of microplastics in consumer products has been demonstrated, opening up the technique to new fields.

Credit author statement

Francisco Laborda, Supervision, Conceptualization, Methodology, Writing - original draft. Celia Trujillo, Investigation, Formal analysis, Validation, Visualization. Ryszard Lobinski, Writing - review & editing.

Declaration of competing interest

The authors declare that they have no known competing financial interests or personal relationships that could have appeared to influence the work reported in this paper.

Acknowledgements

This work was supported by the Spanish Ministry of Science, Innovation and Universities and the European Regional Development Fund [project RTI2018-096111-B-I00 (MICINN/FEDER)]. C. Trujillo thanks University of Zaragoza for a pre-doctoral research contract (PI-PRD/2018–001).

The authors acknowledge Josefina Pérez-Arantegui and the Servicio de Apoyo a la Investigación for the FESEM analysis, Miguel Baya for the ATR-FT-IR analysis, Carlos Celaya for the separation and characterization of microplastics in personal care products and Ingeniatrics for providing the nebulizer.

Appendix A. Supplementary data

Supplementary data to this article can be found online at https://doi.org/10.1016/j.talanta.2020.121486.

References

[1] D. Mozhayeva, C. Engelhard, A critical review of single particle inductively coupled plasma mass spectrometry – a step towards an ideal method for nanomaterial characterization, J. Anal. At. Spectrom. 35 (2020) 1740–1783, https://doi.org/10.1039/C9JA00206E.
[2] M.D. Montaño, J.W. Olesik, A.G. Barber, K. Challis, J.F. Ranville, Single Particle ICP-MS: advances toward routine analysis of nanomaterials, Anal. Bioanal. Chem. 408 (2016) 5053–5074, https://doi.org/10.1007/s00216-016-9676-8.
[3] F. Laborda, E. Bolea, J. Jiménez-Lamana, Single particle inductively coupled plasma mass spectrometry: a powerful tool for nanoanalysis, Anal. Chem. 86 (2014) 2270–2278, https://doi.org/10.1021/ac402980q.
[4] F. Laborda, J. Jiménez-Lamana, E. Bolea, J.R. Castillo, Selective identification, characterization and determination of dissolved silver(i) and silver nanoparticles based on single particle detection by inductively coupled plasma mass spectrometry, J. Anal. At. Spectrom. 26 (2011) 1362–1371, https://doi.org/10.1039/c0ja00098a.
[5] P.N. Shaw, A. Donard, Nano-particle analysis using dwell times between 10μs and 70μs with an upper counting limit of greater than 3x10 7 cps and a gold nanoparticle detection limit of less than 10nm diameter, J. Anal. At. Spectrom. (2016) 1234–1242, https://doi.org/10.1039/C6JA00047A.
[6] R. Santamaria-Fernandez, Precise and traceable carbon isotope ratio measurements by multicollector ICP-MS: what next? Anal. Bioanal. Chem. 397 (2010) 973–978, https://doi.org/10.1007/s00216-010-3561-7.
[7] J. Vogl, K.G. Heumann, Development of an ICP-IDMS method for dissolved organic carbon determinations and its application to chromatographic fractions of heavy metal complexes with humic substances, Anal. Chem. 70 (1998) 2038–2043, https://doi.org/10.1021/ac971283p.
[8] C. Smith, B.P. Jensen, I.D. Wilson, F. Abou-Shakra, D. Crowther, High-performance liquid chromatography/inductively coupled plasma mass spectrometry and tandem mass spectrometry for the detection of carbon-containing compounds, Rapid Commun. Mass Spectrom. 18 (2004) 1487–1492, https://doi.org/10.1002/rcm.1504.
[9] B. Stolpe, M. Hassellöv, K. Andersson, D.R. Turner, High resolution ICPMS as an on-line detector for flow field-flow fractionation; multi-element determination of colloidal size distributions in a natural water sample, Anal. Chim. Acta 535 (2005) 109–121, https://doi.org/10.1016/j.aca.2004.11.067.
[10] V. Nischwitz, N. Gottselig, A. Missong, T. Meyn, E. Klumpp, Field flow fractionation online with ICP-MS as novel approach for the quantification of fine particulate carbon in stream water samples and soil extracts, J. Anal. At. Spectrom. 31 (2016) 1858–1868, https://doi.org/10.1039/c6ja00027d.
[11] D.A. Frick, D. Günther, Fundamental studies on the ablation behaviour of carbon in LA-ICP-MS with respect to the suitability as internal standard, J. Anal. At. Spectrom. 27 (2012) 1294–1303, https://doi.org/10.1039/c2ja30072a.

[12] D. Deiting, F. Börno, S. Hanning, M. Kreyenschmidt, T. Seidl, M. Otto, Investigation on the suitability of ablated carbon as an internal standard in laser ablation ICP-MS of polymers, J. Anal. At. Spectrom. 31 (2016) 1605–1611, https://doi.org/10.1039/c6ja00020g.
[13] F. Li, D.W. Armstrong, R. Houk, Behavior of bacteria in the inductively coupled plasma: atomization and production of atomic ions for mass spectrometry, Anal. Chem. 77 (2005) 1407–1413. http://pubs.acs.org/doi/abs/10.1021/ac049188l. (Accessed 21 March 2011).
[14] M. Riisom, B. Gammelgaard, I.H. Lambert, S. Stürup, Development and validation of an ICP-MS method for quantification of total carbon and platinum in cell samples and comparison of open-vessel and microwave-assisted acid digestion methods, J. Pharmaceut. Biomed. Anal. 158 (2018) 144–150, https://doi.org/10.1016/j.jpba.2018.05.038.
[15] E. Bolea-Fernandez, A. Rua-Ibarz, M. Velimirovic, K. Tirez, F. Vanhaecke, Detection of microplastics using inductively coupled plasma-mass spectrometry (ICP-MS) operated in single-event mode, J. Anal. At. Spectrom. 35 (2020) 455–460, https://doi.org/10.1039/C9JA00379G.
[16] L. Ebdon, M. Foulkes, K. Sutton, Slurry nebulization in plasmas, J. Anal. At. Spectrom. 12 (1997) 213–229.
[17] P. Goodall, M.E. Foulkes, L. Ebdon, Slurry nebulization inductively coupled plasma spectrometry-The fundamental parameters discussed, Spectrochim. Acta, Part B 48 (1993) 1563–1577.
[18] L. Mueller, H. Traub, N. Jakubowski, D. Drescher, V.I. Baranov, J. Kneipp, Trends in single-cell analysis by use of ICP-MS, Anal. Bioanal. Chem. 406 (2014) 6963–6977, https://doi.org/10.1007/s00216-014-8143-7.
[19] Perkin Elmer Inc, Patented Asperon Single Cell Spray Chamber Delivering Intact Individual Cells to the ICP-MS Plasma, 2017.
[20] G. Expansion, High Sensitivity Single-Cell Sample Introduction System for ICP-MS, 2019. http://www.geicp.com/site/images/flyers/single_cell_flyer.pdf. (Accessed 1 January 2020).
[21] P. Alexy, E. Anklam, T. Emans, A. Furfari, F. Galgani, G. Hanke, A. Koelmans, R. Pant, H. Saveyn, B. Sokull Kluettgen, Managing the analytical challenges related to micro- and nanoplastics in the environment and food: filling the knowledge gaps, Food Addit. Contam. 37 (2020) 1–10, https://doi.org/10.1080/19440049.2019.1673905.
[22] M. Oliveira, M. Almeida, I. Miguel, A micro(nano)plastic boomerang tale: a never ending story? TrAC Trends Anal. Chem. (Reference Ed.) 112 (2019) 196–200, https://doi.org/10.1016/j.trac.2019.01.005.
[23] Q. Zhang, E.G. Xu, J. Li, Q. Chen, L. Ma, E.Y. Zeng, H. Shi, A review of microplastics in table salt, drinking water, and air: direct human exposure, Environ. Sci. Technol. 54 (2020) 3740–3751, https://doi.org/10.1021/acs.est.9b04535.
[24] SAPEA, A Scientific Perspective on Microplastics in Nature and Society, SAPEA, Berlin, 2019, https://doi.org/10.26356/microplastics.
[25] S. Huppertsberg, T.P. Knepper, Instrumental analysis of microplastics—benefits and challenges, Anal. Bioanal. Chem. (2018) 1–10, https://doi.org/10.1007/s00216-018-1210-8.
[26] M. Correia, K. Loeschner, Detection of nanoplastics in food by asymmetric flow field-flow fractionation coupled to multi-angle light scattering: possibilities, challenges and analytical limitations, Anal. Bioanal. Chem. 410 (2018) 5603–5615, https://doi.org/10.1007/s00216-018-0919-8.
[27] G. Renner, T.C. Schmidt, J. Schram, Analytical methodologies for monitoring micro(nano)plastics: which are fit for purpose? Curr. Opin. Environ. Sci. Heal. 1 (2018) 55–61, https://doi.org/10.1016/j.coesh.2017.11.001.
[28] J.L. Xu, K.V. Thomas, Z. Luo, A.A. Gowen, FTIR and Raman imaging for microplastics analysis: state of the art, challenges and prospects, TrAC Trends Anal. Chem. (Reference Ed.) 119 (2019) 115629, https://doi.org/10.1016/j.trac.2019.115629.
[29] R. Peñalver, N. Arroyo-Manzanares, I. López-García, M. Hernández-Córdoba, An overview of microplastics characterization by thermal analysis, Chemosphere 242 (2020), https://doi.org/10.1016/j.chemosphere.2019.125170.
[30] R. Thom, H. Marchandise, E. Colinet, The Certification of Monodispersed Latex Spheres in Aqueous Suspensions with Nominal Diameter 2.0 Mm, 4.8 Mm and 9.6 Mm (RM 165, 166 and 167), 1985. Luxembourg.
[31] J. Heroult, V. Nischwitz, D. Bartczak, H. Goenaga-Infante, The potential of asymmetric flow field-flow fractionation hyphenated to multiple detectors for the quantification and size estimation of silica nanoparticles in a food matrix, Anal. Bioanal. Chem. 406 (2014) 3919–3927, https://doi.org/10.1007/s00216-014-7831-7.
[32] C.D.B. Amaral, R.S. Amais, L.L. Fialho, D. Schiavo, A. Rita, A. Nogueira, J. A. Nóbrega, Determination of carbon in digested samples and amino acids by inductively coupled plasma tandem mass spectrometry, Microchem. J. 122 (2015) 29–32, https://doi.org/10.1016/j.microc.2015.04.007.
[33] H.E. Pace, N.J. Rogers, C. Jarolimek, V.A. Coleman, C.P. Higgins, J.F. Ranville, Determining transport efficiency for the purpose of counting and sizing nanoparticles via single particle inductively coupled plasma mass spectrometry, Anal. Chem. 83 (2011) 9361–9369, https://doi.org/10.1021/ac201952t.
[34] F. Laborda, A.C. Gimenez-Ingalaturre, E. Bolea, J.R. Castillo, Single particle inductively coupled plasma mass spectrometry as screening tool for detection of particles, Spectrochim. Acta Part B At. Spectrosc. 159 (2019) 105654, https://doi.org/10.1016/j.sab.2019.105654.
[35] I. Abad-Álvaro, E. Peña-Vázquez, E. Bolea, P. Bermejo-Barrera, J.R. Castillo, F. Laborda, Evaluation of number concentration quantification by single-particle inductively coupled plasma mass spectrometry: microsecond vs. millisecond dwell times, Anal. Bioanal. Chem. 408 (2016) 5089–5097, https://doi.org/10.1007/s00216-016-9515-y.
[36] F. Laborda, A.C. Gimenez-Ingalaturre, E. Bolea, J.R. Castillo, About detectability and limits of detection in single particle inductively coupled plasma mass spectrometry, Spectrochim. Acta Part B At. Spectrosc. 169 (2020) 105883, https://doi.org/10.1016/j.sab.2020.105883.
[37] J.W. Olesik, P.J. Gray, Considerations for measurement of individual nanoparticles or microparticles by ICP-MS: determination of the number of particles and the analyte mass in each particle, J. Anal. At. Spectrom. 27 (2012) 1143, https://doi.org/10.1039/c2ja30073g.
[38] F. Laborda, J. Jiménez-Lamana, E. Bolea, J.R. Castillo, Critical considerations for the determination of nanoparticle number concentrations, size and number size distributions by single particle ICP-MS, J. Anal. At. Spectrom. 28 (2013), https://doi.org/10.1039/c3ja50100k.
[39] M. Aghaei, A. Bogaerts, Particle transport through an inductively coupled plasma torch: elemental droplet evaporation, J. Anal. At. Spectrom. 31 (2016) 631–641, https://doi.org/10.1039/c5ja00162e.
[40] C. Guerranti, T. Martellini, G. Perra, C. Scopetani, A. Cincinelli, Microplastics in cosmetics: environmental issues and needs for global bans, Environ. Toxicol. Pharmacol. 68 (2019) 75–79, https://doi.org/10.1016/j.etap.2019.03.007.
[41] L.M. Hernandez, E.G. Xu, H.C.E. Larsson, R. Tahara, V.B. Maisuria, N. Tufenkji, Plastic teabags release billions of microparticles and nanoparticles into tea, Environ. Sci. Technol. 53 (2019) 12300–12310, https://doi.org/10.1021/acs.est.9b02540.
[42] L.A. Currie, Limits for qualitative detection and quantitative determination: application to radiochemistry, Anal. Chem. 40 (1968) 586–593, https://doi.org/10.1021/ac60259a007.

TECHNICAL NOTE

ICP - Mass Spectrometry

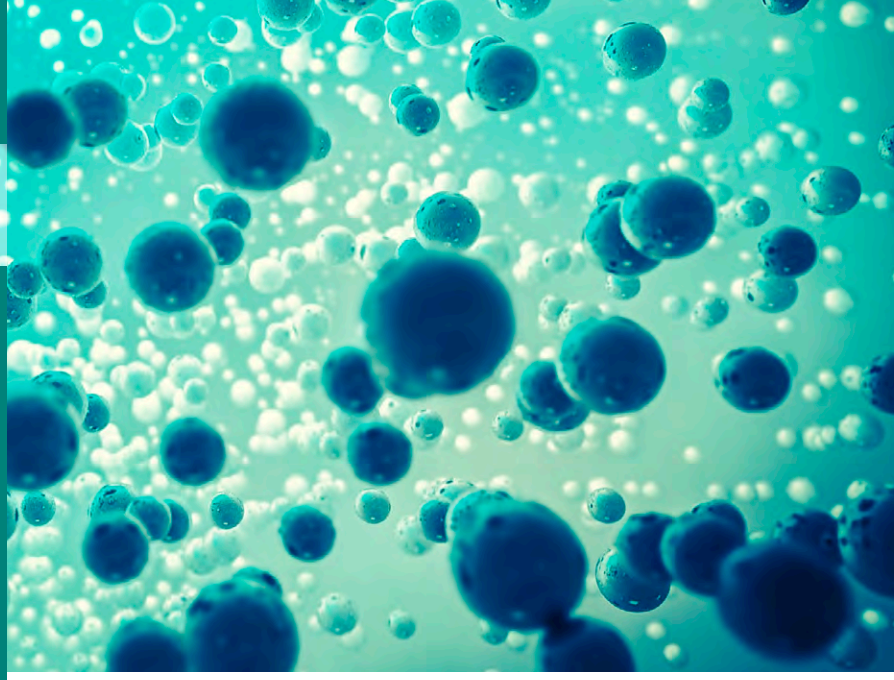

AUTHORS

Francisco Laborda
Celia Trujillo
University of Zaragoza
Zaragoza, Spain

Ryszard Lobinski
Université de Pau et des Pays de L'Adour
Pau, France

Unlocking Carbon-13 with Single Particle ICP-MS: Feasibility Study for Microplastic Detection

Introduction

Carbon is difficult to measure with ICP-MS because of its high ionization potential (11.3 eV) and its presence in both the argon used to generate the plasma (primarily in the form of CO_2, as an impurity) and in reagents, including acids and water. As a result, extremely high backgrounds exist at both of the naturally occurring isotopes of carbon: C12 (99.9% abundance) and C13 (1.1% abundance). With no easy way to remove these sources of carbon, limits of detection with either isotope are severely affected.

One way to greatly reduce backgrounds is by shortening the measurement times using dwell times in the range of microseconds, as is typically done with single particle ICP-MS (SP-ICP-MS)[1,2]. Working at these short dwell times in SP-ICP-MS mode, the background signal is reduced whereas the overall signal from the particles remains unaffected, allowing particles to be detected and measured at levels that were previously unattainable[3].

By using SP-ICP-MS, the C13 background is reduced significantly, permitting carbon-containing particles to be detected, counted, and measured. As a result, SP-ICP-MS may be used as a screening tool for the detection of microplastics, as discussed in detail by Laborda *et al.*[4]. This work summarizes the principles involved in the detection of microplastics with SP-ICP-MS, and also shows examples.

PerkinElmer®
For the Better

Reduction of Carbon Background

All measurements were made on a NexION® ICP-MS due to its ability to use microsecond dwell times, leveraging the Syngistix™ for ICP-MS Nano Application software module, which combines real-time single particle acquisition with fast data processing for routine analytical use. However, in this work, dwell times between 100-200 µs were found to give the best limits of detection for microplastic particles because of the relatively large size of these particles. Although the backgrounds for both C12 and C13 are greatly reduced, C13 was selected for this work since it had a lower background. As shown in Figure 1, the average C13 background acquired with a dwell time of 200 µs is less than 50 counts, which allows for the detection of typical microplastic particles. While acquiring multiple data points per particle provides the highest accuracy [1], it also decreases the height of the particle signals, and hence their detectability. Since the particles detected in this study were in the micron range [4], a dwell time of 200 µs was found to provide the best compromise between accuracy and detection limits.

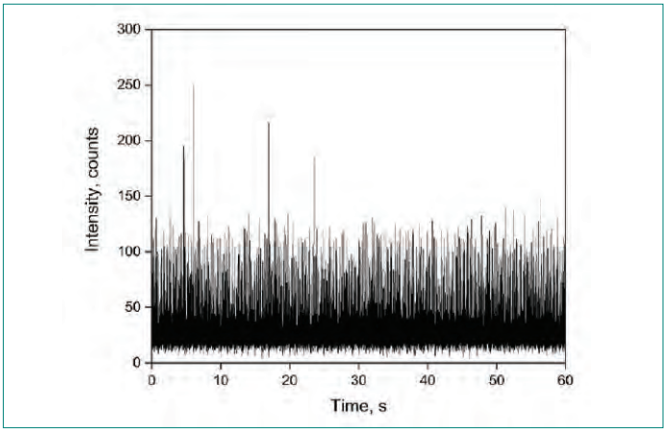

Figure 1: C13 background in SP-ICP-MS acquired with a dwell time of 200 µs.

Sample Transport of Microplastic Particles to the Plasma

With the carbon background reduced, but before the detection of microplastic particles can be evaluated, the transport of microplastic particles from solution to the plasma must be optimized. Transport efficiencies of conventional sample introduction systems (i.e., concentric pneumatic nebulizer with a cyclonic spray chamber) are ≈2% for liquids, where the spray chamber is designed to prevent droplets of about 4 µm and larger from reaching the plasma. Most SP-ICP-MS work has focused on nanometer-size particles (generally smaller than 100 nm), which have transport efficiencies to the plasma of ≈10% with conventional sample introduction systems: the smaller particles pass more efficiently through the spray chamber than larger droplets. However, typical microplastic particles are in the micron-size range, where conventional spray chambers limit them from reaching the plasma.

This issue has been addressed with the development of the Asperon™ spray chamber [5] for single cell ICP-MS (SC-ICP-MS) where cells up to 50 µm must be transported to the plasma. Asperon is a unique linear-pass spray chamber where a sheath flow tangential to the spray chamber wall reduces the number of impacts of cells with the wall, and the laminar flow within the spray chamber carries more cells to the plasma. As a result, the transport efficiency of the Asperon spray chamber is typically ≈30% for micron-sized particles and cells [6,7], making it ideal for the analysis of micron-sized microplastic particles. Therefore, the Asperon spray chamber was used in these studies of microplastic particles.

Detection of Polystyrene Microparticle Standards

For these studies, seven commercially available polystyrene microparticle suspensions with nominal diameters ranging from 1-5 µm were evaluated. The transport efficiencies of the various spheres were evaluated and found to vary from 26-28% for both the 2.2 and 4.8 µm spheres, which corresponds to the transport efficiency measured for cells [6,7]. With the transport of polystyrene spheres to the plasma confirmed, the next step was detection and measurement.

Figure 2 shows a typical particle event distribution and the corresponding size distribution for 2.2 µm polystyrene spheres. The particle event distribution clearly shows that 2.2 µm particles can be detected, with the size distribution being centered on the nominal size, demonstrating accuracy.

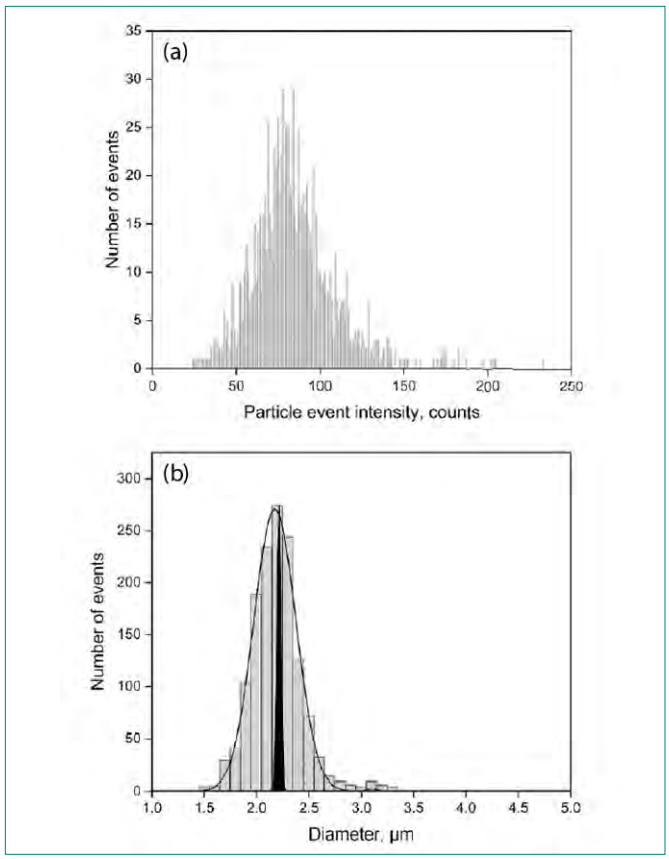

Figure 2: (a) Particle event intensity and (b) corresponding size distribution histogram of 2.2 µm polystyrene spheres.

To determine the accuracy at different sizes, the seven polystyrene microparticle standards were analyzed, with the results shown in Table 1. These results show accurate size measurements for particles from 2-5 µm, while the 1 µm particles (close to the size detection limits) are overestimated, suggesting that SP-ICP-MS can accurately size microplastic particles down to 2 µm.

Table 1: Particle Size Measurements for Seven Different Polystyrene Microparticle Standards.

Particle Standard	Certified Diameter (µm)	Measured Mean Diameter (µm)	% Bias
1	1.04 + 0.03	1.69 + 0.07	140
2	1.98 + 0.01	1.83 + 0.01	93
3	2.02 + 0.02	1.93 + 0.01	96
4	2.22 + 0.01	2.10 + 0.02	94
5	3.03 + 0.09	2.74 + 0.01	91
6	4.00 + 0.04	3.56 + 0.06	91
7	5.00 + 0.04	4.55 + 0.05	92

Detection of Polystyrene Microparticles in Consumer Products

Plastic microparticles are added to exfoliants as abrasives. Three different exfoliants were prepared by mixing with water, sonicating, and filtering through 10 µm filters prior to analysis. As shown in Figure 3, the size distributions differ between the products, as do the particle number concentrations, with the middle exfoliant containing significantly more particles than the other two samples (numerical results in Table 2). This emphasizes the importance of particle concentration: when unknown samples are analyzed, the sample preparation should be adjusted so that the particle concentration is less than ≈250,000 particles/mL, as higher concentrations may result in multiple particles being ionized at the same time, leading to inaccurate results. Therefore, the appropriate sample dilution is a bit of trial and error.

Table 2: Carbon-Containing Particle Results from Exfoliants.

Sample	Mean Diameter (µm)	Particle Concentration (g^{-1})
Blank	---	---
Exfoliant 1	2.89	3.6×10^{7}
Exfoliant 2	3.08	3.1×10^{11}
Exfoliant 3	2.11	4.4×10^{10}

Next, three different plastic tea bags were examined by first removing the contents, washing and drying, and then heating for 5 minutes at 100 °C in ultrapure water to replicate the process of making tea. Figure 4 shows that incidental carbon-containing particles were found in all samples, with all having roughly the same number and size of microparticles, as shown in Table 3. While the particle size is similar to that of the the exfoliants, the particle concentrations are significantly lower in the tea bags: in the exfoliants, microparticles are added to aid in scrubbing, while in tea bags, they most likely originate from leaching or from the breakdown of the tea bags themselves.

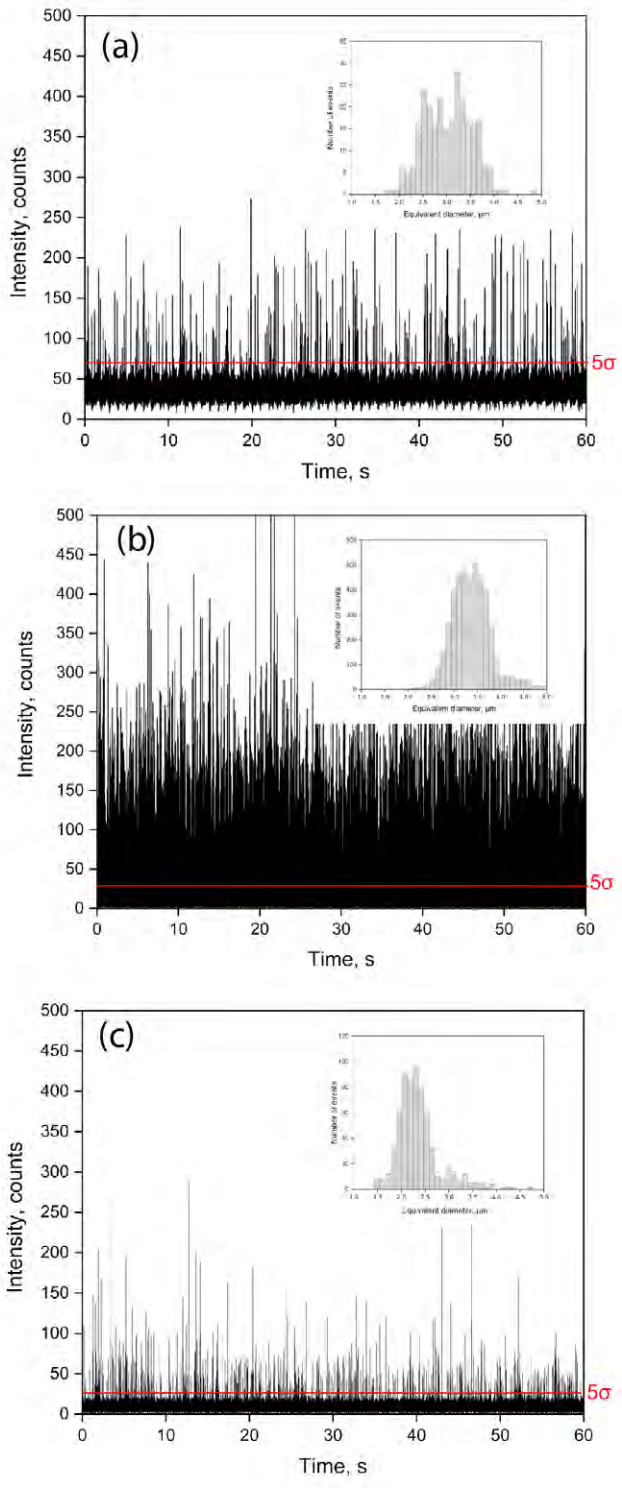

Figure 3: Time scans and size distributions of carbon-containing particles in three different exfoliants, where: (a) Exfoliant 1 has the broadest size distribution; (b) Exfoliant 2 contains the most particles; and (c) Exfoliant 3 has the smallest particle sizes.

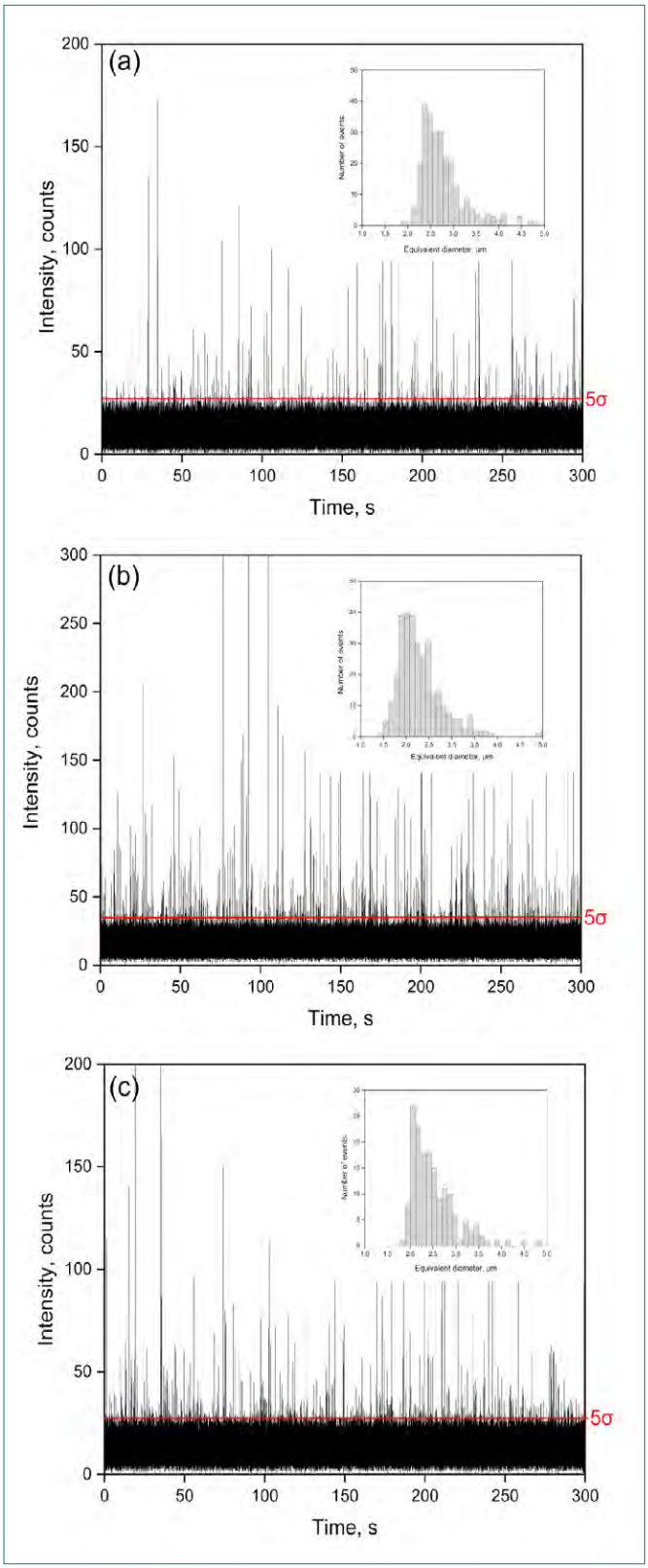

Figure 4: Time scans and size distributions of carbon-containing particles in three different plastic tea bags, each containing similar numbers and sizes of microparticles.

Table 3: Carbon-Containing Particle Results from Plastic Tea Bags.

Sample	Mean Diameter (µm)	Particle Concentration (g^{-1})
Blank	---	---
Tea Bag 1	2.70	2.2×1^{04}
Tea Bag 2	2.18	5.5×10^{4}
Tea Bag 3	2.26	1.9×10^{4}

Conclusions: SP-ICP-MS as a Screening Technique for Microplastics

Since any carbon-containing microparticles will produce carbon signals, the signals achieved using SP-ICP-MS in the determination of microplastic particles cannot be unambiguously linked to microplastics. As such, SP-ICP-MS is regarded as a complementary technique for the characterization of microplastics. To determine if the microparticles are plastic, additional techniques are required. In this work [4], both microscopy and ATR-FT-IR (PerkinElmer Spectrum 100) were used to confirm the presence and identity of the microparticles as plastics (polystyrene, polylactic acid, polyethylene terephthalate).

In order to obtain accurate particle size and number results for carbon in microplastics, the mass fraction of the carbon in the particles must be known. However, since the mass fraction can vary depending on the composition of the plastic, the carbon mass fraction can only be estimated (i.e., use the carbon mass fraction for polystyrene, which is 0.9231). However, because of its analysis speed, SP-ICP-MS can sample many more particles in much shorter times than conventional analytical techniques, providing more information about particle size distribution and particle concentration within a short space of time. Consequently, SP-ICP-MS is an ideal technique to be used in screening for microplastics.

In summary, SP-ICP-MS using the NexION system can be successfully used as either a screening tool or complementary technique for microplastic determination by monitoring the signal of C13. By taking advantage of analysis speed, the background from C13 is greatly reduced, allowing microplastic particles as small as 2 µm to be accurately sized and measured. By combining SP-ICP-MS with techniques which can identify the composition of microplastics, such as ATR-FT-IR, more thorough information about microplastics can be attained.

References

1. "Single Particle Inductively Coupled Plasma Mass Spectrometry: Understanding How and Why", White Paper, PerkinElmer, 2014.
2. "A Comparison of Microsecond vs. Millisecond Dwell Times on Particle Number Concentration Measurements by Single Particle ICP-MS", Application Note, PerkinElmer, 2016.
3. "Analysis of SiO2 Nanoparticles in Standard Mode with Single Particle ICP-MS", Application Note, PerkinElmer, 2015.
4. Laborda, F., Trujillo, C., Lobinski, R. *Talanta*, 2021, 221, 121486. https://doi.org/10.1016/j.talanta.2020.121486
5. "Patented Asperon Single Cell Spray Chamber: Delivering Intact Individual Cells to the ICP-MS Plasma", Technical Note, PerkinElmer, 2019.
6. "Iron Content Measurement in Individual Bacterial Cells Using SC-ICP-MS", Application Note, PerkinElmer, 2018.
7. Merrifield, R.C., Stephan, C., Lead, J.R. *Environ Sci. Technol.,* 2018, 52, (4), 2271-2277.

PerkinElmer, Inc.
940 Winter Street
Waltham, MA 02451 USA
P: (800) 762-4000 or
(+1) 203-925-4602
www.perkinelmer.com

538518 PKI

ECOLE DOCTORALE :
Sciences Exactes et leurs Application ED211

LABORATOIRE :
IPREM UMR5254 – CNRS/UPPA
Université de Saragosse-GEAS

Résumé:

Aujourd'hui, le plastique est un matériau largement utilisé dans de nombreux secteurs. Par conséquent, une grande partie du plastique finit en déchets dans l'environnement, ce qui en fait un problème mondial. On estime qu'environ 80 % des plastiques produits sont rejetés dans l'environnement. Certains de ces plastiques se retrouvent sous forme de nanoplastiques et de microplastiques dans les systèmes aquatiques. La présence de ces plastiques pose des problèmes en raison de leur taille et de leur capacité à adsorber et transporter les polluants émergents, et donc à faciliter leur ingestion par les organismes vivants. La compréhension des effets des micro- et nanoplastiques est encore limitée, en grande partie à cause du manque de méthodes robustes pour leur détection et leur quantification.

Dans ce contexte, cette thèse de doctorat a eu pour objectif le développement d'une méthode analytique pour la détection, la caractérisation de la taille et la quantification des microparticules de plastique par ICP-MS fonctionnant en mode particule unique avec des temps de séjour de l'ordre de la microseconde. Cette méthode a permis la détection de particules de polystyrène d'une taille allant jusqu'à 1,2 µm par traçage isotopique 13C et a été utilisée pour analyser les microplastiques dans les produits de soins personnels et ceux libérés par les emballages alimentaires. Une plateforme analytique a également été développée pour l'analyse d'échantillons environnementaux, tels que l'eau de rivière, en combinant l'ICP-MS à particule unique, la microscopie électronique à balayage à émission de champ et la spectroscopie Raman. L'utilisation de cette plateforme nous a permis de déterminer la présence et l'identité chimique des microparticules de plastique dans les échantillons d'eau de rivière analysés. Nous avons également étudié la capacité d'adsorption des nanoplastiques environnementaux pour les polluants émergents, tels que les agents de contraste à base de gadolinium, et leur capacité à agir comme concurrents des colloïdes naturels. La capacité des nanoplastiques à agir comme des vecteurs de polluants émergents dans des conditions environnementales a été démontrée.